Production of DARPins in the Yeast *Pichia pastoris*

A thesis submitted to
UNIVERSITY COLLEGE LONDON

For the degree of
DOCTOR OF PHILOSOPHY

By

Maria Livanos

Supervised by Professor Kerry Chester, Professor Nigel Titchener-Hooker and Professor Daniel Bracewell

The Advanced Centre for Biochemical Engineering
Department of Biochemical Engineering
University College London
Torrington Place, London, WC1E 7JE, UK

Declaration of Originality

I, Maria Livanos, confirm that the work presented in this thesis is my own. Where information has been derived from other sources, I confirm that this has been indicated in the thesis.

Signed:……

Date:……

Acknowledgements

To the people who made this possible – Thank you.

Your support, extreme patience and goodwill, shall not be forgotten nor left unreciprocated.

Abstract

Designed Ankyrin Repeat Proteins (DARPins) are industrially relevant small non-immunoglobulin scaffold proteins that bind their target with high affinity. G3 is a DARPin designed to target the receptor tyrosine kinase protein HER2 (human epidermal growth factor receptor 2). Overexpression of HER2 is prevalent in many cancer types and development of targeting agents for imaging during the course of treatment is an unmet need. The research aims to develop a bioprocess for the production of clinical grade DARPin from *Pichia pastoris*.

In the pilot stage, the effects of the common hexahistidine (His_6) purification tag on biodistribution and tumour targeting were assessed *in vivo*. Three constructs were created; the $(His)_6$-, the histidine-glutamate $(HE)_3$- and the regulatory standard, untagged G3 DARPin. The final products were characterised in terms of purity, identity and functionality prior to testing in mice. The $(HE)_3$-tagged G3 was the superior product in terms of non-target specific uptake and was taken forward as a clinically relevant example for bioprocess development.

A regulatory compliant bioprocess for G3 was established in the yeast *P. pastoris*. The fermentation procedure was transferred to a 20-L bioreactor and a 5 hour induction run implemented. Tangential flow filtration (TFF), immobilised metal affinity (IMAC), size exclusion (SEC) and anion exchange (AEX) chromatography steps were utilised to generate ~60 mg of fully functional homogenous G3. The level of host cell protein (HCP) and endotoxin was within regulatory compliance at <1 ng/mg and <0.05 EU/mg, respectively. The process was then adapted for production of an imaging agent and enabled the addition of maleimide-DOTA via the free cysteine on the C-terminal of the DARPin. This yielded 38-42 mg / run of high purity DOTA_G3 which radiolabelled with ^{111}In at greater than 95% efficiency.

Sites of proteolytic cleavage were identified and protein engineering carried out to mitigate breakdown. Mutation of the amino acid methionine (30) to leucine resulted in notable inhibition of proteolytic activity and allowed for increased fermentation times, improving titre by ~75%. The mutation did not alter DARPin binding affinity nor baseline expression. The bioprocess and identified mutation were tested on an independent DARPin (E69) to assess the potential of a 'universal' DARPin production platform. As with the G3 the mutated E69 DARPin proved to be far more resistant to proteolytic activity than its wild type counterpart and the bioprocess generated 40 mg of fully functional E69 of equivalent purity at <0.05 EU/mg endotoxin and <3.4 ng/mg HCP.

In summary, this study has generated a holistic and innovative end to end development strategy for the production of DARPins in the yeast *P. pastoris*.

IMPACT STATEMENT

The work described in this thesis was designed and executed to develop a clinically relevant bioprocess for the production of DARPins in the yeast *P. pastoris*. A model protein, the anti-HER2 DARPin was selected based on its clinical potential as a whole body-imaging agent for HER2 positive cancer. Overexpression of HER2 is prevalent in many cancer types and development of targeting agents for imaging prior to and during the course of treatment is an unmet need. DARPins had not previously been manufactured in *P. pastoris* allowing opportunity for challenge and novelty in developing a new bioprocess. Additionally as scaffold proteins DARPins share the same conserved framework and as such the potential to build a platform process for their production.

This thesis successfully developed an effective platform process for DARPin production in the yeast *P. pastoris.* DARPins have previously been produced at shake-flask level in *E.coli.* Despite relatively high yields of 100-200 mg/L, extraction and purification of intracellular proteins from bacteria remains an arduous procedure which is greatly hindered by the presence of endotoxins. The *P. pastoris* bioprocess described is regulatory compliant, cost effective and easy to implement, utilising a secreted expression system, combined clarification / capture event, size exclusion chromatography and anion exchange chromatography. From inoculation to fill the procedure takes no more than five days and the product generated of high purity.

An easily scalable and GMP compliant conjugation process for labelling and purifying large quantities of DARPin was also developed. The conjugation process could easily be fitted to the platform process to facilitate imaging agent production. The product generated was fully functional, of high purity and stable for the assessed timeframe of two years post fill. With the advent of personalised / precision therapies this area of diagnostics is increasingly under demand in order for the successful delivery of stratified medicines. Therefore a means of production that is both cost-effective, efficient and of technical ease is of great importance in taking these products forward.

Table of Contents

TABLE OF FIGURES

List of Tables

List of Abbreviations

% ID/g	Percentage of injected dose per gram of tissue
^{68}Ga	Gallium-68
^{111}In	Indium-111
A	Adenine
aa	Amino Acid
AEX	Anion Exchange
AOX	Alcohol Oxidase
BMGY	Buffered Glycerol-complex medium
BMMY	Buffered Methanol-complex medium
BL	Blood
BO	Bone & Marrow
bp	Base Pair
BSA	Bovine Serum Albumin
C	Cytosine
CDR	Complementary Determining Region
cm	Centimetre
CRUK	Cancer Research UK
Cys	Cysteine
Da	Dalton
DAB	3,3'-*diaminobenzidine*
DARPin	Designed Ankyrin Repeat Protein
dH20	Deionized Water
dNTP	Deoxyribose Nucleoside Triphosphates
DOTA	1,4,7,10-tetraazacyclododecane-1,4,7,10-tetraacetic acid
DSP	Downstream Process
DTT	Dithiothreitol
E.coli	Escherichia coli
ECD	Extracellular Domain
ECL	Enhanced Chemiluminescence
EDC	N-(dimethylaminopropy)l-N-ethylcarbodiimide hydrochloride
EDTA	Ethylenediaminetetraacetic acid
EGFR	Epidermal growth factor receptor
ELISA	Enzyme-linked Immunosorbent Assay
EU	Endotoxin Units

FACS	Fluorescence-activated Cell Sorter
Fc	Fragment Crystallisable Region
FDA	US Food and Drug Administration
FPLC	Fast protein liquid chromatography
g	Gram
G	Guanine
GBM	Glioblastoma Multiforme
GLP	Good Laboratory Practice
GMP	Good Manufacturing Practice
HCD	High Cell Density
HCP	Host Cell Protein
$(HE)_3$	Histidine_Glutamate Tag
HE	Heart
HER1	Human Epidermal Growth Factor Receptor 1
HER2	Human Epidermal Growth Factor Receptor 2
His_6	Hexahistidine Tag
HPLC	High Performance Liquid Chromatography
HRP	Horse Radish Peroxidase
HRV	Human Rhinovirus
Ig	Immunoglobulin
IMAC	Immobilised Metal Affinity Chromatography
INS+	Intestine with content
K_{ass}	On Rate or Association
K_{diss}	Off Rate or Dissociation
K_D	Binding Affinity
KI	Kidney
KR	Lysine-Arginine
L	Litre
LB	Luria Bertani
LC-MS	Liquid Chromatography Mass Spectrometry
LOD	Lower Limit of Detection; ‘Concentration corresponding to a signal two standard deviations above the mean of the zero standard.’
LOQ	Lower Limit of Quantification; Lowest concentration where concentration coefficients of variation (CV) are <20%.
LU	Lungs
M	Molar

MALDI	Matrix-Assisted Laser Desorption/Ionization
MBq	Megabecquerel
mg	Milligram
µg	Microgram
ml	Millilitre
µl	Microlitre
mM	Millimolar
µM	Micromolar
Min	Minute
MHRA	Medicines and Healthcare Products Regulatory Agency
MW	Molecular Weight
NaCl	Sodium Chloride
NaOH	Sodium Hydroxide
ng	Nanogram
OD_{280}	Optical Density Measured at 280 nm
OD_{600}	Optical Density Measured at 600 nm
OPD	O-phenylenediamine dihydrochloride
PBS	Phosphate Buffered Saline
PBS-T	Phosphate Buffered Saline + 0.1% Tween20
PCR	Polymerase Chain Reaction
PET	Positive emission tomography
pI	pH of Isoelectric Point
P. pastoris	Pichia pastoris
PVDF	Polyvinylidene Difluoride
RT	Room Temperature
Rpm	Revolutions per Minute
rProtein	Recombinant Protein
scFv	Single-Chain Variable Fragment
SD	Standard Deviation
SDS-PAGE	Sodium Dodecyl Sulfate Polyacrylamide Gel Electrophoresis
SP	Spleen
SPECT	Single Photon Emission Computed Tomography
SPR	Surface plasmon resonance
T	Thymine
TAE	Tris-Acetate-EDTA
TFF	Tangential Flow Filter
TU	Tumor

U	Unit
UK	United Kingdom
US	United States
VL	Variable Light Chain
VH	Variable Heavy Chain
VOI	Volume of Interest
v/v	Percentage of Volume per Volume
w/v	Percentage of Weight to Volume
YEPD	Yeast Extract Peptone Dextrose medium
YPD	Yeast Extract Peptone Dextrose
YPDS	Yeast Extract Peptone Dextrose Sorbitol

CHAPTER ONE

INTRODUCTION

1.0 INTRODUCTION

1.1 Biotherapeutic Industry

Recombinant DNA was introduced to the world in 1972 (Paul Berg) and by 1973 Herbert Boyer's team had successfully transformed *E.coli* with recombinant plasmid. Almost 10 years later in 1982 the biopharmaceutical industry emerged with the commercial introduction of the world's first recombinant protein, Insulin (Humulin), for the treatment of diabetes (Pavlou *et al.* 2004). Over the next 30 years this highly competitive and rapidly growing sector of the pharmaceutical industry has generated hundreds of such proteins and has taken a prominent position within the pharmaceutical industry with a present global worth in excess of 100 billion dollars.

Targeting agents in the form of monoclonal antibodies (mAb) currently dominate this sector but with the emergence of next generation formats such as bispecific, antibody drug conjugates, antibody fragments and scaffold proteins competition is fierce. Antibodies hold such a prominent position in the biotherapeutic landscape as their antigen specificity can circumvent the broad off target effects that conventional treatments, such as chemotherapy, generate.

1.2 Immunoglobulins (Ig)

Immunoglobulins are an essential component of the body's natural defence mechanism against pathogenic challenge. Although five Ig isotypes exist; IgG, IgM, IgA, IgD and IgE, they are not expressed equally with IgG being the most predominant immunoglobulin in nature (Holliger *et al.* 2005).

IgG is a large multi-chain protein of 150 kDa which can be broken down into two heavy chains (50 kDa) and two light chains (25 kDa), as shown in Figure 1.0. The chains associate largely through disulphide bonds and non-covalent inter-domain interactions. Antigen binding is facilitated by the complimentary determining regions (CDRs) three of which are present on both the V_H and V_L chains (Holliger *et al.* 2005; Liu *et al.* 2012).

Derivatives of the full length antibody with maintained binding capability are also used as targeting entities and constructs are largely either the antigen-binding fragment (Fab) or single chain variable fragment (scFv) constructs (Holliger *et al.* 2005), shown in Figure 1.0. The

smaller antibody domains are typically used when Fc receptor engagement is undesirable, for the penetration of solid tumours and for faster in blood clearance (Blažek *et al*. 2003; Anderson *et al.* 2004).

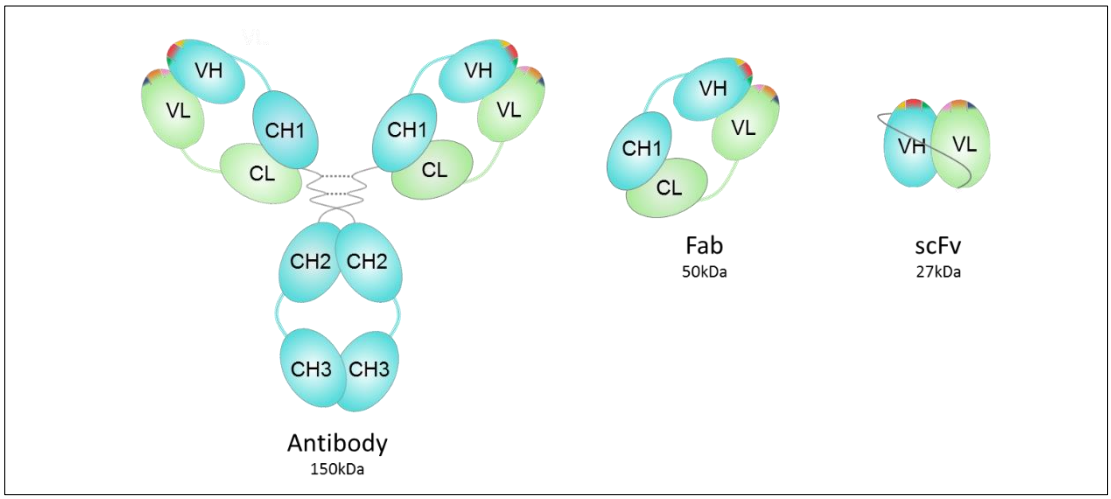

FIGURE 1.0. Structural illustration of a full length antibody (IgG) and commonly used antibody fragments.
Antibody, IgG full length antibody. **Fab,** antigen-binding fragment. **scFv,** single chain variable fragment. *Figure kindly provided by the Kerry Chester Group.*

1.2.1 Antibody Production

In the early years of antibody discovery, production of antibodies relied on the use of poly-serum from antigen immunized mice. The antibodies generated by B cells were a mixed population targeting the whole antigen not specific regions. Each B cell has a limited number of replication cycles and therefore this process was unsuitable for large scale manufacturing.

In 1975 pioneering hybridoma technology was developed by Köhler and Milstein allowing for the cultivation of continuously dividing cells under appropriate conditions. The generation of this *in vitro* culture is a result of fusing the antigen exposed mouse's B-cells to an immortalised myeloma cell line and thus creating a clonal hybridoma (Köhler & Milstein 1975). This technology broke ground in the ability to produce large quantities of antibodies, thereby permitting their emergence in the biotherapeutic sector in 1986 with the first approved antibody therapeutic, muromonab-CD3 / Orthoclone. (Duvall *et al.* 2011; Elgundi *et al*. 2017). Despite the success of hybridoma technology it is labour-intensive, suffering from genetic instability and with production yields often low (Elgundi *et al*. 2017). Aside from the problems with production these antibodies faced they carried murine sequences and therefore could elicit an adverse immune reaction in humans (Tjandra *et al.* 1990).

To counter the immunogenicity associated with murine antibodies, recombinant DNA technology was used to replace the mouse constant regions with constant regions from human antibodies. This thereby created a chimeric construct with reduced foreign party regions exposed to the hosts' immune system. The technology has progressed to fully humanised constructs with the first commercialisation of a fully humanised antibody, trastuzumab (Herceptin), in 1998 by Roche (Bryant *et al.* 2006).

Antibodies are now standardly produced recombinantly in Chinese Hamster Ovary (CHO) cells yielding titres of 8 g/L culture with cell densities of $\geq 1x10^7$ cells/mL (Hacker *et al.* 2009). Despite the high yields possible with mammalian culture the cost associated remain extremely high by comparison to microbial and yeast culture. A mammalian host system is necessary due to the complexity of the molecule as antibodies have multiple disulphide bonds and also require post-translational modification (Elgundi *et al*. 2017). Thus a simpler targeting molecule that could be made to high titres in microbial/yeast expression platforms would be advantageous.

1.3 Non-Immunoglobulin Scaffold Proteins

Non-immunoglobulin (non-Ig) scaffold proteins are a category of affinity proteins often viewed as an alternative to antibodies in imaging and therapeutics. The attractive properties, which set them apart from antibodies, are their small (~40-100aa) single domain structure that is often devoid of cysteines and requires no post-translational modification. This simplicity thus enables them to undergo with ease both multimerization and production, circumventing the need for costly mammalian production platforms. At least 20 structurally and functionally unrelated scaffold proteins have been reported and from these 139 binders developed covering 102 distinctive targets, several of which are in pre-clinical and clinical development (Skrlec *et al.* 2015; Lofblom *et al.* 2011).

One such promising non-Ig scaffold subclass is the Designed Ankyrin Repeat Protein (DARPin) (Boersma *et al.* 2011).

1.3.1 Designed Ankyrin Repeat Proteins (DARPins)

Designed Ankyrin Repeat Proteins (DARPins) are a class of small synthetic non-immunoglobulin binding proteins derived from the ankyrin repeat protein in nature. Ankyrin

repeat proteins in nature aid in the mediation of protein-protein interactions in both the cytoplasmic and extracellular environment. They consist of a framework of repeating structural motifs that stack together, through hydrogen bonds and/or hydrophobic interactions, to form an enlarged stable structure (Plückthun 2015), Figure 1.1. This increase in surface area consequently delivers the potential of a larger binding domain than would ordinarily be available within many globular proteins. Each repeat displays variable surface residues, which upon stacking form the interface for target interaction much like the CDR of an antibody (Tamaskovic *et al.* 2012; Plückthun 2015).

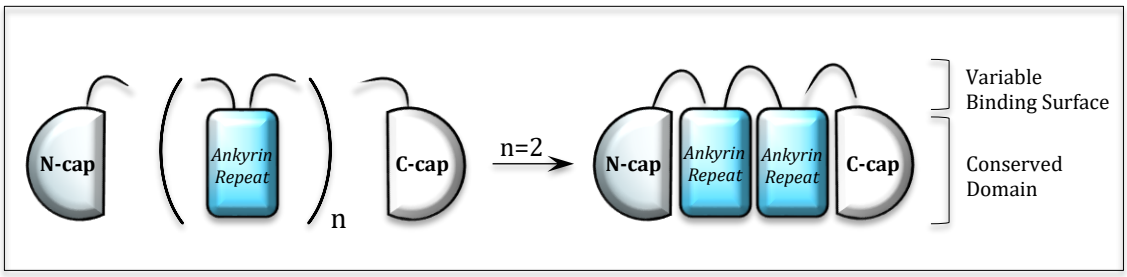

FIGURE 1.1 Schematic representation of DARPin constituents and general module function.

1.3.2 Structure of DARPin proteins

A single DARPin repeat unit comprises of 33 amino acids these form a β-turn followed by two antiparallel α-helices giving a right-handed solenoid structure. Residues present within the β-turn and first of the two anti-parallel α-helices of each repeat facilitate target interaction. Each repeat has the potential for target interaction and this generates high binding affinities between the DARPin and its antigen. N- and C-terminal hydrophilic capping domains (Figure 1.1) are utilised to shield the hydrophobic core of the stacked ankyrin repeats and this allows for a highly soluble molecule.

Protein design using consensus-based engineering emerged in the 1990's and used multiple sequence alignments of as many related proteins as possible to predict the most probable amino acid for each position based on statistical occurrence. It was thought that stabilizing amino acids would occur with greater frequency within the sequence and therefore this strategy would not only specify the protein fold but also generate proteins of increased stability. This underlying hypothesis has proven true for many proteins generated by consensus-based design and variations thereof (Kajander *et al*. 2007).

This principal of consensus design was used in developing the DARPin library. Multiple alignments of naturally occurring Ankyrin repeat proteins were used to design a scaffold of

fixed framework harbouring randomised interaction residues. In total each DARPin module typically consists of 26 fixed framework residues, 6 randomised interaction residues and 1 randomised framework residue (Figure 1.2). These seven randomised amino acid residues when taken together confer a theoretical diversity of 7.2 X 10^7 per unit (Plückthun A. 2015).

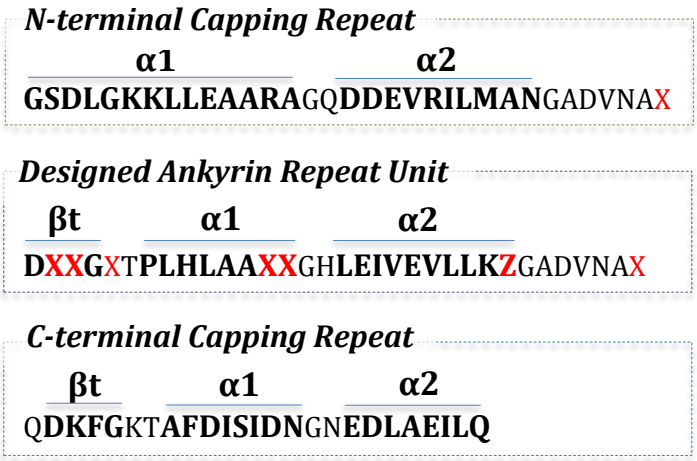

X: Any natural amino acid.

Z: Typically Asparagine, Histidine or Tyrosine.

βt: Beta- turns.

α1/2: Alpha helices 1 & 2, respectively.

FIGURE 1.2 Template amino acid sequences of Designed Ankyrin Repeat protein constituents: N-Cap, C-Cap and Repeat Unit.
Components forming secondary structures (**α1/2 & βt)** are shown above their respective emboldened amino acid sequences. DARPin repeat units ordinarily consist of 26 predefined framework residues of which six are randomized 'interaction' residues, **X** and one is a randomized framework residue, **Z**.

1.3.3 DARPins in development

There are three DARPins currently undergoing phase II and III clinical trials in oncology and ophthalmology (Table 1) and many more in pre-clinical development.

Table 1.0 DARPin agents currently undergoing clinical trial.

AMD, Age-related macular degeneration; **DME,** Diabetic macular edema; **NSCLC,** Non-small-cell lung carcinoma.

Product	Area to be used	Partner	Mode of Action	Clinical Trial
MP0250	Oncology (Multiple Myeloma)	Molecular Partners	Inhibits VEGF and HGF receptor binding.	Phase II
MP0250	Oncology (NSCLC)	Molecular Partners	Inhibits VEGF and HGF receptor binding.	Phase I
MP0274	Oncology (Breast Cancer)	Molecular Partners	Inhibits HER1/2/3 mediated signalling	Phase I
Abicipar	Ophthalmology (wet AMD)	Allergan	Anti-VEGF	Phase III

Abicipar	Ophthalmology (DME)	Allergan	Anti-VEGF	Phase II

1.4 Targeting Cancer

Cancer is a global health problem with a WHO predicted rate of incidence that is rapidly climbing from 12 million in 2012 to 22 million by 2030, this translates to an approximate 65% increase in less than 20 years. Mainstream therapy for cancer tends to revolve around surgical resection, systemic chemotherapy and radiotherapy which whilst proving effective does have limitations in terms of resistance, long-term side effects and poor penetration of solid tumours (Baxevanis *et al.* 2009; Prelaj *et al*. 2018). An emerging field that addresses many of these issues and has shown promise is that of targeted therapies. Targeted therapies utilise our increasing understanding of cancer specific biology to target cancer specific markers. One such widespread marker occurring throughout many forms of cancer is the overexpression and/or mutation of the ErbB receptor family, predominately Erb1 and Erb2.

1.4.1 ErbB Receptor Family

The ErbB family of receptors are type I transmembrane receptor tyrosine kinase and consist of four identified members: EGFR (Erb1/HER1), HER2 (ErbB2), HER3 (ErbB3) and HER4 (ErbB4). Activation of said receptors occurs via a multitude of different ligands including but not exclusively EGF (Epidermal Growth Factor), Amphiregulin, Epiregulin, TGF-α (Transforming Growth Factor Alpha) and Neuregulin's. Ligand induced activation triggers receptor hetero- or homo-dimerization with another ErbB receptor and signalling plays a role in cellular events such as proliferation, DNA synthesis, apoptosis inhibition, differentiation and migration. HER2 is the only family member with no known natural ligand and functions as a constitutively active receptor in native state or through heterodimerization with other family members (Schettini *et al*. 2016).

1.4.2 Targeting interventions for HER2 positive metastatic cancer

The aggressive nature of disease attributed to HER2 overexpression amongst many forms of cancer has been well documented. This has led to an influx of targeted HER2 therapies especially in breast and gastric / gastro-oesophageal junction cancer. Current therapeutic

interventions for HER2+ metastatic cancer involves the use of monoclonal antibodies; trastuzumab (Herceptin) & pertuzumab (Perjeta), small molecule dual tyrosine kinase inhibitor; lapatinib (Tykerb) and antibody-drug conjugate; trastuzumab emtansine (T-DM1, Kadcyla) (Schettini *et al.* 2016). Despite the successful application of these anti-HER2 therapies in treating HER2+ cancer there are as yet no validated means of visualising tumour HER2 expression and distribution prior to and during treatment (Gebhart *et al.* 2016). The production of an imaging agent, which does not interfere with these therapies and allows a system whereby therapies are selected based on the "right patient for the right drug at precisely the right point in their cancer journey" would potentially avoid unnecessary side effects whilst improving treatment outcomes.

1.4.4 Anti-HER2 DARPin; G3

G3 is an anti-HER2 DARPin with a low molecular weight of 14-15 kDa and pica-molar affinity to HER2 (Epa *et al*. 2013). Although G3 and trastuzumab both bind to subdomain 4 (Figure 1.3), their epitopes are non-overlapping and very much discrete; the binding of one does not affect the binding of the other (Epa *et al*. 2013). This could make it an ideal imagining agent allowing for the accurate assessment of cell surface levels of HER2 during and prior to the course of treatment.

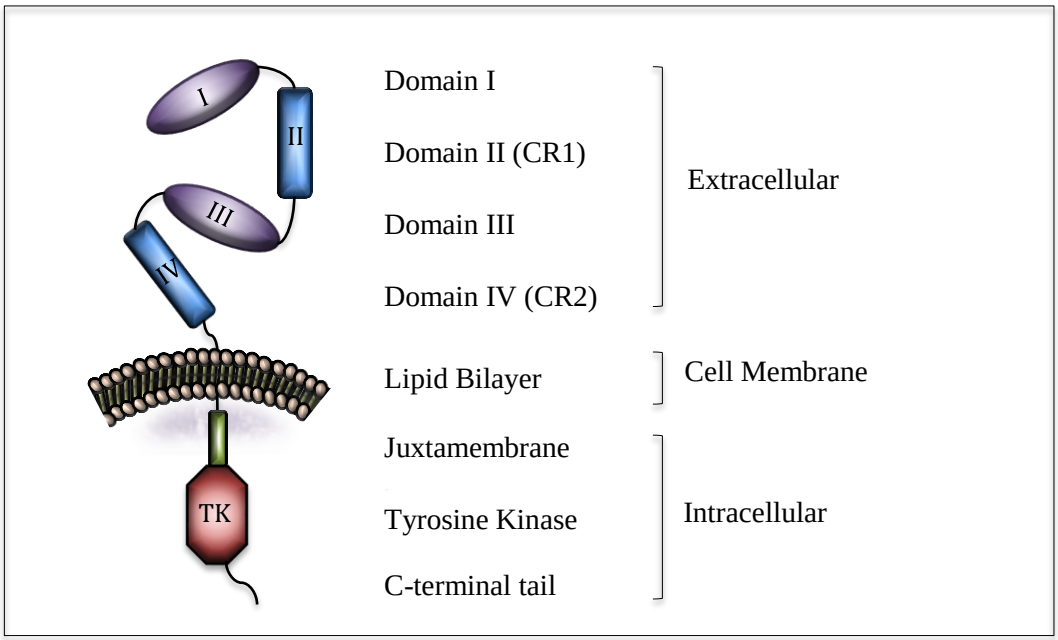

FIGURE 1.3 A schematic representation of the key structural componants of tyrosine kinase receptor, HER2.

1.4.5 G3 DARPin Properties

G3 DARPin represents the smallest in DARPin constructs and consists of a mere two internal repeat modules (Figure 1.4) and as such never quite forms a tertiary structure. Despite this it is a stable hydrophilic protein with an isoelectric point (pI) of 4.7. It has a high affinity for the HER2 receptor at 90 pmol/L by SPR and ~60 to 100 pmol/L when assessed on the HER2+ cell line, BT474. In comparison to the consensus framework given in Figure 1.1 the G3 DARPin has four framework mutations, placed to enhance its affinity in relation to its 'WT' consensus form (Zahnd, *et al.* 2007; Zahnd *et al.* 2010).

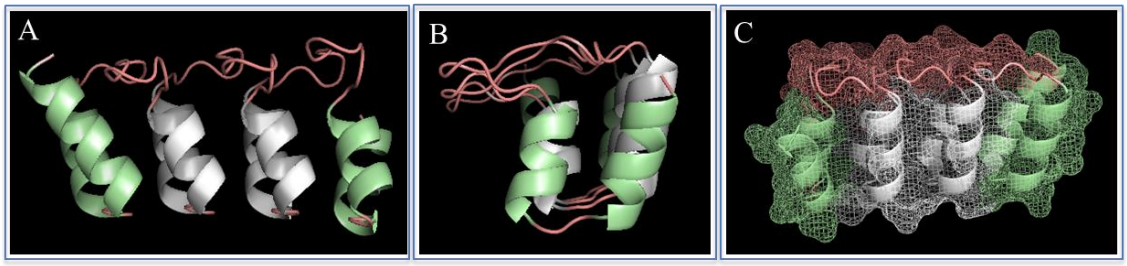

FIGURE 1.4 Structure of anti-HER2 DARPin; G3 in schematic representation.
A. Front profile. **B.** Side profile. **C.** Space-fill.
Green-coloured ribbon represents the N- and C-terminal stabilizing modules. Silver-coloured ribbon indicates the internal repeats. (*Designed using PyMOL*)

1.5 Host Systems for Recombinant DARPin Production

1.5.1 Previous production of DARPins

DARPins have previously been produced at shake-flask level in *E.coli.* Despite relatively high yields of 100-200 mg/L, extraction and purification of intracellular proteins from bacteria remains an arduous procedure which is greatly hindered by the presence of endotoxins.

The procedure kindly provided by The Plückthun Lab (UZH) and outlined in Figure 1.5 highlights the difficulties and time-consuming practises required to capture an intracellular product from *E. coli* and rid the process stream of bacterial endotoxins. This procedure generates high purity product but presents challenges if taken forward to current good manufacturing practice (cGMP).

As an in-house procedure the cells were cultured in shake-flasks and harvested 4-5 hours post IPTG induction. Extensive sonication and homogenization steps were required to sufficiently lyse the cells prior to solid/liquid separation by centrifugation. The now clarified supernatant

was applied to an immobilised metal affinity column; His_6-tagged DARPin was captured and partially purified via overloading. The column was washed extensively (~150CV) with detergent containing buffer before the captured protein was finally eluted.

As regulatory bodies largely frown upon the release of a 'tagged' product, a protease cleavage step is utilised coupled with reverse IMAC to liberate the product from the tag. The product undergoes polishing using an anion exchange chromatography step prior to dialysis into an appropriate buffer.

This procedure generates product of high specificity but has multiple units of operation due largely to the host organism and product localisation. Therefore a move to an easier to handle system would be beneficial.

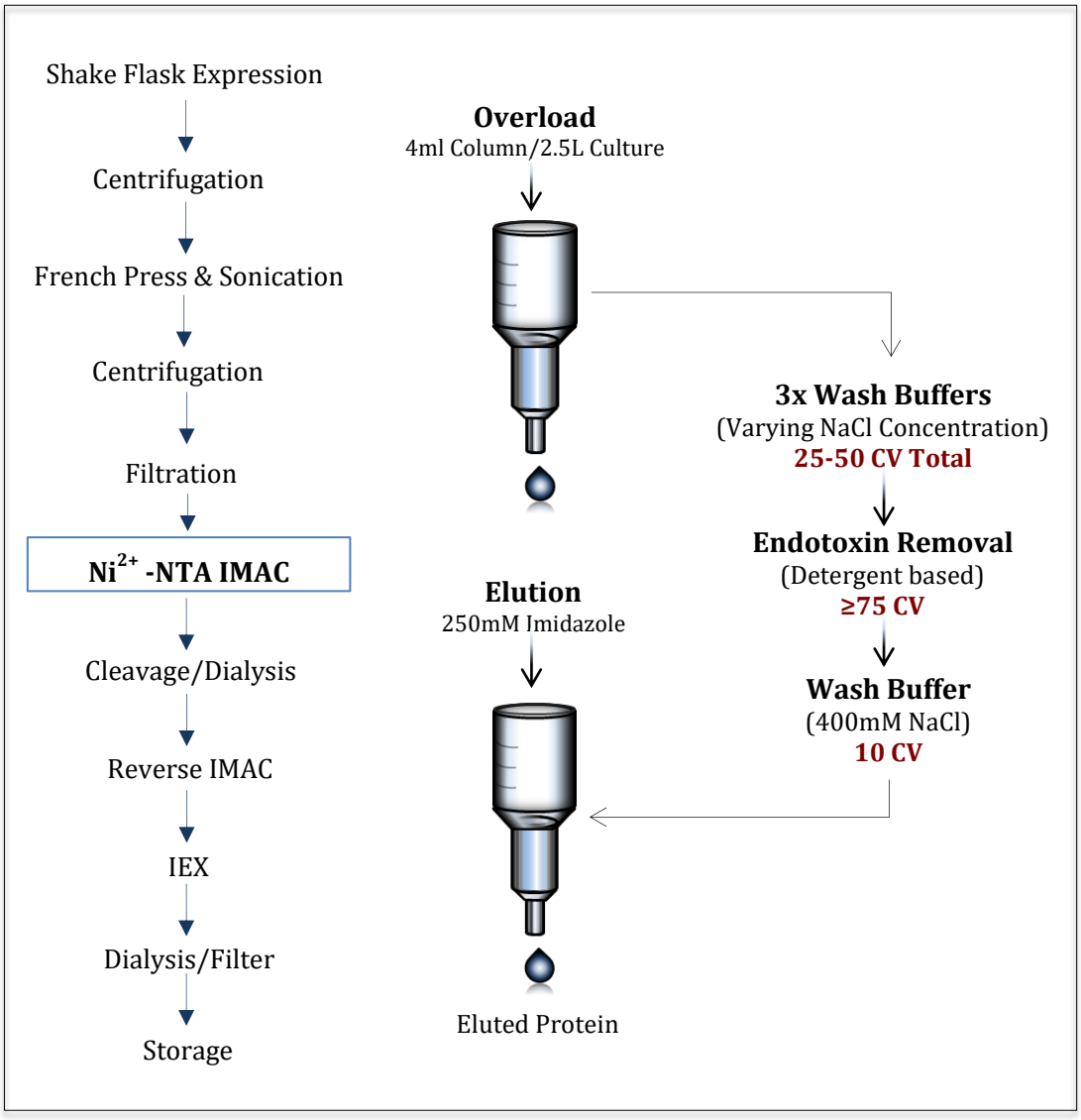

FIGURE 1.5 An illustration of the *E. coli* produced DARPin purification process.

1.5.2 Pichia pastoris

Pichia pastoris (synonym. *Komagataella pastoris***)** initially appeared for commercial use in the early 1970's as a cost-effective source of single cell protein (SCP) for use as animal feed. It was during this process that a procedure for its high cell density culture was developed (Macauley-Patrick, 2005). With this success and the advent of recombinant protein production it was only a matter of time before *P. pastoris* was developed as a host cell for therapeutic protein manufacture.

Host systems differ in their ability to successfully secrete recombinant proteins. *E.coli* are often described as the workhorse of recombinant protein production but a significant percentage of these proteins, even with a secretory module, are intracellularly expressed and often in the form of inclusion bodies. In contrast the methylotrophic yeast *P. pastoris* has the ability to readily express and secrete a variety of recombinant proteins into the surrounding media whilst very few endogenous proteins are secreted. Recombinant proteins placed under the *S. cerevisiae* a-mating factor secretory signal, present within the vast majority of *P. pastoris* expression vectors, are efficiently trafficked, processed and secreted directly into the surrounding media (Damasceno, 2012). The extracellular localisation of a product would greatly reduce time, equipment costs and handling associated with intracellular expression. Beyond the ease at which *P. pastoris* secretes recombinant proteins there are many additionally positive attributes all of which contribute to make it a strong host system. These contributory features are; its lack of endotoxins, strong tightly regulated promoter, relatively short doubling time, stable gene integration, cost-effective growth media, ability to perform post-translational modifications and the capacity to grow to a high cell density. (Razaghi *et al*., 2017)

There are several FDA approved biopharmaceuticals expressed in the yeast *S. cerevisiae*. During the past 30 years there have been products such as Leukine® (1991), Regranex® (1997) and Gardasil® (2006). By contrast *P. pastoris* is a newer candidate having gained its first FDA approval in 2006 for the production of KALBITOR® (Dynax Corp.), a kallikrein inhibitor. This was followed by the enzyme Ocriplasmin, trade name JETREA® (ThromboGenics) by NICE in 2009 and by the FDA in 2012. These approvals and as a consequence the recognition of *P. pastoris* as a GRAS (generally recognised as safe) organism have paved the way for its further use in the therapeutic industry. Currently numerous therapeutics utilising a *P. pastoris* production platform are in clinical development with at least two nanobody-based therapeutics (Ablynx) and two antibody therapeutic leads, ALD518 and ALD403 (Alder

Biopharmaceuticals) employing this versatile expression system (Meehl and Stadheim, 2014; Mizukami *et al.* 2018).

1.6 Bioprocessing of Therapeutic Proteins

The assembly of a regulatory compliant bioprocess for the production of a recombinant therapeutic needs to take into account and address multiple parameters within a strict timeframe. The process needs to produce a highly pure product and each unit operation assessed not only by its ability to achieve high levels of purity and yield but also on both throughput and cost. The time pressure to complete a bioprocess is often governed by the need to utilise the 20 year IP protection afforded by a patent, with the average time to market being 10 years, and the competition to be first to market on 'similar' products and the recognition and financial rewards that potentially come with it (DiMasi and Grabowski 2007).

Despite the fact that recombinant therapeutics can differ greatly from one another their production processes will typically follow one of three largely preordained routes as shown in Figure 1.6. All routes start with a cell generation / protein production stage after which the localisation of the product largely dictates the purification stream that follows with by and large a soluble secreted product being far easier and less costly to manufacture than intracellularly located proteins and inclusion body formats.

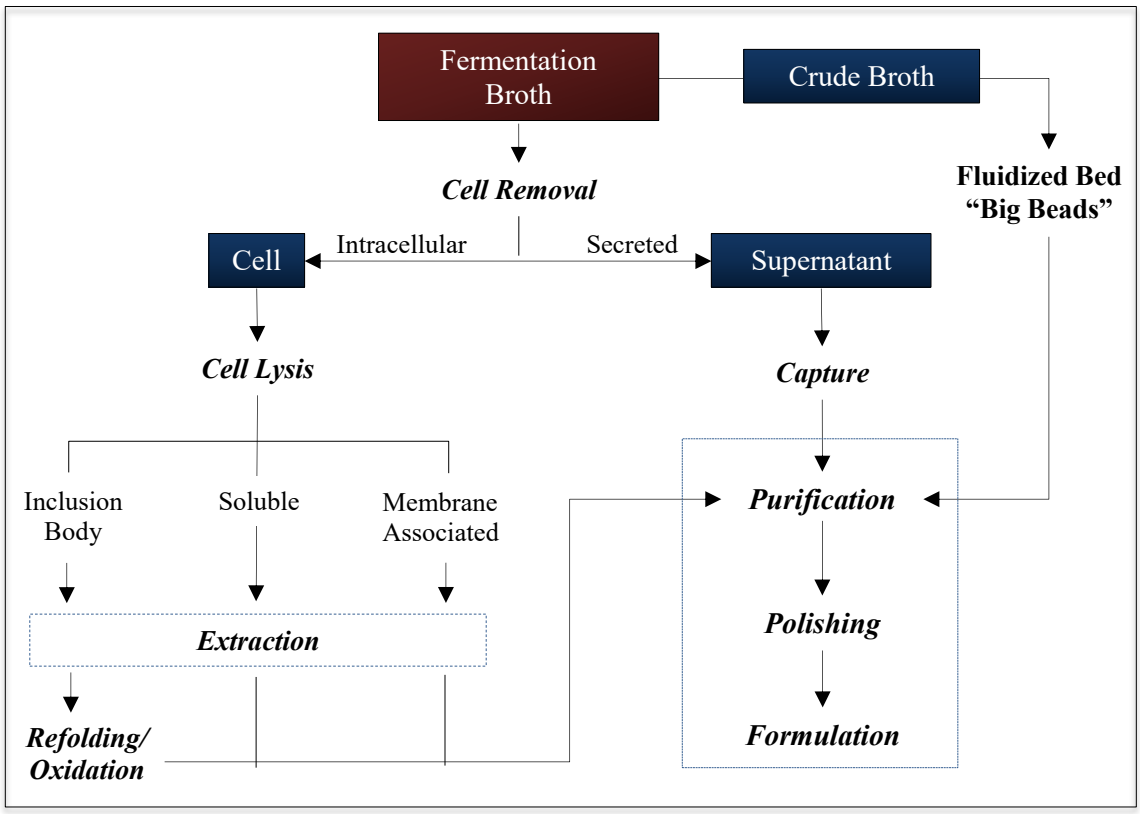

FIGURE 1.6 An overview of the general bioprocess pathways employed in relation to host system and product localisation.

1.7 Downstream Purification

The overall manufacturing cost of biological therapeutics continues to be high with 50-80% of this cost being attributed to downstream processing. With the ever increasing demand for this market of products, further cost effective strategies to downstream purification need to be developed. (Somasundaram *et al.*, 2018)

1.7.1 Liquid Chromatography

Liquid chromatography is one of the principal separation and purification procedures used in the downstream processing of large scale bioprocesses (Rathore *et al.* 2018). In chromatography the isolation or partitioning of target proteins from their current environment depends on the ability to segregate proteins between a stationary phase (resin/medium) and a mobile phase (buffer). Typically the stationary phase is contained within a column and the sample / buffer is applied and allowed to flow through. The type of chromatography used is dependent on both the inherent properties of the protein product, such as size, charge and hydrophobicity, and the contaminants present within the feed stream.

1.7.2 Expanded Bed Adsorption (EBA)

Expanded bed adsorption chromatography was the first chromatographic means of combining clarification, capture and initial purification in a single unit operation from unclarified feed stock. This integrated approach has a number of advantages including reduced processing times, heightened process efficiency, decreased requirements for capital investment/consumables and greater overall yield (Hubbuch J. *et al.* 2005; Ebrahimpour *et al.* 2009).

In expanded bed adsorption chromatography the liquid is pumped upwards through a bed of adsorbent beads, confined by a flow adapter. As a result of this upward flow the beads are distributed from large to small from the bottom to the top of the column, Figure 1.7. This enlarged area of distribution increases the void space amongst the beads allowing larger particles such as cells and cell debris to flow unobstructed through the column (Ebrahimpour *et al*. 2009). The means of capture can be affinity, charge or hydrophobicity dependent on the chromatographic resin used.

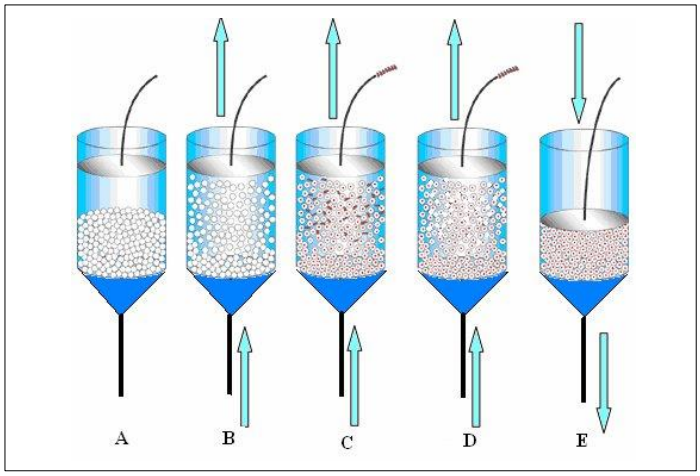

FIGURE 1.7. Expanded Bed Adsorption: An illustration of the operating procedure.

A, No flow - the resin is settled with little space between beads. **B**, Column equilibration – resin becomes dispersed and void volume around beads increases. **C**, Application of feed – due to the increased space between beads cells, particulates and cellular debris can flow unhindered whilst product is captured directly on the resin. **D**, Wash buffer – applied to remove contaminants and any residual cells/cell debris. **E**, Change in flow direction and adapter lowered to compress resin bed. Elution of capture product. Figure taken from Ebrahimpour *et al.* 2009.

Despite the ability of EBA to successfully capture product from crude broth (Tolner *et al*. 2006) and homogenized lysate (Xu *et al.* 2013) there are some drawbacks to this technology such as ease of fouling, low flow rates and large buffer consumption (Tolner *et al.* 2012). In an attempt to address and thus circumvent these limitations radial flow chromatography was developed.

1.7.3 Radial Flow Chromatography (RFC)

First described in 1947 by Hopf (Hopf, P. 1974) in which he created a device that utilized a centrifugal force to drive liquid from a central feed pipe outwardly in a radial direction, termed a 'Chromatofuge'. This device was both overly complicated and expensive to realistically take forward and consequently never took hold in the biotech industry. It was almost 30 years later before radial flow columns had an appropriate design and mode of action to enable them to take their first steps in industry. To date there are few companies concerned with the production and marketing of RFC columns. Two of today's possibly biggest suppliers are Sepragen Corporation in California and Proxcys Downstream Biosystems in The Netherlands marketing the Superflo (50mL-200L) and CRIO (50mL-1200L) series of RFC columns respectively (Cabanne *et al.* 2007).

Traditionally chromatography utilised an axial flow of buffer/sample as depicted in Figure 1.8A. This flow design results in large pressure drops, limited flow speed and increased

compression of the resin upon scaling up. Radial flow addresses some of these factors with the use of concentric cylindrical porous frits in between which the chromatographic resin is held. The sample/buffer flows from the outer to the inner surface as depicted in Figure 1.8B. Since the flow path transverses horizontally across the radius of the column this in essence represents the effective bed height. This unique design of flow enables RFC to operate with a minimal pressure drop, high operational flowrates and enhanced elution peak resolution (Cabanne *et al.* 2007; Besselink *et al.* 2013).

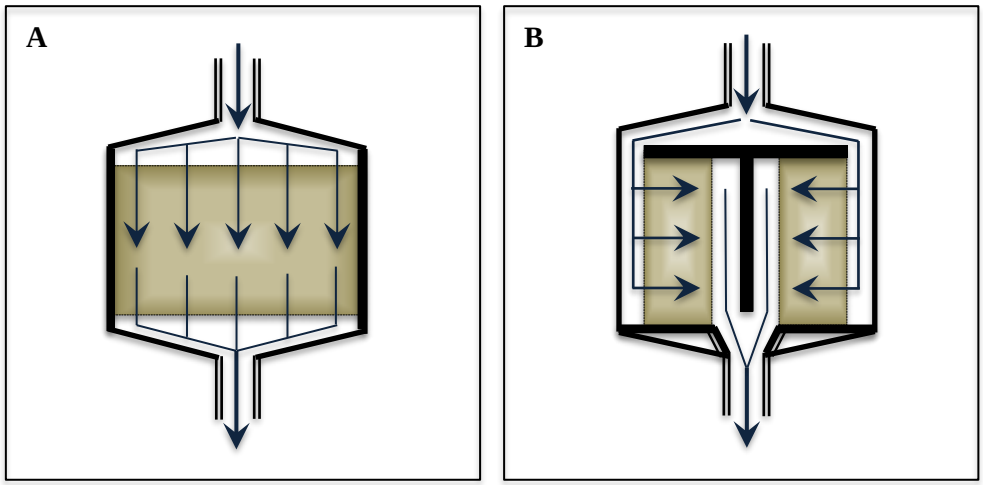

FIGURE 1.8 A schematic depiction of the flow paths induced during axial and radial flow chromatography.
A, Axial flow chromatography. **B**, Radial flow chromatography.

Capture steps do not need great resolution but speed to separate product from contaminants and potential proteases whilst still maintaining a high yield of product. The simpler and more efficient a procedure the cheaper and easier to implement. With a faster turnover and increased likelihood of being straightforwardly translatable to a regulatory compliant bioprocess.

As shown by Tolner *et al.* 2012, it is possible to utilise radial flow chromatography for the direct capture of $(histidine)_6$- tagged product from crude *P. pastoris* fermentation broth without the need for prior clarification steps. The use of IDA (iminodiacetic acid) Chelating Cellthru™ BigBead (300-500µm) technology (Sterogene), marketed capacity of ≥ 30 mg/mL resin, allowed for the successful application of crude whole cell broth to the chromatography column thereby circumventing the need for solid/liquid clarification events.

1.8 Residual Impurities and Immunogenicity

The production of recombinant therapeutics involves the use of multiple units of operation and consequently generates both process-related impurities and openings for product contamination. These factors need to be identified and taken into account so as to deliver a process and product of high quality and at low risk of process failures.

1.8.1 Host Cell Proteins (HCPs)

Cellular proteins from the expression organism of choice by and large constitute the main bulk of process related impurities. The degree to which they are present varies considerably with organism selection and product localization. Products expressed intracellularly regardless of host system will generate far more impurities in the process stream through cellular disruption, required for product capture, than secreted products where there's minimal cell lysis during primary capture steps. Additionally the release of intracellular proteases into the process stream can have significant effects on product degradation and hence final yield generated.

1.8.2 Nucleic Acids

In using biological host organisms for recombinant protein production there will inevitably be some degree of polynucleotide release into the extracellular media in the forms of deoxyribonucleic acid (DNA) and ribonucleic acid (RNA). Polynucleotides are large filamentous entities that are exceptionally stable and hydrophilic. A single nucleotide is composed of a nitrogenous nucleoside core, a sugar group and an acidic phosphate group. At pH values greater than 4 these backbone phosphate groups have an overall negative charge.

1.8.3 Endotoxins (Pyrogens)

Endotoxins are a lipopolysaccharide (LPS) component found in the outer membrane of gram-negative bacteria. Despite their association with the cell wall endotoxins are not solely liberated during cell death / lysis but are continuously expelled into the environment during growth and division. They are an essential component for survival and play a major role in the protection of gram-negative bacteria from harmful environmental stresses. A monomeric endotoxin consist of three distinct domains: a conserved hydrophobic Lipid-A moiety tethering it to the cell membrane, followed by an extended core region of sugar residues, which conclude in an O- or S-antigen (Wakankar *et al*. 2009).

Endotoxins have a potent biological effect in humans and upon entering the bloodstream interact with immune responsive cells eliciting symptoms from inflammation to septic shock and as a consequence possible death. Endotoxin toxicity varies, in humans' severe hepatic toxicity and haematological disorders are notable when exposed to a mere 8 ng endotoxin/ kg body weight. As a result of this sensitivity biopharmaceuticals with intravenous (non-intrathecal) applications can have no more than 5 endotoxin units (EU) / kg body weight / hour (Malyala P & Singh M. 2008). Where 1 EU corresponds to a biological activity of 100 pg of endotoxin standard (EC-5) derived from *E.coli* strain O113:H10K (Braude strain) (Dawson M. 1993).

The removal of endotoxins from the process stream during the production of bio-therapeutics is a particularly challenging and arduous task. The sheer quantity of endotoxins present in a standard bacterial culture is astounding with an average of 70-500 thousand EU ml^{-1} from a filtered supernatant following shake-flask culture to >>1-million EU ml^{-1} from a homogenized HCD fermentation. Couple this with an exceptionally high thermal stability and a broad range in size, typically 10-200 kDa; their removal is far from straightforward.

1.8.4 (1→3)-ß-D-Glucans

Glucans are chains of predominantly branched and occasionally cross-linked glucose moieties found associated with the cell wall of fungi, algae, plants and a few bacteria. They assist in maintaining cell wall conformation and structural strength. Since (1→3)-ß-D-Glucans can vary in length and structure this affects both their physical and chemical properties and therefore biological activity. Beta-glucans can be found in process streams through choice of host organism and pharmaceutical processing reagents such as cellulose based filters. They are capable of eliciting an inflammatory response though to a far lesser degree than endotoxins (Barton et al. 2016; Wakankar *et al*. 2009).

1.8.5 Leachables

Impurities in the form of leachables are a result of process stream / product contact with the physical elements used in the bioprocess and storage of the product such as tubing, gaskets, cartridges, storage vessels…etc. The presence of leachables can compromise product safety and final product quality. This was demonstrated for Eprex®, a synthetic erythropoietin, whereby an adverse immunological response was noted to have occurred in 175 cases between 1998 and 2004. These reaction were determined to be a result of leaching in the form of

phenolic derivatives from a rubber stopper in the prefilled syringes (Wakankar *et al*. 2009). The leaching was induced by a change in product formulation with the second generation drug employing polysorbate 80 instead of human serum albumin for stabilisation. Moving forward a Teflon coated stopper replaced the original uncoated version and cases of the adverse immunological reaction (epoetin-associated pure red-cell aplasia) dropped significantly (Wakankar *et al*. 2009).

1.9 Summary of Aims

The overarching goal of the project is to develop a bioprocess for the production of clinical grade DARPin in *P. pastoris*. The work was focussed on developing G3 DARPin as a whole body-imaging agent for HER2 positive cancer; there are currently no clinical products to achieve this. G3 has shown potential as an imaging agent due to its high affinity for the target and small size (14 kDa) that should facilitate rapid clearance, fast tumour penetration and high tumour: blood ratios at early time points. In addition, G3 is biologically inert and does not compete with therapeutic anti-HER2 antibodies trastuzumab and pertuzumab.

This goal will be reached by achieving the following objectives:

1. Cloning a HER2 DARPin in an X33 *P. pastoris* strain. This particular strain is to be used, as it is compatible for clinical use. HER2 was chosen as a target because of its relevance in cancer.

2. To design a clone that meets the needs of a radio-imaging product. Design would include an N-terminal tag for purification by immobilised metal affinity chromatography and a HRV 3C cleavage site to remove the tag for experimental studies. The clone should also contain a unique C-terminal cysteine for attachment of labelling tracers or to other proteins. Two tags were chosen for IMAC the standard hexahistidine tag and a (Histidine-Glutamate)$_3$ or (HE)$_3$ tag. The more negatively charged (HE)$_3$ tag was selected as it had been previously shown to reduce liver uptake with another targeting agent (Tolmachev *et al.* 2010). This is important as an imaging agent because of HER2+ cancer metastasis can occur in the liver. (**Chapter 3**)

3. To express and purify the His$_6$ tagged G3, (HE)$_3$ tagged G3 and untagged G3 in *P. pastoris* to allow preclinical testing of the variants for comparison to determine a lead to take forward for bioprocess development. (**Chapter 3**)

4. To clone and manufacture the lead DARPin without the HRV 3C cleavage site and evaluate it in terms of MW, binding affinities, preclinical biodistribution and tumour targeting. Use this data to select a principal protein for development as a clinical product for whole body imaging of HER2+ cancer. (**Chapter 4**)

5. To develop a bioprocess suitable for regulatory compliance and apply this process for production of (HE)$_3$ –tagged DARPins. As scaffold proteins DARPins share the same

conserved framework and as such the potential to build a platform process for their production. (**Chapter 5**)

6. To design a process for the manufacture of DARPin imaging agents as an extension of the previously determined bioprocess (**Chapter 5**). Allowing for the possibility of a seamless follow on from the platform process to an end-product specific agent with minimal impact on the unit operations themselves. This process is to include a scalable, efficient maleimide-DOTA conjugation and free linker removal (for product radiolabelling). (**Chapter 6**)

7. Employ molecular cloning to address protease breakdown of DARPins thereby permitting longer fermentations and increased yield. Apply what's been discovered to another DARPin and assess whether both the means to address cleavage and the bioprocess developed could work as a platform for DARPin production. (**Chapter 7**)

CHAPTER TWO

MATERIALS AND METHODS

2.0 Materials and Methods

2.1.1 Suppliers

Table 2.1. List of Suppliers.

Company Name	Company Address
American Type Culture Collection	Manassas, Virginia, United States
Amresco	Solon, Ohio, United States
Anachem	Luton, United Kingdom
Baxter	Berkshire, United Kingdom
Beckman Coulter (UK)	High Wycombe, United Kingdom
Becton Dickinson	Oxford, United Kingdom
Bioline Reagents	London, United Kingdom
Bio-Rad Laboratories	Hemel Hempstead, Hertfordshire, United Kingdom
Charles River	Erkrath, Germany
DNA Technologies	Leuven, Belgium
Eppendorf UK	Cambridge, United Kingdom
Fisher Scientific	Loughborough, United Kingdom
GE Healthcare	Buckinghamshire, United Kingdom
Generon	Maidenhead, Berkshire, United Kingdom
GenScript	Piscataway, New Jersey, United States
Integrated DNA Technologies	Leuven, Belgium
Life Technologies	Paisley, United Kingdom
Macrocyclics	Dallas, Texas, United States
Marvel	Dublin, United Kingdom
Merck Millipore	Billerica, Massachusetts, United States
Nalgene	Derbyshire, United Kingdom
New England BioLabs	Hitchin, Hertfordshire, United Kingdom
NuSep	Wasserburg, Germany
PAA Laboratories	Yeovil, Somerset, United Kingdom
Pall Life Science	Portsmouth, United Kingdom
PerkinElmer	Llantrisant, United Kingdom
Proxcys Downstream Biosystems	Nieuw-Amsterdam, Netherlands
Promega	Southampton, United Kingdom
Qiagen	Crawley, West Sussex, United Kingdom
Roche Diagnostics	Burgess Hill, United Kingdom
Sartorius Stedim	Epsom, Surrey, United Kingdom
Sigma-Aldrich	St. Louis, Missouri, United States
Thermo Scientific	Runcorn, Cheshire, United Kingdom
UCL Advanced Diagnostics	London, United Kingdom
UCL Cancer Institute	London, United Kingdom
Whatman	Maidstone, Kent, United Kingdom

2.1.2 Buffers, media and solutions

Table 2.2 Buffers used in DNA manipulation and protein analysis

Buffers	Composition
Agarose Gel Electrophoresis	
Tris-acetate-EDTA (TAE) stock (50x) (2M Tris-acetate, 0.05 M EDTA)	-242 g Tris Base -57.1 mL glacial acetic acid -100 mL of 0.5 M EDTA (pH 8.0) solution -Made up to 1-L with dH_2O.
TAE (1x)	0.04 M Tris-acetate, 0.001 M EDTA
DNA loading buffer (10x)	For 20 mL volume -6.25 mL of dH2O -0.025 g of Xylene cyanol -0.025 g of Bromophenol Blue -1.25 mL of 10% SDS -12.5 mL of glycerol
New England BioLabs 1kb DNA Ladder	40 µL dH2O, 10 µL 6x Blue Loading Dye (provided), 10 µL DNA Ladder
Promega 1kb DNA ladder	40 µl dH_2O , 10 µl 6x Blue Loading Dye (provided), 10 µl DNA Ladder
Bioline HyperLadder I (BioLine)	Purchased in ready to use form
Restriction Enzymes and Buffers	
XbaI	Concentration 100,000 units/mL (New England Biolabs)
XhoI	
PmeI	
SDS-PAGE	
SDS-PAGE running buffer (10x)	10 g SDS, 30.3 g Tris-base, 144 g glycine and add dH2O to make up to 1-L
Protein Transfer Buffer (10x)	30.3 g Tris-base and 144 g glycine made up to 1-L with dH2O
Protein Transfer Buffer (1x)	100 mL 10x Protein Transfer Buffer, 200 mL methanol, 700 mL dH_2O (Final concentration 25mM Tris-base, 192mM glycine, 20% (v/v) Methanol)
Coomassie Staining	
Coomassie stain (final concentration)	1.25 g coomassie brilliant blue, 50 mL glacial acetic acid, 150 mL methanol and 300 mL dH_20.
De-stain	200 mL glacial acetic acid, 600 mL methanol and 1.2 L dH_20
Wizard SV Gel and PCR Clean-Up System (Promega)	
Membrane Binding Solution	4.5 M guanidine isothiocyanate, 0.5M potassium acetate (pH 5.0) (purchased in this form)
Membrane Wash Solution (Following addition of ETOH)	10 mM potassium acetate (pH 5.0), 80% ethanol,16.7 µM EDTA (pH 8.0) (purchased in this form)

Table 2.3 Plates and Media used for Growth of *E.coli.*

Media	Composition
Low Salt Luria–Bertani (LSLB) Media with Zeocin	10g tryptone (1% w/v), 5g sodium chloride (NaCl) (0.5% w/v) and 5g Yeast Extract (0.5% w/v) fill to 1 litre with dH_2O. Autoclave and once cooled add Zeocin for a final concentration of 25µg/ml.
2TY Media with Zeocin	
Low Salt Luria–Bertani (LSLB) Agar with Zeocin™	Add dH_2O to 10g tryptone, 5g sodium chloride, 5g Yeast Extract and 15g agar so that volume reaches 1 litre. Autoclave and once cooled to approximately 55^oC add Zeocin™ to a final concentration of 25µg /ml. Pour plates and allow to set before inverting and storing at 4^oC.

Table 2.4 Plates and Media used for Growth and Protein Expression in *P. pastoris* (Vector with an AOX Promotor)

Media	Composition
Selection and Growth	
Yeast Extract Peptone Dextrose Medium (YPD) +/- 100µg/mL Zeocin	900 mL dH_20, 10g Yeast Extract, 20g Peptone. Autoclave and then add 20% Glucose (filter sterilized).
YPD with Sorbitol (YPDS) Agar with 100µg/mL Zeocin	900 mL dH_20, 10g Yeast Extract, 20g Peptone, 182.2g Sorbitol and 20g Agar. Autoclave and then add 20% Glucose (filter sterilized) and Zeocin to a final concentration of 100µg/ml.
Expression Studies	
Buffered Glycerol complex medium (BMGY) with 100µg/ml Zeocin	Composition for 1L final Volume: 600 mL dH_2O, 10gram yeast extract, 20gram peptone and autoclave. Once cooled add the following sterile filtered items; 100ml 1M potassium phosphate buffer pH 6.0, 100ml 10X YNB, 600µl 500X Biotin, 100ml 10X glycerol and 100ml case amino acid.
Buffered Methanol complex medium (BMMY) with 100µg/ml Zeocin	Composition for 1L final Volume: 600 mL dH_2O, 10 gram yeast extract, 20 gram peptone and autoclave. Once cooled add the following sterile filtered items; 100ml 1M potassium phosphate buffer pH 6.0, 100ml 10X YNB, 600 µl 500X Biotin, 100 mL 10X Methanol and 100 mL case amino acid.

Table 2.5 New Brunswick Fermentation of *P. pastoris* (Vector with an AOX Promotor)

Media	Composition
Basic salt medium	For 5.3 L final volume, dissolve 5.4g CaSO4 , 88g K2SO4, 70g MgSO4: 7H2O, 54 g (NH4)2SO4 and 300ml glycerol into 5.0L dH20 and then autoclaved in the bioreactor.
Sodium Hexametaphosphate	Dissolve 150g Hexametaphosphate in 1L dH20 and filter.
Trace elements (Amresco)	5.99g CuSO4.(H2O)5 0.08g NaI 3.0g MnSO4.H2O, 0.20g Na2MoO4.(H2O)2 0.50g CoCl2.(H2O)6 20.04g ZnCl2.(H2O)5 65.05g FeSO4.(H2O)7 0.02g H3BO3 19.2ml 96.2% H2SO4 0.40g D-biotin Add dH_2O to make final volume 1L (purchased in this form)
Secondary culture medium	300ml basic salt medium 30ml sodium hexametaphosphate, 1.2ml trace elements, then filter sterilised.
Fermentation media	To 5-L of autoclaved basic salt medium, add 970ml hexametaphosphate, 24ml trace elements and 1ml antifoam.
Limited glycerol feed	300ml 100% glycerol, 300ml water, then autoclaved. Then add 7ml trace elements.
Limited methanol feed	2L methanol and 24ml trace elements.

Table 2.6 Solutions used for Radial Flow Ni-NTA IMAC

Solution	Composition
0.1M Nickel (II) Sulphate	52.56g NiS04 . 6H2O in 2L dH2O
4xBinding Buffer	584g NaCl (2M) and PBS 96 g (2x PBS) in 5L dH2O
1x Equilibration/Wash Buffer	292g NaCl (0.5M) and PBS 48 g (0.5x PBS) in 10L dH2O
Elution Buffer (200mM Imidazole)	58.4g NaCl (0.5M), PBS 9.6g (0.5x PBS) and 27.2g imidazole in 2L dH2O. pH adjusted to 7 with 4M HCl.

Table 2.7 Solutions used for Downstream Processing

Solution	Composition
Low Salt: Buffer A (20mM Tris, 20mM NaCl & 5mM DTT, pH 7.5)	975g dH20, 20ml 1M Tris pH 7.5, 5ml 1M DTT and 1.17g NaCl.
High Salt: Buffer B (20mM Tris, 1M NaCl, 5mM DTT, pH 7.5)	970g dH20, 20ml 1M Tris pH 7.5, 5ml 1M DTT and 58.44g NaCl.

All downstream buffers were prepared using endotoxin free water (Baxter) and Filter Sterilised.

Table 2.8 Column and TFF Cleaning and Storage Buffers

Solution	Composition
0.5M NaOH	10g NaOH, 495g dH_20
20% Ethanol	200mL EtOH and 800mL dH_20

Table 2.9 Buffers used in radio-labelling and Maleimide-DOTA conjugations to G3 DARPin

Solution	Composition
0.1M Phosphate (pH 7)	1.17g Sodium phosphate monobasic, 2.16g Sodium phosphate dibasic, 250mL WFI
0.2M Ammonium acetate (pH 7)	3.95g Ammonium acetate in 250mL WFI.
0.2M Ammonium acetate (pH 6.5) for dialysis	15.42g Ammonium acetate, 10g Chelex-100 in 1L WFI.

2.1.3 Materials

2.1.3.1 Strains, vectors, reagents & enzymes

The *Pichia pastoris* strain, X33 and the vector pPICZαB were purchased from Invitrogen. The *Escherichia coli* strain TG1 was purchased from and DH5α from Agilent Technologies. All Gene-blocks and primers were purchased from Integrated DNA Technologies.

2.1.3.2 DNA Ladders

DNA ladders used were the Hyper Ladder I from Bioline and the 1 Kb Ladder from NEB (Figure 2.0).

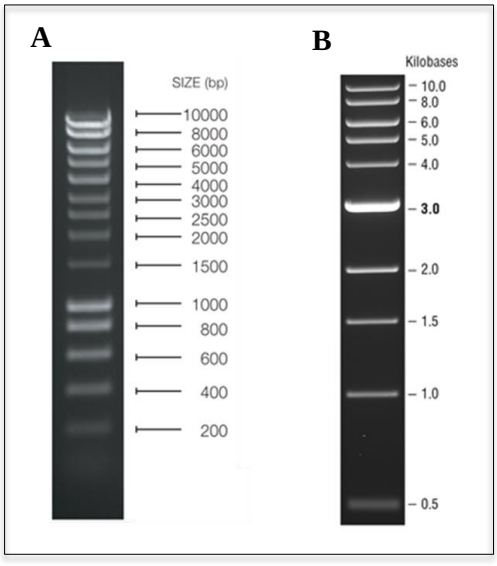

Figure 2.0: DNA Ladders used in agarose gel electrophoresis.
A, Hyper Ladder I (Bioline).
B, 1 Kb Ladder (NEB).

2.1.3.3 Protein Ladders

Proteins ladders used for both SDS-PAGE and Western Blot were the SeeBlue Plus2 Pre-stained Standard (Life Technologies) and Spectra Multicolour Broad Range Protein Ladder (Thermo Scientific) (Figure 2.1).

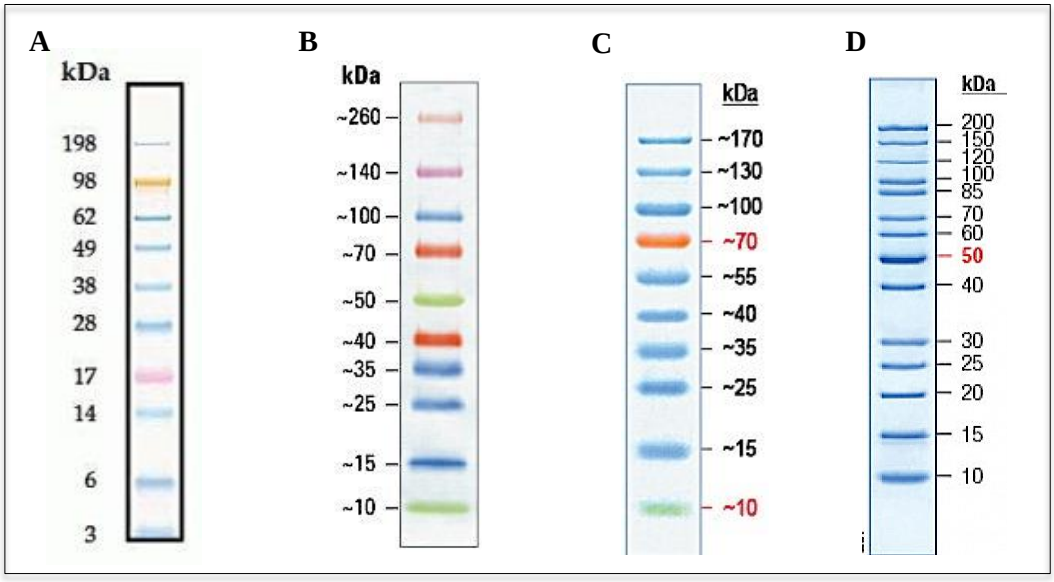

FIGURE 2.1: Molecular Weight Protein Ladders used in SDS-PAGE and Western Blot analysis.
Approximate Molecular Weights of **A.** SeeBlue Plus2 Pre-Stained Standard (Life Technologies), **B.** Spectra Multicolour Broad Range Protein Ladder (Thermo Scientific) and **C**. PageRuler Prestained Protein Ladder (Thermo Scientific), in an SDS-PAGE Tris-Glycine Buffer System.

2.2 Methods

2.2.1 Construction of pPICZaB_(HE)$_3$-G3 from gene-blocks

The lyophilized gene blocks encoding the sequences of the DARPin constructs were centrifuged for 5 seconds at >3000 xg to pellet material after which 20 µL dH_20 was added to the tube for a final concentration of 10 ng/µL This was briefly vortexed to facilitate gene block re-suspension and stored at -20^{o}C until further use.

2.2.1.1 Gene Block digest and ligation

The coding sequence of the DARPins was enzymatically digested with *XhoI* & *XbaI* and ligated into the previously digested pPICZαB vector to produce pPICZαB-[DARPin] plasmids. The plasmids were isolated through Phenol/Chloroform precipitation as follows.

All 20 µL of ligated plasmid reaction had 20 µL of phenol solution (Sigma) mixed thoroughly and centrifuged at 15,000xg for 10mins. The top layer was removed and placed into a fresh microcentrifuge tube prior to an equivalent volume of Phenol: Chloroform addition (Sigma) this was once again mixed thoroughly and centrifuged at 15,000xg in a benchtop centrifuge. The upper layer was removed and placed into a fresh 1.5mL centrifuge tube to which 1:10 of the volume 3M Sodium Acetate at a pH of 6, 2.5 times the volume of ethanol and 1 µL of glycogen was added. The mixture was then left ON at -20oC before centrifugation at 15,000xg for 10mins and removal of the supernatant. A white pellet of DNA should be visible at the bottom of the tube and this was washed with 70% ETOH before centrifugation (15,000xg, 10mins), removal of supernatant and air drying of the DNA pellet. Once dried the DNA was resuspended in 10 µL of dH_20 stored at -20°C. Both vector PCR (AOX3'; 5'-GCAAATGGCATTCTGACATCC-3', AOX5'; 5'-GACTGGTTCCAATTGACAAGC-3') and vector sequencing verified the successful ligation of the gene fragment into the plasmid.

2.2.1.2 Vector Propagation

2 µL of phenol/chloroform purified expression plasmid pPICZαB-[DARPin] was added to 100 µL of ice-thawed electro-competent TG1 or DH5alpha cells. The mixture was then transferred to a pre-chilled 0.2cm MicroPulser™ Electroporation Cuvette (Bio-Rad Laboratories). The cells were electroporated (2500V for 5ms) using the MicroPulser™ electroporator (Bio-Rad Laboratories). After which 1 mL of SOC or low salt LB media was added to the mixture and left to incubate with shaking at 37°C for 1 hour. Following incubation 20-100 µL of cells were spread onto LSLB plates containing 25µg/mL Zeocin™ and incubated for 24 hours at 37°C. *E. coli* cells with plasmids were selected and cultured aerobically at 37 °C in Luria–Bertani low salt medium containing 25 µg/mL Zeocin™. Before centrifugation and plasmid extraction using the QIAGEN Plasmid Midi Extraction kit, according to the manufacturer's instructions.

2.2.2 Test Expression in P. pastoris X33

2.2.2.1 Preparation of electro-competent cells

5 mL of YPD was inoculated with a stab of frozen *X33* glycerol stock and grown at 30°C at 225 rpm. The following day 100 µL was used to inoculate 500 mL of YPD and grown overnight at 30°C at 225 rpm to an OD_{600} of 1.3-1.5. The culture was centrifuged at 1,500 xg for 5 minutes and the supernatant removed. The pellet was gently re-suspended in 500 mL of ice cold dH_20 and centrifuged at 1,500xg at 4°C for 5 minutes. The supernatant was discarded and the pellet re-suspended in 250 mL ice cold dH_20 and centrifuged at 1,500 xg at 4°C for 5 minutes. The

supernatant is discarded and the cell pellet is re-suspended in 20 mL of ice cold 1M sorbitol before being centrifuged for 1,500xg for 5 minutes at 4ºC. The supernatant is for the final time discarded and the pellet re-suspended in 0.5 mL ice cold 1M sorbitol and stored on ice for same day electroporation.

2.2.2.2 Transformation and selection of colonies

The pPICZaB_[DARPin] plasmids were linearised overnight at 37ºC with the restriction enzyme *PmeI*, cleaving at the AOX1 promotor region, prior to phenol / chloroform extraction and transformation into the genome of freshly competent *P. pastoris* X33 cells by electroporation. Transformants were selected on YPDS agar plates containing 100 µg/mL Zeocin™. Colony PCR using 5' & 3' AOX primers (AOX3'; 5'-GCAAATGGCATTCTGACATCC-3', AOX5'; 5'-GACTGGTTCCAATTGACAAGC-3') were used to confirm the integration of pPICZaB-[DARPin] into the genome. Briefly several colonies of each construct were picked and used to inoculate 10 µl of dH_20, 1 µL of this was added to 9 µL of PCR reaction mixture. The reaction was placed in a thermocycler (Personal Cycler, Biometra) and the following program initialised. Initialisation, 95ºC for 3min. PCR cycles (n=30): Denaturation, 95ºC for 60s; Annealing, 60ºC for 60s; Elongation, 72ºC for 90s. Following the 30 cycles there is a final elongation step of 72ºC for 10 min and then a hold step at 4ºC.

2.2.2.3 Expression of DARPins in a shake flask

Colonies positive for the pPICZaB-$(HE)_3$-G3 constructs were inoculated into 5 mL BMGY to an OD_{600} of 5 and kept in a shaking incubator overnight at 30ºC, 200-220 rpm. The culture was centrifuged and re-suspended in 25 mL BMMY and cultured at 30ºC, 200-220rpm for a period of 72 hours. Samples were taken and 100 µL 100% Methanol was added at 24, 48 & 72 hours post induction to the culture medium. Samples were centrifuged and the supernatant analysed by 18% (Novex), 16% (Novex) or 4-20% (NuPage) Tris-glycine SDS-PAGE gels and visualized using coomassie brilliant blue R250 staining or western blot.

2.2.2.4 10L BioFlo3000 Fermentations

For large-scale production a single clone of highest protein expression from each construct was taken forward. High cell density fermentations in a BioFlo3000 10-L Bioreactor (New Brunswick) were carried out in accordance to previously described work (Tolner *et al*. 2006) and with the help of Gaurav Bhavsar and Berend Tolner. Briefly 230 mL of YPD was

inoculated with a vial of *X33* and incubated at 30ºC, 220rpm overnight. The following day 1 mL of overnight culture was used to inoculate 330 mL of minimal media and was grown overnight at 30ºC 220rpm to an approximate OD_{600} of 5. The entirety of this secondary culture was used to inoculate 5L of Basal Salt media at 30ºC, pH of 5 and agitated at 500-1000rpm to maintain a 30% dO_2 level. The pH was maintained by used of ammonium hydroxide and orthophosphoric acid.

After approximately 24hr all the glycerol had been consumed and a spike in $d0_2$ was notable. At this point a limited glycerol feed was initiated (100 mL/hr) and the pH set-point of the bioreactor adjusted to 5.5. The glycerol feed was slowly wound down to zero over a period of 4 hr. MEOH (20 mL) was added 1 hour post dO2 spike to initiate recombinant expression and to prime for transition to methanol limited feed. The MEOH limited feed was initiated directly after conclusion of the glycerol limited feed and reached a maximum flow rate of 45 mL/hr.

2.2.2.5 20-L BIOSTAT® Cplus Fermentations

As before fermentations were carried out with the help of Gaurav Bhavsar and Berend Tolner. Glycerol stock, of the DARPin constructs in X33, was used to inoculate 50 mL YPD media containing 100 µg/mL Zeocin. The primary culture was grown ON at 30ºC and 200 rpm to an OD_{600} of approximately 20. 360 mL of basal minimal media was put into each of two 2-L flasks and inoculated with 2 mL of primary culture per flask. Secondary seeding culture was grown for 16-24 hours and a final $OD_{600} > 4$.

Temperature was set at 30ºC, stirrer 500 rpm, airflow 15 L/min and pH 5 for inoculation. Pressure on compressed air line and oxygen cylinder was at 1.5 bar. All 720 mL of secondary culture was used to inoculate the BIOSTAT® Cplus (Sartorius) vessel to a starting OD_{600} of approximately 0.1 and an initial volume of 8-L. The dO_2 was maintained at 30% in auto mode by increasing the stirrer speed first to 1000 rpm and then adding pure oxygen with air through the sparger in GFR mode.

Post dO_2 spike the profile for glycerol feed (1000 mL: 50% Glycerol + 14 mL of PTM1 trace elements) is initiated in 'auto mode' as outlined in Table 2.10, and the pH is switched to 6.5. One hour post dO_2 spike 20 mL of MEOH is injected directly into the vessel. Following four hours of glycerol feed the carbon source is switched to limited MEOH feed at 15% set point. The methanol feed is run for an hour before the fermenter is harvested.

Table 2.10: 50% Glycerol feeding profile for biomass accumulation.

Step	Time (hour : min)	Set Point (%)
1	1:30	40
2	2:00	30
3	2:30	20
4	3:00	18
5	4:00	15

2.2.3 DARPin capture and purification

2.2.3.1 Radial Flow IMAC

The DARPins were captured directly from the culture media using Radial Flow (CRIO-MD 62, Proxcys Downstream Biosystems) Cellthru BigBead™ IMAC technology (Sterogen) with copper or nickel ions. The fermentation broth without any prior clarification steps was mixed with 4x Binding buffer at a 4:1 ratio and passed through a 125 mL Radial flow Ni^{2+}-IDA IMAC column pre-equilibrated in Binding Buffer at a flowrate of 200 mL/min. The column was then washed with Binding buffer ± imidazole and eluted in 50 mL fractions with elution buffer containing 200mM Imidazole. Fractions containing DARPin (approximately 550 mL total) were collected and passed through a 0.22 micron filter.

2.2.3.2 TFF; Concentration and Dialysis

DTT (Sigma Aldrich) was added to the pool at a final concentration of 5 mM and applied to a Millipore TFF system for concentration and dialysis. The sample was concentrated by ultrafiltration to ~50 mL through Pellicon® cassettes (Millipore) with a molecular cut-off of 5 kDa before dialysis into PBS and 5 mM DTT, pH 7.5 (Buffer A) and further concentration to approximately 30 mL.

2.2.3.3 Size Exclusion Chromatography; SEC1

The dialyzed protein was loaded onto an XK 26/100 column (GE Healthcare) packed with 500 mL Superdex 75 prep grade resin (GE Healthcare) pre-equilibrated in either PBS (±10 mM DTT) (Chapter 3 and 4) or Tris Low Salt Buffer (+5 mM DTT)(Chapter 5, 6, 7). The column was run at 4 mL/min and ≤ 0.3 MPa. A wide peak at appropriate millilitre elution was collected in 5 mL fractions and pooled.

2.2.3.4 Anion Exchange Chromatography

A 200 mL AEX column (XK 50, GE Healthcare) containing Source 30Q resin (GE Lifesciences) was pre-equilibrated in Tris-Low salt buffer pH 7.5. Sample was loaded using a super-loop at 3 mL/min, < 0.3 MPa. Following the load step 0.5 column volumes (CV) of Low Salt Tris Buffer was applied to the column. The higher salt wash conditions and elution were tailored to each DARPin and are set out below, Figure 2.2. Eluent was collected in 5 mL fractions.

A	**For G3 DARPin**
Apply ½ CV 20 % B to the column at a speed equal or less than 5 mL / min.	
Start gradient 20 to 30 % B over 150 mL (15mL per % = 15x10).	
Set flow rate to max 5 mL / min.	

B	**For E69 DARPin**
Apply ½ CV 28% B to the column at a speed equal or less than 5 mL / min.	
Start gradient 28 to 50 % B over 330 ml (15mL per % = 15x22).	
Set flow rate to max 5 mL / min.	

FIGURE 2.2: Wash and elution conditions for G3 and E69 DARPin.
A, G3 DARPin protocol. **B,** E69 DARPin protocol.

2.2.3.5 Size Exclusion Chromatography; SEC2

A 500 mL Superdex 75 XK 26/100 Column was pre-equilibrated in PBS. The sample from 2.2.3.4 was either loaded directly onto the next SEC column (Chapter 5) or first mixed with 0.1M EDTA and incubated for 30 min prior to loading (Chapter 7). The column was run at ≤ 4 mL/min and ≤ 0.25 MPa. T

he eluted 5 mL fractions containing DARPin were pooled and either, aliquoted and stored at -80ºC (Chapter 5) or taken forward for maleimide-DOTA conjugation (Chapter 7).

2.2.4 Conjugation Process [G3-DOTA]

2.2.4.1 Maleimide-DOTA Addition

The product pool from SEC2 (2.2.3.5) was quantified using OD280 and maleimide-DOTA added at a four molar excess to DARPin. The mixture was incubated overnight at room

temperature before purification by SEC (2.2.4.2).

2.2.4.2 Free Linker Removal; SEC3

Sample following incubation with maleimide-DOTA (2.2.4.1) was applied to a 500 mL Superdex 75 column pre-equilibrated in 0.2M ammonium acetate pH 6.5 and run at ≤ 4 mL/min, ≤ 0.25 MPa. Eluted protein was collected in 5 mL fractions. Appropriate fractions were pooled and OD_{280} measure. The final concentration of the DARPin pool was adjusted to 1 mg/mL with 0.2M ammonium acetate.

The product pool was aliquoted into cryo-vials in 0.5 mL fractions before storage at -80°C.

2.2.5 Process and Product Assessment

2.2.5.1 SDS-PAGE and Western Blot Analysis

2.2.5.1.1 Detection of DARPins

Protein samples were resolved by either 18% (NOVEX), 16% (NOVEX) or 4-20% (NuPage) SDS-PAGE gels and stained with Coomassie Blue R-250. Assessment of DARPin specific expression was performed using western blot analysis. Briefly protein samples were resolved by SDS-PAGE gel electrophoresis and then transferred to a PVDF membrane (Millipore), Figure 2.3.

The membrane was blocked with PBS containing 5% (w/v) dry skimmed milk with shaking for 1 hour at room temp. Anti-DARPin serum (1:1000) in 1% (w/v) PBST was then added to the membrane and incubated for 1 hour. This was then detected using an HRP-conjugated Anti-Mouse-IgG secondary (1:1000) in 1% (w/v) PBST for 1 hour and visualized using enhanced-chemiluminescence (ECL) reagent (GE Healthcare), according to the manufacturer's instructions.

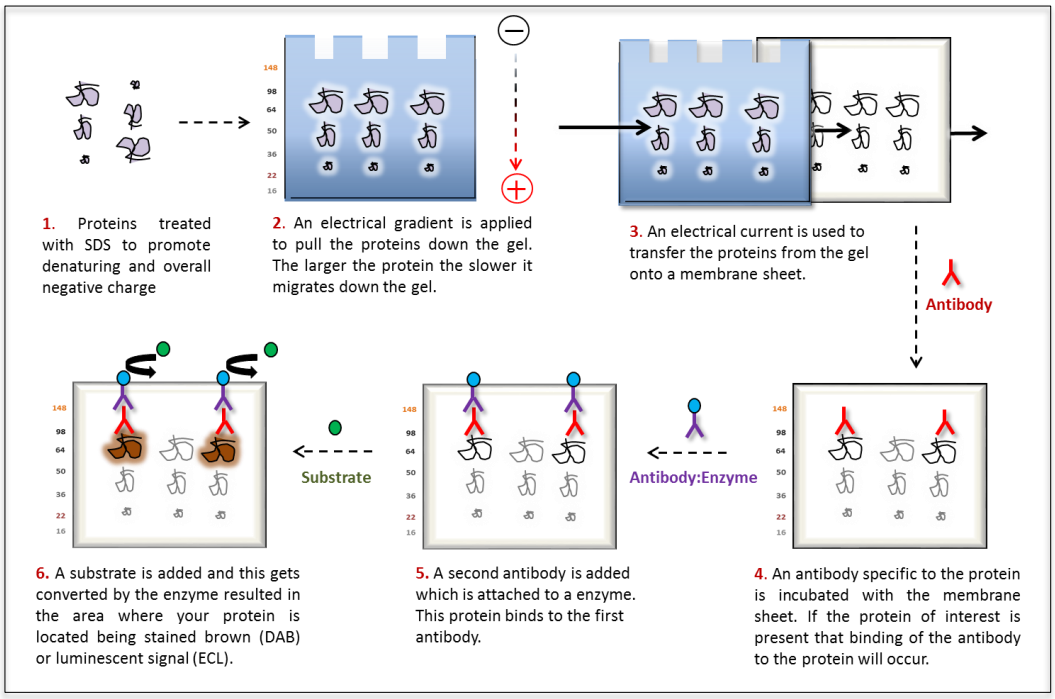

FIGURE 2.3: A schematic representation of the technique, SDS-PAGE and subsequent western blotting.

2.2.5.1.2 Detection of P. pastoris HCP

For the detection of *P. pastoris* HCP by western blot, SDS-PAGE and Western Blotting were performed as stated above. After which probing of the membrane utilised anti-*P. pastoris* conjugated HRP antibodies from the *Pichia pastoris* HCP WB kit (Cygnus Technologies) and was performed according to the manufacturer's instructions.

2.2.5.2 ELISA's for functional assessment

The Maxisorp plate was coated with 100 µL of 1 µg/mL HER2 and stored overnight at 4ºC. The plate was then washed 2 times with 1x PBS-T (PBS + 0.1 % Tween) and beaten dry on paper. 300 µL PBS-TB (PBS + 0.1%Tween + 5% BSA) was added to the wells and incubated on a shaker for 1 hour at room temperature. Following which the plate was washed with 3x PBS-T and beaten dry. 100 µL of sample was then added to the wells. This was then, once again, incubated for 1 hour at room temperature with shaking. The wells were then washed three times with PBS-T. Binding of DARPin was detected using 100 µL/well of anti-DARPin polyclonal mouse serum at 1:1000 in PBS-TB and incubated for an hour on a shaker at RT. The plate was then washed three times with PBS-T and dried before the addition of HRP-conjugated antibody. The anti-mouse-IgG-HRP conjugate in a final volume of 100 µL of PBS-TB was added to each well at a dilution of 1:3000. This was incubated for 1 hour at RT on a

shaker before being washed four times with PBS-TB. The ELISA was developed using 100 µL/well of OPD substrate in 0.1 M-citrate buffer, 4 M HCL was used to stop the reaction and the plate was read at 490 nm.

2.2.5.3 Determining binding kinetics and affinity

Surface Plasmon Resonance (SPR) evaluation of the G3 binding took place using a ProteOn XPR36 (Bio-Rad Laboratories). The extracellular domain of recombinant human HER2 (EMP Genentech) or EGFR/HER1 facilitated the role of antigen for G3 and E69 DARPin respectively. Dr G. Nagy-Davidescu (UZH) performed all tests.

2.2.5.4 Mass Spectrometry & N-terminal sequencing.

Samples were sent for Mass Spectrometry to either Dr G. Nagy-Davidescu (UZH) or Dr E. Samuel (UCL) and N-terminal sequencing to Alta Bioscience LTD. Prior to N-terminal sequencing the sample was run on an 18% SDS-PAGE gel before staining with Coomassie blue R250 and excision of the relevant protein band.

2.2.5.5 Endotoxin Detection and Quantification

Samples were taken throughout the process and analysed for endotoxin level using the Endosafe-PTS system (Charles River), as per the manufacturer's guidelines. Briefly, the cartridge is then loaded into the reader (Figure 2.4A) and 25 µL of your sample of choice is loaded into each of the four sample reservoirs present on the cartridge, Figure 2.4B. Testing is run in duplicate with and without a spiked control introduced to the applied sample, hence the need for four reservoirs. For the non-spiked channels the sample is drawn directly to the LAL reagent and mixed, whilst for the spiked channels the sample is mixed with both endotoxin and LAL reagent. After mixing all pathways are combined with chromographic substrate, incubated and then mixed prior to being drawn to the optical cell and colour intensity measured.

The intensity can be directly correlated to the concentration of endotoxin present and the reaction time to the manufacturers Archived Standard Curve. The reader's software then calculates endotoxin present (EU) and the spike recovery (%).

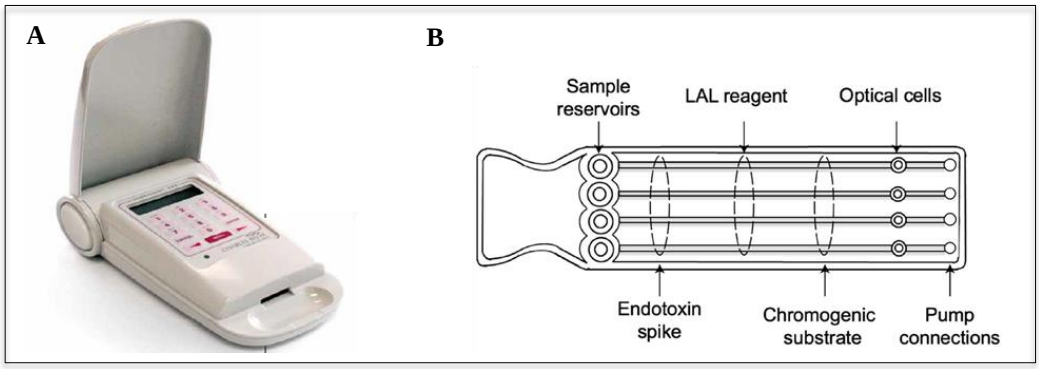

FIGURE 2.4: Layout of the Charles River Endosafe System for Endotoxin Quantification.
A, Endosafe® reader. **B**, Endosafe® cartridge.

2.2.5.6 Quantification of P. pastoris Host Cell Protein

Quantification of host cell protein was performed using the *Pichia pastoris* HCP ELISA Kit (Cygnus Technologies) outlined in Figure 2.5. Briefly 25 µL of standards and samples were added to the wells following with 100 µL of HRP conjugated anti-*P. pastoris*. The reaction was incubated with shaking (400-600 rpm) at RT for either 1.5 hours for the rapid protocol (LOD <1 ng/mL) or 3 hours for the regular protocol (LOD <0.3 ng/mL), the more sensitive of the two methods. The wells were then washed three times with 350 µl of 1x Wash Buffer before the addition of 100 µL of TMB substrate and an incubation of 30 minutes at RT without shaking. After which 100 µL Stop Solution was added and the plates were read at 450/650 nm.

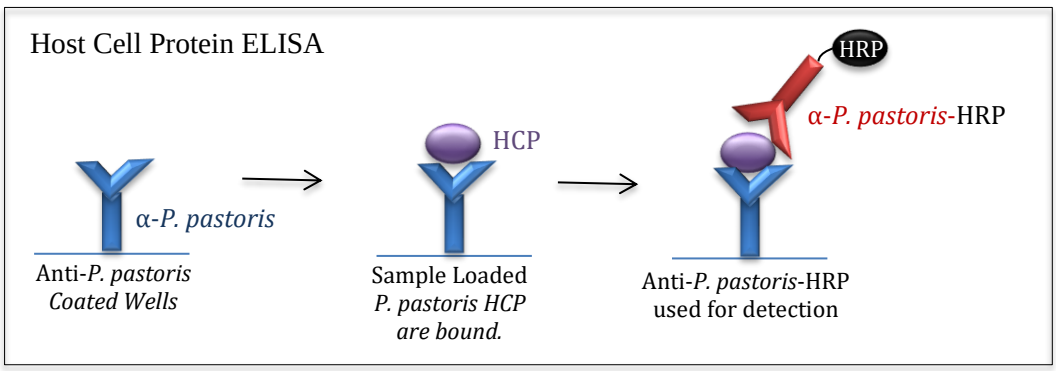

FIGURE 2.5: An outline of the Cygnus *P. pastoris* HCP ELISA assay.

CHAPTER THREE

THE EFFECT OF PURIFICATION TAGS ON DARPIN BIODISTRIBUTION IN AN ANIMAL MODEL

3.0 The effect of purification tags on DARPin biodistribution in an animal model.

3.1 Introduction

The His_6 tag is an excellent first capture step for IMAC purification of recombinant proteins. However, if the tag remained on the final product it could have unwanted effects, including modification of bio-distribution. To address this, the pilot study aimed to compare His_6 tagged G3 with the regulatory standard, untagged version. In addition, as it had been reported that a histidine glutamate $(HE)_3$, tag, which has a negative overall charge at physiological pH, could lead to a reduction of background liver uptake (Hofstrom et al. 2011; Hofstrom et al. 2013), a $(HE)_3$ – and an untagged G3 was also proposed for testing. As with all targeting agents the principle of highly specific binding with low/no non-specific interaction is key to their successful application and, as such, any means to reduce that background binding/localisation would be highly sought after.

All DARPin constructs were expressed in the *P. pastoris* strain *X33* utilising the *S. cerevisiae* alpha-mating factor for secreted expression (Figure 3.0). Though proven to be an effective means of facilitating the extracellular transport of proteins to the extracellular environment inefficient cleavage by *Ste13* of the preproprotein sequence leads to N-terminal heterogeneity (Yang S. *et al.* 2013). In taking a product through to clinical trial homogeneity of the final protein therapeutic/agent is of great importance. It has been shown that removal of the *Ste13* cleavage site, in a number of recombinant proteins, can still allow for their efficient secretion into the extracellular media whilst allowing for a homogeneous n-terminal (Joshi *et al.* 2010).

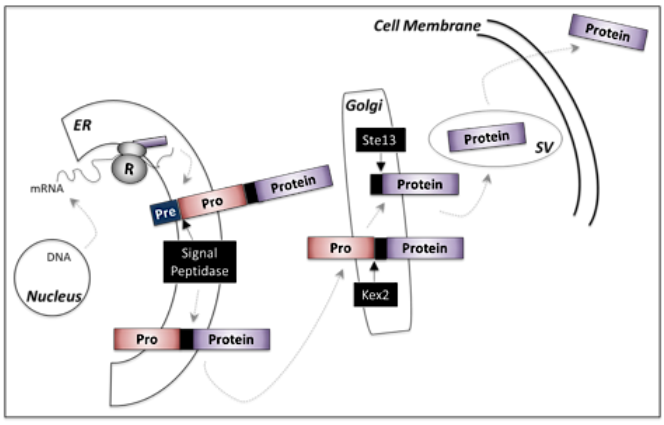

FIGURE 3.0: An illustration of a protein under the *S. cerevisiae* α-mating factor secretory pathway.
The α-mating factor secretory signal consists of a short 19aa pre-sequence followed by a larger 66aa pro-sequence. The pre-sequence is cleaved in the ER before entering the golgi where upon, the KEX2 protease cleaves the pro-peptide. Late in the Golgi the *ste13* cleaves the final adjacent EAEA amino acids to generate a protein ready for secretory vesicle (SV) packaging and export. Adapted from Ostergaard *et al.* 2000.

Aim:

In total five DARPin constructs (Figure 3.1); the EAEA$(His)_6$-G3, EAEA$(HE)_3$-G3, KR$(His)_6$-G3, KR$(HE)_3$-G3, and Cleavable-G3, are to be cloned and expressed using a *P. pastoris* system. All of the G3 constructs are to be cloned with either a full length human rhinovirus (HRV) 3C cleavage site or the remaining amino acids post-cleavage downstream of the tags. This will result in an engineered GP (glycine proline) site between the tags and the DARPin for experimental comparison. The work in this chapter provided the protein products investigated in a peer-reviewed publication (Goldstein et al, 2015) given in appendix 1. The publication looked at these constructs in an *in vivo* system using a variety of radio-isotopes / chelators; this labelling and *in vivo* assessment was carried out by Dr Robert Goldstein.

Objectives:

- To clone the EAEA$(His)_6$-G3, EAEA$(HE)_3$-G3, KR$(His)_6$-G3, KR$(HE)_3$-G3, and Cleavable-G3 with a C-terminal free Cysteine for site specific labelling.
- Express and purify the constructs under a *P. pastoris* system.
- Assess the efficiency of cleavage by *Ste13* of the α-mating factor preproprotein.
- Proteolytic removal of the cleavable-tag and purification to generate a tag-less G3.
- Take the tag-less, $(His)_6$- and $(HE)_3$- tagged DARPins forward for *in vivo* biodistribution studies.

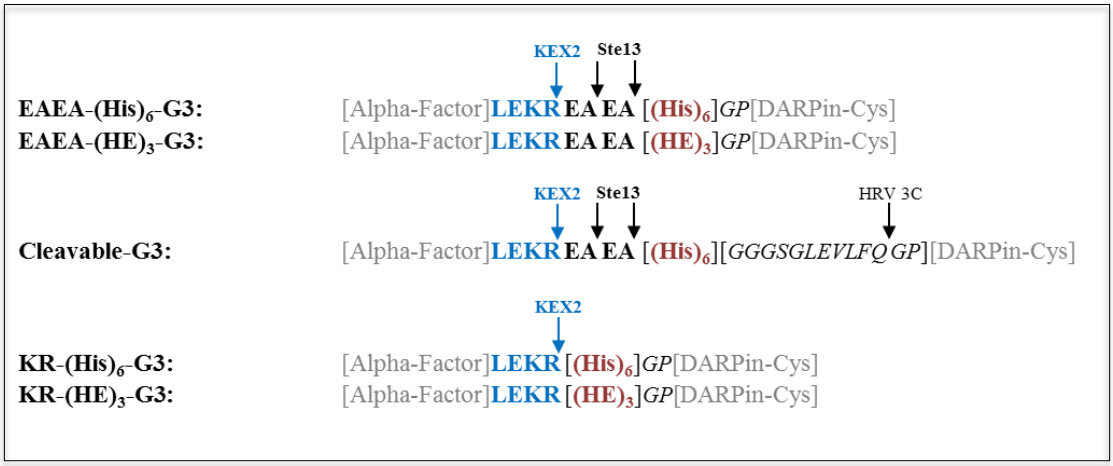

FIGURE 3.1. DARPin Constructs; EAEA$(His)_6$-G3, EAEA$(HE)_3$-G3, KR$(His)_6$-G3, KR$(HE)_3$-G3, and Cleavable-G3 (tag-less).
KEX2, yeast serine endoprotease which cleaves after –Lys/Arg-Arg residues. **Ste13**, dipeptidyl aminopeptidase (*Ste13*) is a Golgi integral membrane protein that cleaves on the C-terminal of repeating -X-Alanine- residues. **HRV 3C**, human rhinovirus 3C protease cleaves after the glutamine residue of –Leu-Glu-Val-Leu-Phe-Gln-Gly-Pro- amino acid sequence. The arrows indicate sites of proteolytic cleavage by KEX2, Ste13 or HRV 3C Proteases.

3.2 Construction of purification tag DARPin variants

3.2.1 Generation of $(His)_6$-, $(HE)_3$- and the cleavable tag G3 DARPin genes

PCR using primers, outlined in Table 3.0, on the ANK-1 plasmid, a plasmid based on the *E.coli* sequence (Provided by Professor Andreas Plückthun, UZH) and optimised for *P. pastoris* expression by GenScript. The encoded gene for G3 DARPin was used to generate a gene fragment containing EAEA-$(His)_6$-G3, EAEA-$(HE)_3$-G3 and EAEA-Cleavable-G3. Removal of the *Ste13* site was carried out by PCR of the EAEA- constructs to generate His-tagged and He-tagged G3 fragments with a KEX2 cleavage site adjacent to the protein. This was generated as it is well documented in literature (Joshi *et al.* 2010; Yang S. *et al.* 2013) that constructs containing both a KEX2 site (LEKR) and a *Ste13* (EAEA) site often result in the inefficient cleavage of the EAEA and therefore variation in the generated proteins MW. This was not an issue for the cleavage tagged DARPin as the N-terminal would be cleaved off following treatment with HRV 3C protease so cloning a construct without the *Ste13* site was not required.

Table 3.0 Primer sequences used in creating G3-tag variants with and without *Ste13* cleavage sites.
Orange, KEX2 cleavage sequence (LEKR). **Bold,** *Ste13* cleavage sequence (EAEA). **Red,** His_6 or $(HE)_3$ purification tags. **Blue,** HRV 3C recognition sequence (GLEVLFQGP) or remaining amino acids (GP). **Green,** Cysteine residue for C-terminal incorporation.

Primer	**Sequence** (bp)	**Melting Temp** (°C)
EAEA$(His)_6$	5'-ATAGAATTCTCGAGAAAAGA**GAGGCTGAAGCT**CATCACCATCATCACCATG GACCAGGTTCTGATTTGGGAAAGAAATTGTTGGAAGCTGCTAGAGCTG -3'	59.5
EAEA$(HE)_3$	5'-ATAGAATTCTCGAGAAAAGA**GAGGCTGAAGCT**CATGAGCATGAACACGAAG GACCAGGTTCTGATTTGGGAAAGAAATTGTTGGAAGCTGCTAGAGCTG-*3'*	71.2
KR$(His)_6$	5'-ATAGAATTCTCGAGAAAAGACATCACCATCATCACCATGGACCAGGTTCT GATTTGG-3'	67.3
KR$(HE)_3$	5'-ATAGAATTCTCGAGAAAAGACATGAGCATGAACACGAAGGACCAGGTTCT GATTTGG 3'	67.4
EAEA(Cleav.)	5'CTCGAGAAAAGA**GAGGCTGAAGCT**CATCACCATCATCACCATGGAGGTGGCT CTGGATTAGAGGTATTGTTTCAAGGACCAGGTTCTGATTTGGGAAAGAAATTGTT GGAAGCTGCTAGAGCTG-3'	71.5
FWD-G3cys	5'-ATAGAATTCTCGAGAAAAGA**GAGGCTGAAGC**-3'	59.5
Rev-G3Cys	5'-TAATTATCTAGATTATTA**GCA**ACCTCCGTTCAACTTTTGCAAAATTTCAG-3'	61.9

The lyophilised primers (Integrated DNA Technologies) were re-suspended with deionised water to either 1 µg/µL or 10 µg/µL depending on their molecular weight. The PCR reactions were composed of 10x denaturing, annealing and elongation cycles with the forward primer

EAEA(His)$_6$ or EAEA(HE)$_3$ or EAEA(Cleav.) and the anti-sense primer Rev-G3Cys. This was subsequently followed by 30x PCR cycles with FWD-G3cys and Rev-G3Cys without further addition of Taq polymerase or Rev-G3Cys. PCR of constructs KR(His)$_6$-G3 and KR(HE)$_3$-G3 were performed using the EAEA(His)$_6$-G3 and EAEA(HE)$_3$-G3 genes generated by the aforementioned reactions. The reaction was set out as before utilising the KR(His)$_6$ or KR(HE)$_3$ sense primers to generate either KR(His)$_6$-G3 or KR(HE)$_3$-G3 respectively.

PCR reactions for each construct were run on 2% agarose gels and the bands of appropriate size, highlighted in Figure 3.2, were excised and purified.

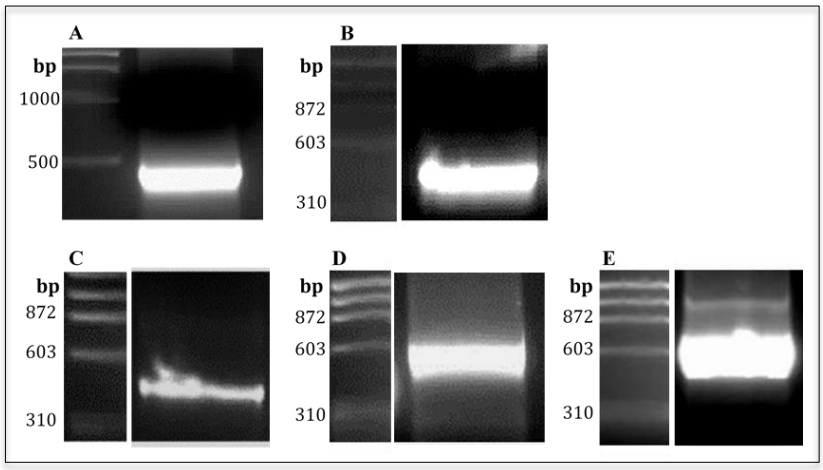

FIGURE 3.2. PCR to generate G3-DARPin Gene of Purification Tag Varients
2% Agarose Gel. **A.** EAEA-(His)$_6$-G3. **B.** EAEA-(HE)$_3$-G3. **C.** EAEA-Cleavable-G3. **D.** KR-(His)$_6$-G3. **E.** KR-(HE)$_3$-G3. 1kb DNA Ladder Promega.

3.2.2 XbaI and XhoI restriction digest of PCR products and vector

5µg of expression plasmid pPICZαB (Invitrogen) and each PCR generated G3 insert underwent restriction digest using *XbaI* and *XhoI* for their subsequent compatible ligation. The digested vector was run on a 1% agarose gel and the band running at approximately 3000 to 4000 bp, as shown in Figure 3.3, was excised and purified. The inserts underwent direct purification through chloroform / phenol extraction without any prior gel separation steps.

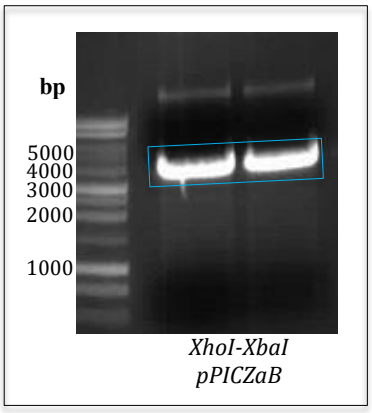

FIGURE 3.3. 1% Agarose gel showing the *XhoI* and *XbaI* restriction digest of pPICZαB.
The digested vector as highlighted by the blue rectangle was excised and purified. Marker; 1kb DNA Ladder (Promega).

3.2.3 Electroporation and Overnight Culture of transformed NEB5-Alpha Cells.

The purified *XhoI* and *XbaI* digested pPICZαB vector and G3 gene inserts were ligated at a 3:1 ratio of vector to insert for 12 hrs at 16 ^{o}C. Before undergoing phenol / chloroform extraction and electroporation into *E.coli* strains TOP10F' and TG1. 50-200 colonies / agar plate displayed resistance to 25µg/ml Zeocin enabled by the Sh ble gene present within the expression vector.

3.2.4 PCR identification of Positive Clones.

Colonies of each construct displaying Zeocin resistance underwent colony PCR using the primers outlined in Table 3.0. The PCR reaction of the tested clones were run on 1.5% agarose gels as shown in Figure 3.4. The DARPin constructs are composed of approximately 450bp and colonies with fragments corresponding to the expected size were sent for sequencing. Since the primers are specific for the insert, not the vector backbone, any colonies as a result of containing the pPICZαB (Zeocin resistant) vector but without ligated insert would not be amplified and this accounts for the empty lanes in the agarose gels of Figure 3.4.

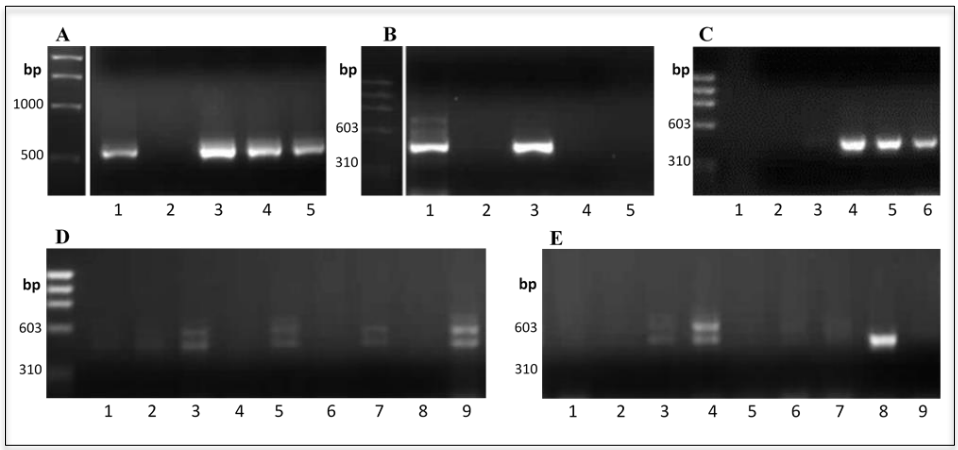

FIGURE 3.4. Colony PCR for the identification of transformed bacterial clones positive for the pPICZaB; EAEA-*(HE)$_3$ /(His)$_6$*, *KR-(HE)$_3$/(His)$_6$* and *Cleavable-tag* G3 constructs.
1.5% Agarose Gel. AOX5' and AOX3' primers. **A,** EAEA-(His)$_6$-G3. **B,** EAEA-(HE)$_3$-G3. **C,** EAEA-Cleavable-G3. **D,** KR-(His)$_6$-G3. **E,** KR-(HE)$_3$-G3. **1-9**, Individual colonies.

3.2.5 Amplification and PmeI linearization of constructs

Sequencing confirmed the presence of appropriate insert for at the very least one of each construct tested. These colonies were grown in LB Zeocin ON for plasmid amplification and midi-prepped for plasmid extraction. The isolated plasmids were linearised with *PmeI* to facilitate integration into the yeast genome. The digested and undigested plasmid underwent agarose gel electrophoresis to confirm plasmid linearization.

All vectors were confirmed to be appropriately digested displaying bands of correct size whilst the undigested controls being non-linear and coiled run faster on the gel giving rise to a main band of smaller size.

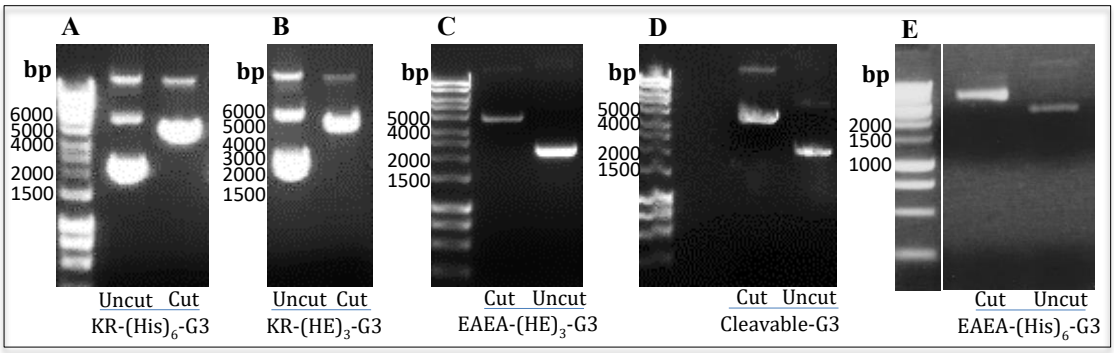

FIGURE 3.5. *PmeI* linearisation of expression vectors; pPICZαB; EAEA-*(HE)$_3$* /*(His)$_6$*, *KR-(HE)$_3$*/*(His)$_6$* and *Cleavable-tag* G3.
1% Agarose Gel. 1kb Ladder from Promega. 10µl of each reaction was loaded.

3.2.6 Transformation of Competent X33

10 µg of linearised plasmid of each construct was added to 80 µL of electro competent *P. pastoris X33* cells. The cell / DNA mix was electroporated and plated onto YPDS plates containing 100 µg/mL Zeocin for selection. After a 72 hour incubation period at 30ºC there were approximately 50 colonies per plate for each construct.

3.3 Production of G3 constructs

3.3.1 Shake-flask test expression

3-6 colonies of each construct were selected and used to inoculate 5 mL of BMGY media containing 100 µg/mL Zeocin. This was incubated at 30ºC overnight to an OD_{600} of 4-6. The

cultures were then centrifuged at 1500xg and the cells re-suspended in MEOH containing media BMMY to an OD_{600} of ~1 in order to initiate recombinant protein expression.

Samples were taken every 24 hours for three days, clarified and the supernatant was combined with reducing buffer and heated at 95ºC for 5mins. The 48hr sample with or without the 72hr sample was loaded onto SDS-PAGE gels and western blotted, Figure 3.6. Protein was detected using either anti-His primary or polyclonal anti-DARPin primary.

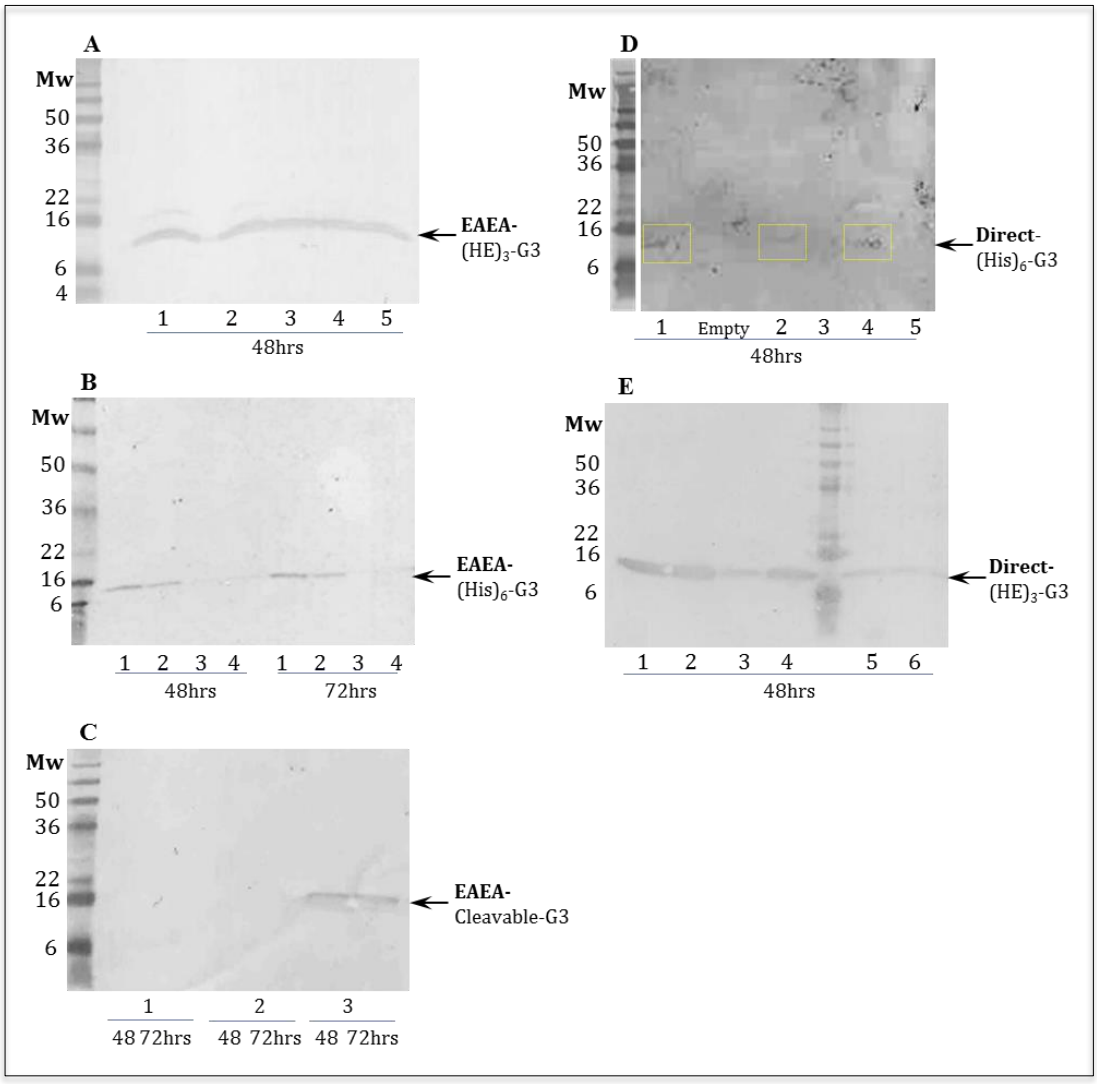

FIGURE 3.6. Shake flask test expression of EAEA- and Direct- G3 purification tag variants in *X33*.
16% SDS-PAGE Western Blots. **His-tagged proteins** detected using anti-His (Mouse) primary and anti-Mouse-IgG-HRP (Sheep) secondary. **$(HE)_3$-tagged protein**s detected using anti-DARPin primary (Rabbit) and anti-Rabbit-IgG-HRP secondary. **A,** EAEA-$(HE)_3$-G3. **B,** EAEA-$(His)_6$-G3. **C,** EAEA-Cleavable-G3. **D,** KR-$(His)_6$-G3, western was of poor quality faint bands are indicated by yellow boxes. **E,** KR-$(HE)_3$-G3.

All five tested colonies of *EAEA-(HE)$_3$-G3* expressed DARPin (Figure 3.6A) and clone 3 was selected to take forward. Two out of the four colonies for construct *EAEA-(His)$_6$-G3* expressed DARPin and clone 1 was chosen for further work (Figure 3.6B). For the cleavable-tagged DARPin, *EAEA-Cleavable-G3* only one out of the three colonies expressed the protein (Figure 3.6C). For the *Ste13*-free constructs, *KR-(His)$_6$-G3* (Figure 3.6D) and *KR-(HE)$_3$-G3 (*Figure 3.6E*)*, 3 out of 5 and all 6 colonies respectively, expressed the G3 DARPin.

The chosen colonies were taken forward for large scale expression and purification to use in further characterisation.

3.3.2 Fermentation and purification of tagged DARPin

A 10-L New Brunswick BioFlo 3000 bioreactor was used at a 5-L working volume for the production of all the DARPin constructs. The 5-L of media in the bioreactor was inoculated with 250 mL of overnight (OD_{600} ~5) seeding culture. A fed-batch glycerol feeding strategy was employed to reach a high cell density prior to methanol induction as described by Tolner *et al.* 2012. Fermentation times ranged from 1 hour (EAEA$(HE)_3$G3) to 23 hours (EAEA(H_6)G3) depending on the construct. A 125 mL Radial Flow IMAC column (Proxys) charged with copper or nickel ions was used to directly capture the tagged proteins from the culture broth. The eluted proteins were then passed through a 0.22 micron filter before being concentrated and dialysed into PBS using a Millipore TFF UF/DF unit. The concentrated protein was loaded onto a 500 mL Superdex 75 size exclusion column for purification and the peak, representative of monomer DARPin, was pooled, aliquoted and stored at -80^{o}C for future protein characterisation.

Product yield following purification ranged from 18 mg to 85 mg as shown in Table 3.1. Samples were taken throughout the bioprocess, clarified, reduced and stored for subsequent SDS-PAGE analysis. Purified end product was sent for mass spectrometry analysis. The results of each construct are evaluated in the sections below.

Table 3.1. Yield of each DARPin construct following fermentation and purification.
Protein measurements took place following HCD fermentation, IMAC capture, TFF concentration / dialysis and SEC facilitated separation to obtain monomer DARPin. The yield of final product for each construct was quantified by absorbance measurements at 280nm.

	G3 DARPin				
	Cleavable tag	EAEA-$(His)_6$ tag	EAEA-$(HE)_3$ tag	$(His)_6$ tag	$(HE)_3$ tag
Final Yield (mg)	18	46	36	32	85

3.3.2.1 EAEA-(His)$_6$-G3

Samples during fermentation, harvest and purification were loading onto a 16% SDS-PAGE gel and run under reducing conditions, Figure 3.7. The fermentation was harvested ~28 hours post dO_2 spike with a faint band visible on the coomassie gel at 14-15 kDa. It is evident once the IMAC captured eluent was concentrated that a significant level of DARPin breakdown had occurred and multiple bands at lower MW to the full length product were present. During the course of dialysis proteins notably lower than 6 kDa appear to have been removed via the TFF membrane (5 kda cut-off). All 25 ml of dialysed protein was loaded onto the SEC column using a super-loop. The chromatogram from the SEC column gave rise to three main peak areas as shown in Figure 3.7D. Samples from the 4 mL eluted fractions, denoted by *2, *14 and *33, were run on SDS-PAGE under both reduced (Figure 3.7A&B) and native (Figure 3.7C) conditions prior to visualisation using coomassie blue.

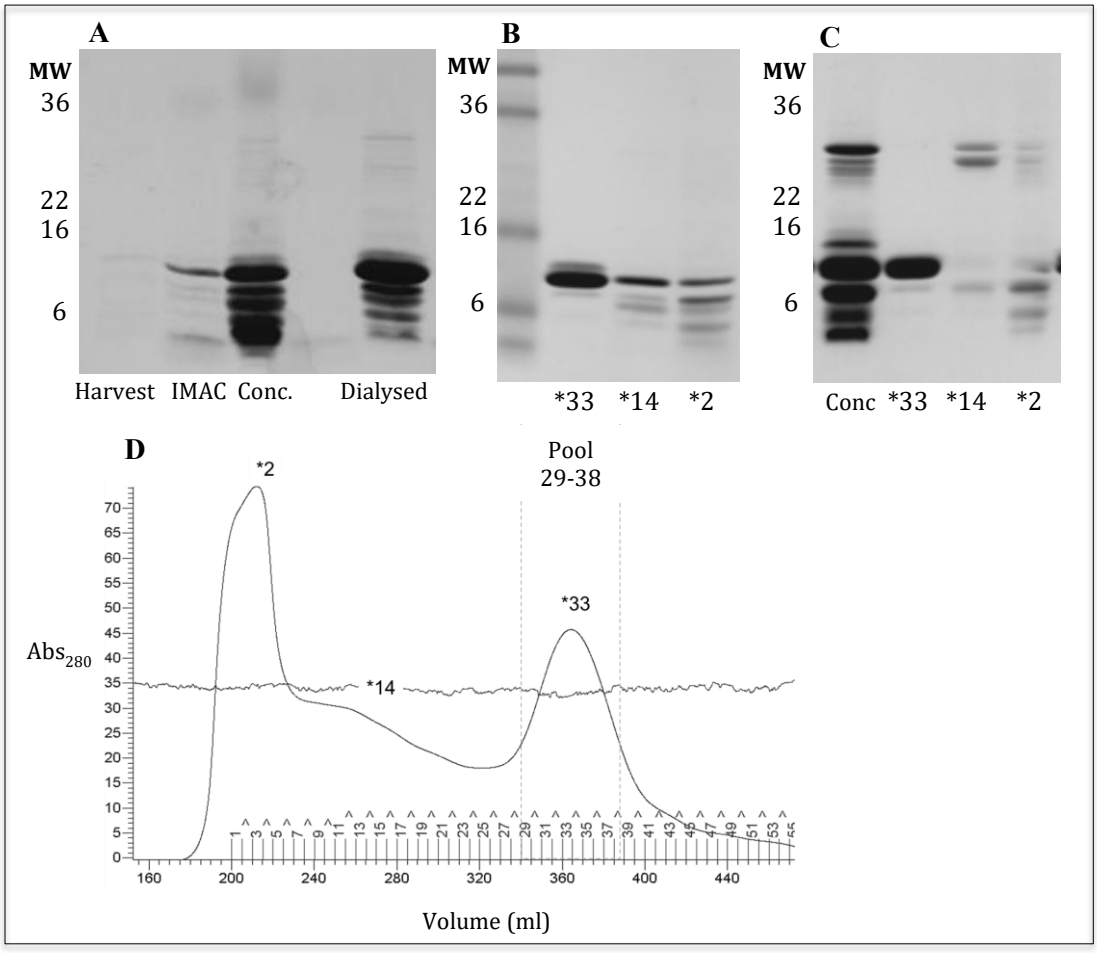

FIGURE 3.7. SDS-PAGE analysis of the fermentation, capture and purification of *X33* pPICZaB_EAEA-(His)$_6$-G3.
16% SDS-PAGE / Coomassie. **A,** Reducing conditions; Capture, Concentration and Dialysis. **Harvest,** clarified supernatant 28hrs post-dO_2 Spike. **IMAC.** Eluent from IMAC. **Conc.,** TFF concentrated IMAC pool. **Dialysed.** Post-concentration pool dialysed into PBS. **B,** SEC fractions run under reduced conditions. **C,** SEC fractions run under non-reducing conditions. ***2, *14**, ***33,** SEC eluted fractions 2, 14 and 33 respectively.

Fractions *2 and 14* are mainly composed of aggregated proteins and lower MW protein / DARPin dimers respectively. Fraction *33 contains largely monomer DARPin with a small amount of contaminating lower MW protein and elutes at the appropriate volume of 360 mL. When measured by OD 280nm the product pool (*33) contained a total of 46 mg.

The SEC pool was run on a 125 mL analytical SEC column and a clear peak at ~90 mL corresponded to the expected elution for G3 DARPin, Figure 3.8B. Analysis by MALDI mass spectrometry, shown in Figure 3.8A, determined the MW of the product to be 14869 Da which confirmed the inefficient cleavage carried out by *Ste13* of the glutamic acid (E) and alanine (A) residues. Fully cleaved $(His)_6$-G3 is 14,536.3 Da whilst EAEA$(His)_6$-G3 and EA$(His)_6$-G3 are 14,936.7 Da and 14,736.5 Da respectively. The evaluated MW was between the two partially cleaved variants validating the need to produce a construct free of the EAEA to enable a product that commences exactly at the histidine tag.

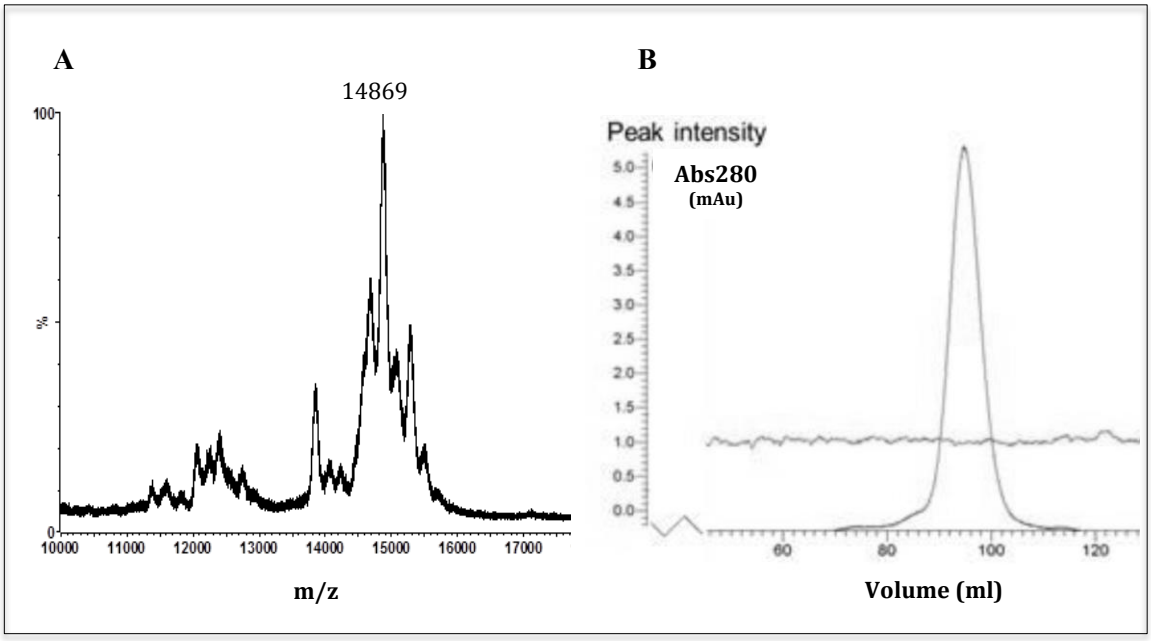

FIGURE 3.8: Final purified EAEA$(His)_6$-G3 analysis.
A, MALDI Mass Spectrometry. **B,** Analytical SEC (125mL Superdex 75).

3.3.2.2 EAEA-$(HE)_3$-G3

Samples during the course of the bioprocess, from fermentation to final purification, were loading onto a 16% SDS-PAGE gel and run under reducing conditions, Figure 3.9. The fermentation was harvested ~28 hours post dO_2 spike with an evident band visible on the coommassie gel at 14-15 kDa. Protein was eluted from the SEC column in three distinctive

peaks (Figure 3.9C), a sample from the centre of each peak was taken, run on SDS-PAGE and stained with coomassie blue (Figure 3.9B). All three fractions appear to contain a 14 kDa and 6 kDa protein, in line with full-length and cleaved G3 respectively. Fraction *4 eluted at ~200 mL representative of high MW and thus probably aggregate. Fraction *20 at 280 mL indicative of dimer formation and fraction *32 at 340 mL is the expected monomer elution value.

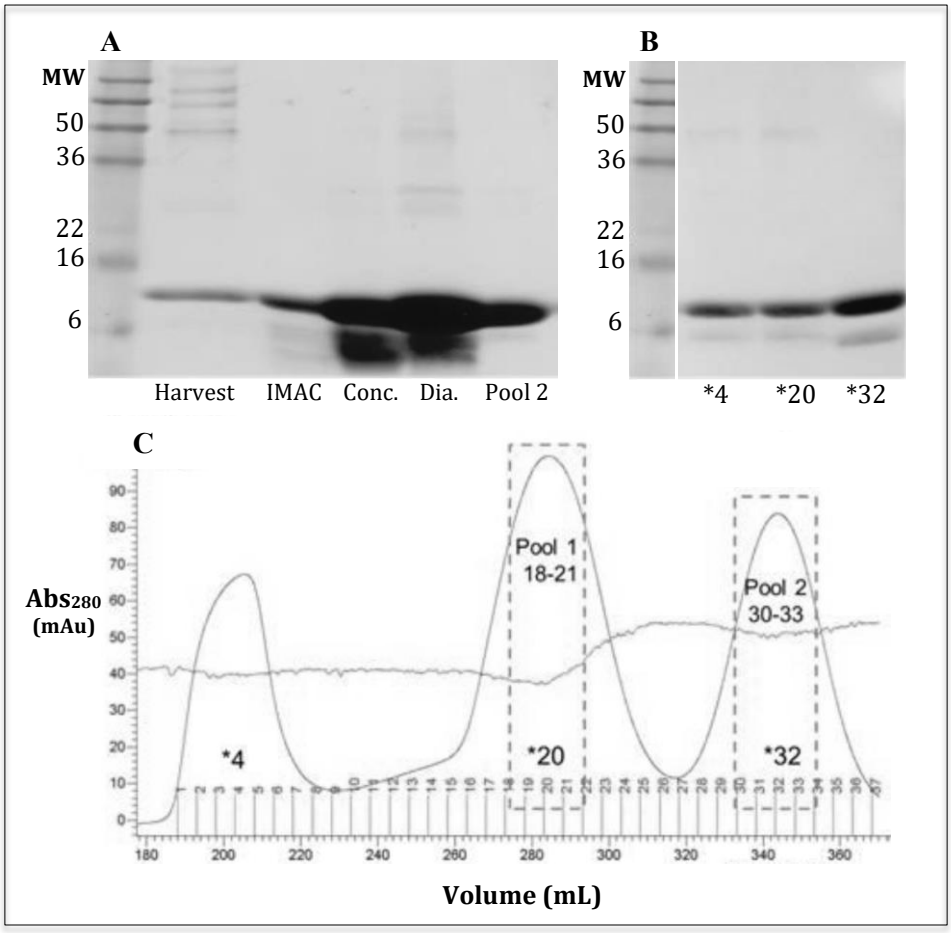

FIGURE 3.9. SDS-PAGE analysis of the fermentation, capture and purification of *X33* pPICZaB_EAEA-(HE)$_3$-G3.
16% SDS-PAGE / Coomassie. **A,** Reducing conditions; Capture, Concentration and Dialysis. **Harvest,** clarified supernatant 5 hours post-dO_2 Spike. **IMAC.** Eluent from IMAC. **Conc.,** TFF concentrated IMAC pool. **Dia.** Post-concentration pool dialysed into PBS. **Pool 1,** pool of dimer DARPin from SEC. **Pool 2**, pool of monomer DARPin from SEC. **B,** SEC fractions run under reduced conditions. **C,** SEC chromatogram of purification run. ***2, *14**, ***33,** SEC eluted fractions 2, 14 and 33 respectively.

The EAEA-(HE)$_3$-G3 pool was analysed by MALDI mass Spectrometry and analytical Superdex75 chromatography, Figure 3.10 -A and -B respectively. The expected mass of the DARPin starting at the (HE)$_3$- tag is 14512,2Da but the molecular weight obtained was shown to be 14846.4Da. This value is indicative of inefficient *Ste13* cleavage as EA-(HE)$_3$- and EAEA-(HE)$_3$-G3 would result in molecular weights of 14912.6 Da and 14712.4 Da

respectively, the determined MW is an average of these values. This is because the DARPin pool contains both partially cleaved and uncleaved *STE13* sites resulting in an averaged peak. Analytical SEC demonstrated a largely monomer product pool with a far smaller peak at 75 mL of residual dimer DARPin.

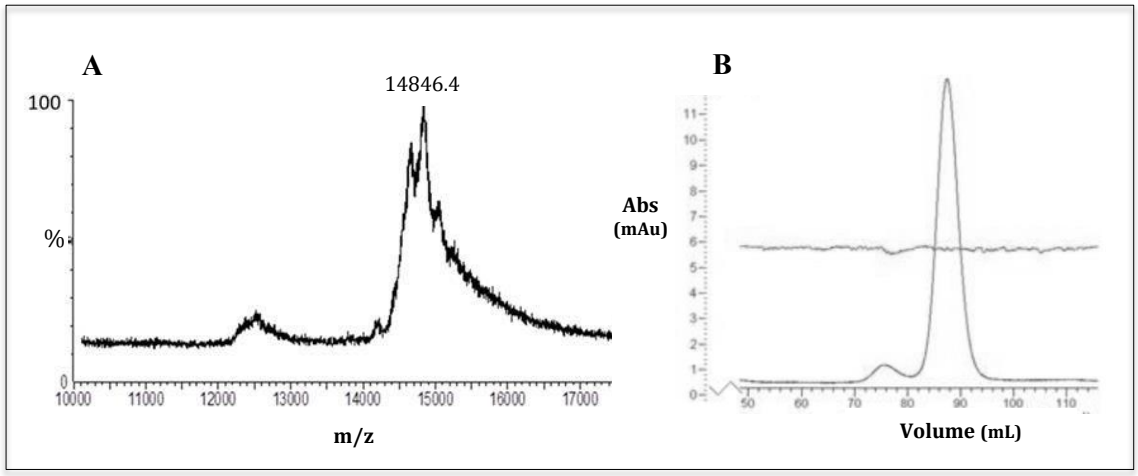

FIGURE 3.10: Final purified EAEA(HE)$_3$-G3 analysis.
A, Mass Spectrometry. **B,** Analytical SEC (125 mL Superdex 75).

3.3.2.3 Cleavable-tag G3

The cleavable tag DARPin was harvested 2 hours post methanol induction (6 hours post dO_2 spike) by Ni^{2+}-IMAC. There were significant loses of DARPin in the flow-through (FT) during the course of loading as shown in Figure 3.11A. This indicates the possibility of suboptimal loading conditions or proteolytic cleavage of the tag during the course of the fermentation to address this a western blot of the flow through probed with an antibody to the His_6-tag was run. This revealed that the tag was present on the unbound DARPin (data not shown) indicating that the FT is a result of the run conditions not proteolytic action. The column was washed with 10mM and 20mM Imidazole, with evident background proteins being eluted in the initial wash step. To reduce the high degree of aggregation and dimerization seen in the previous G3 runs during TFF and SEC unit operations a final concentration of 10mM DTT, a strong reducing agent, was added. The DTT was added into the IMAC eluted pool and then into the dialysis buffer and running buffer for TFF and SEC, respectively. This increased the fraction of monomeric DARPin obtained, reducing the level of aggregate and dimer. Following SEC the eluted pool contained a total of 18 mg cleavable-tag G3 of monomer DARPin.

The anticipated molecular weight of the product starting directly prior to the tag is 15581.5 Da the value obtained for the purified product following mass spectrometry was 15934 Da (Figure

3.11B) indicating yet again the inefficient cleavage of the EAEA site by the *Ste13* protease. In the case of this construct this is not problematic as further processing with the human rhinovirus 3C protease, to generate a tag-less product, would allow the DARPin to have a uniform N-terminus initiating at the engineered glycine-proline (GP) site adjacent to the DARPin.

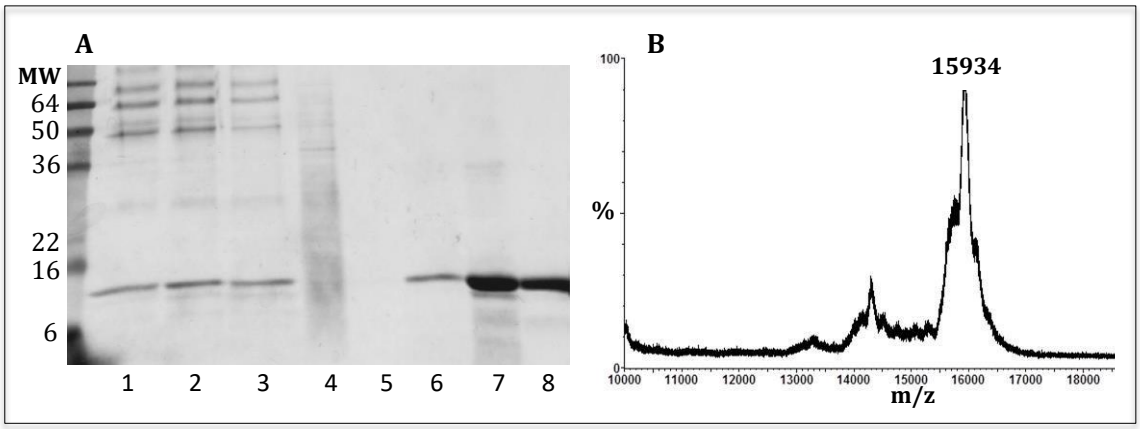

FIGURE 3.11: SDS-PAGE and Mass Spectrometry analysis of the production and purification of pPICZaB_Cleavable-G3.
A. 16% SDS-PAGE / Coomassie run under reducing conditions. **B.** Mass Spectrometry. **1.** 2 hours post MEOH induction, **2.** 3 hours post-MEOH induction, **3.** IMAC Flow through (1-L) **4.** 10 mM Imidazole Wash. **5.** 20 mM Imidazole Wash. **6.** IMAC Eluent. **7.** TFF; Dialysis and concentration, **8.** SEC pool.

3.3.2.3.1 HRV 3C Protease mediated cleavage to create tag less G3

To evaluate the effects of differing buffer conditions on HRV 3C protease cleavage 10 mL of His-tagged DARPin was concentrated from ~0.2 mg/mL to ~0.6 mg/mL using a spin column. 0.5 mL was then dialysed in a 3.5 kDa MWCO Slidalyzer (Pierce) against three different buffers; PBS, Cleavage Buffer (150 mM NaCl, 50 mM Tris-HCl at pH 7.5) and High Salt Cleavage Buffer (800 mM NaCl, 50 mM Tris-HCl at pH 7.5). HRV 3C Protease was added to a final concentration of 40 units per mL and incubated for 18 hours at 4^{o}C. The samples were loaded onto a 16% SDS-PAGE gel, run under reducing conditions and identical loading conditions. Protein was visualised by Coomassie Brilliant Blue-250 staining (Figure 3.12A) and also western blot with an anti-His (1:1000) primary and anti-mouse IgG-HRP (1:1000) secondary, Figure 3.12B.

Cleavage was most efficient when using the high salt cleavage buffer and under these conditions the tag was removed from all the G3 product within 18 hours of incubation using 76 U/mg HRV 3C protease and therefore this buffer system was chosen to take forward.

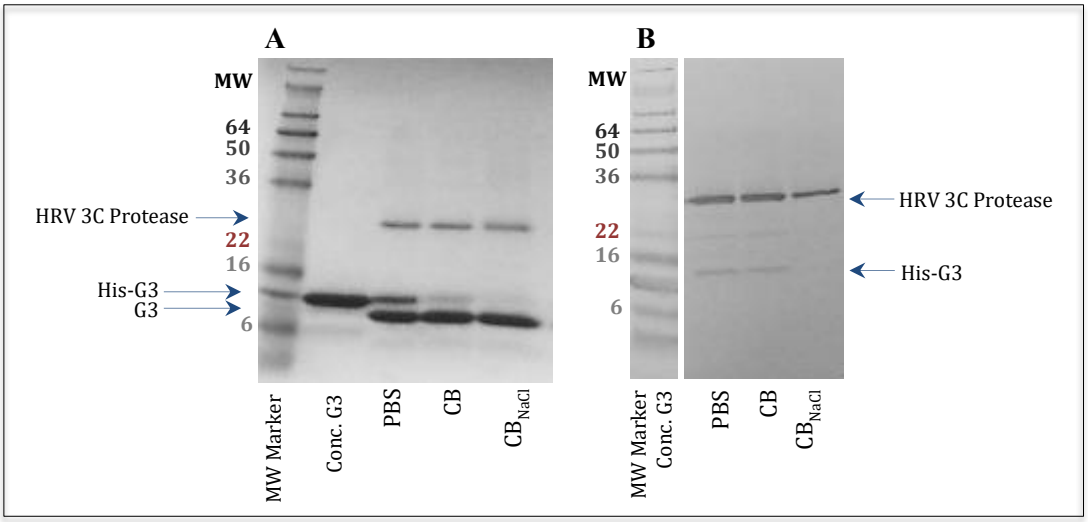

FIGURE 3.12. An evaluation of His-tag cleavage by HRV 3C protease.
A. Coomassie Stain, **B.** Western Blot; anti-His (1:1000). 16% SDS-PAGE, 20µl Loaded. ***Conc. G3*;** Concentrated His_6-tagged G3 prior to dialysis and cleavage. ***PBS;*** Reaction mixture in PBS. **CB;** Reaction mixture in Cleavage Buffer. ***CB_{NaCl}*;** Cleavage Buffer with 0.8 M final conc. NaCl.

Due to the high cost associated with buying in enzymes the protease was titrated from 1x (76 U/mg) to 100x (0.76 U/mg) and cleavage efficiency investigated over an 18 hour period, Figure 3.13.

At a concentration of 76 U/mg the tag can be cleaved in a timeframe of 2 hours, at 7.6U/mg an overnight incubation would need to be applied to get appropriate levels of tag-free DARPin. Concentrations lower than this were deemed not feasible as there were high levels of un-cleaved product still visible following 18 hours of incubation.

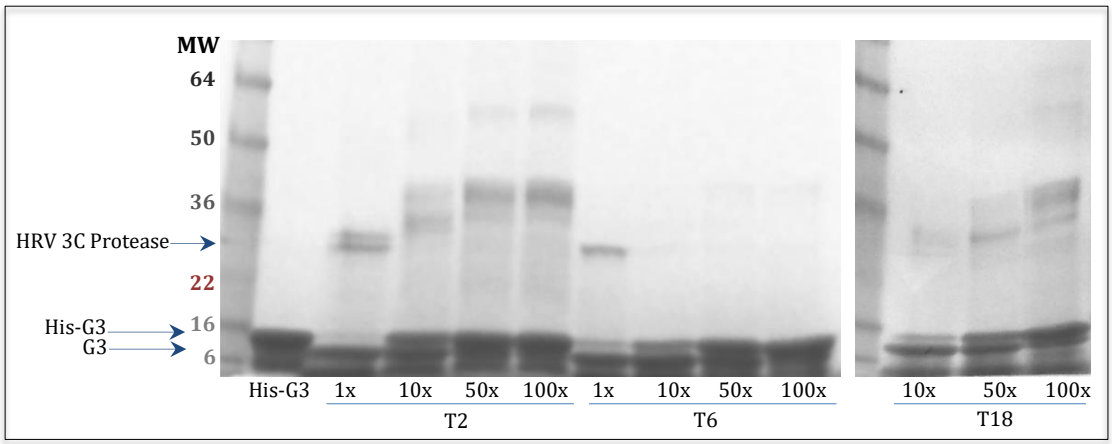

FIGURE 3.13. Titrated HRV 3C Protease and its Subsequent Effect on Cleavage.
12 % Gel. Coomassie Stain, 20ul Loaded. Cleavage Buffer with 0.8M final conc. NaCl. ***1x, 10x, 50x, 100x;*** 1-100 fold dilution in HRV 3C Protease used***. T2, T6 & T18***; 2, 6 & 18hrs incubation with HRV 3C Protease respectively.

Taking into account the above-mentioned cleavage studies, 18 mg of cleavable-tag G3 produced in Section 3.3.2.3 was dialysed into HS-CB containing 10 mM DTT. A total of 76 units of HRV 3C protease was used per mg of DARPin and took place over the course of 2 hours at 4ºC. As before the his_6-tagged protease and any remaining un-cleaved DARPin were removed by Ni^{2+} IMAC. This process allowed the cleaved product, now without a tag, to pass unhindered within the flow through whilst retaining the still tagged remnants.

The tag-less G3 DARPin was pooled and stored at -80ºC for future studies.

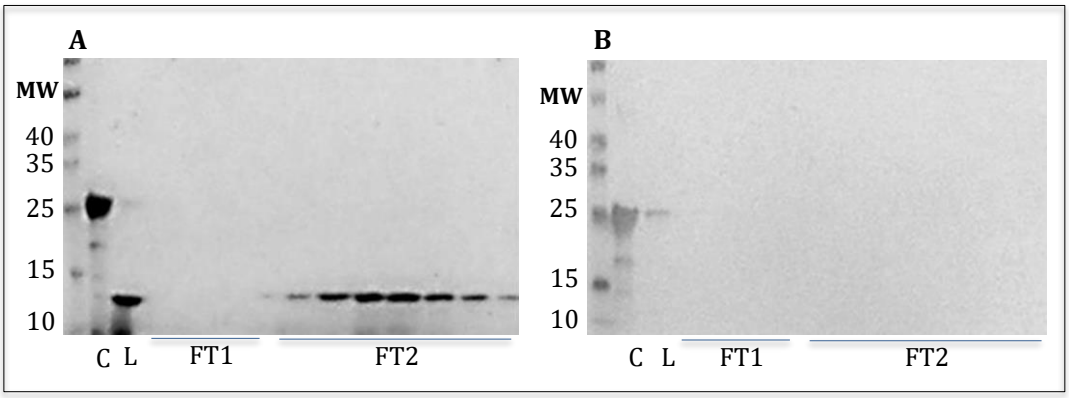

FIGURE 3.14. Large scale cleavage and purification to create a tag-less DARPin.
A. Coomassie Stain, **B.** Western Blot; anti-His (1:1000). 16% SDS-PAGE, 20 µL Loaded. ***C*;** His_6-tagged HRV 3C Protease. ***L;*** Load – Cleavage reaction mixture. **FT1;** Flow-through during Load (2 mL). **FT2;** Flow-through during wash with high salt cleavage buffer containing 10mM DTT (5 mL).

3.3.2.5 KR-$(His)_6$-G3

The His_6-tagged G3 free of a *Ste13* cleave site (EAEA), KR-$(His)_6$-G3, was harvested 23 hours post methanol induction. Removal of the cleavage site did not notably affect expression or secretion of the construct with product detectable in the extracellular media. Samples from throughout the fermentation and purification were taken and run under reducing conditions on a 16% SDS-PAGE gel, Figure 3.15A. Having seen the aggregation and dimerization propensity of the first DARPin construct EAEA-$(His)_6$-G3 (Section 3.3.2.1) during concentration and size exclusion chromatography the use of a reducing agent was implemented. As such the TFF and SEC unit operations were performed under reducing conditions with the addition of 10mM DTT.

In comparison to constructs purified in the absence of DTT there was far less aggregate and dimer formation visible on the SEC chromatogram with an increased proportion of protein being monomer DARPin eluting between 280-400 mL (Figure 3.15 B).

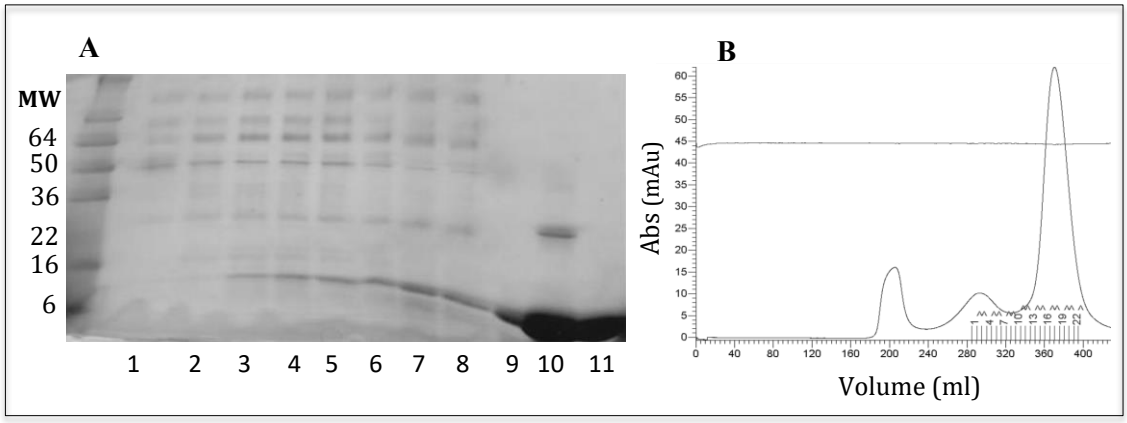

FIGURE 3.15: SDS-PAGE analysis of a high cell density fermentation and subsequent capture and purification of *X33* pPICZaB_KR-(His)$_3$-G3.
A, 16% SDS-PAGE Gel run under reducing conditions. **B,** Analytical Superdex75 prep-grade, SEC. **1.** dO_2 Spike, **2.** 1hr post-spike, **3.** 2hrs post-spike **4.** 3hrs post-spike, **5.** 4hrs post-spike, **6.** 6hrs post-dO_2 spike (2hrs on MEOH limited feed), **7.** 20hours on MEOH limited feed. **8**, Harvest, **9,** IMAC eluent **10**, TFF; Dialysis and concentration. **11,** SEC monomer pool.

When analysed by mass spectrometry the molecular weight obtained at 14447 Da matched closely with the anticipated value of 14536.3 Da indicating clean removal of the alpha factor secretory peptide in the absence of the *Ste13* cleavage site, Figure 3.16A.

The purified KR-(His)$_6$-G3 gave a clean peak on the chromatogram when run on analytical SEC with no visible dimers present within the pool as shown in in Figure 3.16B.

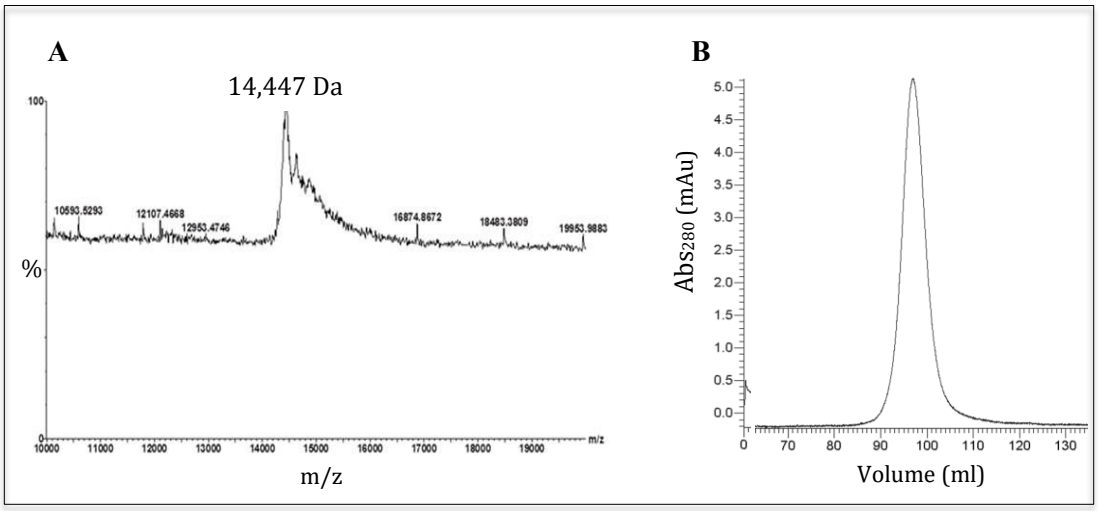

FIGURE 3.16: Final purified KR(His)$_6$-G3 analysis.
A, Mass Spectrometry. **B,** Analytical SEC (125 mL Superdex 75).

3.3.2.6 KR-(HE)$_3$-G3

The (HE)$_3$-tagged G3 construct, free of the *Ste13* cleavage site; KR-(HE)$_3$-G3, was harvested 6 hours post dO_2 spike / 3 hours post methanol induction. As with the KR-(His)$_6$-G3, the removal of the EAEA cleavage site did not affect the products secretion into the surrounding media as shown in Figure 3.17A.

Unlike with the His$_6$-tagged constructs whereby 20 mM imidazole was present in the wash step the (HE)$_3$- constructs were washed without the presence of imidazole. This decision was made due to the (HE)$_3$- tag containing only three available histidine's and therefore its affinity for binding to metal ions would be lessened by comparison to the hexahistidine tag. Therefore harsh wash conditions could result in significant loses during IMAC. Despite this there was still a loss of product in the flow-through throughout loading of the fermentation broth. Use of the reducing agent DTT (10mM final concentration) during concentration and dialysis resulted in lowered aggregate and dimer formation noted during the SEC unit step where the chromatogram shown in Figure 3.17B showed that the majority of the product protein was in monomeric form (~320-380 mL), with far reduced dimer (~260-300 mL) and aggregate (~180-230 mL) formation.

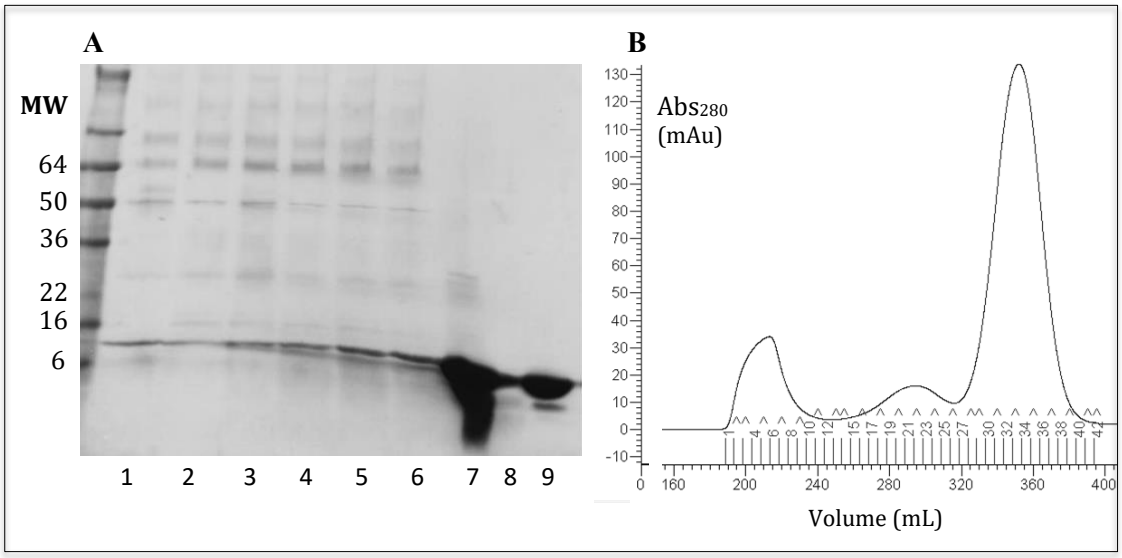

FIGURE 3.17: Analysis of a high cell density fermentation and subsequent capture and purification of *X33* pPICZ*α*B_KR-(HE)$_3$-G3.
A, 16% SDS-PAGE / Coomassie run under reducing conditions. **B**, 500mL Superdex75 SEC. **1.** dO_2 Spike, **2.** 1hr post-spike, **3.** 2hrs post-spike **4.** 3hrs post-spike, **5.** 4hrs post-spike, **6.** 6hrs post-dO_2 spike (3hr post MEOH induction), **7.** TFF; Dialysis and concentration, **8.** IMAC eluent, **9.** SEC eluted pool.

Following SEC the peak representative of monomer DARPin was pooled and assessed by analytical SEC which showed a tight monomer peak with an almost indistinguishable amount of dimer DARPin as shown in the chromatogram in Figure 3.18A.

Mass Spectrometry revealed the DARPin to be 14511.7 Daltons this correlates well with the anticipated molecular weight of 14,512.2 Da, revealing that the removal of the *Ste13* cleavage site indeed results in a homogenous N-terminal product (Figure 3.18B).

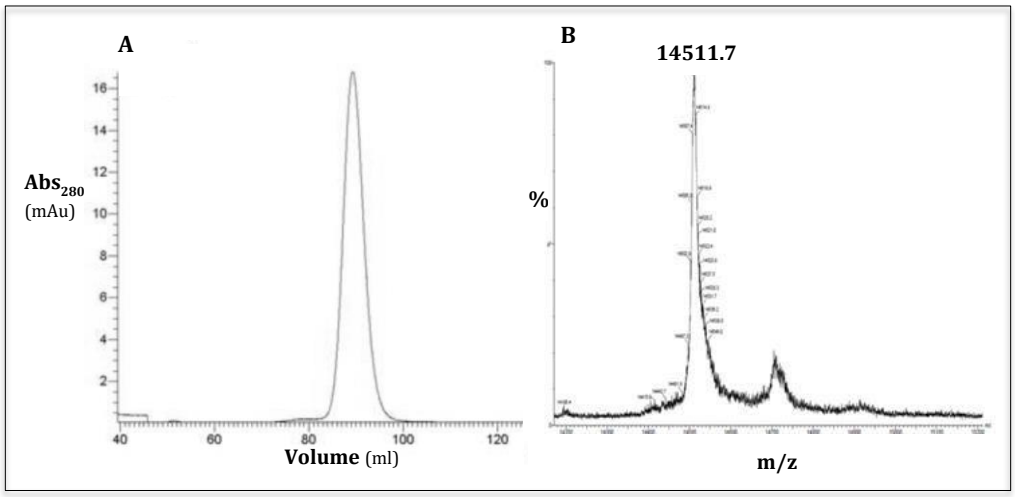

FIGURE 3.18: Final purified KR(HE)$_3$-G3 analysis.
A, Analytical SEC (125 mL Superdex 75). **B,** Mass Spectrometry.

3.3.3 In vivo biodistribution

3.3.3.1 Non-tumour bearing model

The effect of the purification tag on DARPin biodistribution was assessed within a mouse model using an indium^{111} radiolabel. The *in* vivo biodistribution studies were carried out by Robert Goldstein (UCL). The free cysteine on the c-terminal of the untagged-, KR$(HE)_3$- and KR(His_6)- G3 was conjugated to a maleimide-DOTA chelator prior to labelling with ^{111}In. The addition of the radio-isotope took place at a very small scale with no more than 5-60 µg of each DARPin used per reaction. Each DOTA-conjugated construct in 0.2 M ammonium acetate (pH 6.5) had 10-30 MBq $^{111}InCl_3$ added and incubated for 2 hours at 37ºC. The reactions were stopped with 5 mM EDTA, buffer exchanged into PBS and the purity was assessed by instant thin layer chromatography, iTLC. Radiochemical purity was determined to be greater than 95% and specific activity between 1-2 MBq/nnmol.

The protein was administered to 8 female BALB/c mice, per G3 construct, with 4 mice being euthanised at 4 hours and 24 hours post-injection. The radiolabelled $(HE)_3$-tagged G3 out performed both the tag-free and His_6- tagged DARPins in terms of overall favourable biodistribution which would allow for lower background and better imaging. This is demonstrated in Figure 3.19 with the $(HE)_3$-tagged construct having lower uptake at 4 hours in the spleen, heart, stomach, liver, pancreas, lung, muscle , bone marrow and blood. At the following time point (24 hr) ^{111}Indium-$(HE)_3$-G3 still had lower uptake, than either other construct, in the spleen, pancreas, intestine, liver, stomach, bone marrow and muscle. The high level of radio-activity seen in the kidneys by all constructs is a result of the excretory pathway for the DARPin molecules with the earlier time-point displaying values from ~250-300% of the injected dose per gram in the kidneys alone.

Given the potential for liver metastasis in HER2 positive breast cancer, non-specific localisation of radiolabelled DARPin is undesirable as any background will affect imaging potential and accuracy. To this affect the indium labelled $(HE)_3$-DARPin had far lower liver uptake at both 4 hours (1.57% ID/g) and 24 hours (1.05% ID/g) post-administration than both the His_6- (3.72 and 3.45% ID/g) and untagged- G3 (4.31 and 3.06% ID/g), Figure 3.19. Given the positive properties afforded to the DARPin by the $(HE)_3$-tag this construct was chosen for future work.

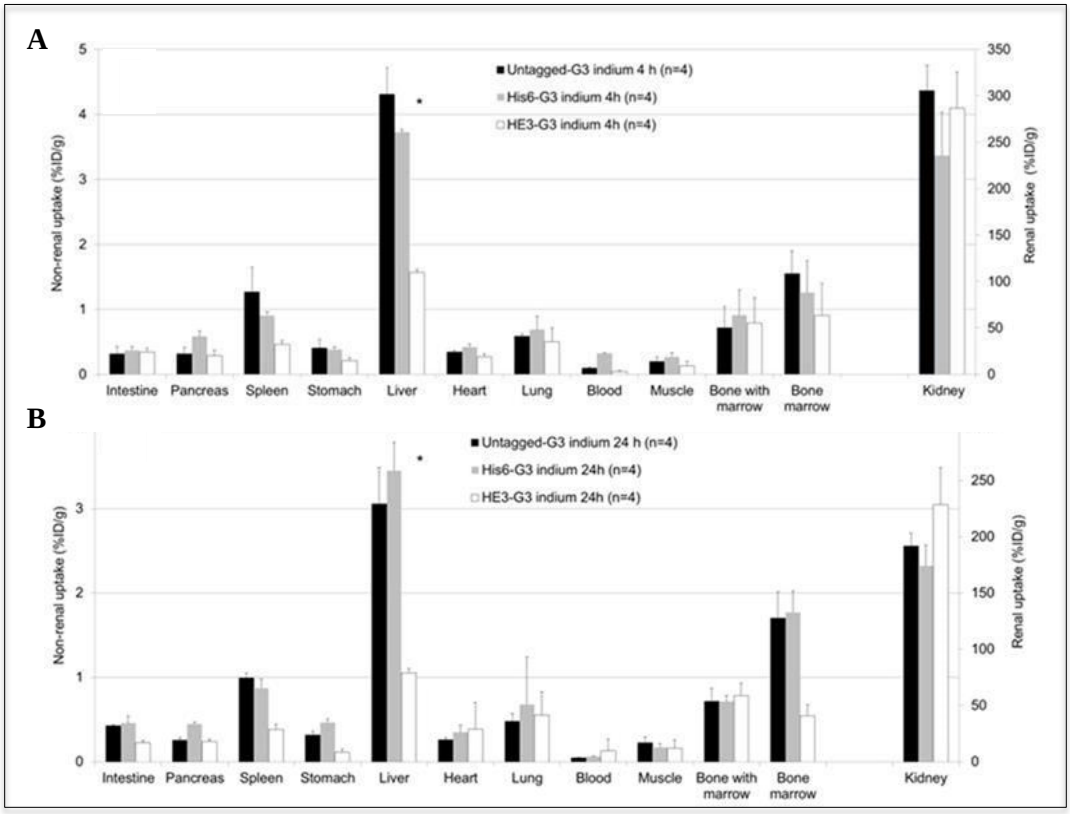

C

	4 hours						24 hours					
Tissue	Untagged-G3		$(HE)_3$-G3		$(His)_6$-G3		Untagged-G3		$(HE)_3$-G3		$(His)_6$-G3	
BL	0.10	± 0.02	0.05	± 0.01	0.33	± 0.24	0.05	± 0.01	0.13	± 0.14	0.06	± 0.01
HE	0.34	± 0.03	0.27	± 0.05	0.42	± 0.07	0.26	± 0.03	0.39	± 0.32	0.35	± 0.08
LU	0.59	± 0.04	0.50	± 0.21	0.69	± 0.45	0.48	± 0.09	0.55	± 0.27	0.68	± 0.56
LI	4.31	± 0.40	1.57	± 0.04	3.72	± 0.39	3.06	± 0.43	1.05	± 0.05	3.45	± 0.34
PA	0.32	± 0.10	0.29	± 0.09	0.58	± 0.1	0.26	± 0.03	0.24	± 0.03	0.45	± 0.02
SP	1.27	± 0.37	0.46	± 0.06	0.91	± 0.08	0.99	± 0.06	0.38	± 0.06	0.87	± 0.11
KI	306	± 27.2	287	± 38.6	236	± 46.6	192	± 11.2	229	± 32.9	174	± 18.8
SO	0.41	± 0.14	0.21	± 0.05	0.38	± 0.27	0.32	± 0.04	0.11	± 0.04	0.47	± 0.04
INS+	0.31	± 0.11	0.35	± 0.06	0.37	± 0.07	0.43	± 0.01	0.23	± 0.03	0.46	± 0.08
MU	0.20	± 0.07	0.13	± 0.07	0.27	± 0.09	0.22	± 0.07	0.16	± 0.10	0.17	± 0.05
BO	0.71	± 0.33	0.79	± 0.39	0.91	± 0.14	0.72	± 0.15	0.79	± 0.14	0.71	± 0.07

FIGURE 3.19. Biodistribution results (%ID/g +/-SD) for the ^{111}In-labelled; Untagged- , $(His)_6$- and $(HE)_3$-G3 DARPin.
The mice were injected unsedated with 1 µg of radiotracer with ex vivo organ distribution assessed at 4 and 24 hours p.i. (n=4).

BL, *Blood*, HE, *Heart*, LU, *Lungs*, PA, *Pancreas*, SP, *Spleen*, KI, *Kidney*, SO, *Stomach*, INS+, *Intestines with content*, MU**,** *Muscle*, BO, *Bone & Marrow*.

3.3.3.2 HER2 positive tumour bearing model

Having shown in section 3.3.3.1 that the $(HE)_3$-tagged G3 had significantly more favourable bio-distribution, in terms of unspecific uptake, than both the His_6-tagged and untagged variants this construct was chosen to be taken forward for testing within a tumour model. Female SCID-beige mice were inoculated on their right flank with the HER2 expressing BT474 (breast cancer) cell line and the tumour was allowed to grow over a period of days. DARPin was radiolabelled in the same manner as for the tumour-free model in Section 3.3.3.1 and had a final purity of >95% and a specific activity of 1-2 MBq/nmol. As shown in Figure 3.20 the radiolabelled G3 DARPin successfully targeted the tumour, with tumour to blood ratios of 175 ±26 at 4 hour and 344 ±161 at 24 hours. The uptake profile in the remaining organs remained consistent with that of the non-tumour baring model.

A

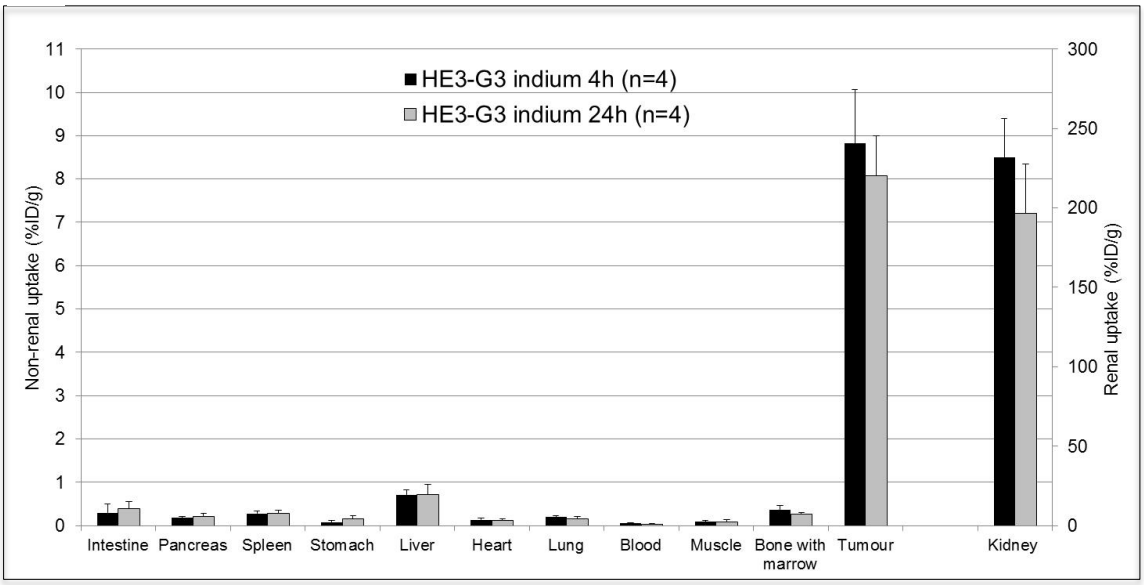

B

	$(HE)_3$-G3 (Tumour : Tissue ratio)			
Tissue	4 hours		24 hours	
BL	175	± 26.1	344	± 161
HE	69.3	± 25.2	66.5	± 8.10
LU	46.4	± 12.6	60.8	± 24.9
LI	12.4	± 1.80	12.0	± 3.60
PA	50.1	± 15.3	41.5	± 12.7
SP	32.3	± 9.60	28.6	± 5.00
KI	0.04	± 0.01	0.04	± 0.01
SO	149	± 91.1	67.5	± 46.6
INS+	39.4	± 21.1	21.8	± 5.10
MU	114	± 55.5	106	± 51.7
BO	25.9	± 8.30	28.1	± 2.70

FIGURE 3.20. Biodistribution of ^{111}Indium radiolabelled $(HE)_3$-G3 DARPin in a tumour bearing model.
HER2-positive human breast tumours derived from the cell line BT474 in female SCID-beige mice. (n=4)
A, Bio-distribution of ^{111}In-$(HE)_3$-G3. Uptake is presented as the mean % ID/g ±SD.
B, Table of tumour to normal tissue ratio at 4 and 24 hours post administration with indium radiolabelled DARPin.

3.3 Discussion

As with all targeting agents the principle of highly specific binding with low/no non-specific interaction is key to their successful application and as such any means to reduce that background binding/localisation would be highly sought after. Tolmachev *et al*. (2010) first purported, using another targeting scaffold protein termed Affibody, that different purification tags elicit varying effects on the biodistribution of proteins. Tolmachev and co-workers showed that the negatively charged $(HE)_3$-tag performed far better in uptake experiments than the His_6- and tag-less variants. To determine if this was the case for DARPins, G3 constructs were produced containing either a His_6-tag, $(HE)_3$-tag or with no tag (cleavable tag) and the biodistribution assessed within a mouse model.

The biodistribution studies established that as with the Affibodys the $(HE)_3$- tagged G3 DARPin was also superior to the no-tag or hexahistidine tagged variants (Goldstein *et al*, 2015). Consequently the superfluous Glycine-Proline (GP) residue, present for HRV 3C protease cleavage and kept as a constant for the tagged constructs, was removed and the now direct $(HE)_3$ tagged G3 was successfully cloned and expressed in *P. pastoris, X33*. All tested clones expressed and clone 6 was taken forward for high cell density (HCD) fermentations based on the qualitative observation of SDS-PAGE band intensity.

3.4 Conclusion

Although the $(His)_6$ tag is an excellent first capture step for IMAC purification of recombinant proteins, it can nevertheless have unwanted effects such as the modification of biodistribution. As a result, the aim of this chapter was to compare the regulatory standard, untagged product with a His_6 -tagged G3 and $(HE)_3$ – tagged G3.

To this end five DARPin constructs were cloned and expressed within a *P. pastoris* system, namely EAEA$(His)_6$-G3, EAEA$(HE)_3$-G3, KR$(His)_6$-G3, KR$(HE)_3$-G3, and Cleavable-G3. After successful cloning and expression of these constructs, the effect of the purification tag on DARPin biodistribution was subsequently assessed using an *in vivo* non-tumour bearing mouse model. The model indicated that radiolabelled $(HE)_3$-tagged G3 out performed both the tag-free and His_6- tagged DARPins in terms of overall favourable biodistribution, which would result in lower background signal and better imaging.

Given that HER2 positive breast cancer can metastasise to the liver, non-specific radiolabelled DARPins would be undesirable as it would affect imaging accuracy. Indium labelled $(HE)_3$-

DARPin had far lower liver uptake at both 4 hours (1.57% ID/g) and 24 hours (1.05% ID/g) post-administration than both the His_6- (3.72 and 3.45% ID/g) and untagged- G3 (4.31 and 3.06% ID/g). Given the aforementioned positive properties of the $(HE)_3$-tag, this construct was chosen for subsequent experiments within a HER2 positive tumour bearing mouse model. The use of this mouse model revealed similar biodistribution of the radiolabelled $(HE)_3$-tagged G3 DARPin to that of the non-tumour bearing mouse model and achieved high a high tumour to blood ratio.

In conclusion, this pilot study indicated that the presence of a His_6 tag did not affect normal tissue uptake, as there was no statistical difference in bio-distribution of the His_6 tagged and untagged G3. Additionally, the $(HE)_3$ tagged DARPin was significantly superior to both the untagged and His_6 tagged variants in both non-tumour bearing and tumour bearing mouse models. Thus, the $(HE)_3$ tagged DARPin was selected as the lead product for the next stage of development. The work formed the basis of a peer-reviewed publication (Goldstein *et al*, 2015) given in appendix 3 and outlined in Figure 3.21.

Finally, the removal of *Ste13* cleavage site (EAEA) allowed for the production of DARPin with a homogenous N-terminal domain. The next chapter involved the evaluation of the final G3 protein design.

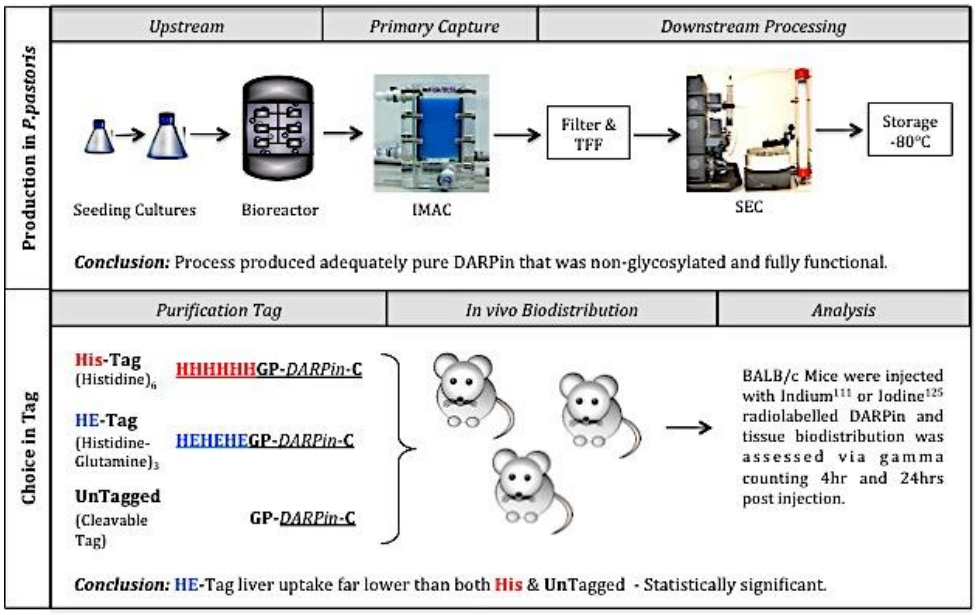

FIGURE 3.21: Schematic overview of production process and affinity tag bio-distribution analysis described in Goldstein *et al*, 2015.

CHAPTER FOUR

PROTEIN DESIGN AND DEVELOPMENT FOR CLINICAL GRADE MANUFACTURE

4.0 Protein design and development for clinical grade manufacture.

4.1 Introduction

The pilot study had identified a lead G3 DARPin and had shown the feasibility of DARPin manufacture in *P. pastoris*, however, the inclusion of the GP moiety that was used for HRV 3C protease cleavage was now redundant. This chapter aimed to construct a GP-free variant, by removing the superfluous GP and creating a direct $(HE)_3$ tagged G3. As with any change to a product it is essential to test if there are any differences between the new $(HE)_3$-DARPin and the previously studied (GP containing) DARPin to provide the best possible support for the decision on which DARPin to select for GMP production and ultimately for the first-in-human whole body clinical imaging trial.

Aim:

To construct and perform an initial assessment, in terms of expression and functionality, of a GP-free $(HE)_3$-tagged G3 ($(HE)_3$-G3) in *P. pastoris*.

Objectives:

- To clone a GP-free anti-HER2 DARPin with an N-Terminal $(HE)_3$-Tag and a C-Terminal free Cysteine for site specific labelling (HEHEHE-DARPin-C), $(HE)_3$-G3.
- To express and purify the $(HE)_3$-G3 from *P. pastoris*.
- To assess the final product in terms of molecular weight, binding affinity and bio-distribution.

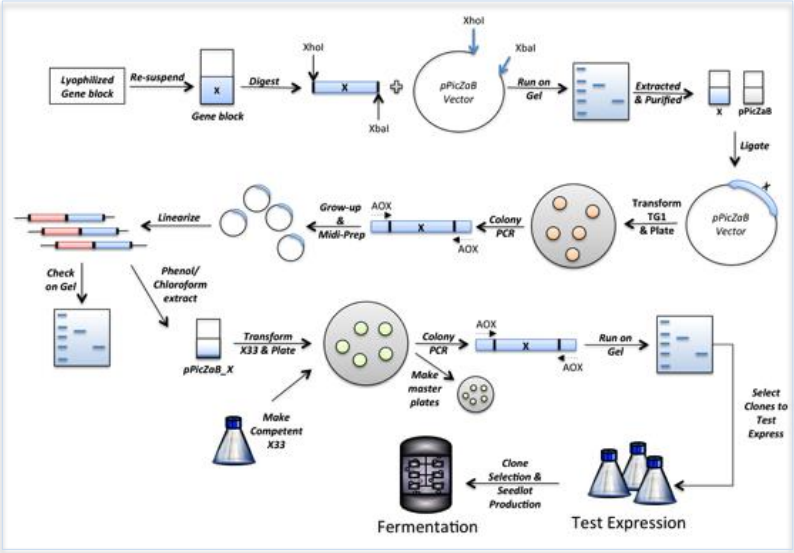

FIGURE 4.0. Overview of the procedures used in the production of the anti-HER2 DARPin in *P. pastoris*.

4.2 Construction of Expression Plasmid pPICZαB-$(HE)_3$-G3

4.2.1 Expression Plasmid pPICZαB-$(HE)_3$-G3

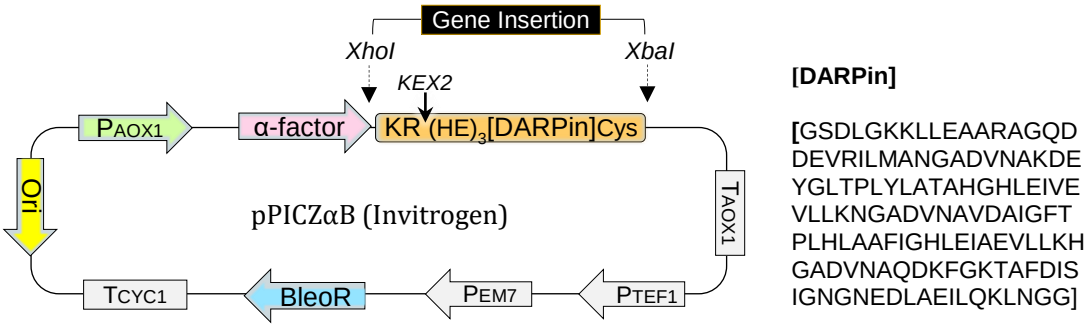

FIGURE 4.1. A schematic depiction of expression vector pPICZαB with $(HE)_3$-G3 insert.

Processing of the leader sequence to the mature protein takes place at a consensus sequence (KR) and is performed by the *P. pastoris* protease Kex2. The expression plasmid contains a sequence encoding this site just adjacent to the gene of interest. The gene sequence was checked for any internal KR sites as they could result in the disadvantageous cleavage of the product. As demonstrated in the above schematic (Figure 4.1) the G3 DARPin contains no internal Kex2 cleavage sites and therefore no modification of the sequence is required.

4.2.2 XbaI and XhoI digested pPICZαB plasmid & G3 gene block

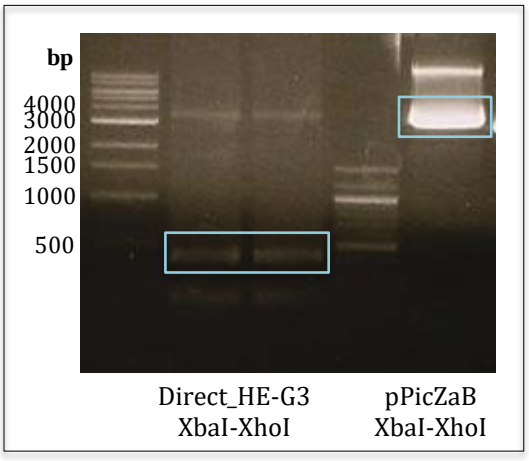

FIGURE 4.2. Agarose gel (1.5%) showing the *XhoI* & *XbaI* restriction digest of both the $(HE)_3$-G3 gene block and the *P. pastoris* expression vector pPICZαB. The digested products to be excised are highlighted by blue rectangles.

The pPICZαB plasmid (3597 bp) and the DNA encoding the $(HE)_3$-G3 (~450 bp) were digested by restriction enzymes *XbaI* and *XhoI*. The digests then underwent gel electrophoresis on a 1%

agarose gel (Figure 4.2) and the bands of appropriate size excised and gel purified for subsequent ligation.

4.2.3 Electroporation & Overnight Culture of transformed NEB5-alpha Cells

Bacterial cells, NEB5-Alpha, transformed with the ligated vector pPICZαB_$(HE)_3$-G3 were identified using antibiotic mediated selection. There were approximately 20 colonies per LSLB/Zeocin (25 µg/mL) plate, which had been able to grow as a result of the resistance inferred by the *Sh ble* gene present within pPICZαB DNA.

4.2.4 PCR identification of Positive Clones

The successful construction of a pPICZαB expression vector encoding the gene for $(HE)_3$-G3 was demonstrated by colony PCR with AOX-3'(5'- GCAAATGGCATTCTGACATCC -3') and AOX-5'(5'- GACTGGTTCCAATTGACAAGC -3') primers yielded a band of approximately 800 base pairs, corresponding to the expected size of pPICZaB_HE-G3-Cys vector, in all of the five tested colonies, Figure 4.3.

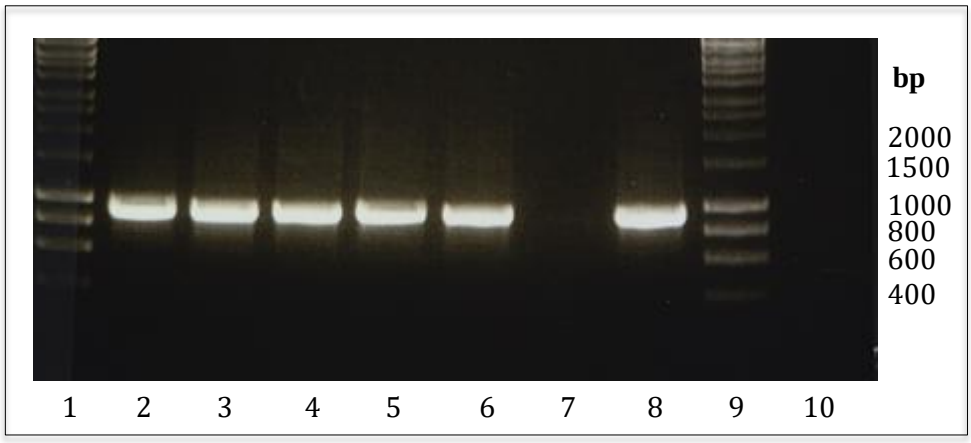

FIGURE 4.3: Agarose gel (1%) showing PCR colony screening for the identification of transformed bacterial clones positive for the pPICZαB_$(HE)_3$-G3 construct.
1. 1kb Ladder, **2-6**. Clones 1 to 5 (*E.coli* NEB-Alpha:: pPICZαB_G3), **7.** Reaction Mixture without Cells, **8.** Reaction mixture plus parental plasmid, **9**. 1kb Ladder, **10**. Clone 1 PCR reaction without primers.

4.2.5 Sequencing of Plasmids Derived from PCR identified Clones

DNA sequencing using the AOX sense and anti-sense primers further validated the correct insertion of G3 cDNA with all sequenced clones (1-5) displaying full length appropriate DNA.

For further analysis Clone 1 was taken forward and the plasmid fully sequenced in both directions (Figure 4.4). Twenty primers were designed to ensure that each area of the vector was covered at least twice in both the 5' prime and 3' prime direction. This allowed for a thorough coverage of the plasmid with the knowledge that any primer resulting error such as a misread could be ruled out.

The molecular biology program SnapGene® was used to create a template vector using the published sequence of pPICZαB with the DARPin sequence appropriately inserted within the multiple cloning site.

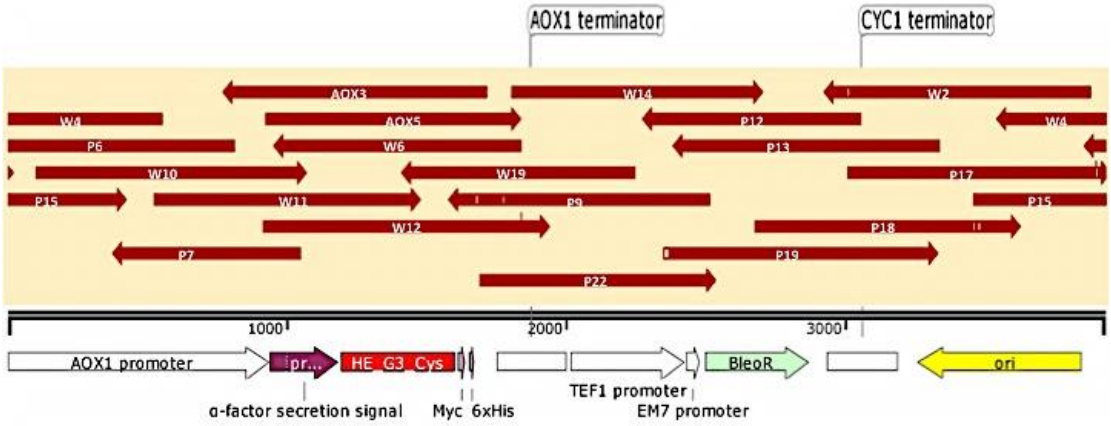

FIGURE 4.4: Whole plasmid sequencing of expression vector $(HE)_3$-G3.

Following whole plasmid sequencing there were found to be deviations in the pPICZαB vector sequence from that of the published model. Whilst the gene encoding the DARPin was as expected the mutations, deletions and additions found in the expression vector had to be further assessed. A new stock of pPICZαB was ordered from Invitrogen and underwent sequencing as previously stated. This generated the 10 identical 'errors' present within the DARPin pPICZαB expression vector (highlighted in Figure 4.5) and demonstrated that these mutations were not a result of the cloning and handling of the vector but generated by the manufacturers themselves.

FIGURE 4.5. Comparison of the published invitrogen pPICZ*α*B sequence versus the actual sequence of the supplied vector.
Origin of replication; (3702): G to A and (3456-7): AT to TA mutation.
TEF1 promoter; (2266-7): Insertion of A, (2278-9) & (2294-5): AG to GA mutation, (2303-4) Insertion of C.
Adjoining sequence between TEF1 and EM7 promoters; (2428): Deletion of a G.
Adjoining sequence between BleoR and CYC1 terminator; (2885): Deletion of a G, (2891-2): Insertion of G, (2900): C to G mutation.

4.3 Transformation and Test Expression of HE-G3-Cys in *P. pastoris*

4.3.1 Amplification and PmeI linearization of pPICZaB_G3

50 mL of overnight culture inoculated with clone 1 was divided in two and midi-prepped (Qiagen) yielding 1200 ng/µL of pPICZαB_$(HE)_3$-G3. The expression plasmid (10 µg) was then linearized with restriction enzyme *PmeI*, chloroform extracted and transformed into the methylotrophic yeast, *P. pastoris X33.*

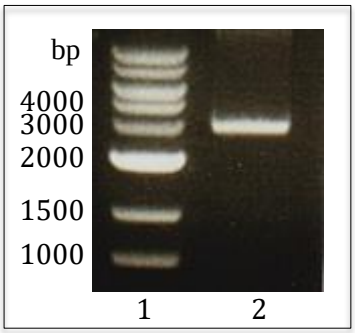

FIGURE 4.6 Agarose gel (1%) depicting the *PmeI* restriction enzyme digest of vector pPICZαB_$(HE)_3$G3.
1. 1kb Ladder, **2.** *PmeI* cut Clone 1 (pPICZαB_G3)

4.3.2 Transformation of Competent X33

The linear pPICZαB_$(HE)_3$-G3 construct (Figure 4.6) was transformed into freshly prepared electro-competent *P. pastoris X33* cells. There were greater than 100 colonies/plate demonstrating resistance to 100 µg/mL Zeocin™. Colony PCR using the AOX-5' and AOX-3' primer set on 10 colonies confirmed the integration of the G3 DARPin coding sequence into the genome (Figure 4.7).

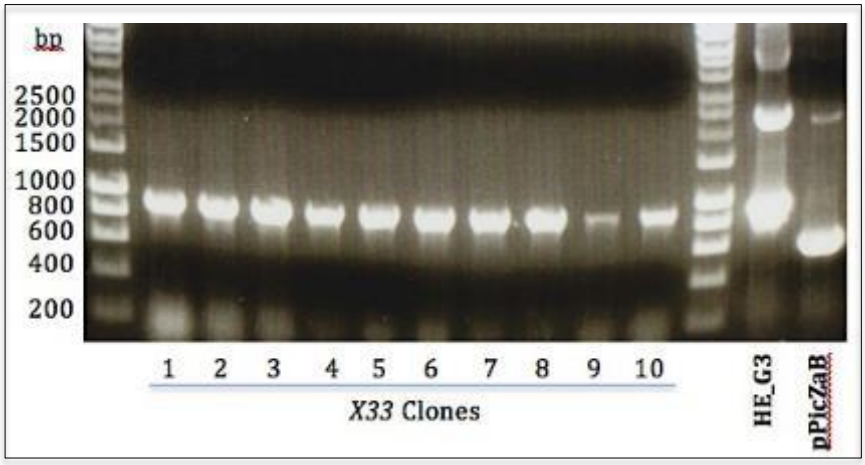

FIGURE 4.7 Agarose gel (1%) showing the PCR of *X33* Colonies transformed with pPICZaB_Direct_$(HE)_3$_G3 using AOX sense and anti-sense primers.
Empty vector (pPICZαB) and vector carrying the G3 gene (pPICZαB_$(HE)_3$-G3) were used as controls.

4.3.3 Shake Flask Expression of Transformed X33 *cells*

Transformants positive for the construct pPICZαB_$(HE)_3$-G3 were cultured in shake flasks and DARPin production assessed. The culture supernatant following cellular clarification was subjected to SDS-PAGE analysis (Figure 4.8). A distinctive band is at its most prominent 48hrs post-MEOH induction of an apparent MW of 14 kDa. Western Blot using polyclonal serum from immunized mice verified the identity of this band to be that of G3. All tested clones appeared to express the anti-HER2 DARPin with clone 6 chosen as lead clone.

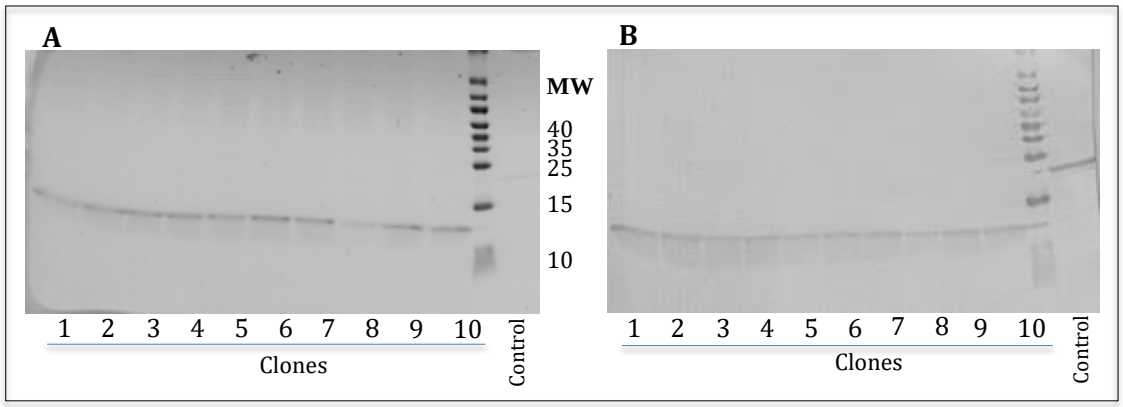

FIGURE 4.8 SDS-PAGE (A) and Western Blot (B) analysis of 10 *X33* colonies positive for the pPICZ*α*B Direct_$(HE)_3$_G3 construct.
Samples run were from 48 hours post MEOH induction 4xSDS-PAGE reducing buffer and 18% Tris-Glycine gel were used. Another DARPin previously known to express in *P. pastoris* was used as a inducible positive control. **(B)** Mouse anti-DARPin primary and sheep anti-Mouse-HRP secondary.

4.3.4 10L Bioreactor Test Expression

Clone 6 was chosen and taken forward for high cell density fermentation. A 10-L Bioreactor used at a 5-L working capacity was inoculated with seeding culture. A fed-batch glycerol feeding strategy was employed to reach a high cell density prior to methanol induction, as described in further detail in Section 4.4.

Highly defined minimal media that is free of animal derived constituents meets regulatory requirements and ensures batch to batch consistency. By and large the most well established media formulation for *P. pastoris* is the minimal salt solution, BSM (Basal salts medium) developed by Invitrogen. In this minimal format the organism will grow at a slower rate than the complex media, YPD, BMGY and BMMY used in the shake flask growth and test expressions.

Samples were taken at 0, 2, 4, 7, 9 and 24 hours post methanol induction (10 mL), clarified via centrifugation, then the supernatant was isolated, mixed with reducing buffer (4x) and run on 16% SDS-PAGE gel (Figure 4.9).

Bioreactor test expression indicated the presence of protein at the appropriate molecular weight of approximately 14 kDa from as early on as 2 hours post methanol induction. During the course of the next 22 hours there was a steady increase of a lower molecular weight protein than that of the full length product. Western blot probed with polyclonal anti-DARPin identified this protein to be of DARPin origin. Therefore this DARPin fragment, of approximately 10-12 kDa, could be the result of proteolytic cleavage of the G3 DARPin or an internal ribosomal reading site. Further experiments would be required to determine the origin and therefore mechanism at work.

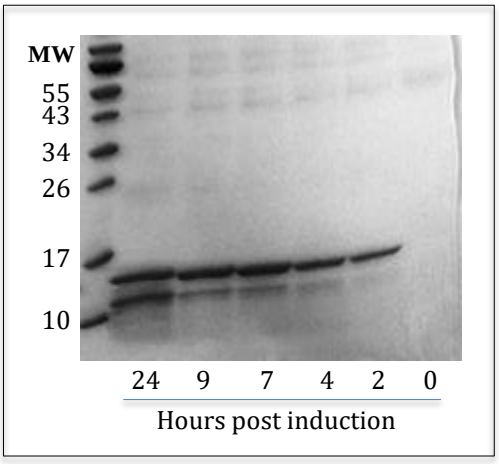

FIGURE 4.9: Expression of $(HE)_3$-G3 in *X33* (Clone 6) during HCD fermentatin.
16% SDS-PAGE gel was run under reducing conditions and stained with Coomassie blue. Samples of clarified supernatant taken from the point of dO_2 spike to 24 hours post induction with methanol were assessed.

4.4 Bioreactor Harvest and Purification

Given the rate of breakdown demonstrated in Section 4.3.4 a short induction time of 4 hours, 1 hour on methanol limited feed, was employed.

The bioreactor (5-L working volume) was inoculated with 300 mL of a 24 hour pre-culture to give a starting OD_{600} of 0.2. The vigorous and continuous aeration of the culture media was enforced by sparging the bioreactor with air at a flow rate of 10 LPM.

A PID cascade system was set up to maintain 30% air saturation by automatically increasing or decreasing the agitation speed (500-1000 rpm) until this DOT set point was reached. When the airflow became limited pure oxygen was also added to the culture media. As demonstrated in Figure 4.10 it took just under 17 hours of cell growth to deplete the dO2 to 30% and initiate the PID cascade, gradually increasing the agitation speed from 500 to 1000 rpm over the course of 4.5 hours. Increased use of base to maintain a pH of 5 is also notable correlating with the increase in biomass, respiration and hence acidic by-products, which lower the pH of the culture environment.

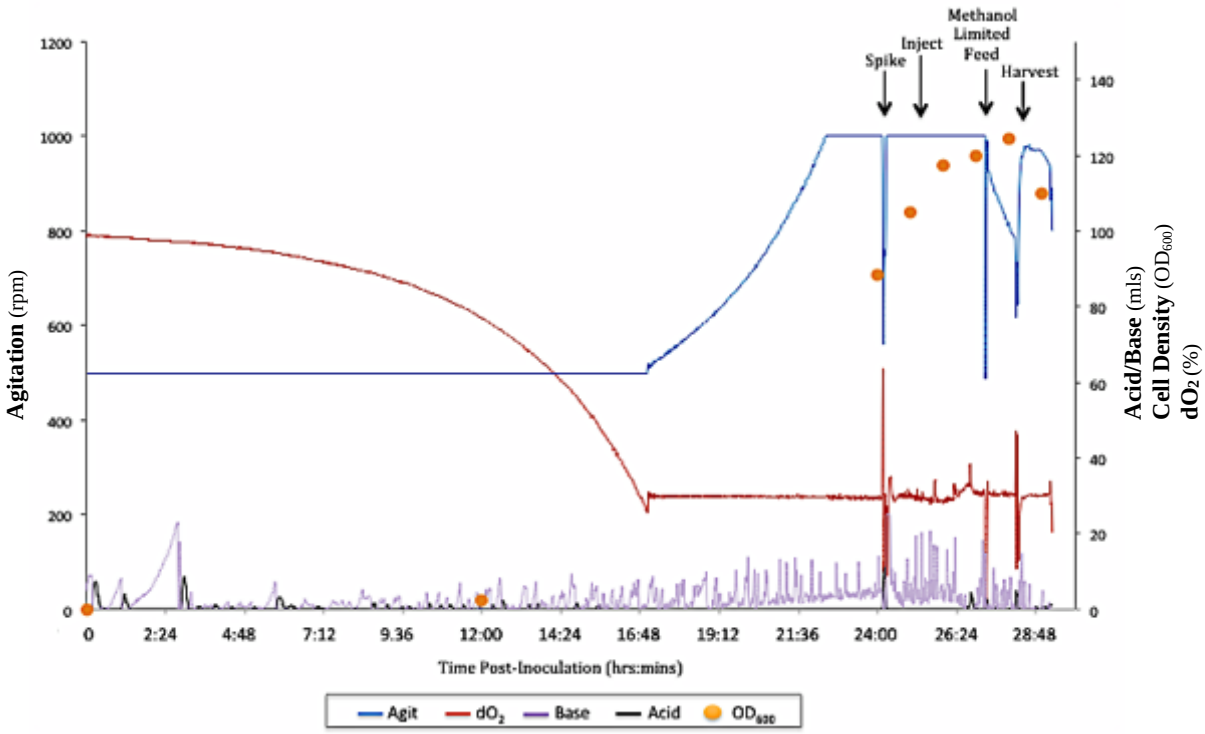

FIGURE 4.10: Fermentation trace in 10L New Brunswick bioreactor.

Agit, Agitation; **dO_2**, Dissolved oxygen concentration; **Base**, Ammonium hydroxide; **Acid**, Phosphoric Acid; **OD_{600}**, Optical density at 600nm.

At 24 hours post inoculation (OD_{600} of ~85 / 28 g/L DCW) the dO_2 concentration spiked and the agitation plummeted indicating the decrease of respiratory activity as a result of complete carbon source consumption. This marks the end of the glycerol batch phase and the start of the glycerol fed-batch phase. At this point the pH is increased from 5 to 6.5 and the glycerol feed is initiated at a starting rate of 100 g/hr gradually decreasing over 4 hours to a final rate of ~20 g/hr (OD_{600} of 120) before transfer to the methanol limited feed. 10 mL of methanol is injected into the bioreactor 1 hr post glycerol fed batch initiation to prime the culture for transfer onto methanol and begin recombinant protein induction. The methanol limited feed was introduced at a rate of 20 g/hr and maintained until fermentation harvest commenced 1 hour later (28 hours post inoculation) at a cell density of approximately 125 at 600nm.

The controlled conditions facilitated by a bioreactor allowed for high viable cell density and consequently high levels of secreted DARPin as shown in Figure 4.11.

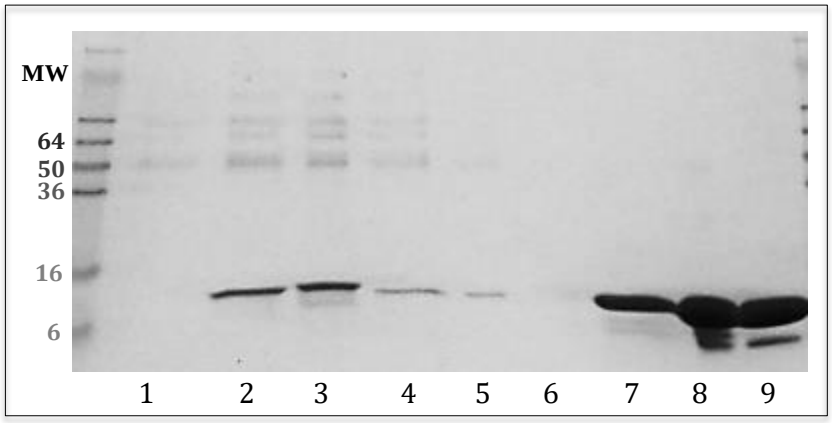

FIGURE 4.11: SDS-PAGE analysis of a high cell density fermentation and subsequent 1hr post MEOH limited feed, capture and purification of *X33* pPICZaB_$(HE)_3$-G3-Cys.
1. dO_2 spike, **2.** 1hr pre MEOH limited feed, **3.** Harvest point (1hr post MEOH limited feed), **4.** 2-L FT, **5.** 4-L FT, **6.** 5-L Wash, **7.** Ni-IMAC eluent, **8.** TFF, **9.** SEC (Final product).

The secreted $(HE)_3$-tagged DARPin was captured directly from the un-clarified broth using radial flow nickel immobilized metal ion chromatography. The use of a 125 mL radial flow system (Proxys) combined with IDA Chelating Cellthru™ BigBead (300-500µm) technology (Sterogene) allowed for the successful application of crude whole cell broth thereby circumventing the need for solid/liquid clarification events.

Following capture the $(HE)_3$-tagged DARPin was competitively eluted from the column using 200 mM imidazole and applied to a Millipore TFF system (5 kDa cut off) for concentration to approx. 30 mL and dialysis into PBS. The protein was then applied to a size exclusion chromatography (SEC) column containing 500 mL of Superdex 75 for size-based purification.

4.5 Assessment of Final Product in *P. pastoris*

4.5.1 HER2 Binding of G3

Binding of G3 to the HER2 receptor was verified by ELISA. Purified $(HE)_3$-G3 was captured by its cognate antigen HER2 in the micro titre plate and subsequently probed with antibody to DARPin. Results, shown in Figure 4.12, demonstrate specific binding of $(HE)_3$-G3 to the extracellular domain of the HER2 receptor.

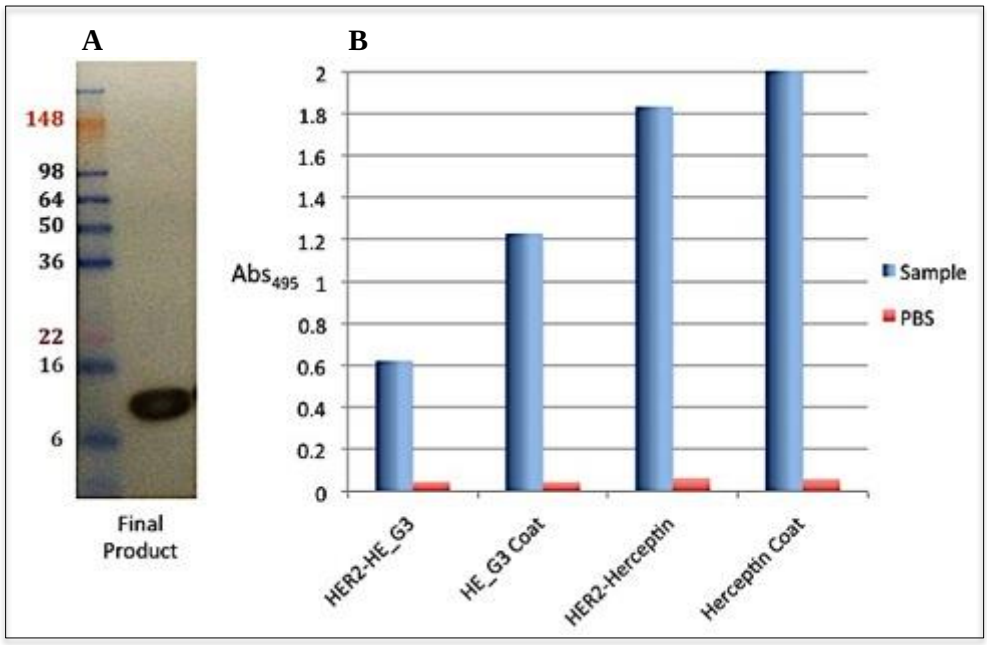

FIGURE 4.12. Detection and Analysis of Anti-HER2 DARPin using polyclonal mouse serum.
A. ECL western blot analysis. 18% SDS-PAGE. 2µL of final product loaded in 4x reducing buffer. Polyclonal mouse serum used at 1:1000 1hr incubation. **B.** ELISA Detection of G3 DARPin. **HER2-HE_G3,** Wells were coated with 1µg/mL HER2, G3 was applied at a concentration of 5µg/mL and detected using polyclonal mouse serum (1:1000) followed by anti-mouse-IgG-HRP. **HE_G3 Coat,** G3 was used to coat the well (5µg/mL) and detected using polyclonal mouse serum (1:1000) followed by anti-mouse-IgG-HRP. **HER2-Herceptin,** Wells were coated with 1µg/mL HER2, Herceptin was applied (5µg/mL) and detected using anti-human-IgG-HRP (1:4000). **Herceptin Coat,** Herceptin (5µg/mL) coated wells detected using anti-human-IgG-HRP (1:4000).

4.5.2 Affinity of Current Batch to Previous Batches of G3

Surface plasmon resonance (SPR) analysis was performed to investigate the reactivity of the extracellular domain of HER2 with the purified *P. pastoris* produced DARPin in comparison with previous *E.coli* batches. Results showed that, in these experiments, the *P. pastoris* GP-free DARPin (K_D 3.59E-10 M) bound to the receptor in the same manner as the previous *E.*

coli DARPin (K_D 2.34E-10 M) and P. pastoris GP- containing DARPin (K_D 1.84E-10 M) as noted by the K_D which in all cases was in the low picamolar range (Table 4.0).

Table 4.0. Comparison of SPR data of the anti-HER2 DARPin G3 (with and without GP site) produced in *P. pastoris* to the previously produced anti-HER2 DARPin using the then standard *E.coli* method.

	Previous batches of G3	*P. pastoris* G3 (with GP)	*P .pastoris* G3 (No GP)
K_{ass} [$M^{-1}s^{-1}$]	6.64E+05	1.0E+06	8.42E+05
K_{diss} [s^{-1}]	1.55E-04	1.9E10-4	3.02E-04
K_D [M]	2.34E-10	1.84E-10	3.59E-10

4.5.3 Product Molecular Weight

The glycosylation status of the produced $(HE)_3$-G3 was assessed using mass spectrometry. *P. pastoris* N-linked glycosylation occurs on asparagine with the consensus sequence N-X-S/T and these sites were not present within the DARPin. O-Linked Glycosylation could not be ruled out. Mass Spectrometry identified the *P. pastoris* produced DARPin to be 14358 Daltons coinciding directly with the expected (theoretical) molecular weight, Figure 4.13A. Analytical SEC of the product pool generated a tight single peak on the chromatogram, 4.13-B

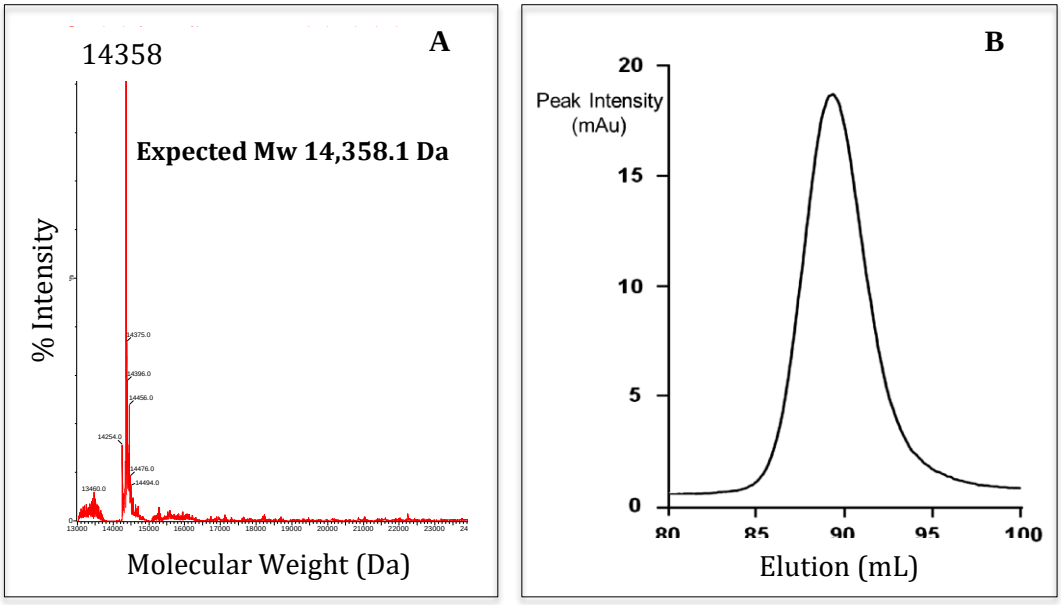

FIGURE 4.13. Analysis of the Final Product.
A. MALDI Mass Spectrometry of $(HE)_3$-G3. The determined molecular weight of the protein mirrored that of the anticipated MW of 14358 Da. **B.** Analytical Superdex75 SEC trace of $(HE)_3$-G3.

4.5.4 Biodistribution; $(HE)_3$-G3 vs. $(HE)_3$-GP-G3

The $(HE)_3$-G3 and $(HE)_3$-GP-G3 DARPin constructs were sent for biodistribution studies to L. Baltzer (Uppsala University). Immuno-competent mice were used in this study to compare normal tissue uptake, which included radiolabelling, control of specific radioactivity, radiochemical purity and control of DARPin purity by SDS-PAGE. Throughout all of this work frequent controls of DARPin quality and radiolabelling efficiencies were conducted using SDS-PAGE and HPLC with a radio-detector.

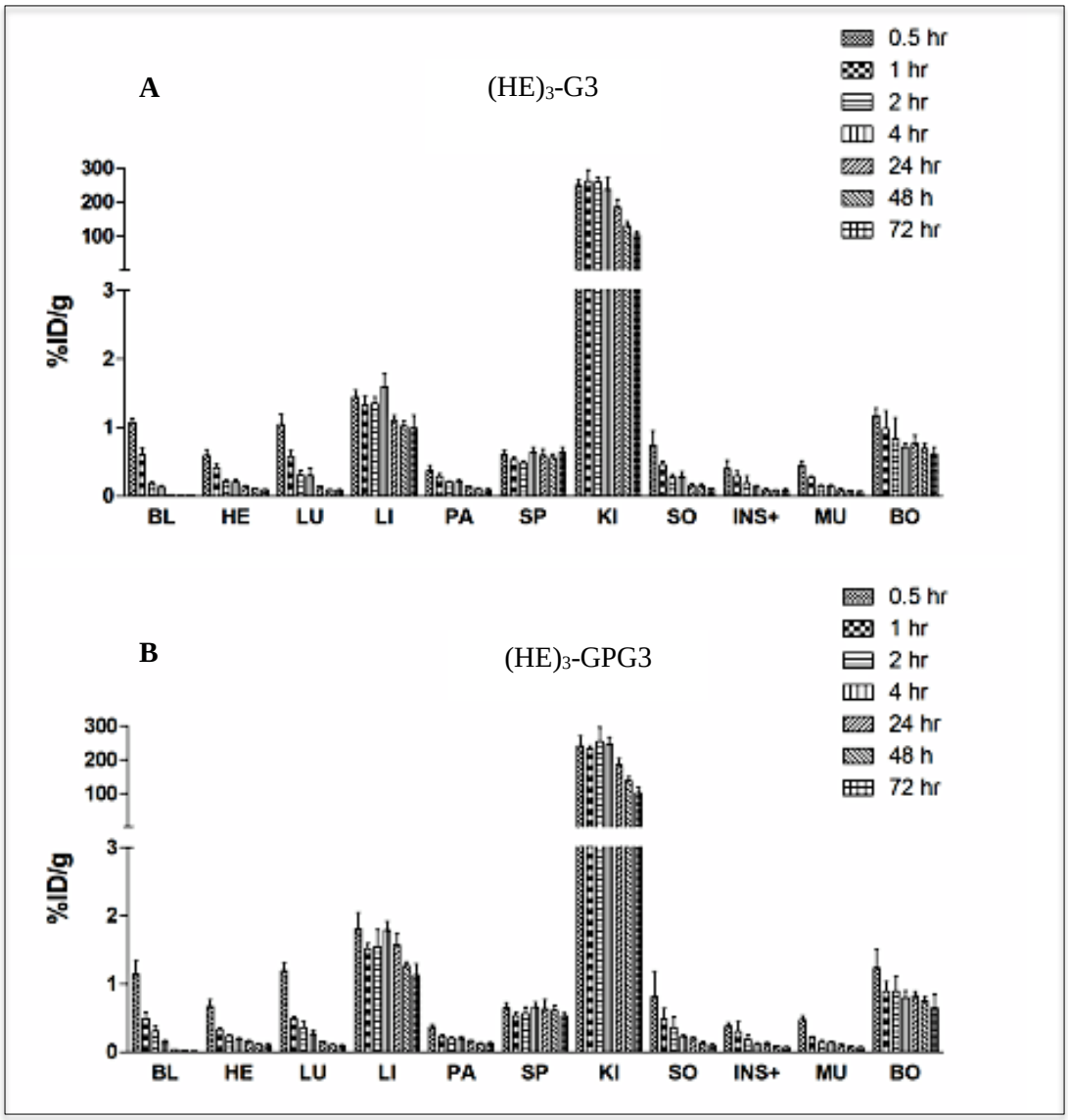

FIGURE 4.14: Distribution of HE_3-G3 DARPin and HE_3-GP-G3 DARPin, in 28 + 28 NMRI mice, monitored over a total of 72 hours.
The mice were injected unsedated with 1 µg of radiotracer with ex vivo organ distribution assessed at 0.5, 1, 2, 4, 24, 48 and 72 hours p.i. (n=4). (Table X) Weights of mice were 25±2g.

BL, *Blood*, **HE**, *Heart*, **LU,** *Lungs*, **PA**, *Pancreas*, **SP**, *Spleen*, **KI**, *Kidney*, **SO**, *Stomach*, **INS+**, *Intenstine with content*, **MU**, *Muscle*, **BO**, *Bone & Marrow*.

Table 4.1 Biodistribution values (%ID/g +/-SD) for GP containing and GP-Free variants of G3 DARPin.

The mice were injected unsedated with 1 μg of radiotracer with ex vivo organ distribution assessed at 0.5, 1, 2, 4, 24, 48 and 72 hours p.i. (n=4). Weights of mice were 25 ± 2 g.

	0.5hr		1hr		2hr		4hr		24hr		48hr		72hr	
Tissue	GP	No GP	GP	No GP	GP	No GP	GP	No GP	GP	No GP	GP	No GP	GP	No GP
BL	**1.14** ± 0.17	**1.08** ± 0.06	**0.49** ± 0.08	**0.60** ± 0.09	**0.31** ± 0.07	**0.18** ± 0.02	**0.14** ± 0.02	**0.13** ± 0.02	**0.03** ± 0.00	**0.02** ± 0.00	**0.02** ± 0.00	**0.01** ± 0.00	**0.01** ± 0.00	**0.01** ± 0.00
HE	**0.67** ± 0.08	**0.59** ± 0.07	**0.33** ± 0.03	**0.41** ± 0.06	**0.24** ± 0.02	**0.22** ± 0.01	**0.19** ± 0.02	**0.21** ± 0.03	**0.16** ± 0.01	**0.14** ± 0.02	**0.12** ± 0.01	**0.11** ± 0.00	**0.10** ± 0.02	**0.10** ± 0.01
LU	**1.20** ± 0.10	**1.04** ± 0.14	**0.48** ± 0.03	**0.58** ± 0.08	**0.36** ± 0.08	**0.30** ± 0.06	**0.27** ± 0.04	**0.30** ± 0.10	**0.15** ± 0.01	**0.14** ± 0.01	**0.10** ± 0.01	**0.09** ± 0.00	**0.09** ± 0.01	**0.09** ± 0.01
LI	**1.81** ± 0.21	**1.45** ± 0.08	**1.52** ± 0.07	**1.33** ± 0.12	**1.54** ± 0.22	**1.35** ± 0.08	**1.78** ± 0.11	**1.59** ± 0.17	**1.57** ± 0.15	**1.11** ± 0.06	**1.26** ± 0.05	**1.02** ± 0.06	**1.13** ± 0.14	**1.00** ± 0.16
PA	**0.36** ± 0.03	**0.37** ± 0.07	**0.23** ± 0.03	**0.29** ± 0.03	**0.20** ± 0.02	**0.21** ± 0.01	**0.20** ± 0.03	**0.20** ± 0.03	**0.17** ± 0.01	**0.14** ± 0.01	**0.12** ± 0.01	**0.11** ± 0.01	**0.12** ± 0.02	**0.09** ± 0.01
SP	**0.64** ± 0.07	**0.61** ± 0.05	**0.53** ± 0.04	**0.53** ± 0.04	**0.57** ± 0.08	**0.49** ± 0.02	**0.66** ± 0.06	**0.65** ± 0.06	**0.63** ± 0.11	**0.59** ± 0.08	**0.61** ± 0.06	**0.56** ± 0.05	**0.53** ± 0.04	**0.64** ± 0.07
KI	**241** ± 25.5	**250** ± 14.1	**233** ± 7.56	**261** ± 29.2	**254** ± 36.3	**258** ± 11.3	**246** ± 17.5	**237** ± 29.9	**185** ± 15.9	**185** ± 19.3	**138** ± 10.8	**130** ± 10.8	**102** ± 15.5	**104** ± 8.07
SO	**0.81** ± 0.33	**0.74** ± 0.18	**0.48** ± 0.13	**0.46** ± 0.04	**0.36** ± 0.13	**0.27** ± 0.04	**0.23** ± 0.03	**0.29** ± 0.06	**0.20** ± 0.02	**0.16** ± 0.02	**0.13** ± 0.02	**0.14** ± 0.04	**0.10** ± 0.01	**0.11** ± 0.01
INS+	**0.38** ± 0.05	**0.40** ± 0.11	**0.30** ± 0.13	**0.29** ± 0.07	**0.18** ± 0.07	**0.19** ± 0.09	**0.12** ± 0.01	**0.14** ± 0.02	**0.13** ± 0.02	**0.10** ± 0.01	**0.08** ± 0.01	**0.08** ± 0.01	**0.07** ± 0.01	**0.08** ± 0.03
MU	**0.47** ± 0.05	**0.45** ± 0.06	**0.21** ± 0.02	**0.27** ± 0.02	**0.15** ± 0.02	**0.15** ± 0.01	**0.14** ± 0.01	**0.14** ± 0.02	**0.11** ± 0.01	**0.10** ± 0.02	**0.08** ± 0.00	**0.07** ± 0.01	**0.07** ± 0.00	**0.06** ± 0.01
BO	**1.24** ± 0.23	**1.17** ± 0.10	**0.89** ± 0.13	**0.98** ± 0.23	**0.67** ± 0.18	**0.84** ± 0.27	**0.80** ± 0.09	**0.72** ± 0.05	**0.82** ± 0.06	**0.76** ± 0.11	**0.74** ± 0.06	**0.69** ± 0.07	**0.65** ± 0.18	**0.62** ± 0.09

GP, Glycine-Proline containing DARPin HE-**GP**G3; **No GP**, Glycine- Proline free DARPin HE-G3.

BL, *Blood*, **HE,** *Heart*, **LU,** *Lungs*, **PA,** *Pancreas*, **SP,** *Spleen*, **KI,** *Kidney*, **SO,** *Stomach*, **INS+,** *Intestines with content*, **MU**, *Muscle*, **BO**, *Bone & Marrow*.

The results shown in Figure 4.14 and Table 4.1 showed no measureable differences in biodistribution between the two DARPins in non-tumour bearing mice and therefore demonstrated that the removal of the Glycine-Proline cleavage site did not affect normal tissue uptake.

4.5.5 Tumour imaging using $(HE)_3$-G3 DARPin radiolabelled with ^{111}In.

Single-photon emission computed tomography (SPECT) images were collected for six of the mice in the study and these showed large uptake in the kidneys but also clear identification of the HER2+ tumours for the $(HE)_3$-G3 DARPin. Images and a detailed biodistribution for one mouse (ID: nr15) with a HER2+ tumour are shown in Figure 4.15.

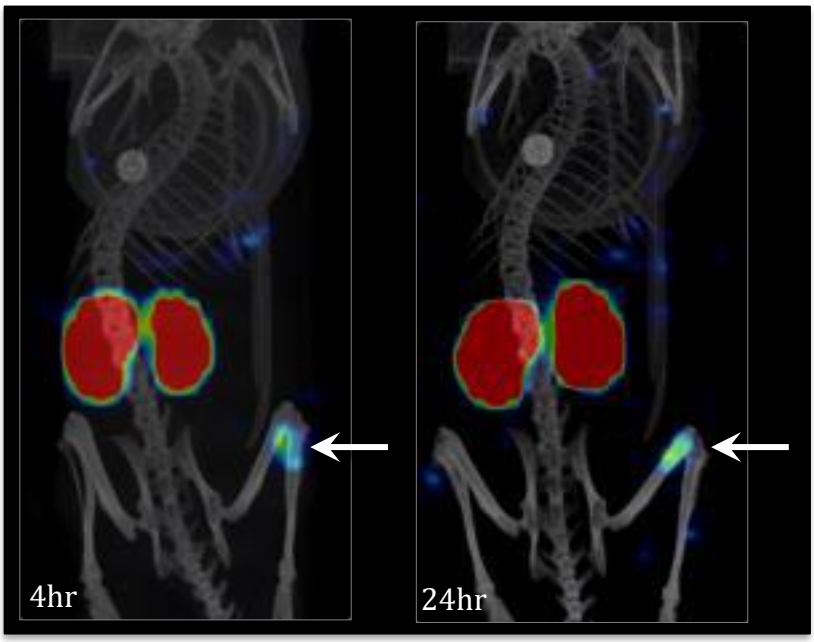

FIGURE 4.15: SPECT-CT of HER2+ Tumour bearing mice 4 hr and 24 hr post injection.

Balb/c nu/nu mice bearing a BT474 tumour mass were injected with 2µg of $(HE)_3$-G3-Cys DARPin radiolabelled with ^{111}In. The tumour is in the right lower back/leg and is indicated with an arrow. A large uptake can also be seen in the kidneys. The injected radioactivity was 2.27 MBq. After the second SPECT scan the mice were sacrificed and various organs dissected and their radioactivity measured.

The radioactivity uptake in the excised organs was expressed as a percentage of the injected dose per gram (%IDG) and is shown in the table below.

Organ	SPECT 24hr (%IDG)
Blood	0,033
Heart	0,122
Lung	0,226
Liver	1,632
Pancreas	0,676
Spleen	0,132
Kidney	127
Stomach	0,186
Intestine with Content	0,090
Muscle	0,067
Bone and Marrow	0,369
Tumour	6,456

4.5 Discussion

It was essential to test if there were any clinical differences between the new $(HE)_3$-DARPin and the previously studied (GP containing) DARPin. Biodistribution was assessed in both a non-tumour and HER+ tumour model in mice at 4 hours and 24 hours. The new $(HE)_3$-DARPin showed no notable difference from the previous GP engineered variant and as such demonstrated once again the that substitution of the His_6 tag of G3 DARPin with a negatively charged and hydrophilic histidine-glutamate $(HE)_3$ tag can reduce liver uptake whilst enabling tag mediated capture and purification via Ni^{2+}-IDA radial flow chromatography. In conclusion the $(HE)_3$-G3 DARPin is comparable in both *P. pastoris* expression and *in vivo* biodistribution to the GP-containing variant, $(HE)_3$-GPG3 and was also able to image HER2+ tumours in a mouse model. Therefore $(HE)_3$-G3 will be taken forward for the clinic as it does not have an unnecessary and potentially disadvantageous GP site.

P. pastoris is capable of complex post-translational modification such as the edition of sugar residues (glycosylation) this modification can present both positive and negative outcomes depending on the required product function (Love *et al*. 2018). Glycosylation of residues leads to a decreased half-life and rapid clearance of molecules in the blood (Jia *et al.* 2016). Mass spectrometry of the *P. pastoris* expressed product indicates no obvious N- or O-linked glycosylated residues on the G3 DARPin construct, with no increase in MW from the theoretical. From this it was concluded that the G3 product quality from *P. pastoris* expression did not deviate from that produced by the previous standard *E.coli* method or from the Glycine-Proline containing variant in terms of glycosylation state. SPR analysis also demonstrated that binding affinity to its cognate antigen, HER2, remained unaffected at picomolar affinity.

Finally, the *Ste13* cleavage site Xaa-Pro/Ala, which in literature had been shown to be responsible for n-terminal heterogeneity as a result of inefficient cleavage (Yang S. *et al.* 2013) proved true for the G3 DARPin. Generating multiple forms of G3 with partially, fully and unaltered N-terminal EAEA residues. In taking a product through to clinical trial homogeneity of the final protein therapeutic/agent is of great importance. To rectify this issue the *Ste13* cleavage site was removed and, as has been the case for a number of other recombinant proteins (Joshi *et al.* 2010; Prabha et al. 2009), its removal did not hamper the efficiency of secretion into the extracellular media and produced DARPin with a homogeneous N-terminal.

4.6 Conclusion

In order for HRV 3C protease cleavage to take place, Glycine-Proline (GP) moieties had to be included (Chapter 3). Given that the $(HE)_3$ tagged G3 DARPin had the most favourable biodistribution and was therefore chosen for future studies, the GP moiety became redundant. Consequently, the aim of this chapter was to construct a GP-free variant of the $(HE)_3$ G3 DARPin that would be suitable for subsequent GMP production and ultimately for the first-in-human whole body clinical imaging trial.

The specific objectives of this chapter were to clone, express and purify the $(HE)_3$-G3 from *P. pastoris* and validate the final GP-free $(HE)_3$-tagged G3 product in terms of molecular weight, binding affinity and biodistribution.

The binding propensity of the G3 DARPin to the extracellular domain of the HER2 receptor was verified by both ELISA and SPR analysis, demonstrating that the GP-free DARPin bound to HER2 in the same manner as the standard *E. coli* produced DARPin, with both proteins displaying K_D values in the picamolar range. The molecular weight of the product was identified via mass spectrometry and correlated directly with the expected MW of the GP-free DARPin at 14358 Daltons. Finally, the biodistribution analysis conducted in both non-tumour and tumour bearing mouse models showed that uptake of radiolabelled GP-free $(HE)_3$-tagged G3 DARPins was not affected by the absence of GP and was successfully used to image a HER2 positive tumour by SPECT/CT.

Based on the results from this chapter, the GP-free $(HE)_3$-tagged G3 DARPin was used for subsequent use for the generation of a clinical grade bioprocess for DARPin production.

CHAPTER FIVE

DESIGN AND CHARACTERISATION OF USP AND DSP CONDITIONS FOR A CLINICAL GRADE G3 DARPIN MANUFACTURING PROCESS

5.0 Design and characterisation of upstream and downstream conditions for a clinical grade G3 DARPin manufacturing process.

5.1 Introduction:

The production of recombinant therapeutics involves the use of multiple units of operation and consequently generates both process-related impurities and openings for product contamination. These factors need to be identified and taken into account so as to deliver a product of low risk and high quality.

The standard laboratory practice of a research / academic setting to that of a GMP compliant facility are very different in terms of both mentality and follow through. In research one assess a wide scope of parameters / experiments / methods in answer to a hypothesis. The processes and how they are undertaken is largely flexible and the answers generated dictate future work. Whilst in a GMP adhering environment the aim is to determine and employ a thoroughly documented methodology that is highly reproducible and without error. This in turn does translate to a process with rather strict and inflexible parameters in both design and implementation. This restrictive setting stems from the need to deliver a biopharmaceutical of exceptional purity and as such, from a regulatory standpoint, the bioprocess itself defines the product (Carta *et al.* 2010).

Aim:

To develop a GMP compliant bioprocess for the production and purification of DARPin in *P. pastoris*.

Objectives:

- Technology transfer to CIP Bioreactor for G3 production.
- Derive a GMP compliant DSP for purification of the anti-HER2 DARPin.
- Determine the yield of product, endotoxin and HCP throughout the developed bioprocess.
- Assess binding affinity and molecular weight of the product.

5.2 Scale up to cGMP compliant CIP Bioreactor

As laid out in the previous chapters all initial fermentations took place in the 10-L BioFlo 3000 Bioreactor (New Brunswick Scientific). Despite the conditions afforded by this bioreactor resulting in high expression of the product the levels of control, sterility and potential for scale up are limited.

The impracticality and sterility concerns raised in using an autoclavable bioreactor is evidenced from the facility layout, as depicted in Figure 5A. It is logistically unsuited for the transfer of what is large and heavy equipment to an external autoclave whenever a cleaning cycling is required. Secondly the process in itself would be putting the facility at greater risk of contamination. To this respect the technology transfer to a clean in place bioreactor which is scalable and falls within regulatory compliance was deemed very much necessary.

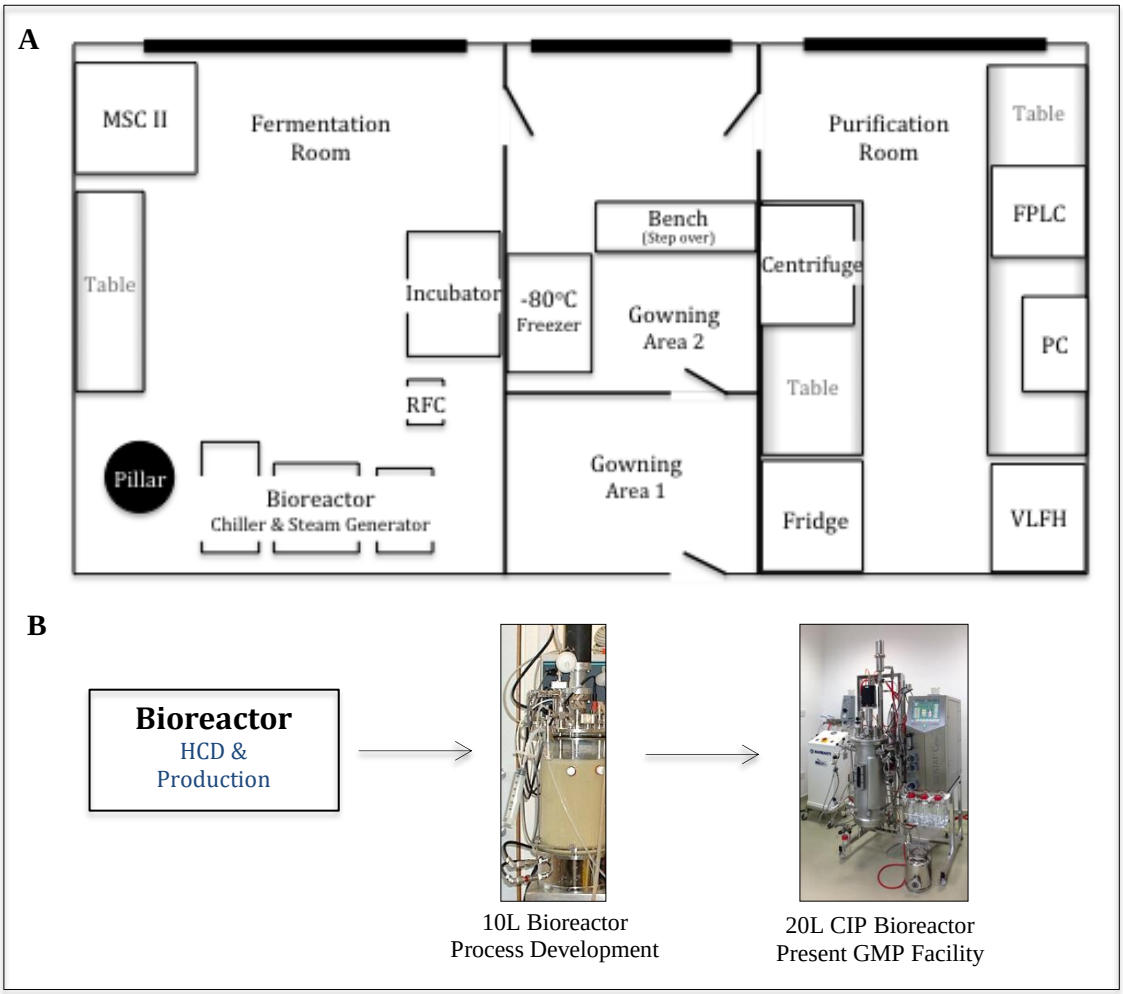

FIGURE 5.0: A. Layout of the Copley May Production Facility. B. Process development from 10-L Autoclavable Bioreactor to 20L Clean-in-Place system.
MSC II, Microbial Safety Cabinet (Class II), **RFC**, IMAC Radial Flow Column, **FPLC**, Fast Protein Liquid Chromatography, **VLFH**, Vertical Laminar Flow Hood, **PC**, Computer connected to FPLC.

The BIOSTAT® Cplus (Sartorius) is a 20-L stainless steel bioreactor that can be cleaned in place (CIP) using a steam generator. Ports can be re-sterilised following sampling, preventing the introduction of contaminants, a feature not possible using the BioFlo 3000.

The procedure previously used for DARPin production in the BioFlo 3000 vessel was adjusted and assessed under the BIOSTAT® Cplus bioreactor. Briefly 50 mL of YPD in a 250 mL flask was inoculated with 5 µl of frozen stock and grown for at least 16 hours at 30°C at 200 rpm. The following day 2 mL of primary culture was added to two 2-L shake-flasks containing 360 mL minimal media and grown overnight at 30°C 220 rpm. The fermenter was pre-equilibrated to the following set points prior to inoculation; pH 5, stirrer speed 500 rpm, temperature 30°C, dissolved oxygen 30%, air flow of 15 L/min and a pressure of 1.5 bar for both air and oxygen. The settings were placed on auto mode so that the dissolved oxygen would be controlled at 30% by firstly increasing the stirrer speed to a maximum of 1000 rpm and when reached by adding pure oxygen with air through the sparger. All 720 mL of the secondary culture at an OD_{600} ~6 was used to inoculate the bioreactor. As noted in Figure 5.1 we see the expectant trace starting with the consumption of the carbon source and cell growth depleting the dO_2 to 30% whereby the stirrer speed gradually increases to 1000 rpm to maintain the dO_2 at 30%. All the carbon source had been consumed at approximately 23 hours post inoculation and this is represented by a spike in the dissolved oxygen levels. At this point glycerol limited feed is initiated, pH adjusted to 6.5 and 15 mL of methanol introduced to the culture to prime for the transition to methanol limited feed. The glycerol is gradually tapered off and at 4 hours post dO_2 spike the culture is switched to methanol limited feed and allowed to grow for a further 1 hour before harvest.

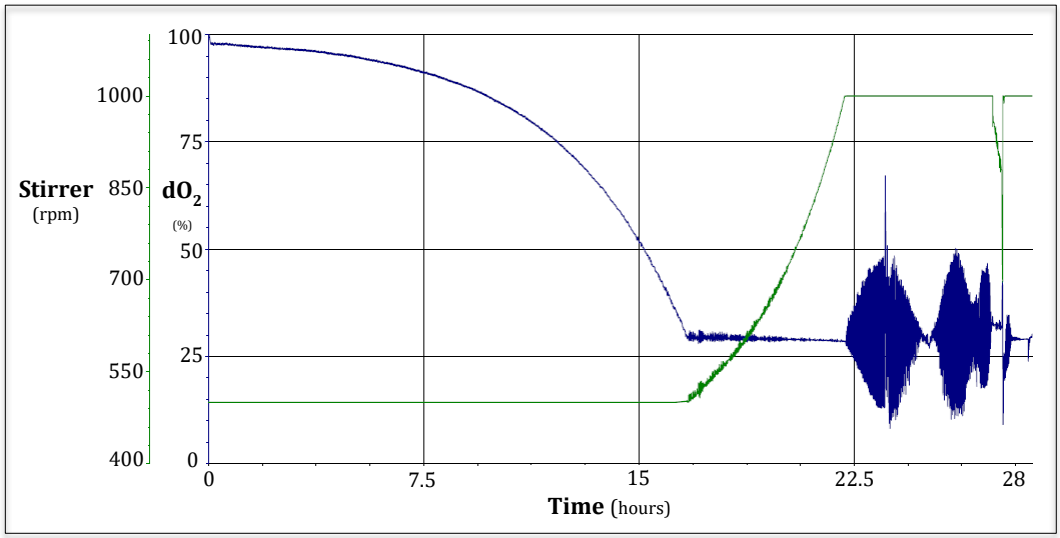

FIGURE 5.1: DARPin fermentation using the BIOSTAT® Cplus (Sartorius) bioreactor.

Expression of the G3 DARPin followed a similar trend to that seen in the BioFlo3000 bioreactor with a visible amount detected by coomassie blue stained SDS-PAGE gel (Figure 5.2A) as early as 2 hours after the introduction of (15 mL) methanol to the culture. The appearance of cleaved DARPin can be seen by western blot when probed with a polyclonal anti-DARPin primary and anti-Rabbit-HRP secondary, Figure 5.2B. From the initial induction to point of harvest there was a steady increase of product to a final concentration of approximately 60 mg/L culture and an OD_{600} of 270, higher than the biomass observed at harvest for the BioFlo 3000 (OD_{600} 180).

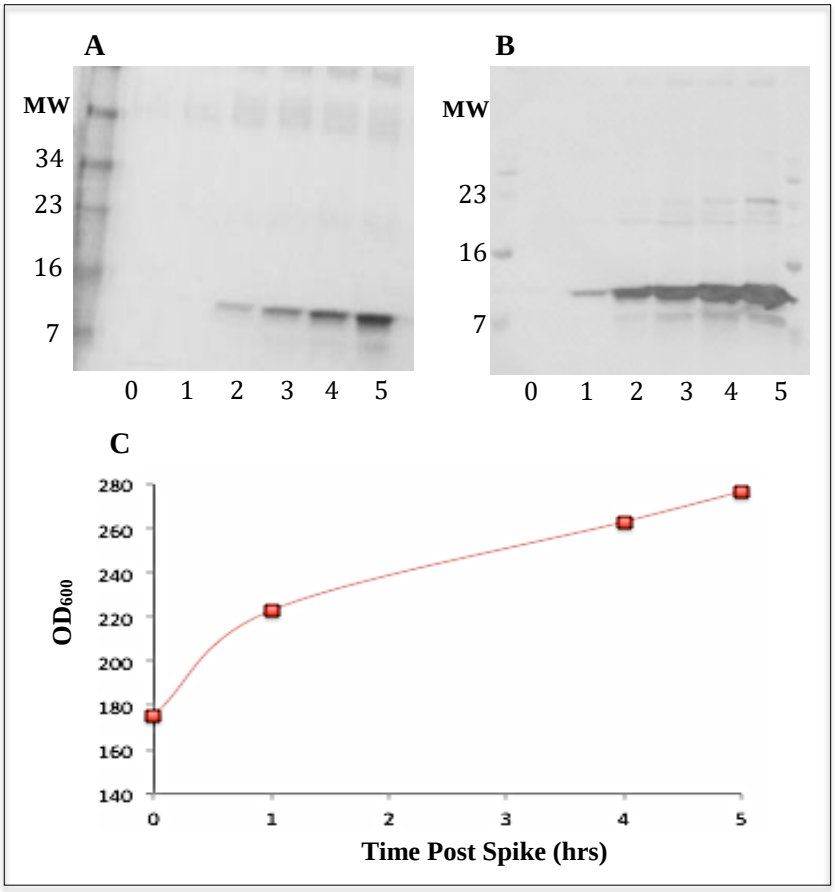

FIGURE 5.2: Expression of $(HE)_3$-G3 in a 20-L Bioreactor.
16% SDS-PAGE / Western blot analysis of G3 DARPin in the supernatant and OD_{600} culture growth post induction.

0-5, hours post methanol induction. **A**, Coomassie stained gel. **B**, Western blot with an anti-DARPin primary, anti-Rabbit-HRP secondary. **C**, Graph depicting cell growth.

5.3 Primary Capture and Purification from Crude Broth

Downstream purification (DSP) represents over 60% of the total cost to manufacture an antibody drug product, with the capture step being the critical step in determining the overall process effectiveness and efficiency. Having demonstrated the successful application of radial flow IMAC for the combined clarification and primary capture of the $(HE)_3$-tagged DARPin in Chapters 3 and 4 this unit operation would remain as the primary capture step for the GMP bioprocess.

A CRIO-MD 62 radial flow column (Proxcys Downstream Biosystems) at 6 cm bed height and a volume of 125 mL was packed with Cellthru BigBead technology resin. The agarose beads are functionalised with the metal chelator iminodiacetic acid (IDA) which has high selectivity for transition metal ions forming a stable complex. This allows for the capture of $(histidine)_6$-tagged proteins from solution as a result of histidine has affinity for metal ions. Whilst the large bead size of 300-500 µm allows the crude culture to flow through without blocking the column.

Nickel ions were chosen over copper ions as specific selectivity is higher for the former thereby theoretically providing less opportunity for HCP association. The wash buffer does not contain imidazole as the $(HE)_3$-DARPin has only three histidine's present as opposed to the conventional six, two alternate histidine's are required for association with the Ni^{2+} as shown in Figure 5.3.

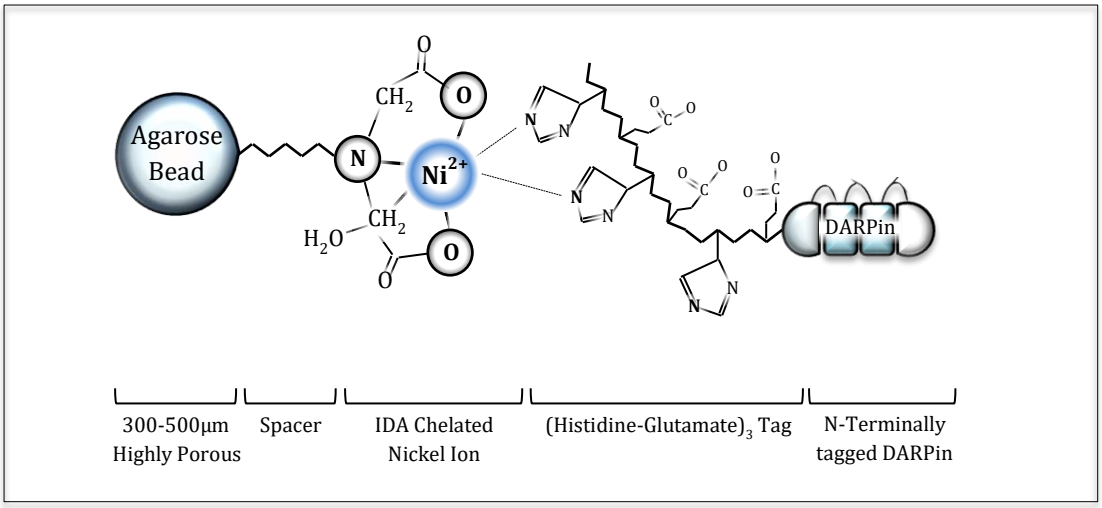

FIGURE 5.3: Schematic representation of Ni^{2+}-IMAC capture of $(HE)_3$-tagged DARPin.

The unclarified broth from the fermentation of section 5.2 (~12.5-L) was mixed 1 in four with 4xBinding Buffer (2xPBS, 2M NaCl pH 8) and loaded onto the radial flow IMAC column at a flowrate of 200 ml/min. Once all the material was applied to the column, the column was washed with 10-L of Binding Buffer in forward and reverse to dislodge any cells and

contaminating proteins. Before the bound protein was competitively displaced using a high imidazole buffer for elution (200 mM imidazole, 0.5xPBS, 0.5M NaCl, pH 7.5). Samples were taken prior to loading, flow-through and from the eluted pool and analysed by SDS-PAGE, Bradford and HCP ELISA.

As shown below in Figure 5.4 at harvest there was approximately 450 mg of DARPin, 5019 mg of HCP and 58 g/L cells. This was loaded onto the column at 200 mL/min, washed extensively and eluted. The eluent was composed of 93% (208 mg) DARPin and only 8% (15.9 mg) of HCP. So although 54% of the product was lost in the flow through, the step had removed 99.7% of the HCP contaminants. Time was favoured over yield in this step with the entire unit step taking no more than 1.5-2 hours, far less than conventional clarification followed by primary capture event.

A

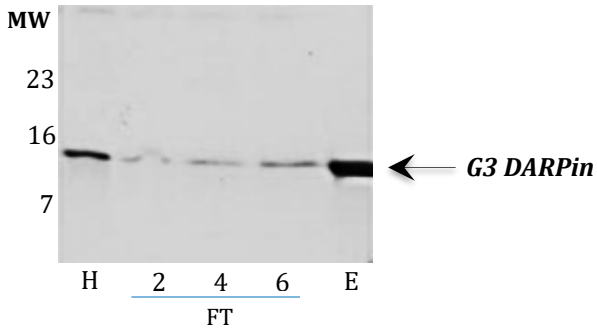

B

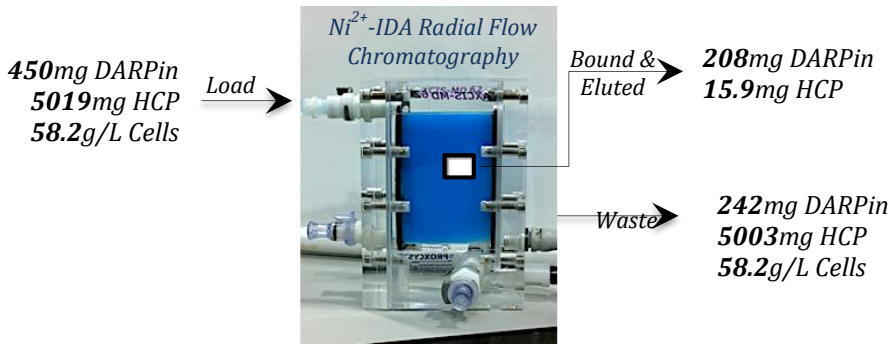

C

Stage	**G3 in Preparation** (% of Total Protein)	**G3 Yield** (%)	**HCP in Preparation** (% of Total Protein)	**HCP Removed** (%)
Cell-free Supernatant	8.23	100	91.8	-
IMAC	92.9	46.2	7.09	99.7

FIGURE 5.4: Analysis of IMAC facilitated primary capture and purification.
A, 18% SDS-PAGE Gel / Coomassie stained. **H,** Material prior to loading. **FT,** Flow through of material during loading at 2, 4 and 6 litres volume applied. **E,** Pooled eluent following IMAC. **B,** Schematic overview of DARPin (mg), HCP (mg) and *X33* Cells (g/L) during IMAC processing of fermentation broth. **C,** Yield and purity analysis of IMAC facilitated capture and purification.

5.4 Downstream Processing of Captured Protein

5.4.1 TFF: Concentration and Dialysis

As before a Labscale™ TFF system was implemented utilising three Pellicon® XL Ultrafiltration modules (Millipore). These modules are manufactured to a regulatory compliant standard and contain a Biomax® Polyethersulfone (PES) ultrafiltration membrane of 50 cm^2 per unit.

The pooled eluent (~550 mL) containing an average of 208 mg of DARPin and 15.9 mg HCP from the preceding IMAC capture step was loaded onto a pre-equilibrated (0.5PBS, 0.5M NaCl, 200mM Imidazole, pH 7.5) TFF system was concentrated to 25 mL and dialysed (5 CV) into Tris Low Salt buffer (20 mM Tris-HCl, 20 mM NaCl, 5 mM DTT, pH 7.5) containing 5 mM DTT in preparation for the SEC step of the following section, 5.4.2.

After application to the TFF system and subsequent UF/DF the protein pool contained 196 mg DARPin and 10.2 mg HCP. This represents a yield of 94.4% product post unit operation, with 35.8% of the HCP present removed. The high retention of product is not wholly unsurprising, given the membranes 5 kDa cut-off, void-free structure and low protein binding, resulting in the 14 kDa G3 remaining within the retentate. Due to the MW of G3 and illustrated need for a very small cut-off this does translate into the somewhat limited removal of HCP's from the product stream with only one third of what was present removed in the permeate.

A

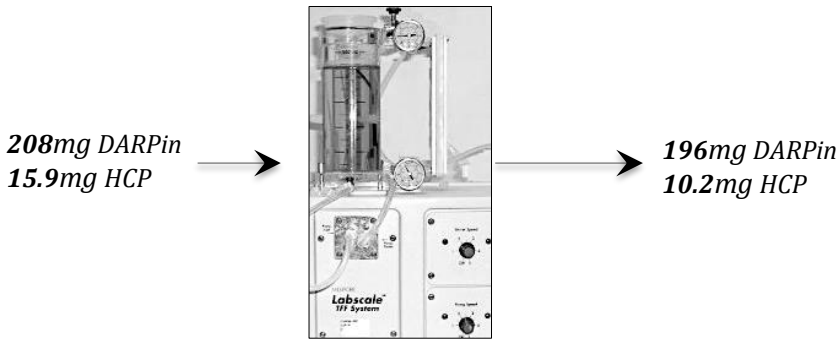

B

Stage	**G3 in Preparation** (% of Total Protein)	**G3 Yield** (%)	**HCP in Preparation** (% of Total Protein)	**HCP Removed** (%)
IMAC	92.9	46.2	7.09	99.7
TFF	95.1	94.4	4.94	35.8

Figure 5.5: Analysis of TFF facilitated concentration and dialysis.
A, Schematic overview of DARPin (mg), HCP (mg) and *X33* Cells (g/L) during TFF concentration and dialysis of IMAC eluent into 20mM Tris-HCl, 20mM NaCl, 5mM DTT pH 7.5 in preparation for SEC1. **B,** Yield and purity analysis of the TFF unit step.

5.4.2 SEC1: Size-based Separation and Buffer Exchange

Size exclusion chromatography (SEC) had been shown to work successfully in previous chapters (3 and 4) both as a unit operation and in generating a product used successfully in animal models for biodistribution, imaging and toxicity. This would remain as a primary purification step in the GMP compliant process.

A XK 26/100 column (GE Healthcare) came prepacked with 500 mL Superdex 75 resin (GE Lifesciences). The resin matrix comprises of 24-44 µm beads of cross-linked dextran (Sephadex) allowing for increased resolution and agarose for physical and chemical stability. This resin allows the high resolution of molecules from 3-70 kDa and as such G3 DARPin with a monomer size of 14 kDa and dimer of 28 kDa falls well within this range.

The manufacturers published guidelines suggest a sample volume of no more than 2% of the column volume in order to obtain maximum resolution. As an initial purification step and seeing how adequate the capture step was in removing HCP's we used a sample load of maximum 5% of the column volume. As such all 25 mL of the pooled eluent from Section 5.4.1 was loaded onto the SEC column, pre-equilibrated in low salt buffer (Buffer A; 20 mM Tris-HCl, 20 mM NaCl, 5 mM DTT pH 7.5) and run at ≤ 4 mL/min with a pressure limit of 0.3 MPa. Unlike in the laboratory runs (Chapter 3 and 4) the facility utilised an ÄKTApurifier FPLC system, not an ÄKTAprime, so standard operating procedures (SOP's) and validating runs were adjusted accordingly.

The main objective of this step was to remove contaminants of largely differing molecular weight, DARPin dimers and protein aggregates and then buffer exchange in preparation for the following purification steps.

As depicted in Figure 5.6A this process resulted in two notable Abs_{280} peaks at 180-260 mL and 280-360 mL correlating to aggregated protein and largely monomer DARPin, respectively. A wide fraction of 40 mL was pooled, as with AEX being the next step resolution capacity is determined by protein quantity and not volume. Approximately ~10-20 mL from the start and end of the peak were removed so as to minimise the inclusion of any DARPin dimer and lower molecular weight proteins.

This unit operation resulted in a loss of 34 mg of DARPin, therefore giving a G3 yield of 82.6% and an HCP removal of 99.7%. The final preparation resulting from this step consisted of 99.98% of G3 DARPin (Figure 5.6 –B &-C), both full-length and truncated.

A

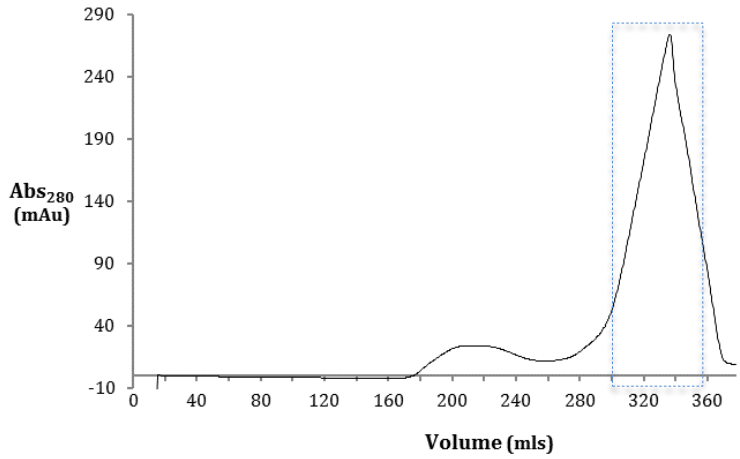

B

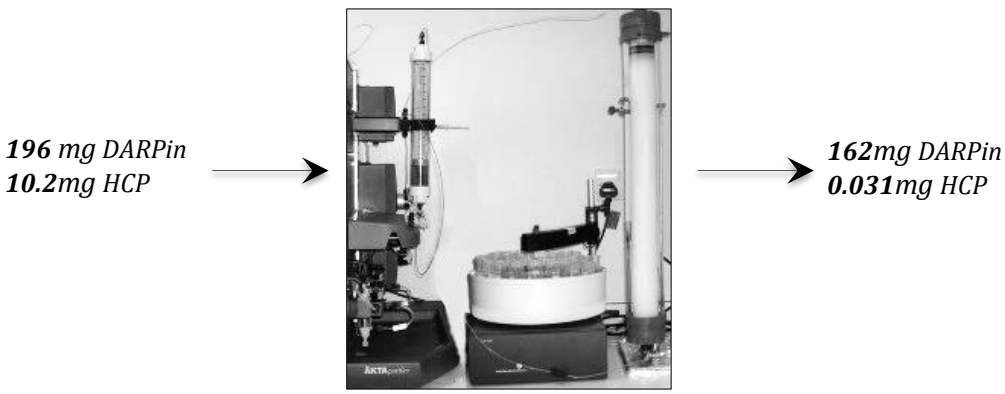

C

Stage	G3 in Preparation (% of Total Protein)	G3 Yield (%)	HCP in Preparation (% of Total Protein)	HCP Removed (%)
TFF	95.06	94.37	4.94	35.76
SEC1	99.98	82.59	0.019	99.69

FIGURE 5.6: Analysis of SEC facilitated purification.
A, Chromatogram of the $(HE)_3$-G3 SEC purification run. **Blue rectangle**, fraction of eluent pooled. **B,** Schematic overview of DARPin (mg) and HCP (mg) during the SEC separation of the concentrated and dialysed pool from section 5.4.1 in preparation for AEX. **C,** Yield and purity analysis of the AEX unit step.

5.4.3 AEX: Charge-based Separation

As demonstrated in the preceding section 5.4.2, SEC1 processing already generates a product pool of high purity with an average 99.98% (162 mg) of the total protein being G3. Though clear of almost all HCP (~0.013 mg), SEC1 doesn't adequately separate cleaved DARPin from full length as demonstrated by the lower MW band visible after SDS-PAGE analysis. G3 DARPin is negatively charged at physiological pH with an isoelectric point of 4.79. So in order to remove these lower MW variants, given cleavage would result in a degree of change in charge, anion exchange chromatography was employed.

A XK 50 column (GE Healthcare) with a length of 20 cm and an internal diameter of 5 cm was packed with 200 mL of the strong anion exchanger resin, Source 30Q (GE Lifesciences) using an AKTA Purifier (GE Healthcare). The uniform 30 µm rigid polystyrene/divinyl benzene polymer matrix allows for low back pressure and high flowrates with a wide range of working conditions. The matrix is modified with the strong anion exchange group, quaternary ammonium (Q).

All ~50 mL of the pooled eluent from section 5.4.2 was loaded onto the AEX column in low salt buffer (Buffer A; 20 mM Tris-HCl, 20 mM NaCl, 5 mM DTT pH 7.5) and run at 5 mL/min. $(HE)_3$-G3 elutes at ~250 mM NaCl so a step wash of 1/2 CV with a 200 mM NaCl containing buffer was implemented (20% Buffer B; 20 mM Tris-HCl, 1M NaCl, 5 mM DTT pH 7.5). This step enables the bulk removal of contaminating proteins, of lower affinity, whilst retaining product binding. An increasing salt gradient of 10 mM NaCl (1% Buffer B) per 15 mL to a final concentration of 300 mM NaCl (30% Buffer B) was employed to separate contaminating proteins, both residual HCP and any cleaved G3, whose affinity for the resin is close to the full length product, $(HE)_3$-G3.

As depicted in Figure 5.7 this process resulted in a sharp peak at approximately 25% Buffer B equating to the previously determined 250 mM NaCl required to elute the G3 DARPin. A tight fraction was pooled to both prevent overloading of the following SEC step and prevent addition of cleaved G3 which elutes at a higher salt concentration than the full length protein. There was a loss of 50 mg of DARPin giving a G3 yield of 69% for the unit operation along with the removal of 79% of HCP, this gave a final prep consisting of 99.99% of full length G3 DARPin as determined by SDS-PAGE.

A

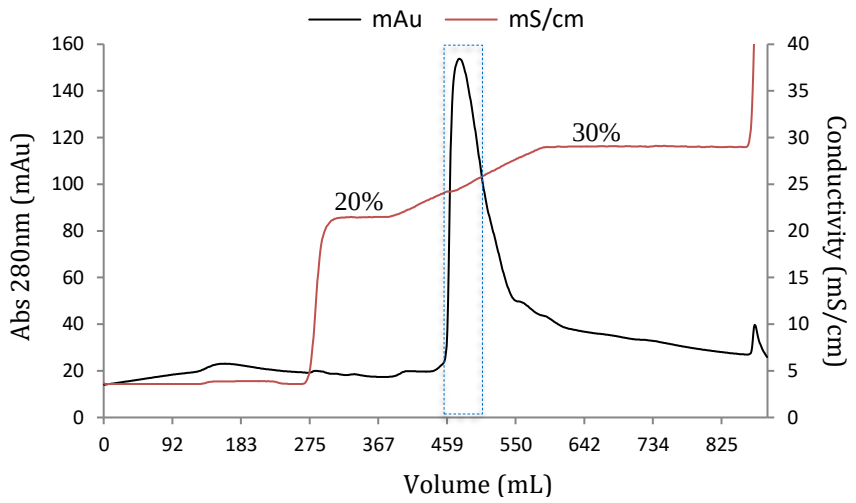

B

C

Stage	**G3 in Preparation** (% of Total Protein)	**G3 Yield** (%)	**HCP in Preparation** (% of Total Protein)	**HCP Removed** (%)
SEC1	99.98	82.59	0.019	99.69
AEX	99.99	69.19	0.006	79.15

FIGURE 5.7: Analysis of AEX facilitated purification.
A, Chromatogram of the $(HE)_3$-G3 AEX purification run. **Blue rectangle**, fraction of eluent pooled. **B,** Schematic overview of DARPin (mg) and HCP (mg) during the AEX separation of the SEC1 pool from section 5.4.2. **C,** Yield and purity analysis of the AEX unit step.

5.4.4 SEC2: Buffer Exchange and Monomer Selection

With AEX generating 112 mg of full length DARPin of high purity (99.99%) the final stage was a means of buffer exchange into appropriate storage buffer. This was achieved by SEC using, as in section 5.4.2, a 500 mL Superdex 75 packed column pre-equilibrated in PBS and without DTT so as not to interfere with any future conjugation experiments/animal studies.

All 35 mL from the preceding step was loaded onto the SEC column and run as before at <4 ml/min and <0.25 MPa. A clean uniform peak was visible on the chromatogram at the expected elution volumes of ~330 mL shown in Figure 5.8. A tight pool was taken from the eluted fraction from approximately 335-365 mL, this was to ensure that the final concentration of DARPin was ≥ 1mg/mL thereby removing the need for any concentration-based unit operations. As a result of this narrow cut of eluent a final product quantity of 60 mg was acquired from the initial 112 mg, this thereby resulted in a 46% loss of G3 DARPin and a six-fold reduction in the already regulatory acceptable HCP content. The final product was stored in cryovials as 1 mL aliquots at -80ºC.

A

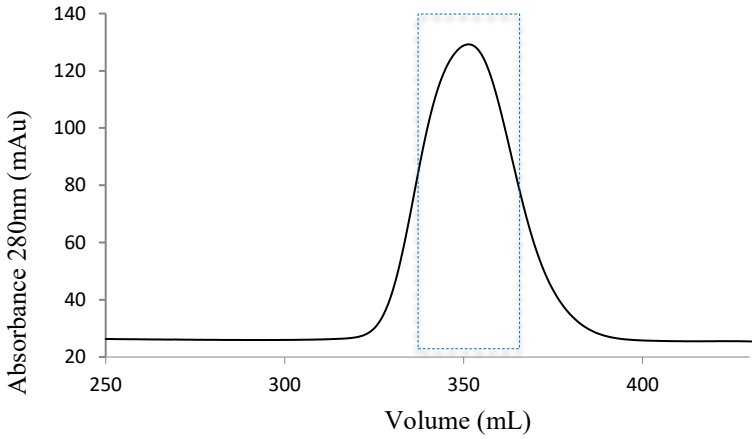

B

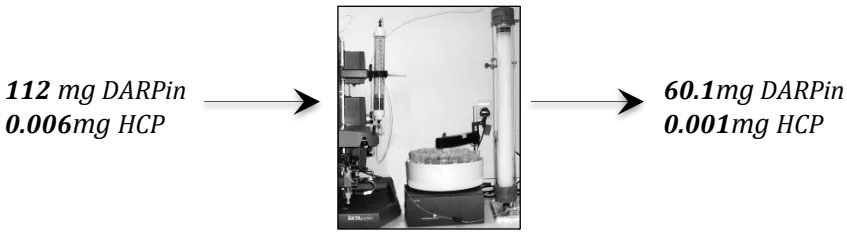

C

Stage	G3 in Preparation (% of Total Protein)	G3 Yield (%)	HCP in Preparation (% of Total Protein)	HCP Removed (%)
AEX	99.99	69.19	0.001	79.15
SEC2	100.00	53.56	0.000	77.04

FIGURE 5.8: Analysis of SEC2 facilitated buffer exchange.
A, Chromatogram of the $(HE)_3$-G3 SEC2 purification run. **Blue rectangle**, fraction of eluent pooled. **B,** Schematic overview of DARPin (mg), HCP (mg) and *X33* Cells (g/L) during the SEC separation of AEX pool from section 5.4.3. **C,** Yield and purity analysis of the SEC2 unit step.

5.5 Final Process

The final process for cGMP production of $(HE)_3$-G3 DARPin takes five days of which almost half the time is required for DSP (Figure. 5.9).

The DSP comprises of **(i)** Primary capture by radial flow immobilized-metal affinity chromatography (IMAC), **(ii)** Concentration/dialysis by means of tangential flow filtration (TFF), **(iii)** Size exclusion chromatography (SEC) using a Superdex 75 prep grade column equilibrated in 20 mM Tris, 20 mM NaCl and 5 mM DTT, pH 7.5; the protein peak containing the monomer DARPin is selected **(iv)** Anion exchange (AEX) chromatography, using a Source 30Q AEX resin and applying a linear gradient of 200 mM to 300 mM NaCl (both in 20 mM Tris, 5 mM DTT pH 7.5) for protein elution; the pooled fraction is stored at 4°C overnight, **(v)** Desalting by SEC on a Superdex 75 column equilibrated in PBS; the fraction containing the monomer $(HE)_3$-G3 is collected and stored at -80°C in PBS.

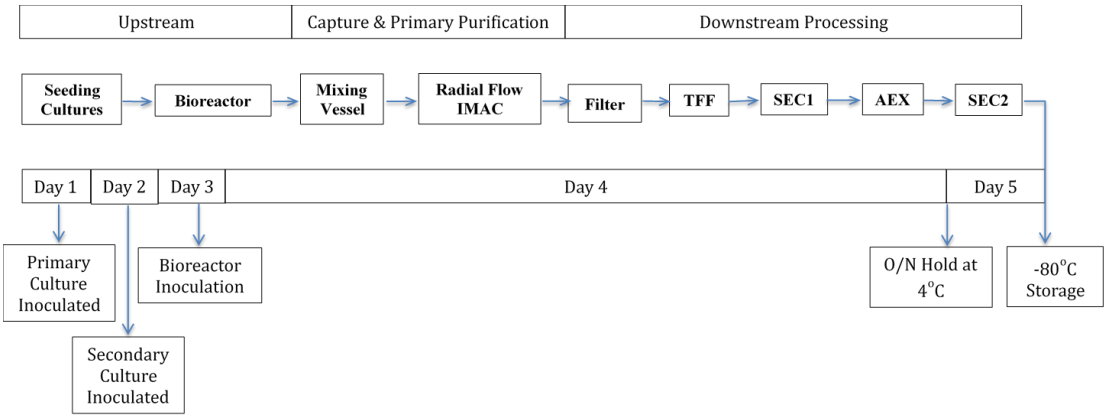

FIGURE 5.9: Bioprocess overview for the production and purification of the anti-HER2 DARPin, G3.

As shown in Figure 5.10, the developed bioprocess started with approximately 5.5 gram of protein of which only 450 mg (8.23%) was DARPin. The capture event using radial flow IMAC removed 99.7% of the contaminating HCP with a final yield of 46.2% G3 DARPin thereby generating a purity of 92.9% from a single unit step. TFF concentrated and dialysed the product pool with minimal losses of DARPin at 6% and limited removal of 35.8% / 5 mg of HCP. SEC1 eliminated most of the remaining HCP leaving just 0.019 mg amongst 162 mg of DARPin, a yield of 82.6 %. Given that SEC1 had already generated product of regulatory acceptable standard of HCP and endotoxin, AEX was tasked primarily with removal of the lower weight truncated DARPin. This was achieved alongside the further subtraction of 79% HCP generating a product pool of 99.99% full length G3 product. SEC2 allowed for the desalting of the AEX

pool into PBS for storage generating a final batch of 60 mg DARPin at 1mg/ml concentration and containing just 1 µg of HCP.

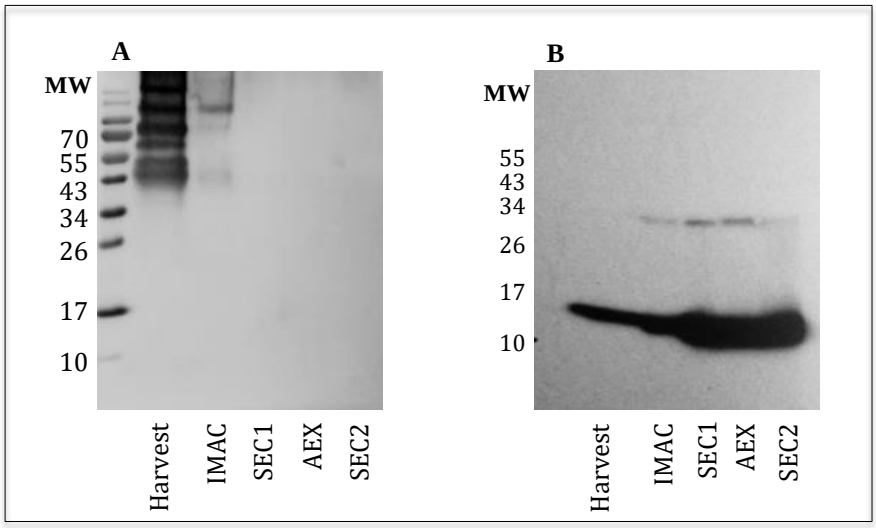

C

Stage	**Total Protein** (mg)	**G3 DARPin** (mg)	**G3 in Preparation** (% of Total Protein)	**G3 Yield** (%)	**Total HCP** (mg)	**HCP in Preparation** (% of Total Protein)	**HCP Removed** (%)
Cell-free Supernatant	5469	450	8.23	100	5019	91.8	-
IMAC	224	208	92.9	46.2	15.9	7.09	99.7
TFF	207	196	95.1	94.4	10.2	4.94	35.8
SEC1	162	162	99.98	82.6	0.031	0.019	99.7
AEX	112	112	99.99	69.2	0.006	0.006	79.2
SEC2	60.1	60.1	100.00	53.6	0.001	0.000	77.0

FIGURE 5.10: Analysis of the G3 DARPin bioprocess.

A & **B**, Visualisation of Host cell protein and DARPin throughout the bioprocess. 16% SDS-PAGE Western blot probed with **A.** anti-*P. pastoris*-HRP and **B.** anti-DARPin primary and anti-Mouse-IgG-HRP secondary. **C,** Quantities of HCP and DARPin prior to and following each unit step. Total protein measured by Bradford assay. HCP measured by P. pastoris HCP kit (Cygnus).

Harvest / Cell-free Supernatant, clarified supernatant at point of harvest. ***IMAC***, eluted pool following capture from harvest broth by radial flow IMAC. ***SEC1***, pool following first size exclusion chromatography. ***AEX***, eluted after anion exchange chromatography of SEC1 pool. ***SEC2***, Eluent following size exclusion chromatography of AEX pool.

5.5 Discussion

Taking into account the actual cohort size of Phase I and II clinical trials (Umscheid *et al*. 2011) the amount of material required to sustain the entire cohort does not necessitate the need for extensive running costs and downstream handling of unwarranted quantities of protein. A short running, easy to implement approach imparts a practical feasibility for the production of DARPins for use in clinical trials.

Transfer to a CIP bioreactor allowed for greater control in terms of decreasing the risk of contamination as ports can be sterilised something the autoclavable bioreactor used in development could not. The fermentation protocol enabled the HCD growth of *P. pastoris* and high titres of secreted G3 over a very small window of induction, ~450 mg following one hour of methanol limited feed. The $(HE)_3$-tagged product was captured directly from crude broth, containing on average 58g cells (DCW), 450 mg DARPin and 5020 mg HCP, using Cellthru™ BigBead technology (Sterogene) coupled with radial flow IMAC. This unit step concurrently clarified the feed stream and captured the G3 DARPin, removing whole cells and 99% of contaminating HCP whilst capturing ~ 50% of the product in < 2 hours of run time. As a unit operation radial flow IMAC is of low maintenance and allows for a small footprint and exceptionally fast process time, combining what is typically two to three pieces of equipment into one thereby saving considerable resources, man-power and time. This technology is additionally easily scalable with indistinguishable hydrodynamic properties to the far larger manufacturing-scale radial flow columns.

A Millipore TFF system provided a closed and fully sanitise-able system from which to concentrate and dialyse the IMAC captured pool. Reducing agent (5 mM DTT) used throughout the process lowered both the quantity of DARPin dimers and the level of protein aggregate formed. The use of a Pellicon® TFF cassette with 5 kDa cut-off membranes, of low protein binding, resulted in a yield of 94% DARPin but also only a 35% loss of HCP as such a low cut-off allows little to get through.

It was noted during the preliminary stages of R&D that the *P. pastoris* culture secreted mainly high MW host proteins into the external media. By using a size separation step they were efficiently removed as were any dimer DARPins present. So a 500 mL Sephadex-75 column was used with a high resolving power from 3-70 kDa. This unit operation resulted in a loss of 34 mg of DARPin, therefore giving a G3 yield of 82.6% and an HCP removal of 99.7%. The final preparation resulting from this step consisted of 99.98% of G3 DARPin, both full-length and truncated. Although unusual to have a SEC unit operation this early in a process, given that

scale up would be restricted, it does work extremely well. As such the pooled DARPin product following this SEC step is largely monomer and already at regulatory compliant levels of both HCP and endotoxin. SEC is an easy to implement and effective technique for use in circumstances where extremely large product quantities are not required, as is the case for clinical trials.

Although SEC generated regulatory compliant product in terms of HCP and endotoxin it was unable to fully remove the lower MW DARPin fragment. In order to remove this and generate a product pool of full length DARPin charge based separation was implemented.

A strong anion exchange resin (Source 30Q) was used and the procedure consisted of a step wash followed by a linear gradient for elution. The uniform 30 μm rigid polystyrene/divinyl benzene polymer matrix allowed for low back pressure and high flowrates with a wide range of working conditions. A tight fraction was pooled to both prevent overloading of the following SEC step and prevent the inclusion of cleaved G3 which elutes at a slightly higher salt concentration than that of the full length protein. There was a loss of 50 mg of DARPin giving a G3 yield of 69% for the unit operation along with the removal of 79% of remaining HCP, this gave a final prep consisting of 99.99% product, all full length G3 as determined by SDS-PAGE and mass spectrometry.

With AEX generating 112 mg of full length DARPin of high purity (99.99%) the final stage was a means of buffer exchange into appropriate storage buffer. This was achieved by SEC using, as before, a 500 mL Superdex 75 packed column pre-equilibrated in PBS and without DTT so as not to interfere with any future conjugation experiments/animal studies. A clean uniform peak was visible on the chromatogram and a tight pool was taken to ensure that the final concentration of DARPin was $\geq$ 1 mg/mL thereby removing the need for any concentration-based unit operations. As a result of this narrow cut of eluent a final product quantity of 60 mg was acquired from the initial 112 mg, this thereby resulted in a 46% loss of G3 DARPin and a six-fold reduction in the already regulatory acceptable HCP content.

5.6 Conclusion

The aim of this Chapter was to develop a bioprocess suitable for regulatory compliance and apply this process for production of $(HE)_3$ –tagged DARPins. As scaffold proteins DARPins share the same conserved framework and as such the potential to build a platform process for their production.

Upstream development involved the successful technology transfer of the G3 DARPin fermentation from the 10-L BioFlo 3000 (New Brunswick) developmental bioreactor, used in Chapters 3 and 4, to the regulatory compliant 20-L clean-in-place BIOSTAT® Cplus (Sartorius). A short induction time of 1 hour on methanol limited feed was implemented due to the potential proteolytic cleavage of the G3. Nether-the-less at harvest the culture was at a biomass of OD_{600} 270 and the product at a concentration of 60 mg/L, both of which are higher than what had been achieved in the BioFlo 3000.

Radial flow IMAC facilitated the combined event of clarification and primary capture, recovering 46% of the DARPin product at 99.6% purity, in under two hours of run time. TFF was used to concentrate and dialyse the eluent in the presence of 5 mM DTT. This step resulted in minimal losses of product (5.4%) and the removal of a third of remaining HCP. Size exclusion chromatography was then utilised to remove contaminants of largely differing molecular weight, DARPin dimers and protein aggregates, whilst simultaneously performing buffer exchange removing a further 99.7% of HCP with a yield of 82.6% G3 at 99.98% purity. AEX chromatography was successfully used to separate full-length DARPin from that of lower MW and resulted in 112 mg of G3 at 99.99% purity. The final step utilised SEC to desalt / buffer exchange the product pool into appropriate storage buffer. Resulting in 60 mg of fully functional G3 DARPin at 1 mg/mL.

In conclusion, the developed DSP for DARPin production consisted of affinity, size and charge based purification events generating a highly homogeneous monomeric product at regulatory compliant levels of HCP and endotoxin, < 0.5 ng /mL and < 0.05 EU / mL, respectively.

CHAPTER SIX

DESIGN AND CHARACTERISATION OF A CONJUGATION PROCESS FOR THE SYNTHESIS OF A CLINICAL IMAGING G3 DARPIN

6.0 Design and characterisation of a conjugation process for the synthesis of a clinical imaging G3 DARPin

6.1 Introduction

Molecular Imaging combines traditional diagnostic imaging techniques with targeting agents/probes to characterise and measure the expression of specific biomarkers present within disease. Imaging can be optical, MRI or radionuclide-based with the latter being more favourable in terms of increased sensitivity and ability to be quantitative with no limit to tissue penetration (Hong *et al.* 2008). Two such techniques, which have been used extensively in cancer patient diagnosis, staging and monitoring, are single photon emission tomography (SPECT) and positron emission tomography (PET).

SPECT uses gamma-emitting isotopes such as ^{99m}Tc ($t_{1/2}$ 6hrs), ^{111}In ($t_{1/2}$ 2.8 days), ^{123}I ($t_{1/2}$ 13.2 hours) and ^{131}I ($t_{1/2}$ 8 days) whilst PET requires positron-emitting isotopes typically ^{18}F ($t_{1/2}$ 109.7 min), ^{11}C ($t_{1/2}$ 20.4 min), ^{13}N ($t_{1/2}$ 9.96 min) and ^{15}O ($t_{1/2}$ 2.07 min). PET is approximately 10 times more sensitive than SPECT but is far more costly and not as readily available (Rahmim *et al.* 2008; Pimlott 2014).

Whether it is SPECT or PET that is employed, both require the addition of a chelator to the targeting agent in order to facilitate the addition of a radio-nucleotide. For use in the clinical setting the chelator must be able to form thermodynamically and kinetically secure complexes to avoid the *in vivo* loss of the radionuclide. DOTA is a non-bridged macrocyclic chelator whose maleimide-DOTA derivative has already been used in clinical trials (Stasiuk *et al*. 2013). The maleimide moiety is electrophilic and displays high selectivity towards free thiols and this property has been widely utilised for the conjugation and labelling of proteins and peptides (De Leon-Rodriguez *et al.* 2008).

G3 DARPin has been produced with a free C-terminal cysteine to permit conjugation through this sulfhydryl chemistry, Figure 6.0. As addressed earlier in Chapter 5 the regulatory compliant bioprocess for G3 DARPin production maintains the presence of a reducing agent (5 mM DTT) throughout the DSP and each unit step selects for monomers. This is to ensure that the thiol's, which are prone to oxidative dimerization, are prevented from forming disulphide bonds (thus available for linker addition) and those that are not reduced are removed.

In our previous work (Goldstein *et al.* 2015) the addition of the maleimide-DOTA took place on a very small scale at ≤ 2 mg G3 per conjugation cycle. The reaction involved using equipment and methods which are far more suited to a research lab than a GMP facility. Many

items were not available at the appropriate standard, were not easily scalable and justifying to the regulatory authorities that the procedure itself could meet the stringent guidelines in terms of reproducibility, sterility and control would be extremely difficult.

This chapter aims to take this small-scale lab process and turn it into a regulatory compliant process capable of labelling and purifying larger quantities of DARPin with the flexibility (if required) for future scale-up.

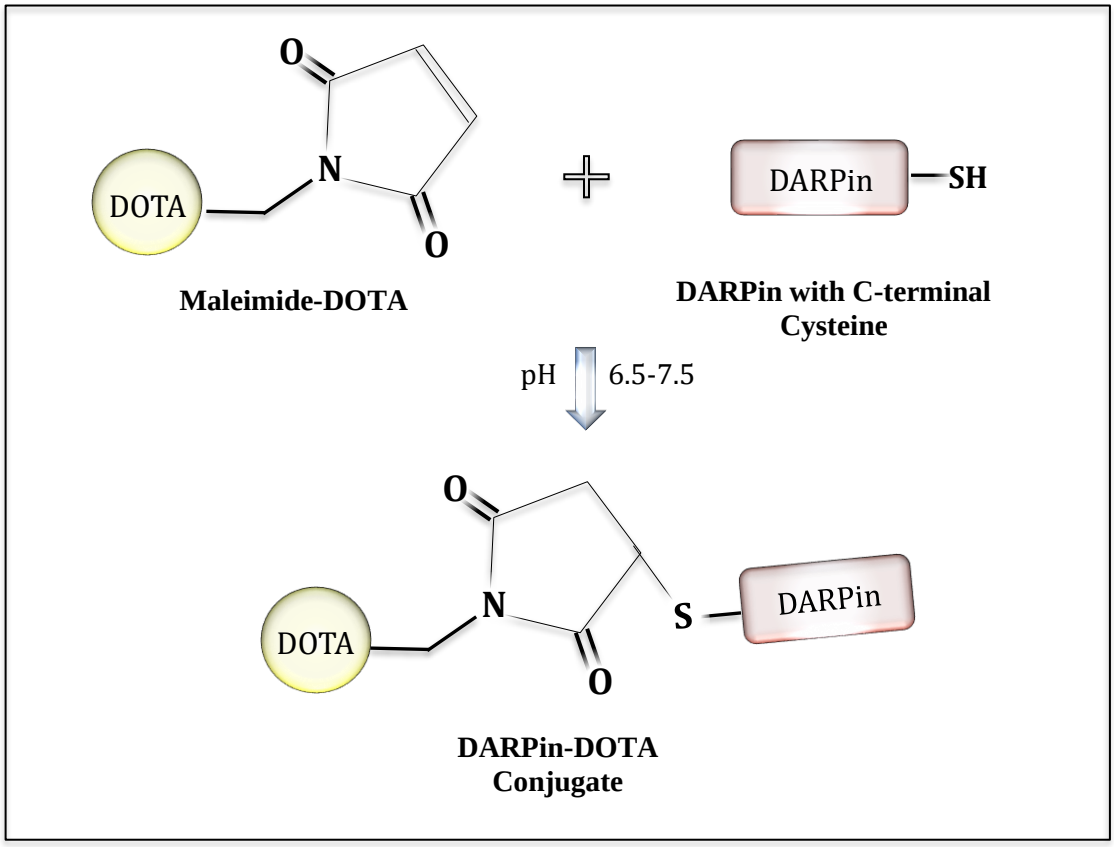

FIGURE 6.0: Schematic depicting the conjugation of maleimide-DOTA to DARPin-Cys.

6.2 Development of a regulatory compliant labelling process

6.2.1 Previous Maleimide-DOTA to G3 DARPin conjugation process

The previously determined conjugation process used by Goldstein *et al.*, 2015 used 4 units of operation over a period of ~6 days to process a maximum of 2 mg of G3 DARPin. (Figure 6.1)

FIGURE 6.1: Overview of small scale Maleimide-DOTA conjugation process used in Goldstein *et al*, 2015.
G3 DARPin stored at -80ºC in PBS/5mM DTT was used in the conjugation. The first step in the process involved the addition of a metal chelator EDTA to remove any free metal ions which would otherwise bind to DOTA and inhibit radiolabelling of the DARPin. The strong reducing agent TCEP was included to reduce any further DARPin dimers thereby freeing the cysteine for maleimide conjugation. Buffer exchange into an appropriate medium (Sodium Phosphate, pH 7) took place using a PD-10 desalting column with a maximum 2mL loading capacity. Following which a 4x molar excess of maleimide-DOTA was added to the DARPin pool and incubated at 4ºC for 72 hours. A PD-10 column was once again used to buffer exchange the DARPin into 0.2M ammonium acetate. A Vivaspin column with a MW cut off of 3.5 kDa facilitated both the removal of free linker and the concentration of DARPin, by lyophilisation and reconstitution. The reconstituted DARPin was then further dialysed in a Maxi GeBAflex-tube (Generon) against ammonium acetate containing Chelex-100 resin (Bio-Rad) to remove any introduced or remaining metal ions prior to radiolabelling.

6.2.2 Design of a regulatory acceptable and easy to implement process

6.2.2.1 Simplifying the conjugation process

The conjugation of maleimide-DOTA was assessed in PBS to determine efficiency of reaction under these buffer conditions. PBS was chosen instead of Sodium Phosphate to determine whether the conjugation could be placed directly after SEC2 of Chapter 4 and combine the first two steps of the lab process into one.

1 mL of G3 (5 mM DTT/PBS) at 1 mg/mL was loaded onto a PD-10 desalting column pre-equilibrated with PBS. The eluted fractions now free of DTT were pooled and a 4x molar excess of maleimide-DOTA to G3 was added, as determined by OD_{280}. 30 µL samples were taken before the addition of the chelator (t = 0) and at 10, 20, 30, 60 and 120 minutes post addition. The samples were loaded onto a 16% SDS-PAGE gel and run under reducing conditions, protein was visualised by coomassie staining (Figure 6.2).

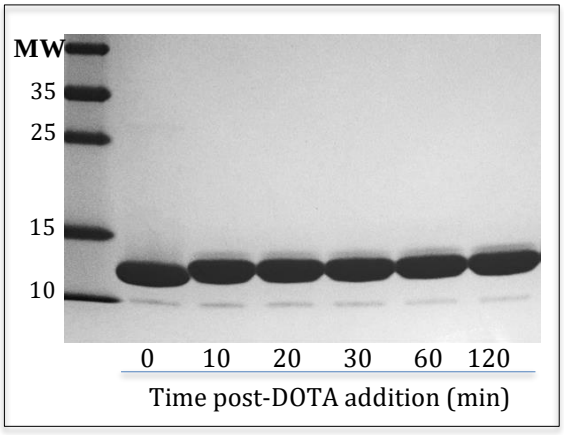

Figure 6.2: 16% SDS-PAGE / Coomassie stained gel depicting Maleimide-DOTA incubation with G3 DARPin over the course of 2 hours in PBS.

Maleimide-DOTA (Chemical formula: $C_{22}H_{34}N_6O_9$) has a MW of 526.54 Da and its conjugation with G3-DARPin to form G3-DOTA results in an increase in MW from 14358 to 14,884 Da, this difference can be resolved by SDS-PAGE. Figure 6.2 shows a clear shift in MW as early as 10 minutes post maleimide-DOTA addition. Extended incubation with the linker of up to 120 minutes did not appear to be any more beneficial nor though was it detrimental. This demonstrates the flexibility of conjugation time in PBS with no need for 72 hour incubations. The process in Chapter 4, from where this product was sourced, had both adequately selected for monomers and prevented the thiols from oxidising with DTT alone, ruling out the need for TCEP addition.

6.2.2.2 Removal of free linker from conjugated product

The previous process required buffer exchange (PD-10) before the removal of unconjugated maleimide-DOTA via a spin column (Vivaspin) with a MW cut-off 3.5 kDa. Centrifugation enabled the linker to pass through the membrane pores whilst retaining the G3-DOTA in an almost lyophilised state on the upper membrane. The protein was then re-suspended in 0.2 M ammonium acetate. This procedure would face many roadblocks on its way to regulatory approval. One would have to validate that the lyophilisation itself did not affect protein function, assess the degree of aggregation induced and circumvent the lack of scalability presented by this process.

To this end G3-DOTA was generated as per Chapter 5 and 1 mg used to assess whether a more regulatory applicable process could be determined. The DARPin was incubated for 30 minutes with maleimide-DOTA in PBS and loaded directly onto a 125 mL Superdex 75 column using a 2 mL super loop. The 125 mL column was used due to the small quantity of G3 that was being conjugated but if this procedure was to be taken forward the 500 mL column used in SEC1 and SEC2 would be applied.

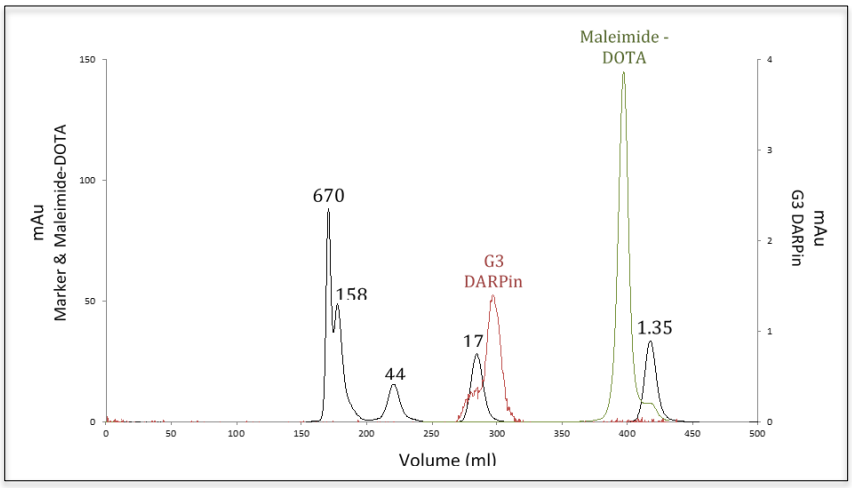

FIGURE 6.3: Separation of key components, G3 DARPin and maleimide-DOTA on a 500ml Superdex75 Size exclusion column.
Black, Molecular weight markers: Thyroglobulin (670kDa), Y-globulin (158kDa), Ovalbumin (44kDa), Myoglobin (17kDa) and Vitamin B12 (1.35kDa). ***Red***, Purified G3 DARPin stored in PBS. ***Green***, Unreacted Maleimide-DOTA (Macrocyclics).

The G3-DOTA was isolated from the unconjugated linker and fractions pooled for further assessment. Factors investigated were, conjugation efficiency, G3-DOTA to antigen binding and the ability to successfully radiolabel. The dialysis step against ammonium acetate containing Chelex-100, which had taken place over 72 hours, was removed. Radiolabelling efficiency would dictate whether there was further need for metal ion removal or whether this measure was no longer necessary.

6.2.3 Assessment of radiolabelling efficiency

The DOTA- conjugated G3 DARPin was sent for radiolabelling studies to Julia Blower (Kings College London). The radio-isotope Indium^{111} was used in this study to evaluate labelling efficiency of the DARPin after undergoing mock process conditions, Figure 6.4.

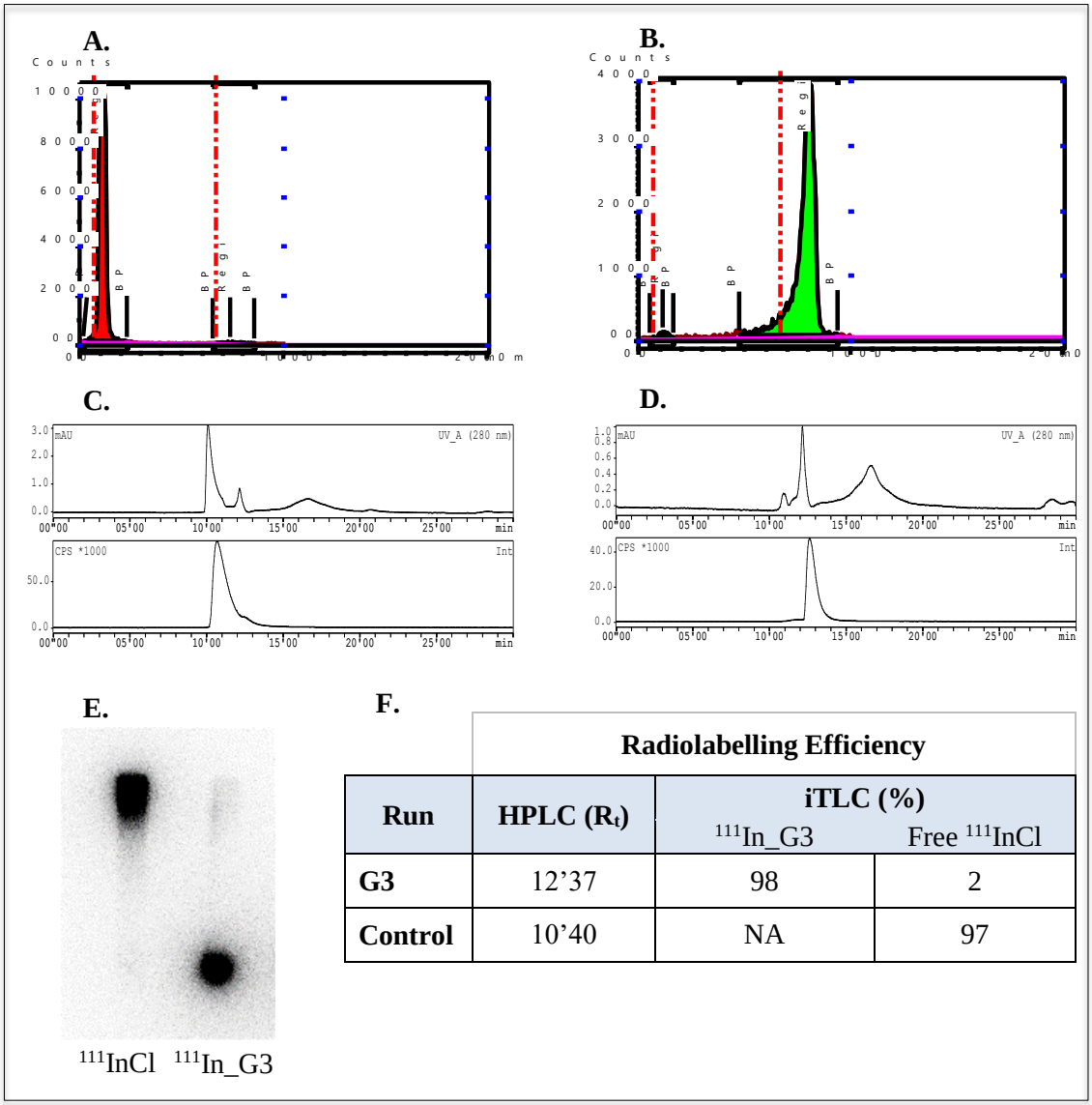

Radiolabelling Efficiency			
Run	**HPLC (R_t)**	**iTLC (%)**	
		^{111}In_G3	Free ^{111}InCl
G3	12'37	98	2
Control	10'40	NA	97

Figure 6.4: Assessment of conditions developed on the radilabelling efficiency of G3-DOTA with Indium^{111}.
^{111}InCl (30 µL, 30 MBq), G3_DOTA DARPin (60 µL, 1mg/mL), and NH_4OAc (0.2 M, 10 µL) were combined and heated at 37ºC for 1h. 20 µL sample taken for SEC HPLC analysis and 1µL sample taken for iTLC. **A and C,** iTLC and HPLC of radiolabelled G3, respectively. **B and D.** iTLC and HPLC of free radiolabel ^{111}InCl, respectively. **E,** Visualisation of radioactivity on iTLC paper. **F,** HPLC and iTLC values for the radiolabelled DARPin (G3) and the unconjugated Indium salt (Control)

6.2.4 Mass Spectrometry pre- and post- Linker addition

Pre- and post-linker addition G3 DARPin was sent for Mass Spectrometry analysis, a clear shift from 14358.1 to 14883.8 Da indicated the successful incorporation of the DOTA-maleimide to the DARPin with ~100% efficiency, Figure 6.5. The trace showed no background protein contaminants or unconjugated DARPin within the final G3-DOTA pool. An internal standard, Myoglobin, was added to the mass spectrometry analysis as a validating control in run performance.

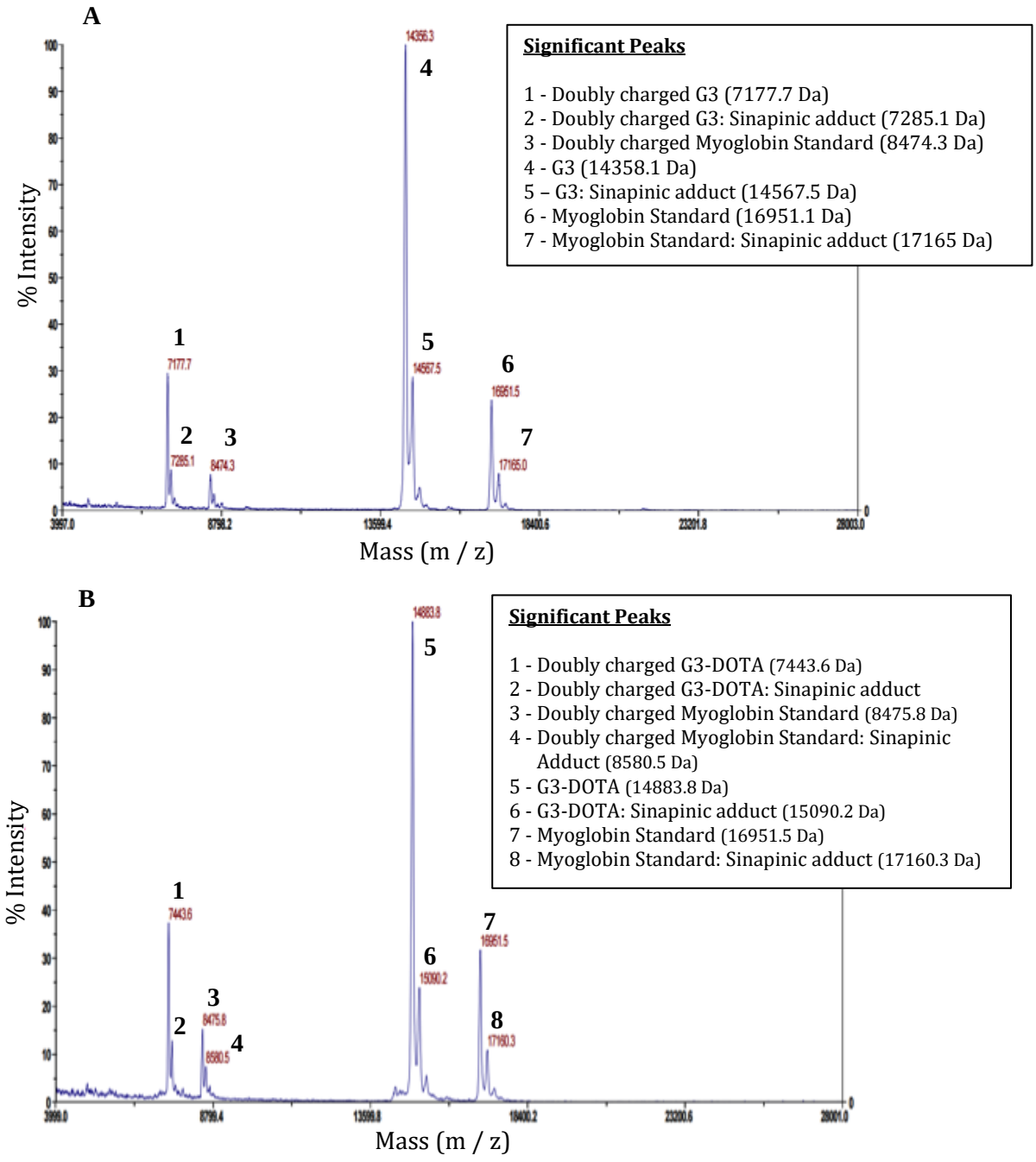

FIGURE 6.5: Mass Spectrometry of G3 DARPin pre- and post-DOTA conjugation.

6.2.5 *Integration and expansion to facilitate imaging agent production.*

As highlighted in the precluding sections the key process parameters for DARPin to maleimide-DOTA conjugation and the generated conjugates ability to radiolabel can be broken down into four predominant components. These components are; availability of accessible thiols, a solution devoid of metal ions, a pH of 6.5-7.5 and DARPin at a final concentration of 1 mg/mL. To minimise the addition of subsequent steps and thereby allow a seamless follow on, the labelling process should, as much as possible, utilise unit steps already present. To this extent the conjugation procedure was initiated following the AEX purification step of the established bioprocess (Figure 5.9, Chapter 5) in a flow-scheme as depicted by Figure 6.6.

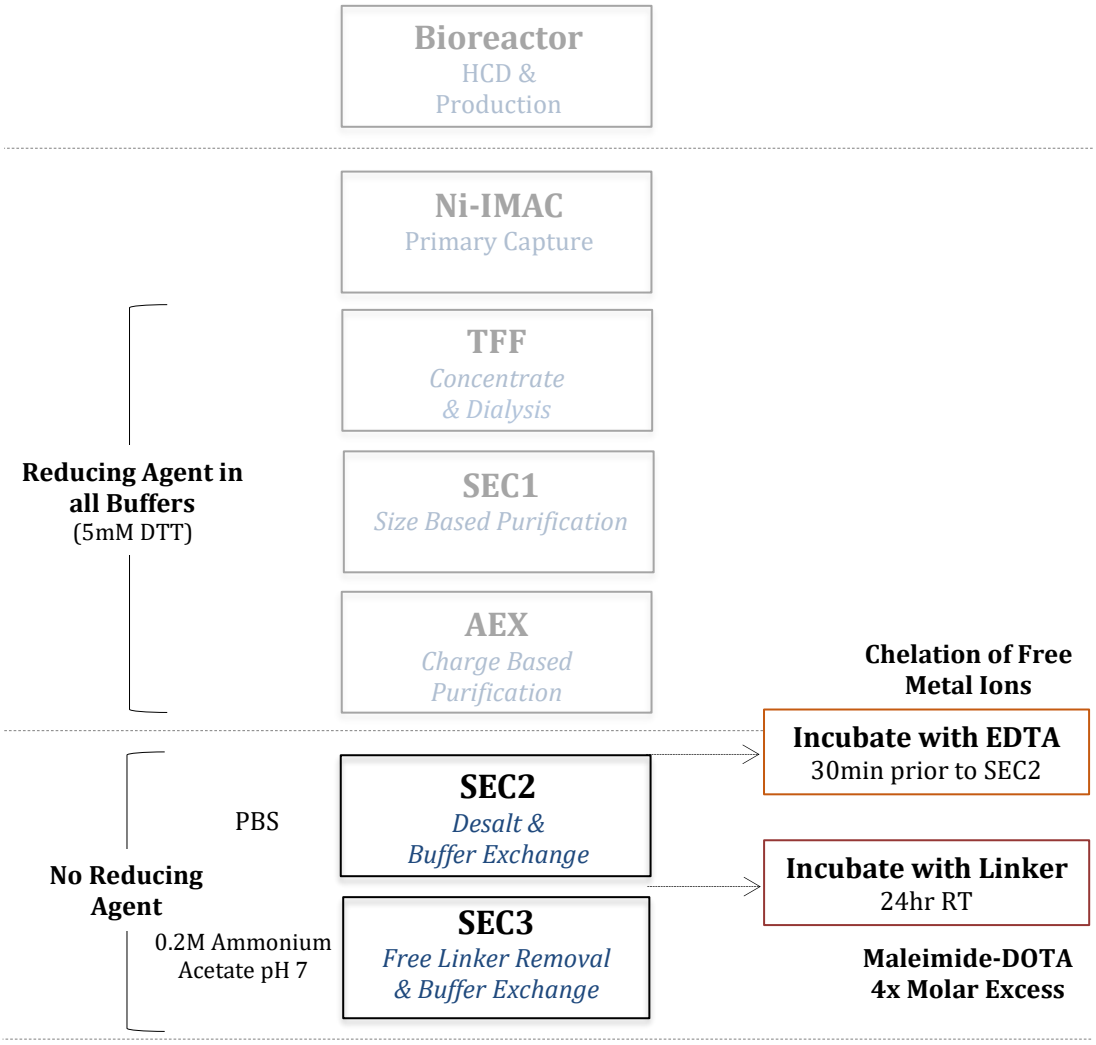

FIGURE 6.6: Postulated bioprocess for the production of a DARPin facilitated imaging agent.

6.2.5.1 AEX purification and ON hold

G3-DARPin was generated as laid out in Chapter 5 with a total of ~100 mg following AEX elution. The eluted pool was held overnight at 4°C before the addition of the metal ion chelator ethylenediaminetetraacetic acid (EDTA) at 1mM final concentration. The sample was incubated with EDTA for 30 minutes at room temperature prior to SEC2 loading.

6.2.5.2 SEC2 and addition of Maleimide-DOTA

The 500 mL SEC column was used instead of the 125 mL SEC column as working at process scale meant a far higher quantity of DARPin to the previous mock run, 2 mg vs 50-60 mg. The column was similarly pre-equilibrated in PBS to facilitate the removal of both EDTA and DTT whilst putting the DARPin in the appropriate buffer conditions for conjugation (Figure 6.7B). The eluted fractions corresponding to monomer DARPin (peak at ~380 mL) were pooled and the OD_{280} determined giving a yield of 54 mg. Maleimide-DOTA was added at a 4 molar excess to DARPin and left overnight at room temperature in a sealed container.

6.2.5.3 SEC3; Free linker removal

The next day the sample was loaded onto another 500 mL Superdex75 column pre-equilibrated with 0.2 M ammonium acetate, SEC3. A different but identical column was used, as when taking this process to the facility the turn-around would be extremely tight with three SEC steps on consecutive days for a single column. There were two clear peaks on the chromatogram at 400 mL and 470 mL corresponding to DARPin-DOTA and free maleimide-DOTA, Figure 6.7-B. A tight cut of the eluted peak was taken in order to maintain DARPin-DOTA concentration equal to or above 1 mg/mL without the addition of a concentration step. The difference in volume at which the peaks elute from one column to another is a result of packing variation as can be seen when protein standards are run and compared. This process generated 40 mg of G3-DOTA at ~ 1 mg/mL

Unconjugated and conjugated samples following SEC2 desalting and SEC3 free linker removal were run under reducing conditions on an 18% SDS-PAGE gel and visualised with coomassie stain. The clear shift in MW post linker addition is evident and treatment under both conditions appears not to affect the integrity of the DARPin with a singular band present in both samples run, Figure 6.7-A. The G3-DOTA was sent for radiolabelling and was determined to be 97% radiolabelled.

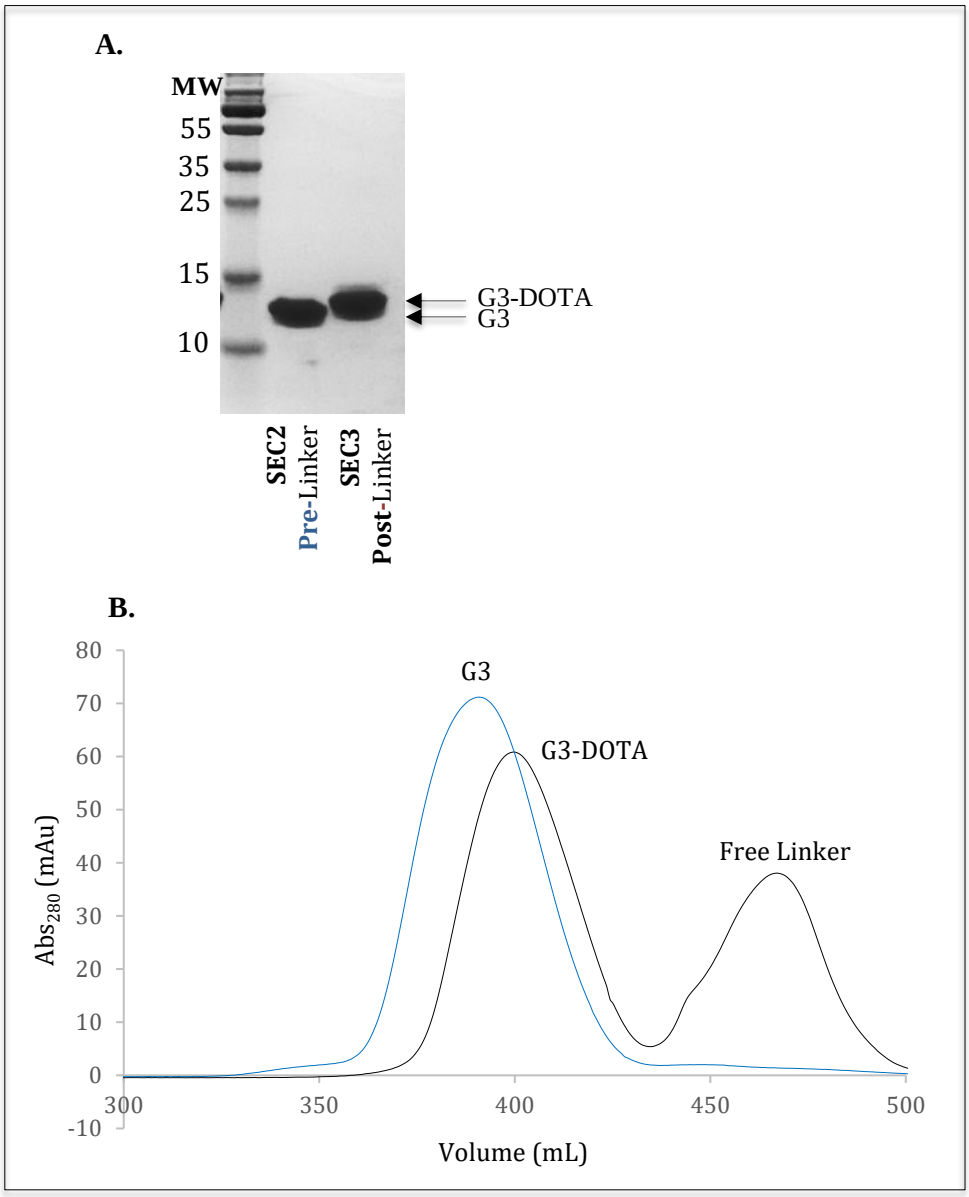

FIGURE 6.7: Chromatogram and SDS-PAGE of SEC2 and SEC3 for the production of a G3 imaging agent.

A, SDS-PAGE analysis of G3 DARPin prior to and after maleimide-DOTA conjugation. Samples were run under reducing conditions on an 18% SDS-PAGE gel and visualised with coomassie stain. **SEC2,** removal of EDTA / DTT and buffer exchange into PBS for maleimide-DOTA conjugation. **SEC3,** separation of G3-DOTA from unconjugated maleimide-DOTA and buffer exchange into 0.2M ammonium acetate in preparation for radiolabelling.

B, Chromatogram of the adapted steps for imaging agent production. Two 500 mL Superdex75 Columns were used. ~25 mL loaded using a 500 mL super loop. **Blue,** SEC2. **Black,** SEC3.

6.3 Final Process Characterization

The developed imaging agent process was characterised in terms of the attributes of the final product generated. To this effect the product was assessed by mass spectroscopy (Section 6.3.1), binding affinity (Section 6.3.2), HCP and endotoxin content (Section 6.3.3) and radiolabelling efficiency (Section 6.3.4).

6.3.1 Mass Spectrometry

The product from the three independent runs was assessed using MALDI-TOF by Dr Emmanuel Samuel (UCL) at fill (t=0), 6 (t=6) and 12 (t=12) months, the results of which are shown in Table 6.0. Myoglobin was once again used as an internal validating control for the run. A pass, in terms of acceptable deviation from the theoretical value as a result of instrumental limitations, was stated as ± 0.05%.

The theoretical mass of $(HE)_3$-G3 DARPin is 14358 Da and the fully conjugated $(HE)_3$-G3-DOTA is 14884.41 Da. As such the product from all three runs had the appropriate MW to be $(HE)_3$-G3-DOTA and proved to be stable over the 12 month period tested, with the percentage difference from the theoretical MW never exceeding ± 0.03%.

Table 6.0: Mass Spectrometry evaluation of three G3-DOTA production runs over a 12 month period.
Product, G3-DOTA conjugate. **Difference,** percentage difference in MW from the theoretical mass of the product.

	Mass Spectrometry MALDI-TOF					
Batch No.	**Fill**		**6 Months**		**12 Months**	
	Product (Da)	Difference (%)	Product (Da)	Difference (%)	Product (Da)	Difference (%)
R09	14886.92	+0.017	14882.85	-0.010	14883.33	-0.007
R04	14882.83	-0.011	14882.60	-0.012	14879.97	-0.030
R01	14879.90	-0.030	14881.80	-0.018	14888.40	+0.027

6.3.2 Binding Affinity

6.3.2.1 Surface Plasmon Resonance

Samples were sent to Dr G. Nagy-Davidescu (UZH) for SPR analysis. The binding affinity of the DOTA conjugated DARPin from the three production runs was tested against the extracellular domain of HER2, as shown in Table 6.1.

The product from all three runs had affinity in the nanomolar to picomolar range with equilibrium dissociation constants (K_D) ranging from 3.78 $x10^{-10}$ to 5.95 $x10^{-10}$ M and the analyte binding capacity of the surface (R_{max}) remaining consistent with values of 29.77 to 30.45 RU. This means that conjugation of the DOTA and the bioprocess as a whole delivers a product of unaltered binding characteristics to the original G3 DARPin reproducibly.

Table 6.1: SPR data of the final DOTA conjugated product from three anti-HER2 DARPin production runs.

	Surface Plasmon Resonance (SPR)			
	K_{ass} [$M^{-1}s^{-1}$]	**K_{diss}** [S^{-1}]	**K_D** [M]	**R_{max}** [RU]
R09	1.15E+06	4.35E-04	3.78E-10	30.45
R04	1.10E+06	4.48E-04	4.08E-10	30.18
R01	8.23E+05	4.90E-04	5.95E-10	29.77

6.3.2.2 EC50 Evaluation

The EC50 (half maximal effective concentration) of the G3 imaging agent from three production runs was determined by ELISA. Briefly the plate was coated with HER2 (2 µg/mL), blocked and incubated with G3-DOTA from 2 µg/mL doubling down to 0.00391µg/mL before probing with anti-G3 polyclonal primary (1:500) and anti-Rabbit-HRP secondary (1:3000).

The three DARPin products from section 6.3.2.1 were run in triplicate and a previously fully characterised reference $(HE)_3$-G3-DOTA was used as a performance control. All three batches were tested from the time of fill to 12 months in storage at -80°C. Regardless of the batch tested or time post fill, all gave values in the nanomolar range from 0.9 to 5.6 nM never deviating more than 0.7 nM from the reference. So even though values for the same product can seemingly double from 2.5nM to 5.4nM, this is not a significant difference and has more to do with the limitations of the assay when working at such high affinity values.

Table 6.2: EC50 values of $(HE)_3$-G3-DOTA from three production runs.

	EC50 (nM)					
Batch No.	**Fill**		**6 Months**		**12 Months**	
	Reference	Product	Reference	Product	Reference	Product
R09	2.5	2.6	5.4	5.6	2.1	2.1
R04	2.3	1.9	3.0	2.3	1.9	2.0
R01	1.0	0.9	2.6	2.9	1.9	2.0

6.3.3 Host Cell Protein and Endotoxin Content

The final DARPin product from runs R09, R04 and R01 was tested for the presence of *P. pastoris* host cell protein (HCP) and endotoxin. HCP was tested using a validated *P. pastoris* HCP kit (Cygnus) utilising a sandwich ELISA protocol. Endotoxin quantity was measured using the regulatory compliant Charles River PTS cartridge system.

All products tested had < 0.5 ng of HCP per mg of DARPin product and endotoxin amounts below the limit of detection for the device (< 0.05 EU/mL) as shown in Table 6.3. All values obtained are well within regulatory limits.

Table 6.3: HCP and Endotoxin measurements for the DARPin imaging agent.

	HCP and Endotoxin			
Batch No.	**Total G3-DOTA** [mg]	**G3-DOTA** [mg/mL]	**HCP** [ng/mL]	**Endotoxin** [EU/mL]
R09	39	1.01	0.45	<0.05
R01	40	0.98	0.21	<0.05
R04	36	1.03	0.16	<0.05

6.3.4 Radiolabelling Efficiency

As in previous chapters the DOTA-conjugated G3 DARPin was sent for radiolabelling studies to Dr Julia Blower (Kings College London). Once again the radio-isotope Indium^{111} was used to evaluate labelling efficiency of the DARPin after undergoing the adapted bioprocess for the specific manufacture of DARPin-based imaging agents, Figure 6.6.

The analytical techniques high performance liquid chromatography (HPLC) and instant thin layer chromatography (iTLC) were used to assess the proportion of radiolabelled product and hence the success of the reaction, Table 6.4. The DOTA conjugated G3 from the three runs, at time of fill and up to two years in -80^{o}C storage, was assessed for radiolabelling efficiency.

All product tested by iTLC, irrespective of storage time, radiolabelled consistently high with ≥ 97% of the final product being ^{111}In-(HE)$_3$-G3. HPLC verified these results with retention times (R_t) of between 10’50 and 10’56 for the product batches tested, whilst free ^{111}In had an R_t of 12’44.

Table 6.4: Analysis of the labelling efficiency of G3 DARPin with radio-isotope ^{111}In using HPLC and iTLC.
0hr, the radiolabelling reaction took place directly after the product was thawed. **24hr,** Radiolabelling took place 24 hours after the product had been thawed and stored at 4°C.

	Radiolabelling Efficiency			
Batch No.	**HPLC (R_t)**		**iTLC (%)**	
	0hr	24hr	0hr	24hr
R09 (At Fill)	10'52	10'53	97	97
R04 (At Fill)	10'54	10'52	100	98
R01 (At Fill)	10'53	10'53	97	97
F16 (~1yr)	10'52	10'52	99	99
F199 (~2yr)	10'56	10'50	99	97

6.5 Discussion

The original conjugation of the bi-functional metal chelator, maleimide-DOTA, to the free cysteine on the C-terminal of the DARPin was designed as a lab scale process using standard documented techniques. As such, no more than 2 mg of protein could be processed per conjugation run, equipment was not wholly regulatory compatible and multiple units of operation were required. This is because a concentration of 1mg/mL of DARPin was shown to be required for efficient conjugation and the components used is the initial process could not process more than 2mL, and therefore we were restricted by volume. The procedure did successfully facilitate conjugation of the chelator to the DARPin, radiolabelling was > 95% efficient and the generated imaging agent used for *in vivo* imaging of HER2 positive breast cancer, Chapter 3 (Goldstein *et al*. 2015). Despite the success of the final product generated, both scaling up this process and making it GMP compliant would be a challenge. As such, stripping back the conjugation process from the conventional multi-unit step to just one operational unit not only increased the overall ease, time and costs but allowed for the efficient integration of the conjugation process to the bioprocess as a whole.

The eluted pool containing DARPin following AEX was held overnight at 4°C before the addition of the metal ion chelator ethylenediaminetetraacetic acid (EDTA), at a final concentration of 1mM. The column was similarly pre-equilibrated in PBS to facilitate the removal of both EDTA and DTT whilst putting the DARPin in the appropriate buffer conditions for conjugation. The next day the sample was loaded onto another 500 mL Superdex-75 column pre-equilibrated with 0.2 M ammonium acetate, SEC3. A tight cut of the eluted peak was taken

in order to maintain DARPin-DOTA concentration equal to or above 1 mg/mL without the addition of a concentration step. This process generated 40 mg of G3-DOTA at ~ 1 mg/mL.

On average 40 mg of conjugated DARPin was generated with this procedure at 1 mg/mL and < 0.5 ng/mL HCP and < 0.05 EU/mL Endotoxin. One vial is enough per patient and therefore a single DARPin production run generates enough product for 80 patient doses. Given that a minimum of three production runs are typically required to satisfy regulatory demands and that a Phase I clinical trial consists of 10-15 patients, these runs would generate enough DARPin for ~200 patients and therefore potentially enough for Phase I, II and potentially Phase III clinical trials, if required.

The final conjugated product from all tested batches was shown to be stable and fully functional for at least two years post-fill with no change in MW (14,884.41 ±0.03%), K_D (3.78 x10^{-10} to 5.95 x10^{-10} M), EC50 (0.9 to 5.6 nM) nor radio-labelling efficiency at > 97%, regardless of the storage time.

6.6 Conclusion

The previously determined conjugation process used by Goldstein *et al.*, 2015 used 4 units of operation over a period of ~6 days to process a maximum of 2 mg of G3 DARPin. Though successful in both conjugation and radiolabelling of the product a more regulatory compliant and easier to implement process was sort after for GMP grade imaging agent production.

The key process parameters for DARPin to maleimide-DOTA conjugation and the generated conjugates ability to radiolabel can be broken down into four predominant components. These components are; availability of accessible thiols, a solution devoid of metal ions, a pH of 6.5-7.5 and DARPin at a final concentration of 1 mg/mL. To minimise the addition of subsequent steps and thereby allow a seamless follow on, the labelling process utilised unit steps already present. To this extent the conjugation procedure was initiated following the AEX purification step of the established bioprocess (Chapter 5). EDTA was added to the AEX derived eluent pool prior to SEC2 loading for the chelation of free metal ions. SEC2 was once again used to desalt and buffer exchange the DARPin into PBS, thereby removing all DTT. A four molar excess of maleimide-DOTA to DARPin was added and the solution incubated ON. The only new unit step added to the process was the addition of a final SEC to facilitate the removal of free linker and buffer exchange into 0.2 M ammonium acetate for direct radiolabelling.

This process generated 40 mg of G3-DOTA at ~ 1 mg/mL and radiolabelling with greater than 97% efficiency. The G3-DOTA was shown to be fully functional and stable with consistent MW, EC50 and radiolabelling efficiency for up to two years post storage.

CHAPTER SEVEN

EMPLOYMENT OF MOLECULAR CLONING TO ADDRESS BREAKDOWN

7.0 Employment of molecular cloning to address breakdown

7.1 Introduction:

As shown in Chapter 4 long fermentation runs for the G3 are hampered by the appearance of a lower molecular weight product in conjunction to the full length DARPin. In order to access the mechanism behind the resultant lower MW DARPin, the portion of G3 that is represented by this fragment needs to be identified. After which methods to investigate and inhibit its formation can be investigated.

To evaluate the developed bioprocess of Chapter 5 as a platform process for DARPin production one needs to assess its success when using another independent DARPin. E69 is a 21.5 kDa anti-EGFR DARPin developed by The Plückthurn Lab (UZH) which binds to an epitope located at the c-terminal end of ectodomain-I and does not interfere with ligand EGF binding (Boersma *et al* 2011). This DARPin is of clinical relevance as the over-expression of EGFR (HER1) has been reported in > 50% of glioblastomas (Kalman *et al*. 2013; Xu et al 2017) and has been used as a target with a variety of therapeutic approaches (Westphal *et al*. 2017). As a contender for another first-in-man clinical trial a cGMP process for its production is of great relevance. Therefore E69 is an ideal model DARPin to test the developed G3 manufacturing procedure for use as a platform process.

Aims:

To evaluate and attempt to address lower MW band formation identified during time course fermentations. To consequently determine if the means of inhibition and the G3 bioprocess itself could work as a platform process for DARPin production.

Objective:

- N-Terminal Sequencing of upper and lower MW bands as resolved by SDS-PAGE. This will aid in determining whether the lower MW weight DARPin is a result of proteolytic cleavage or internal ribosome initiation site.

- Substitution of the Methionine at position 30 to Leucine generating G3 M30L so as to investigate whether removal of this internal methionine inhibits truncated product formation.

- Time course fermentation of X33 expressing G3M30L to assess the propensity of this new construct to form two variants in comparison to the WT.

- SPR analysis of G3 M30L to determine whether the mutation of the Methionine to Leucine has altered the binding affinity of the DARPin.

7.2 Investigation of Lower MW Protein

7.2.1 N-Terminal Sequencing

Clarified supernatant from an overnight induced G3 DARPin *P. pastoris* culture in the BioFlo 3000 vessel (New Brunswick) was run under reducing conditions on an 18% Tris-Glycine SDS-PAGE gel and underwent coomassie staining. Two notable bands were present of an approximate molecular weight of 14 kDa and 10 kDa; these were excised and sent to Alta Bioscience LTD for N-terminal analysis, Figure 7.0A.

N-terminal sequencing of the first 5 amino acids confirmed the band of higher molecular weight to be full length G3 whilst the lower molecular weight band appeared to be truncated in the N-cap region immediately before an internal methionine at amino acid position 30, Figure 7.0B. This action could have been a result of proteolytic cleavage or an internal ribosomal reading site. Regardless of the underlying cause the action was causing the removal of almost a quarter (29aa, 3.25 kDa) of the required G3 product resulting in a tag-less G3 of 135aa, 14.36 kDa and a pI of 4.79.

In order to dually determine the underlying cause for the truncated product and attempt to inhibit the action the methionine at position 30 was changed to the amino acid leucine. Leucine was chosen as its sidechain is similarly of a hydrophobic nature and size and would therefore less likely affect protein structure and stability.

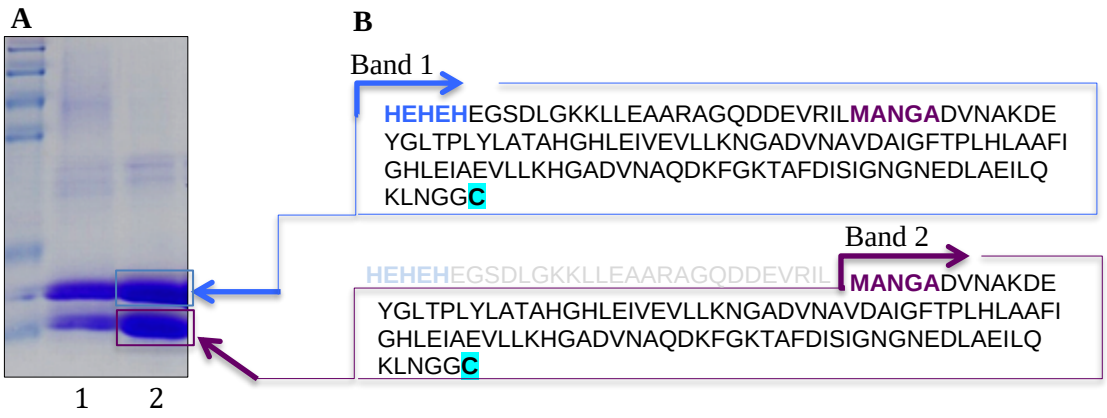

FIGURE 7.0: N-Terminal amino acid analysis of two notable proteins present in the supernatant following O/N induction of G3 in a 10-L Bioreactor.
18% SDS-PAGE run under reducing conditions. Reducing agent was added at a 1:4 ratio to clarified supernatant and heated to 95ºC for 5 minutes. **1,** 10 µL Loaded **2,** 20 µL Loaded. **Blue, Red Rectangle** denote higher MW and lower MW bands, respectively, which were excised and sent for N-terminal sequencing without further processing.

7.3 Cloning of G3 DARPin Methionine to Leucine Variant

7.3.1 XbaI and XhoI digested pPICZαB plasmid & G3M30L gene block

The pPICZαB plasmid (3597 bp) and the DNA encoding the G3 DARPin with the methionine to leucine mutation (G3 M30L) (~450 bp) were digested by restriction enzymes *XbaI* and *XhoI*. The pPICZαB digest underwent gel electrophoresis on a 1% agarose gel (Figure 7.1) and the bands of appropriate size excised before being gel purified for subsequent ligation. The digested gene block fragment underwent phenol/chloroform extraction prior to ligation at a 3:1 insert to vector molar ratio.

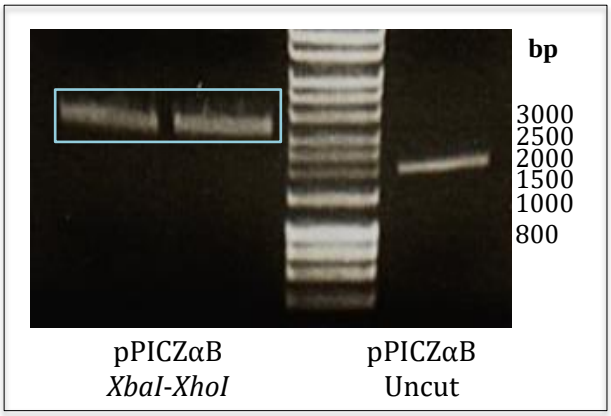

FIGURE 7.1: 1% Agarose Gel depicting cleavage of vector pPICZαB with restriction enzymes *XbaI-XhoI*.
Uncut pPICZaB was run alongside the digested vector as a negative control. **Blue rectangle,** DNA bands isolated from the gel and column purified for ligation with G3M30L insert.

7.3.2 Electroporation & Overnight Culture of transformed TG1 Cells

The *E. coli* strain TG1, was transformed with ligated vector pPICZαB_G3M30L and identified using antibiotic mediated selection. There were approximately twelve colonies per low salt LB/Zeocin™ (25 µg/mL) plate.

7.3.3 PCR identification of Positive Clones

Construction of a pPICZαB expression vector encoding the gene for G3M30L was demonstrated by colony PCR with primers AOX3' (5'- GCAAATGGCATTCTGACATCC -3') and AOX5' (5'- GACTGGTTCCAATTGACAAGC -3'). The AOX primers amplify the DNA from either side of the MCS in the pPICZαB vector generating a far larger fragment upon successful gene insertion than what would be present from the MCS alone. As demonstrated in Figure 7.2, where the AOX PCR yielded a band of approximately 500 bp for the empty

vector and a band of approximately 700-800 base pairs, corresponding to the expected size of pPICZαB_G3M30L, in both of the tested colonies.

FIGURE 7.2: Colony PCR of pPICZ*α*B-G3M30L transformed *TG1* cells.
1% Agarose Gel with each PCR reaction equally split amongst 3 wells. **Colony 1 / 2,** TG1 colony 1 and 2 respectively, selected by zeocin resistance (25 µg/mL) for vector integration. **pPICZ*α*B,** native expression vector.

7.4 Transformation and Expression Testing of G3M30L

7.4.1 Amplification and PmeI linearization of pPICZαB_G3M30L

50 mL of overnight culture inoculated with clone 1 was divided in two and midi-prepped (Qiagen) yielding 1700 ng/µL of pPICZαB_G3M30L. The expression plasmid (5-10 µg) was then linearized with *PmeI*, which cleaves at the 5-prime region of the AOX promotor allowing integration into the yeast genome. The linearised construct was run on a DNA agarose gel along with the uncut supercoiled vector as a control. Linear plasmid runs slower and as one band in comparison to supercoiled DNA which runs faster and has multiple forms present, Figure 7.3.

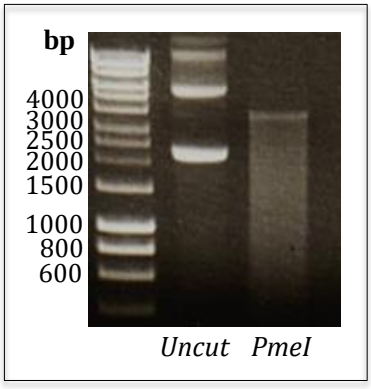

FIGURE 7.3: Agarose gel (1%) depicting the *PmeI* restriction enzyme digest of pPICZ*α*B containing construct G3 M30L.
Uncut, the undigested vector. ***PmeI*,** the *PmeI* treated vector.

Following confirmation of linear state by agarose gel electrophoresis the vector was chloroform extracted and re-suspended into 5 µL of sterile dH_2O prior to electroporation into freshly made electro-competent, *P. pastoris* X33. The electroporated cells were incubated at 30ºC and

subsequently plated onto YPDS plates containing 100 µg/mL Zeocin™. The plates were incubated for a period of 72 hours at 30°C and resulted in ~50 colonies per plates

7.4.2 Shake Flask Test Expression of Transformed X33 cells

Four clones of pPICZαB_G3M30L were isolated from the aforementioned plates and glycerol stock generated. This stock was used to inoculate 5mL of BMGY, grown over night and spun down and re-suspended to an OD_{600} of 1 in BMMY media in 250 mL shake flasks. The cultures were incubated at 30°C 220 rpm for 72 hours and DARPin production assessed. The culture supernatant 48 hours post methanol induction underwent cellular clarification and SDS-PAGE analysis, Figure 7.4. Three of the four chosen clones (Clone 2-4) appeared to express a protein of appropriate molecular weight at 14 kDa. Clone 1 either didn't express or expressed below the threshold of sensitivity for visualisation, in the case of a coomassie stained gel typically <50 µg/mL. Clone 3 whose band is qualitatively perhaps most evident was chosen as lead clone.

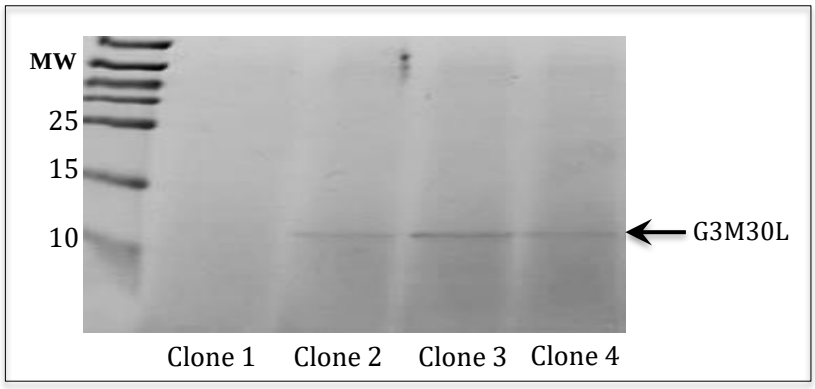

FIGURE 7.4: Shake-flask test expression of construct $(HE)_3$-G3 M30L in *X33*.
Clarified supernatant 48 hours post methanol induction was run under reducing conditions on an 18% SDS-PAGE prior to coomassie staining. **Clone 1-4**, four individual clones' isolated following Zeocin™ selection of transformed *X33* cells.

7.4.3 10L Bioreactor Test Expression

Clone 3 was then taken forward for high cell density fermentation. A 10-L BioFlo3000 Bioreactor used at a 5-L working capacity was inoculated with seeding culture. A fed-batch glycerol feeding strategy was employed to reach a high biomass prior to methanol induction as described in Chapter 3.

Bioreactor test expression indicated the presence of possible breakdown 33 hours post dO_2 spike (Figure 7.5) far later than that observed for the wild type G3 DARPin.

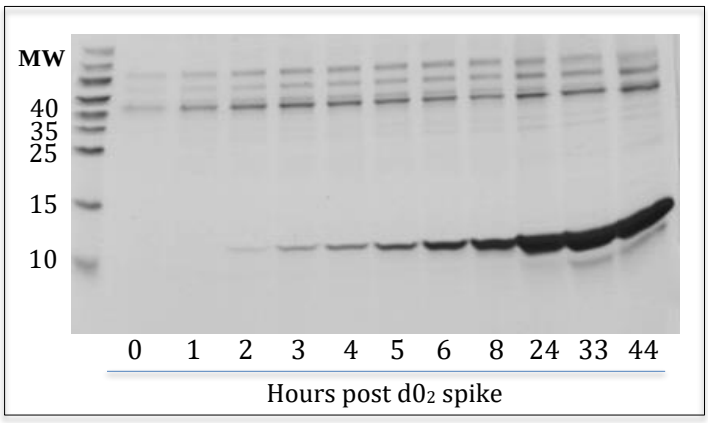

FIGURE 7.5: Bioreactor test expression of $(HE)_3$-G3 M30L over a period of 44 hours.
18% SDS-PAGE run under reducing conditions and coomassie stained.

7.5 Product analysis; $(HE)_3$-G3 M30L

7.5.1 N-terminal Sequencing

Supernatant from the 44 hour time point of the fermentation in section 7.4.3 was clarified via centrifugation and run under reducing conditions on an 18% SDS-PAGE gel, Figure 7.6 -B. The coomassie brilliant blue-250 stained gel showed the clear resolution of two protein bands at an approximate molecular weight of 10 kDa and 13-14 kDa. Both protein bands were excised and sent to Alta Bioscience LTD for N-terminal analysis. N-terminal analysis showed that the lower molecular weight band was truncated DARPin initiating at the leucine at amino acid position 30. So although the proteolytic action seen by the original G3 construct had been slowed by the change of methionine to leucine that region was still susceptible as seen by the appearance of the lower MW DARPin product, Figure 7.6 -C.

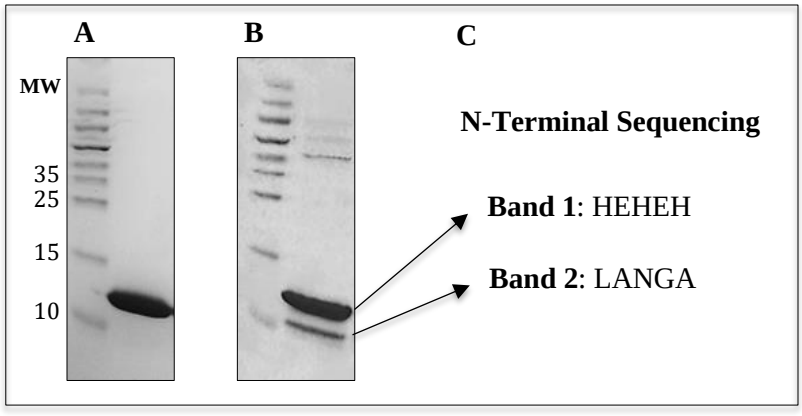

FIGURE 7.6: Identification of the first five N-terminal amino acids.
A. Protein following capture and purification (IMAC, TFF & SEC). **B.** Clarified fermentation broth 44 hours post dO_2 spike. **C.** N-terminal sequencing of two proteins isolated following SDS-PAGE. **Band 1**, Protein of MW ~14 kDa. **Band 2**, Protein of MW ~10 kDa.

7.5.2 Binding Affinity

Surface Plasmon Resonance (SPR) analysis was performed by Dr G. Nagy-Davidescu (UZH) to assess whether the change from methionine to leucine had any effect on the binding affinity of the DARPin to its cognate antigen (HER2). Samples were run in duplicate on both the wild type G3 and G3 M30L. As shown in Table 7.0, there was no significant difference in binding affinity between both the wild type and the methionine to leucine G3 variant with both constructs displaying binding affinities (K_D) in the nanomolar to low picomolar range, Table 7.0. Thus indicating that the methionine to leucine modification does not affect the binding affinity of the DARPin and would therefore in future be a plausible means of inhibiting cleavage of that constant region.

Table 7.0. SPR affinity data for wild type G3 and methionine to leucine variant G3 M30L.

Construct	K_{ass} [$M^{-1}s^{-1}$]	K_{diss} [s^{-1}]	K_D [M]	Rmax [RU]
G3	3.26E+05	3.76E-04	1.15E-09	46.91
G3	3.03E+05	3.88E-04	1.28E-09	48.41
G3M30L	1.20E+06	3.17E-04	2.63E-10	52.29
G3M30L	1.08E+06	3.27E-04	3.02E-10	52.39

7.6 Cloning of Anti-EGFR DARPin Wild-type and M30L Variant

7.6.1 Sequence of Constructs E69 and E69M30L

The E69 WT and M30L mutant were designed to have, as with the G3, an N-terminal $(HE)_3$-tag and C-terminal cysteine as shown in Figure 7.7.

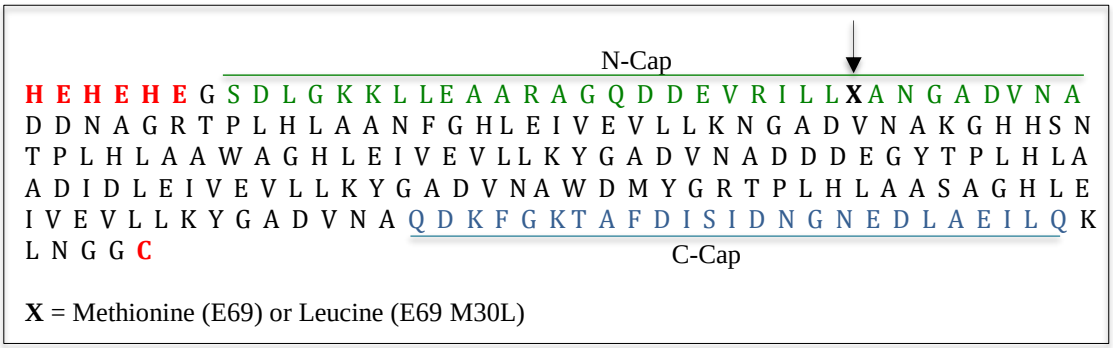

FIGURE 7.7: Amino acid sequence of E69 WT and M30L variant.
Green and **Blue**, the amino acids of the conserved N-Cap and C-Cap regions respectively. **Arrow,** site of mutated residue.

Processing of the leader sequence to the mature protein takes place at a consensus sequence (KR) and is performed by the *P. pastoris* protease KEX2. The expression plasmid contains a sequence encoding this site just adjacent to the gene of interest. The gene sequence was checked for any internal KR sites as they could result in the disadvantageous cleavage of the product.

As demonstrated in the above schematic (Figure 7.7) the E69 DARPin contains no internal KEX2 cleavage sites and therefore no modification of the sequence was required.

7.7.2 XbaI and XhoI digested pPICZαB plasmid & E69 WT and M30L gene block

The E69 WT and E69 M30L gene blocks were digested with restriction enzymes *XhoI* and *XbaI* before being run on a 1% agarose gel. As highlighted by the blue rectangles in Figure 7.8, these DNA bands of appropriate size were excised and purified. Following this the DARPin gene constructs were ligated at a 3:1 ratio with 50 ng of the *XhoI* and *XbaI* digested and purified pPICZαB vector.

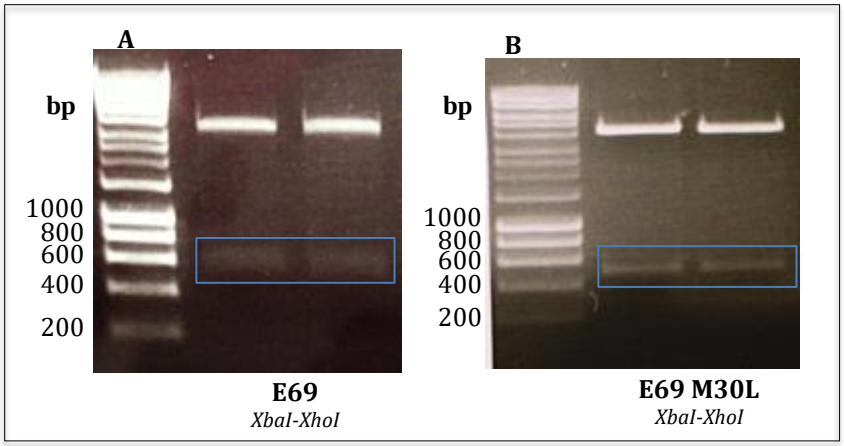

FIGURE 7.8: Digest of Gene Blocks E69 and E69 M30L using restriction enzymes *XhoI* and *XbaI*.
A. E69 WT **B.** E69 containing the methionine to leucine mutation. **Blue rectangle,** DNA bands isolated from gel and column purified.

7.7.3 Electroporation and culture of transformed E. coli

The ligated expression plasmids underwent phenol / chloroform extraction prior to electroporation into competent TG1 cells. The transformed cells were plated onto to low salt LB agar containing 25 µg/mL Zeocin™ for selection. Following an ON incubation at 37ºC there were approximately 100 colonies per plate. Three colonies of each construct were re-plated (YPD/Zeocin™ plates) and used to inoculate 5mL of YPD media containing 25µg/mL Zeocin™. The cultures were grown ON at 37ºC and mini-prepped to isolate the plasmid DNA before being sent for sequencing using primers AOX5'(5'-GACTGGTTCCAATTGACAAGC -3') and AOX3' (5'-GCAAATGGCATTCTGACATCC-3') to confirm the presence of the E69 WT and E69 M30L gene insert.

7.7.4 Vector amplification and linearization

Sequencing confirmed the presence of appropriate insert for all colonies tested for both E69 WT and E69 M30L. One of each of these colonies per construct was chosen and grown in LB

Zeocin™ ON for plasmid amplification and midi-prepped for plasmid extraction. The isolated plasmids were linearised with *PmeI* to facilitate integration into the yeast genome. Digested and undigested plasmid underwent agarose gel electrophoresis to confirm plasmid linearization.

7.7.5 Transformation of competent X33

5 µg of linearised plasmid of each construct was added to 80 µL of freshly prepared electro competent *P. pastoris X33* cells. The cell/DNA mixture was electroporated and plated onto YPDS plates containing 100 µg/mL Zeocin™ ($C_{60}H_{89}N_{21}0_{21}S_3$) for selection. After a 72 hour incubation period at 30°C there were approximately 15-20 colonies per YPDS plate for both the wild-type and mutated constructs.

7.7.6 Shake flask test expression of WT and M30L E69

Four colonies of both the E69 WT and E69 M30L were selected and used to inoculate 5 mL of BMGY media containing 100 µg/mL Zeocin™. This was incubated at 30°C overnight to an OD_{600} of 4-6. The cultures were then centrifuged at 1500 xg for 5 minutes and the cells re-suspended in the methanol containing induction media BMMY to an OD_{600} of ~1 in order to initiate recombinant protein expression.

Samples were taken at 24 and 48 hours post induction, clarified, the supernatant was combined with 4x reducing buffer and heated at 95°C for 5 minutes. The samples were loaded onto SDS-PAGE gels and coomassie blue R250 stained, Figure 7.9.

All eight tested clones expressed their respective DARPin constructs from as early as 24 hours post-induction. The *X33* colony denoted by the number 2 of both E69 and E69 M30L in Figure 7.9 –A & -B, were chosen to be taken forward for future work. The decision was qualitative in nature based on the band intensity of their respective SDS-PAGE gels.

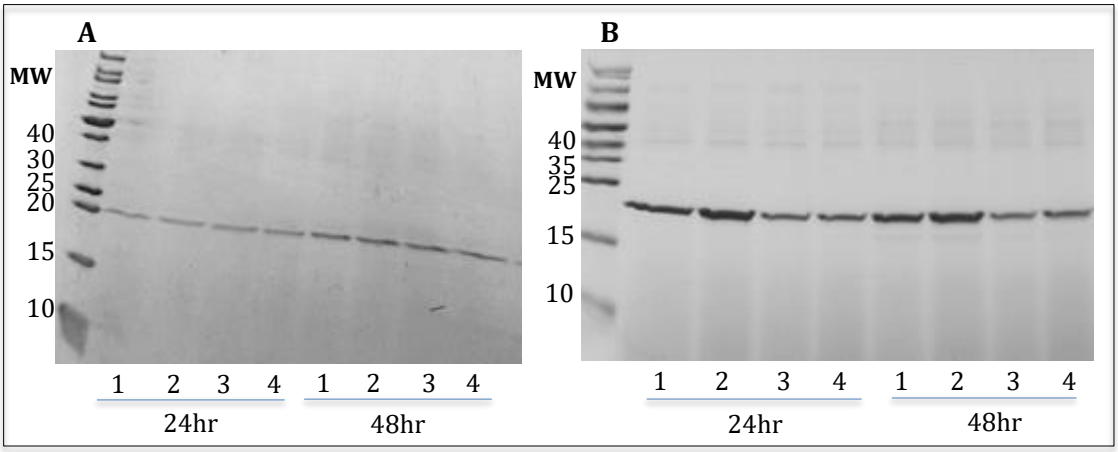

FIGURE 7.9: Shake flask test expression of clones positive for the E69 (A) and E69 M30L (B) constructs.

18% SDS-PAGE / Coomassie Stained. **24/48hr**, Hours post methanol induction. **1-4**, Individual colonies 1, 2, 3 or 4.

7.7.7 10-L Bioreactor Test Expression of WT and M30L E69

A 10-L New Brunswick BioFlo3000 bioreactor was used at a 5-L working volume for the production of both the DARPin constructs. The bioreactor was inoculated with 250 mL of overnight (OD_{600} ~5) seeding culture. A fed-batch glycerol feeding strategy was employed to reach a high cell density prior to methanol induction as previously described. The E69 WT and M30L constructs were cultured for 18 hours and 45 hours respectively. Supernatant was taken throughout the fermentations, clarified and run under reducing conditions on SDS-PAGE gels. Protein was visualised by staining with coomassie brilliant blue-R250, Figure 7.10.

The E69 M30L variant appeared to have significantly less susceptibility to the proteolytic breakdown than the WT E69, with product still visible 45 hours post dO_2 spike, Figure 7.10-B. By comparison the WT E69 was almost completely cleaved into two lower MW band products of 15 kDa and 10 kDa, as early as 18 hours post dO_2 spike, Figure 7.10-A.

Samples from the 8 hour time point for E69 wild -type and the 18 hour time point for E69 M30L were resolved on an 18% SDS-PAGE gel, coomassie brilliant blue-250 stained and sent to Alta Bioscience for N-terminal sequencing. N-terminal sequencing demonstrated that, as for the G3 DARPin, cleavage was taking place before the methionine at position 30 for the WT and prior to the leucine at position 30 for the mutated construct (E69 M30L). This demonstrates that the same mechanism of action is occurring for G3 and E69 DARPin and that the means of inhibition developed are indeed applicable to both.

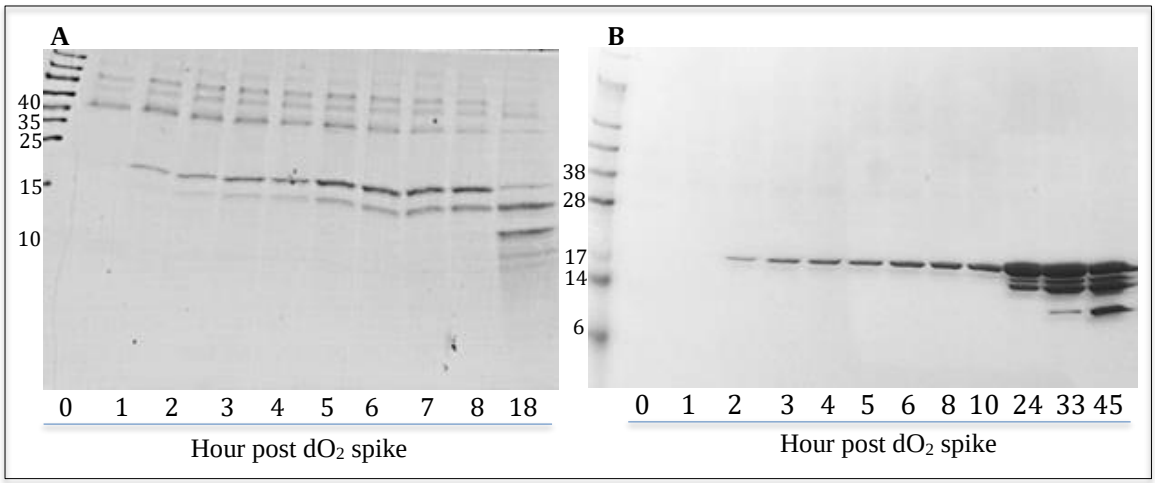

FIGURE 7.10: 10L Bioreactor Test Expression of E69 (A) and E69 M30L (B).
A, 18% SDS-PAGE gel. **B**, 16% SDS-PAGE gel. 20µL loaded. Coomassie brilliant blue-250 stained.

7.8 Production and purification of E69 M30L using the G3 established bioprocess

7.8.1 10-L Bioreactor production of E69 M30L

To assess if the established G3 bioprocess of Chapter 5 could work as a platform process for DARPin production an independent secondary DARPin was chosen to undergo the procedure.

E69 M30L was selected and produced in the BIOSTAT® Cplus bioreactor as stated in section 7.7.7. E69 M30L was harvested early at 4 hours post initial MEOH induction / one hour on MEOH limited feed to keep parameters as consistent as possible with the G3 DARPin runs and not overload the DSP.

The DARPin expressed well with protein visible by coomassie as early as 1 hour post induction Figure 7.11A. Western blot (Figure 7.11B) of the same samples showed breakdown bands from the 2 hour time point which were not evident in the coomassie blue stained gel. Over representation of the quantity of breakdown in the western blot is a result of the over-exposure of the film during development.

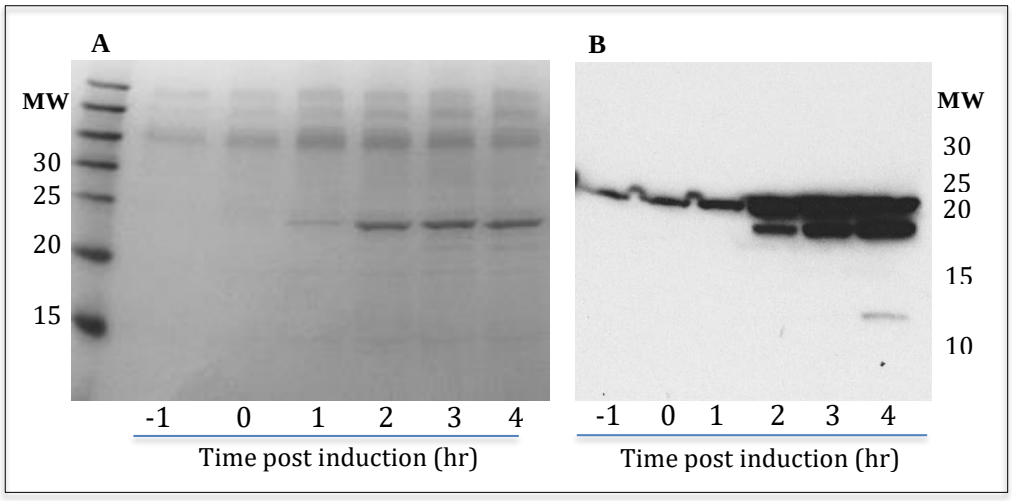

FIGURE 7.11: SDS-PAGE analysis of E69M30L during HCD fermentation.
A, 16% SDS-PAGE / Coomassie under reducing conditions of E69 M30L during HCD fermentation. **B,** Western blot using anti-DARPin primary and anti-rabbit-IgG-HRP secondary.

7.8.2 Bioreactor Harvest and Purification

Bioreactor harvest and purification followed the procedure set out in Chapter 5. Briefly the DARPin was captured by radial flow Ni^{2+}-IMAC, concentrated and dialysed by TFF, size purified by SEC, charge purified by AEX before undergoing buffer exchange and final monomer selection using a second size exclusion chromatography (SEC2) step.

The initial IMAC capture step generated approximately 60 mg of E69 M30L in the 550 mL eluent pool as determined by densitometry. What was similarly noted was a significant proportion of DARPin in the flow through when analysed by SDS-PAGE [Data not shown]. As with the G3 DARPin this unit operation succeeded in removing a significant quantity of the host cell protein with very little, and of a largely high molecular weight, visible by western blot using polyclonal anti- *P. pastoris*-HRP (Cygnus), Figure 7.12. This kit has a reported sensitivity limit of 1 ng / protein band.

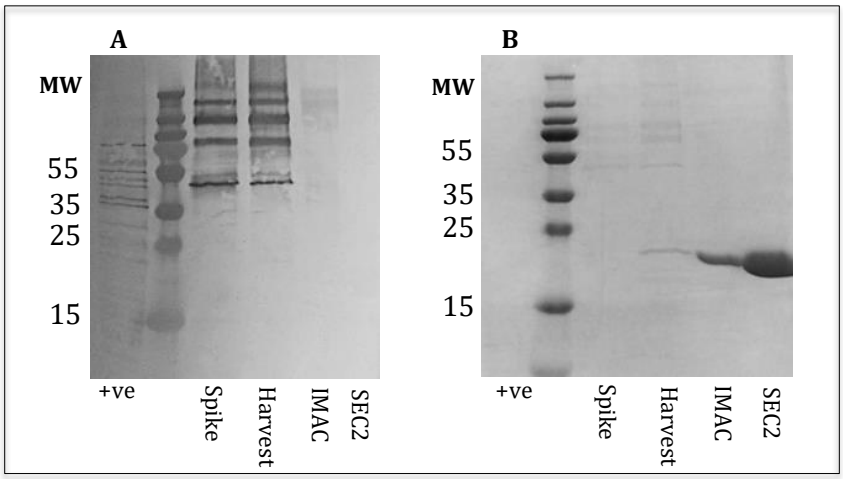

FIGURE 7.12: Analysis of HCP levels during fermentation, after IMAC and final product.
A & B, Visualisation of Host cell protein and E69 M30L DARPin throughout the bioprocess. 16% SDS-PAGE loaded identically. **A.** Western blot probed with anti-*P. pastoris*-HRP and **B,** Coomassie stained. **+ve**, Positive *P. pastoris* HCP standard Cygnus kit. **Harvest**, clarified supernatant at point of harvest. **IMAC**, eluted pool following capture from harvest broth by radial flow IMAC. **SEC1**, pool following first size exclusion chromatography. **AEX**, eluted after anion exchange chromatography of SEC1 pool. **SEC2**, Eluent following size exclusion chromatography of AEX pool / final product.

Purity of the E69 protein fraction at various stages of DSP is illustrated in Figure 7.13. The protein fractions mainly contain E69 following primary capture (IMAC) but impurities are revealed after concentration and dialysis (TFF). This concentrated fraction is further purified during successive DSP steps. As with the G3 the initial size exclusion step (SEC1) removes the majority of HCP contaminants but retains the lower molecular breakdown product, Figure 7.13-A & -B. The parameters for anion exchange chromatography (AEX) were modified for the E69 DARPin as with a pI of 4.64 it is lower than that of G3 at 4.79 and therefore requires a higher salt concentration to be displaced. In this case the wash step contained 28% Tris High Salt Buffer (20mM Tris, 1M NaCl, 5mM DTT, pH 7.5) and a gradient of 28% to 50% Tris High Salt Buffer was applied over 330 mL for elution. E69 M30L elutes at a NaCl concentration of 350 mM in comparison to the 250 mM NaCl observed for the G3 DARPin. SEC2 facilitates the buffer exchange of the DARPin into suitable storage buffer, the chromatogram generated in Figure 713-D is of a single peak eluted at the appropriate volume for monomer E69 M30L.

A total of 40 mg was generated using this procedure and this was taken forward for SPR, mass spectrometry, endotoxin and HCP analysis.

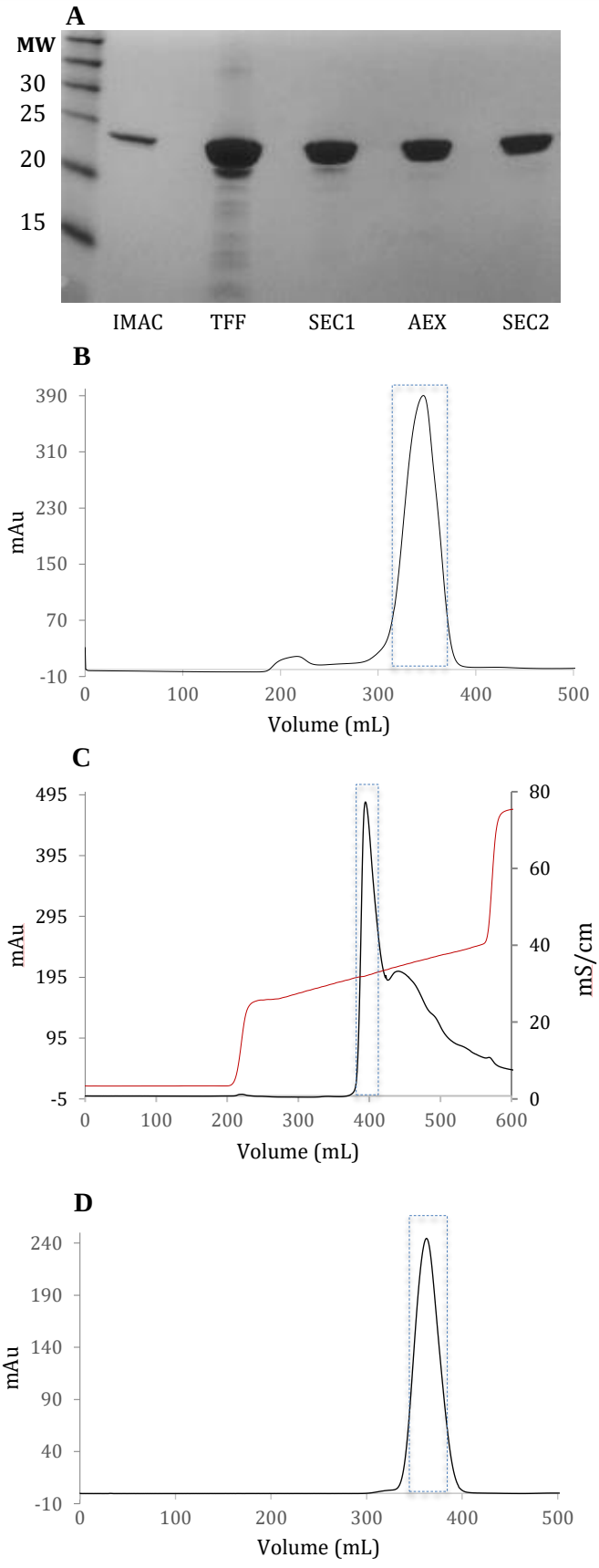

Figure 7.13: Downstream processing of E69 M30L using the bioprocess developed in Chapter 5.

A, 18% SDS-PAGE / Coomassie analysis of E69 M30L following primary capture and subsequent purification.

IMAC, eluent following nickel IMAC capture from culture broth. **TFF**, Pool following concentration and dialysis. **SEC1,** eluent following size exclusion of TFF pool. **AEX,** Pool following Anion Exchange chromatography of SEC1 product. **SEC2**, Buffer exchange of AEX pool and removal of any remaining DARPin dimers.

FPLC Chromatograms;

B, SEC1

C, AEX

D, SEC2

7.9 Binding Affinity of E69 M30L

The binding affinity of both the wild-type and M30L E69 were assessed by Dr G. Nagy-Davidescu (UZH). SPR evaluation of the anti-EGFR DARPins took place using a ProteOn XPR36 (Bio-Rad Laboratories) and the extracellular domain of recombinant human EGFR/HER1 (EMP Genentech). Previous batches of E69 DARPin made in *E. coli* were compared to the *P. pastoris* E69 M30L mutant.

As shown in Table 7.1 the original E69 wild-type and the *P. pastoris* expressed M30L DARPin had no significant difference in their binding affinities with a K_D of 41.1 nM and 38.8 nM respectively. Thus demonstrating that the mutation and the host system used is once again successfully applicable to DARPins.

Table 7.1: SPR analysis of the original E69 WT (*E. coli*) and mutant E69 M30L (*P. pastoris*).

	Previous Batches E69	***P. pastoris* E69M30L**
K_{ass} [$M^{-1}s^{-1}$]	37262.2	41672.9
K_{diss} **[s^{-1}]**	1.532e-3	1.616e-3
K_D [nM]	41.1	38.8

7.10 Product Analysis

Final product analysis by Electrospray Mass Spectrometry was performed by Dr G. Nagy-Davidescu (UZH), Figure 7.14-A. The profile shows a predominant single peak of 21, 490 Dalton, which is similar to the theoretical molecular weight of E69 M30L. Application of the final sample onto a 125 mL size exclusion column (Superdex 75) generated a single peak on the chromatogram at the appropriate location for monomer DARPin. This purity was dually confirmed by SDS-PAGE analysis of the final product, showing upon staining with Coomassie Brilliant Blue R-250 a single band of the expected size of E69 M30L and no contaminating proteins.

Once again the FDA-approved Endosafe Portable Test System (PTS) from Charles River was used to measure endotoxin levels in the DARPin preparations and the *P. pastoris* HCP kit by Cygnus for any remaining host cell protein. The host cell protein (HCP) and endotoxin levels in this product were less than 3.5 ng/mg and 0.05 EU/mg, respectively.

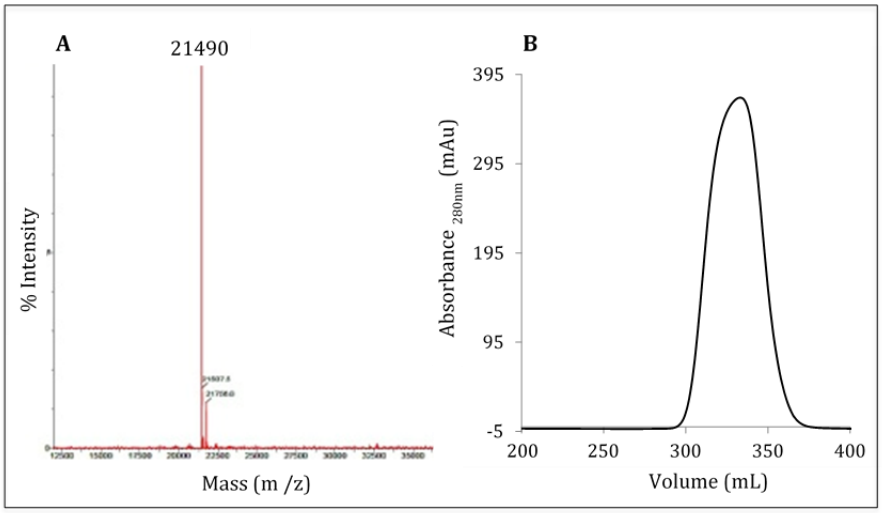

FIGURE 7.14: Assessment of E69 M30L molecular weight and monomeric state.
A, Mass Spectrometry. **B,** FPLC trace using analytical SEC. 1 mL of 0.5 mg/mL E69 M30L was loaded onto a 125 mL column packed with Superdex 75 resin. Run at 1 mL/min.

7.11 Conclusion

The aim of the work presented in Chapter 6 was to a) evaluate and attempt to address the formation of a lower MW DARPin constituent and b) assess the developed bioprocess (Chapter 5) and knowledge gained for use as a platform process.

N-terminal sequencing of the truncated G3 DARPin identified the area being affected to be directly before a methionine in the conserved N-cap region of the DARPin. To assess whether this was a result of internal ribosomal reading or proteolytic activity the methionine was mutated to a leucine. An amino acid with a similarly hydrophobic side chain was chosen to minimize any interference with structure and hence stability and binding. As such this substitution did not affect DARPin binding nor baseline expression. It did however greatly inhibit the appearance of the lower MW DARPin fragment but did not completely abolish it, indicative of proteolytic action. Further mutation of the N-Cap region in question would be required to potentially completely abolish the cleavage of DARPin product.

Both the mutation and developed bioprocess were tested on an independent anti-EGFR DARPin, E69. As with the G3, the mutated E69 DARPin proved to be far more resistant to proteolytic activity than its wild type counterpart and the bioprocess could be used as a platform process, generating 40 mg of fully functional E69 M30L of equivalent purity at <0.05 EU/mL endotoxin and < 3.5 ng/mg HCP.

CHAPTER EIGHT

FINAL DISCUSSION AND LOOKING TO THE FUTURE

8.0 Final Discussion and Looking to the Future

8.1 Discussion

The work described in this thesis was designed and executed to develop a clinically relevant bioprocess for the production of DARPins in the yeast *P. pastoris*. A model protein, the anti-HER2 DARPin was selected based on its clinical potential as a whole body-imaging agent for HER2 positive cancer. DARPins had not previously been manufactured in *P. pastoris* allowing opportunity for challenge and novelty in developing a new bioprocess.

8.1.1 P. pastoris expression and selection of affinity tag.

As with all targeting agents the principle of highly specific binding with low/no non-specific interaction is key to their successful application and as such any means to reduce that background binding/localisation would be highly sought after. Tolmachev *et al*. (2010) first purported, using another targeting scaffold protein termed Affibody, that different purification tags elicit varying effects on the biodistribution of proteins. Tolmachev and co-workers showed that the negatively charged $(HE)_3$-tag performed far better in uptake experiments than the His_6- and tag-less variants. To determine if this was the case for DARPins, G3 constructs were produced containing either a His_6-tag, $(HE)_3$-tag or with no tag (cleavable tag) and the biodistribution assessed within a mouse model.

The biodistribution studies established that as with the Affibodys the $(HE)_3$- tagged G3 DARPin was also superior to the no-tag or hexahistidine tagged variants (Goldstein *et al,* 2015). Consequently the superfluous Glycine-Proline (GP) residue, present for HRV 3C protease cleavage and kept as a constant for the tagged constructs, was removed and the now direct $(HE)_3$ tagged G3 was successfully cloned and expressed in *P. pastoris, X33*. All tested clones expressed and clone 6 was taken forward for high cell density (HCD) fermentations based on the qualitative observation of SDS-PAGE band intensity.

It was essential to test if there were any clinical differences between the new $(HE)_3$-DARPin and the previously studied (GP containing) DARPin. Biodistribution was assessed in both a non-tumour and HER+ tumour model in mice at 4 hours and 24 hours. The new $(HE)_3$-DARPin showed no notable difference from the previous GP engineered variant and as such demonstrated once again the that substitution of the His_6 tag of G3 DARPin with a negatively charged and hydrophilic histidine-glutamate $(HE)_3$ tag can reduce liver uptake whilst enabling tag mediated capture and purification via Ni^{2+}-IDA radial flow chromatography. In conclusion

the $(HE)_3$-G3 DARPin is comparable in both *P. pastoris* expression and *in vivo* biodistribution to the GP-containing variant, $(HE)_3$-GPG3 and was also able to image HER2+ tumours in a mouse model. Therefore $(HE)_3$-G3 will be taken forward for the clinic as it does not have an unnecessary and potentially disadvantageous GP site.

P. pastoris is capable of complex post-translational modification such as the edition of sugar residues (glycosylation) this modification can present both positive and negative outcomes depending on the required product function (Love *et al*. 2018). Glycosylation of residues leads to a decreased half-life and rapid clearance of molecules in the blood (Jia *et al.* 2016). Mass spectrometry of the *P. pastoris* expressed product indicates no obvious N- or O-linked glycosylated residues on the G3 DARPin construct, with no increase in MW from the theoretical. From this it was concluded that the G3 product quality from *P. pastoris* expression did not deviate from that produced by the previous standard *E.coli* method or from the Glycine-Proline containing variant in terms of glycosylation state. SPR analysis also demonstrated that binding affinity to its cognate antigen, HER2, remained unaffected at picomolar affinity.

Finally, the *Ste13* cleavage site Xaa-Pro/Ala, which in literature had been shown to be responsible for n-terminal heterogeneity as a result of inefficient cleavage (Yang S. *et al.* 2013) proved true for the G3 DARPin. Generating multiple forms of G3 with partially, fully and unaltered N-terminal EAEA residues. In taking a product through to clinical trial homogeneity of the final protein therapeutic/agent is of great importance. To rectify this issue the *Ste13* cleavage site was removed and, as has been the case for a number of other recombinant proteins (Joshi *et al.* 2010; Prabha et al. 2009), its removal did not hamper the efficiency of secretion into the extracellular media and produced DARPin with a homogeneous N-terminal.

8.1.2 Design of a GMP compliant DARPin production process

Taking into account the actual cohort size of Phase I and II clinical trials (Umscheid *et al*. 2011) the amount of material required to sustain the entire cohort does not necessitate the need for extensive running costs and downstream handling of unwarranted quantities of protein. A short running, easy to implement approach imparts a practical feasibility for the production of DARPins for use in clinical trials.

Hauling a research project through to clinical trial requires a multi-disciplinary team and is very much labour intensive. Typically within an industrial setting a facility will be fitted to a pre-determined and regulatory compliant production process. Whilst in an academic led endeavour all must occur during the lifetime of the project grant itself and within the agreed upon budget.

Consequently process development alone does not wholly dictate facility layout but rather a combination of both factors play a role in what is the concluding manufacturing process. As such the development of the G3 DARPin bioprocess was not fully dictated by theoretical design, but rather, took into account pre-existing parameters such as facility dimensions, already available equipment and the working success of previous unit operations during the R&D phase of G3 development, in determining a suitable manufacturing process for clinical grade material.

Transfer to a CIP bioreactor allowed for greater control in terms of decreasing the risk of contamination as ports can be sterilised something the autoclavable bioreactor used in development could not. The fermentation protocol enabled the HCD growth of *P. pastoris* and high titres of secreted G3 over a very small window of induction, ~450 mg following one hour of methanol limited feed.

The $(HE)_3$-tagged product was captured directly from crude broth, containing on average 58g cells (DCW), 450 mg DARPin and 5020 mg HCP, using Cellthru™ BigBead technology (Sterogene) coupled with radial flow IMAC. This unit step concurrently clarified the feed stream and captured the G3 DARPin, removing whole cells and 99% of contaminating HCP whilst capturing ~ 50% of the product in < 2 hours of run time. As a unit operation radial flow IMAC is of low maintenance and allows for a small footprint and exceptionally fast process time, combining what is typically two to three pieces of equipment into one thereby saving considerable resources, man-power and time. This technology is additionally easily scalable with indistinguishable hydrodynamic properties to the far larger manufacturing-scale radial flow columns.

A Millipore TFF system provided a closed and fully sanitise-able system from which to concentrate and dialyse the IMAC captured pool. Reducing agent (5 mM DTT) used throughout the process lowered both the quantity of DARPin dimers and the level of protein aggregate formed. The use of a Pellicon® TFF cassette with 5 kDa cut-off membranes, of low protein binding, resulted in a yield of 94% DARPin but also only a 35% loss of HCP as such a low cut-off allows little to get through.

It was noted during the preliminary stages of R&D that the *P. pastoris* culture secreted mainly high MW host proteins into the external media. By using a size separation step they were efficiently removed as were any dimer DARPins present. So a 500 mL Sephadex-75 column was used with a high resolving power from 3-70 kDa. This unit operation resulted in a loss of 34 mg of DARPin, therefore giving a G3 yield of 82.6% and an HCP removal of 99.7%. The final preparation resulting from this step consisted of 99.98% of G3 DARPin, both full-length

and truncated. Although unusual to have a SEC unit operation this early in a process, given that scale up would be restricted, it does work extremely well. As such the pooled DARPin product following this SEC step is largely monomer and already at regulatory compliant levels of both HCP and endotoxin. SEC is an easy to implement and effective technique for use in circumstances where extremely large product quantities are not required, as is the case for clinical trials.

Although SEC generated regulatory compliant product in terms of HCP and endotoxin it was unable to fully remove the lower MW DARPin fragment. In order to remove this and generate a product pool of full length DARPin charge based separation was implemented.

A strong anion exchange resin (Source 30Q) was used and the procedure consisted of a step wash followed by a linear gradient for elution. The uniform 30 μm rigid polystyrene/divinyl benzene polymer matrix allowed for low back pressure and high flowrates with a wide range of working conditions. A tight fraction was pooled to both prevent overloading of the following SEC step and prevent the inclusion of cleaved G3 which elutes at a slightly higher salt concentration than that of the full length protein. There was a loss of 50 mg of DARPin giving a G3 yield of 69% for the unit operation along with the removal of 79% of remaining HCP, this gave a final prep consisting of 99.99% product, all full length G3 as determined by SDS-PAGE and mass spectrometry.

With AEX generating 112 mg of full length DARPin of high purity (99.99%) the final stage was a means of buffer exchange into appropriate storage buffer. This was achieved by SEC using, as before, a 500 mL Superdex 75 packed column pre-equilibrated in PBS and without DTT so as not to interfere with any future conjugation experiments/animal studies. A clean uniform peak was visible on the chromatogram and a tight pool was taken to ensure that the final concentration of DARPin was ≥ 1 mg/mL thereby removing the need for any concentration-based unit operations. As a result of this narrow cut of eluent a final product quantity of 60 mg was acquired from the initial 112 mg, this thereby resulted in a 46% loss of G3 DARPin and a six-fold reduction in the already regulatory acceptable HCP content.

8.1.3 Development of a conjugation process for imaging agent production

Taking imaging agents to market is an expensive and time consuming endeavour, yielding an annual revenue, at best, of $400 million far less than that of therapeutic drugs at $3.4 billion, and consequently is driven largely by academia and smaller biotech's (Agdeppa *et al*. 2009; von Gall *et al.* 2017). But with the advent of personalised / precision therapies this area of

diagnostics is increasingly under demand in order for the successful delivery of stratified medicines. As such imaging agents have been shown to reduce the cost of treatments and increase survival across a wide range of cancers by providing accurate data as to which patients would benefit from which treatments depending on individual tumour markers (von Gall *et al.* 2017). A means of production that is both cost-effective, efficient and of technical ease would be required to take these products forward.

The original conjugation of the bi-functional metal chelator, maleimide-DOTA, to the free cysteine on the C-terminal of the DARPin was designed as a lab scale process using standard documented techniques. As such, no more than 2 mg of protein could be processed per conjugation run, equipment was not wholly regulatory compatible and multiple units of operation were required. This is because a concentration of 1mg/mL of DARPin was shown to be required for efficient conjugation and the components used is the initial process could not process more than 2mL, and therefore we were restricted by volume. The procedure did successfully facilitate conjugation of the chelator to the DARPin, radiolabelling was > 95% efficient and the generated imaging agent used for *in vivo* imaging of HER2 positive breast cancer, Chapter 3 (Goldstein *et al*. 2015). Despite the success of the final product generated, both scaling up this process and making it GMP compliant would be a challenge. As such, stripping back the conjugation process from the conventional multi-unit step to just one operational unit not only increased the overall ease, time and costs but allowed for the efficient integration of the conjugation process to the bioprocess as a whole.

The eluted pool containing DARPin following AEX was held overnight at 4°C before the addition of the metal ion chelator ethylenediaminetetraacetic acid (EDTA), at a final concentration of 1mM. The column was similarly pre-equilibrated in PBS to facilitate the removal of both EDTA and DTT whilst putting the DARPin in the appropriate buffer conditions for conjugation. The next day the sample was loaded onto another 500 mL Superdex-75 column pre-equilibrated with 0.2 M ammonium acetate, SEC3. A tight cut of the eluted peak was taken in order to maintain DARPin-DOTA concentration equal to or above 1 mg/mL without the addition of a concentration step. This process generated 40 mg of G3-DOTA at ~ 1 mg/mL.

On average 40 mg of conjugated DARPin was generated with this procedure at 1 mg/mL and < 0.5 ng/mL HCP and < 0.05 EU/mL Endotoxin. One vial is enough per patient and therefore a single DARPin production run generates enough product for 80 patient doses. Given that a minimum of three production runs are typically required to satisfy regulatory demands and that a Phase I clinical trial consists of 10-15 patients, these runs would generate enough DARPin

for ~200 patients and therefore potentially enough for Phase I, II and potentially Phase III clinical trials, if required.

The final conjugated product from all tested batches was shown to be stable and fully functional for at least two years post-fill with no change in MW (14,884.41 ±0.03%), K_D (3.78 x10^{-10} to 5.95 x10^{-10} M), EC50 (0.9 to 5.6 nM) nor radio-labelling efficiency at > 97%, regardless of the storage time.

This stripped-down conjugation procedure could be incorporated into almost any available bioprocess for imaging agent production and is not solely limited to DARPins. This would limit the requirement of extensive further training of operators and minor adjustments to the already existing template documentation.

8.1.4 Protein engineering to alleviate product cleavage during production

Time course HCD fermentations of the *P. pastoris X33* $(HE)_3$-G3-Cys resulted in the formation of a lower molecular weight band in addition to the expected product. Western blot probed with anti-DARPin highlighted this lower band to be DARPin indicating potential protease action or incorrect ribosomal reading. The full length and lower MW DARPin were N-terminally sequenced. The DARPin fragment was shown to initiate within the conserved N-cap domain directly prior to a methionine residue. To determine whether this was due to internal ribosomal reading or proteolytic cleavage the methionine, at amino acid position 30, was mutated to a leucine. Leucine was chosen as it has a similarly hydrophobic side-chain and would be less likely to confer detrimental structural abnormalities. SPR analysis determined that the change in amino acid had no effect on the binding affinity of the DARPin to its cognate antigen (HER2) with continued K_D values in the picomolar range. This mutation resulted in the inhibition of the protease activity but not its complete abolishment, as would have been the case with an internal ribosomal reading site. Although the mutation did not entirely prevent the proteolytic action it did allow for increased fermentation times from < 6 hours to 44 hours post-dO_2 spike, with minimal cleavage present, and consequently a 75% increase in product yield, as assessed by densitometry.

For the production of large quantities of DARPin and the need for far longer fermentations this breakdown would indeed need to be further addressed. Proteolytic action is well documented in *P. pastoris* (Cregg *et al.* 1993; Sinha *et al.* 2003) and means of tackling it from the addition of protease inhibitors and protein engineering to confer resistance to protease deficient cell lines and media supplementation are well illustrated (Zhang *et al.* 2007).

8.1.5 A platform process for DARPin manufacture

To evaluate the developed bioprocess as a platform process for DARPin production one needs to assess its success when using another independent DARPin. E69 is a 21.5 kDa DARPin developed by The Plückthurn Lab (UZH) which binds to EGFR (HER1) (Boersma *et al* 2011). This DARPin is of clinical relevance as the over-expression of EGFR has been reported in > 50% of glioblastomas and has been used as a target with a variety of therapeutic approaches (Kalman *et al*. 2013; Xu et al 2017; Westphal *et al*. 2017). As a contender for another first-in-man clinical trial a cGMP process for its production was of great relevance. Therefore E69 was chosen as an ideal model DARPin by which to test the developed G3 manufacturing procedure for use as a platform process, including the removal of the inefficient *Ste13* cleavage site and the methionine to leucine mutation, which as present in a conserved region would potentially affect both DARPins.

8.1.5.1 P. pastoris expression and cleavage inhibition

Wild-type E69 and the E69 methionine to leucine variant were cloned and expressed in *P. pastoris*. Both constructs were run under identical fermentation conditions using the BioFlo 3000. Removal of the *Ste13* site did not prevent efficient secretion of the E69 DARPins into the extracellular media. The original E69 wild-type and the *P. pastoris* expressed M30L DARPin had no significant difference in their binding affinities with a K_D of 41.1 nM and 38.8 nM respectively and no indication of N- or O- glycosylation as determined by mass spectrometry.

As with the G3, the E69 M30L variant appeared to have pointedly less susceptibility to the proteolytic breakdown than the WT E69, with product still visible 45 hours post dO_2 spike. By comparison the WT E69 was almost completely cleaved into two lower MW band products of 15 kDa and 10 kDa, as early as 18 hours post dO_2 spike. N-terminal sequencing demonstrated that, as for the G3 DARPin, cleavage was taking place before the methionine at position 30 for the WT and prior to the leucine at position 30 for the mutated construct (E69 M30L). This determines that the same mechanism of action is occurring for G3 and E69 DARPin and that the means of inhibition developed are indeed applicable to both.

Thus demonstrating that the *P. pastoris* host system, removal of the *Ste13* site and the methionine to leucine mutation are applicable to other DARPins.

8.1.5.2 Production process

E69 M30L was used to assess the developed production process. Bioreactor harvest and purification followed the procedure used for $(HE)_3$-G3 (8.1.2) . Briefly the DARPin was captured by radial flow Ni^{2+}-IMAC, concentrated and dialysed by TFF, size purified by SEC, charge purified by AEX before undergoing buffer exchange and final monomer selection using a second size exclusion chromatography (SEC2) step.

The protein fractions mainly contained E69 M30L following primary capture (IMAC) but impurities were revealed after concentration and dialysis (TFF). This concentrated fraction was further purified during successive DSP steps. As with the G3, the initial size exclusion step (SEC1) removed the majority of HCP contaminants but retains the lower molecular breakdown product, visible by SDS-PAGE. The parameters for anion exchange chromatography (AEX) were modified for the E69 DARPin as with a pI of 4.64 it is lower than that of G3 at 4.79 and therefore requires a higher salt concentration to be displaced. In this case the wash step contained 28% Tris High Salt Buffer (20 mM Tris, 1 M NaCl, 5 mM DTT, pH 7.5) and a gradient of 28% to 50% Tris High Salt Buffer was applied over 330 mL for elution. E69 M30L elutes at a NaCl concentration of 350 mM in comparison to the 250 mM NaCl observed for the G3 DARPin. SEC2 facilitated the buffer exchange of the DARPin into suitable storage buffer, the chromatogram generated is of a single peak eluted at the appropriate volume for monomer E69 M30L. Approximately 40 mg of E69 M30L were generated well within regulatory compliant levels of host cell protein (HCP) and endotoxin.

As with the G3, the mutated E69 DARPin proved to be far more resistant to proteolytic activity than its wild type counterpart and the bioprocess could be used as a platform process, generating 40 mg of fully functional E69 M30L of equivalent purity at <0.05 EU/mL endotoxin and < 3.5 ng/mg HCP. In conclusion, this study has generated a holistic and innovative end to end development strategy for the production of DARPins in the yeast *P. pastoris*.

8.2 Future Work

8.2.1 Radial Flow IMAC; combined clarification and capture event

8.2.1.1 RF-IMAC vs. Standard practice

To truly take forward radial flow IMAC as a challenger to the conventional clarification and primary capture events favoured by industry one would need to demonstrate the overwhelming benefit of this combined system in a head-to-head comparison.

Though radial and axial flow have previous been compared in terms of dynamics and capture from formerly clarified supernatant (Demirci *et al.* 2012; Cabanne *et al.* 2007), there is limited literature discussing combined clarification/capture events using this technology (Kinna *et al.* 2016; Goldstein *et al.* 2015; Tolner *et al* 2012). In industry the established use of centrifugation generates a largely clarified feedstock but still requires it to subsequently undergo another clarification event, typically depth filtration, before capture steps can be implemented (Gupta *et al*. 2017; Jacquemart *et al*. 2016). As yet no extensive analysis has been conducted to assess the benefit of radial flow to the overall bioprocess in comparison to the conventional clarification / capture events.

Critical parameters to be taken into consideration include, but are not limited to, overall cost implications, effects of shear, product yield / purity, process scalability / flexibility and the effect on subsequent DSP operations. With BigBead™ technology (Sterogene) commercially available in varying formats, such as IEX and Protein A, and many other manufacturers providing a range of resins (Besselink *et al*. 2013; Saraswat *et al*. 2013), this unit step and the scope of this investigation is not necessarily limited to an IMAC dependent process and as such could be used in a far wider field. As for cost analysis, software to model the cost dynamics of a bioprocess has been well documented in literature and used extensively in process change comparisons to assess feasibility (Pollock *et al.* 2017; Felo M. 2013).

8.2.1.2 Optimisation of Radial Flow IMAC

The greatest loss of DARPin product (~ 50%) occurred during the primary capture / clarification event which utilised radial flow IMAC. The unit step had not undergone optimisation due to both time constraints and already exceeding the required product quota to facilitate a clinical trial. Radial flow has great potential to facilitate the combined clarification

and primary capture events not typically seen in conventional processes and optimising this unit step would increase the overall yield of the process considerably.

Figure 8.0 shows a preliminary investigation into whether the extremely fast flow rates of 200 mL/min could be maintained but with an increase in yield of captured product by residence time alone. To achieve this two identical 125 mL radial flow IMAC columns were set up in tandem thereby theoretically doubling the overall residence time. The eluted protein was quantified by OD_{280} and demonstrated that the combined columns allowed for an increase in captured protein from the original 45-50% to 75% of the G3 DARPin present in the load. A column of identical height but double the path length is available for purchase (Proxcys) and in future could be put in place instead of the tandem approach. These columns have such small footprints that even when scaling up, process space is not an overriding issue. This is because radial flow columns do not increase in width when scaling up but in height so the foot print itself remains small.

Beyond residence time other parameters that play a significant role in chromatography-based applications include buffer compositions, choice of chelating ligand, metal ions, cell density upon application and flowrate, even if restricted to the upper margins to maintain speed of process. A means of going from a largely trial and error method of optimisation to a more cost-effective and systematic approach, where multiple parameters and their interactions can be concisely studied, include methods such as Design of Experiments (DOE) (Shekhawat *et al.* 2018; Hibbert 2012) and Simplex-based approaches (Konstantinidis *et al.* 2016; Konstantinidis *et al.* 2017).

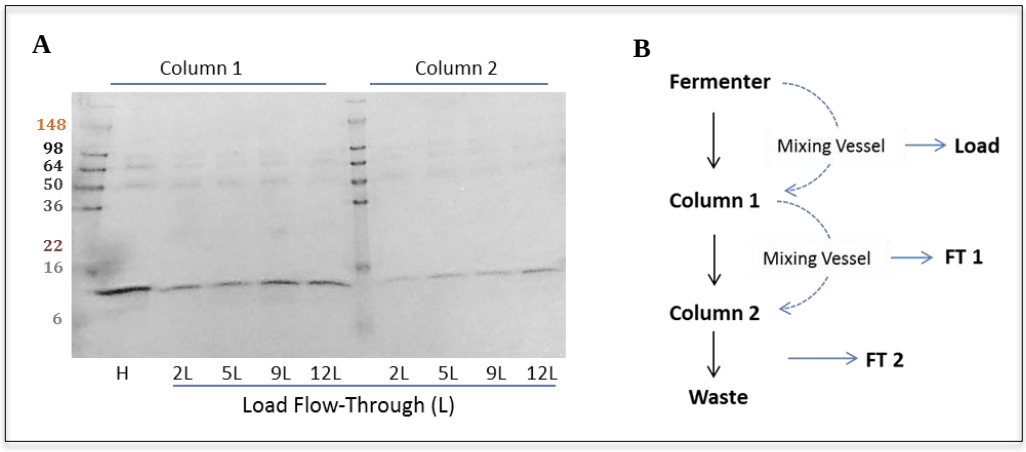

FIGURE 8.0: The effect of residence time on $(HE)_3$-G3 IMAC capture.
A, 18% SDS-PAGE gel run under reducing conditions and coomassie stained. **B,** schematic of the process setup. **H,** the IMAC load at harvest. **Column 1,** the first IMAC column in the tandem set up. **Column 2,** the second IMAC column in the tandem set up.

8.2.2 Streamlining the DARPin production bioprocess.

The fewer the unit steps and more non-complex a bioprocess is, the more likely it is to be cost efficient, easier to validate, perform and take to regulatory compliance. As such removing the initial SEC step from the DARPin DSP and going straight to AEX would reduce cost and time whilst potentially improving yield.

A preliminary experiment has been carried out using IMAC captured E69 M30L from a 52 hour fermentation. The process stream from a long fermentation run was used as this would theoretically represent the highest level of contaminants both in terms of HCP and degraded DARPin fragments. The pool from IMAC was concentrated to 200 mL and dialysed, in the same manner as for the original DARPin process (Chapter 5), and 50 mL loaded onto a 30 mL AEX (SOURE 30Q) column. The column was eluted in a stepwise manner up until 320 mM NaCl whereupon a gradient of 320-620 mM NaCl over 100 mL was initiated to remove remaining protein. As shown in Figure 8.1-A, the eluted DARPin (280 mL - 310 mL, Fractions 1 and 2) was easily separated from, HCP, lower molecular weight species and dimer DARPin as shown by Figure 8.1-B. Further characterisation of this substitution is required in terms of actually unit step HCP and product removal / yields and the effect on the subsequent established DSP steps. But the initial data looks promising and beyond the aforementioned advantages it would cut down run times by a day with minimal changes to existing SOP's and as a bioprocess be amendable to scale-up, if needed.

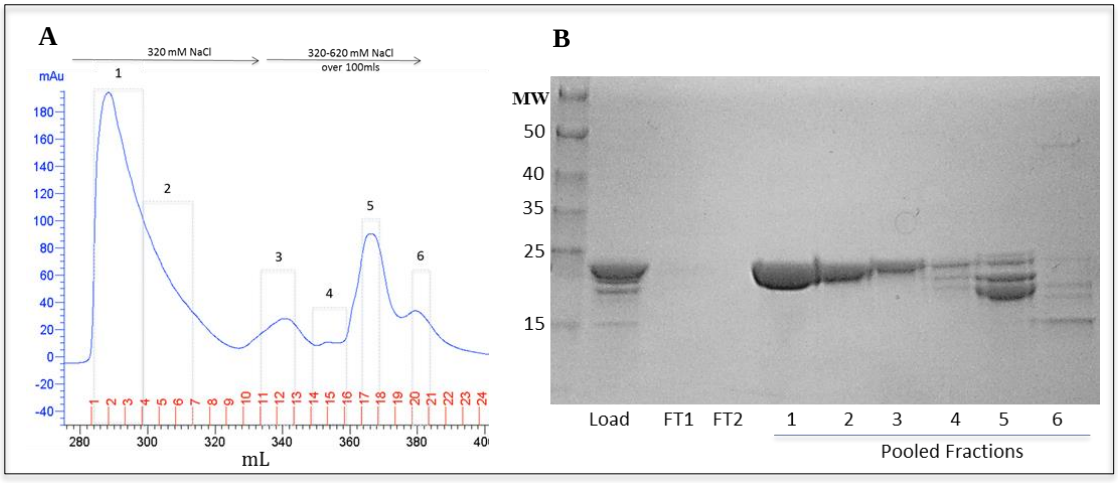

FIGURE 8.1: AEX as a secondary purification event following IMAC and TFF.
A, AEX Chromatogram of DARPin elution and proteins of similar pI. **B,** 18% SDS-PAGE run under reducing conditions. **Load**, TFF concentrated and dialysed pool that was loaded onto the AEX column. **FT1,** Load flow through. **FT2,** Binding buffer wash flow through. **1-6,** fractions from eluted protein pools as indicated on the chromatogram (A).

8.2.3 PET/SPECT imaging studies

8.2.3.1 Imaging potential for gastric / gastro-oesophageal junction cancers

Uptake of the HE_3-G3 DARPin in human tumour xenografts of gastro-oesophageal junction cancer were evaluated because, similarly to breast carcinoma, 7-34% of metastatic gastric cancers can show HER2 over expression and/or amplification, and this percentage increases to 24-32% gastroesophageal junction tumours (Fazlollahi *et al.* 2018; Abrahao-Machado *et al.* 2016). Thus, as in breast carcinoma, pathologists are now asked to evaluate HER2 status in gastric carcinoma samples and there is great need for whole body imaging to establish the extent and HER2 status of the tumour burden (Lee *et al.* 2017; Ahn *et al.* 2013). Results, illustrated in Chapter 6, showed excellent tumour uptake and favourable tumour: healthy tissue ratios in this model. Therefore imaging studies using the G3 DARPin for whole body imaging of gastric / gastro-oesophageal junction cancers would be of great clinical benefit.

8.2.3.2 Sensitivity of HER2 detection

Although the ability of the HER2 DARPin for tumour imaging has been demonstrated, Chapters 3 and 6, its potential for being able to differentiate between differing levels of HER2 expression has not. It would therefore be of benefit to assess the limits of detection for this imaging agent and whether quantifiable differences can be achieved.

Use of a heat shock protein 90 (HSP 90) inhibitor, such as 17-AAG (Tanespimycin) (Smith-Jones *et al.* 2004), 17-DMAG (Alvespimycin) (Hertlein *et al.* 2010), AUY922 (Luminespib) and PUH-71 (Holland *et al.* 2010; Li *et al*. 2016) for the downregulation of HER2 on cells would allow the assessment of differing amounts of receptor under controlled conditions. These inhibitors have already demonstrated their antitumor activity in numerous preclinical cancer models (Okui *et al*. 2011; Speranza *et al.* 2018; Wang *et al.* 2016; Mellatyar *et al.* 2018) and in the downregulation of HER2 levels in imaging studies (van de Ven *et al*. 2012; Berezowska *et al.* 2013; Wang *et al.* 2017).

Therefore HSP 90 inhibitors could be used to provide controlled levels of HER2 for assessment of imaging potential by the G3 DARPin. Techniques such as immunohistochemistry, flow cytometry and PET/CT have been previously used to validate and attempt to correlate perceived results using antibodies (Oude Munnink *et al.* 2010; Capala *et al.* 2012) and provide a sound basis from which to approach these experiments.

8.2.4 Development of Antibodies against DARPin and $(HE)_3$-tag

The development of monoclonal antibodies against DARPin would provide an invaluable tool in allowing their detection during production process development, further laboratory studies and use in Human Anti-DARPin detection Assays (HADA). A recombinant antibody would enable a 'single-batch' use policy from start to finish during the actual GMP production and clinical trial assessment studies. This would eliminate the need for mouse/rabbit immunization and the generation of polyclonal pools. Allowing for large quantities of recombinant, homogeneous and well characterised antibodies.

In order to develop and then select a library of antibodies against DARPin the well-established and proven technique of phage display would enable generation and selection of potential binders (Shim, 2017). Phage display is a powerful technology and has generated antibodies to multiple targets including blockbuster antibodies such as adalimumab (Humira®), ranibizumab (Lucentis®) and trastuzumab (Herceptin®) (Nixon *et al*. 2014; Frenzel *et al.* 2016).

As shown in Figure 8.2 the polyclonal pools generated are cross reactive amongst DARPins indicating the presence of antibodies to the conserved domains and potentially the $(HE)_3$-tag, which as yet has no commercially available antibody for its detection. Recombinant antibodies to these targets would enable flexibility over format for the required application such as mouse or human Fc, scFv or Fab, fluorophore conjugated or HRP. The efficacious development of biological therapeutics requires reliable bioanalytical methods for characterization in all phases of development and ultimately market (Harth *et al.* 2019). Having highly characterised agents from which to run these test would make this system a 'platform' in terms not only of bioprocess but of evaluation.

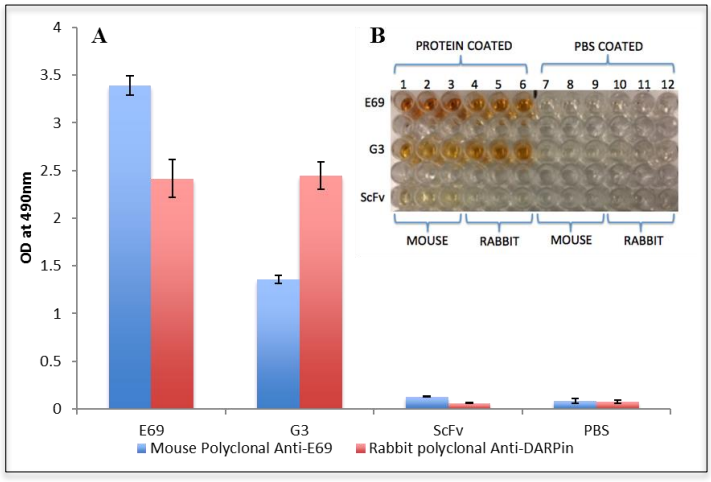

FIGURE 8.2: Testing of mouse serum from E69 immunised mice for DARPin reactivity / cross reactivity.
A, ELISA against E69, G3 or scFv. **B**, Visual display of the developed ELISA plate.

SUPPLEMENTARY DATA

Appendix 1 Supplementary Data

Primer	Sequence	Tm (℃)	GC (%)	↔	Vector Binding Region (bp)
F10	5’-GTCTGACGCTCAGTGGAAC-3’	56	58	Fwd	Between Ori-AOX1p (4072-4090)
F9	5’-GAAGGAAGCTGCCCTGTCTTAAACC-3’	61	52	Fwd	AOX1 Promotor (790-814)
F8	5’-GATCTGAATAGCGCCGTCGAC-3’	59	57	Fwd	Between Myc-His (1830-1850)
F7	5’-CTTCTCGTACGAGCTTGCTCC-3’	58	57	Fwd	AOX1 Terminator (2054-2074)
F6	5’-CACTCCTCTTCAGAGTACAGAAG-3’	55	48	Fwd	AOX1 Terminator (2161-2183)
F5	5’-CGGTCTTCAATTTCTCAAGTTTCAG-3’	56	40	Fwd	TEF1 Promotor (2522-2546)
F4	5’-GACGACGTGACCCTGTTCATCAG-3’	60	57	Fwd	BleoR (2824-2846)
F3	5’-GTTATGTCACGCTTACATTCACGCC-3’	60	48	Fwd	CYC1 Terminator (3146-3170)
F2	5’-CTGGAGACCAACATGTGAGC-3’	56	55	Fwd	Between CYC1-Ori (3386-3405)
F1	5’-GATACCTGTCCGCCTTTCTC-3’	55	55	Fwd	Ori (3606-3625)
AOX5	5’-GACTGGTTCCAATTGACAAGC-3’	55	48	Fwd	AOX1 Promotor (855-875)
AOX3	5’-GCAAATGGCATTCTGACATCC-3’	56	48	Rev	AOX1 Terminator (1954-1974)
Primer10	5’-CATACCTCGCTCTGCTAATCCTG-3’	58	52	Rev	Ori (3820-3842)
Primer9	5’-GGAACAGGAGAGCGCACGAG-3’	61	65	Rev	Ori (3569-3588)
Primer8	5’-CGTACACGCGTCTGTACAG-3’	56	58	Rev	CYC1 Terminator (3299-3317)
Primer7	5’-GCGTGAATGTAAGCGTGACATAAC-3’	58	46	Rev	CYC1 Terminator (3146-3169)
Primer6	5’-GATGAACAGGGTCACGTCGTC-3’	58	57	Rev	BleoR (2824-2844)
Primer5	5’-GTCGGTCCAGAACTCGACCG-3’	60	65	Rev	BleoR (2750-2769)
Primer3	5’-GCTTGTCAATTGGAACCAGTCG-3’	58	50	Rev	AOX1 Promotor (854-875)
Primer2	5’-CCAAATGACCATGAGCAGTAG-3’	54	48	Rev	G3 DARPin
Primer1	5’-GTGCTGTTGGAAAATGGC-3’	53	50	Rev	α-Factor (1099-1116)
FW3390	5’-GGTATCTGCGCTCTGCTGAAGC-3’	61	59	Fwd	Ori (3908-3929)
FW3140	5’-CTCACGCTGTAGGTATCTCAG-3’	55	52	Fwd	Ori (3655-3675)
FW2690	5’-CTGTACAGACGCGTGTACGCATG-3’	61	57	Fwd	CYC1 Terminator (3299-3321)
FW2170	5’-CCAAGTTGACCAGTGCCGTTC-3’	59	57	Fwd	BleoR (2699-2719)
FW1770	5’-CTTCAAAACACCCAAGCACAGC-3’	58	50	Fwd	TEF1 Promotor (2295-2316)
FW1430	5’-GGATGTCAGAATGCCATTTGC-3’	56	48	Fwd	AOX1 Terminator (1954-1974)
FW1140	5’-CTACTATTGCCAGCATTGCTGC-3’	58	50	Fwd	α-Factor (1143-1164)
FW850	5’-GACTGGTTCCAATTGACAAGC-3’	55	48	Fwd	AOX1 Promotor (855-875)
FW480	5’-GGTTCGTTGAAATGCTAACG-3’	53	45	Fwd	AOX1 Promotor (475-494)
FW70	5’-CGACATCCACAGGTCCATTCTC-3’	58	55	Fwd	AOX1 Promotor (49-70)
R2960	5’-CGATTTTTGTGATGCTCGTCAG-3’	56	45	Rev	Ori (3477-3498)
R2530	5’-GACGTGTCAGTCCTGCTCCTC-3’	60	62	Rev	BleoR (3055-3075)
R2110	5’-CTATGCCGATATACTATGCCGATG-3’	56	46	Rev	EM7 Promotor (2642-2665)
R1960	5’-CAATGGAGGTCACTGAAAGAG-3’	54	48	Rev	TEF1 Promotor (2287-2307)
R1570	5’-CAAGATATTCATCAGCTGCGAG-3’	55	45	Rev	AOX1 Terminator (2087-2108)
R1020	5’-GTTGTAGTGTTGACTGGAGCAG-3’	56	50	Rev	α-Factor (996-1017)
R600	5’-GTTCAGAAGCGATAGAGAGACTGC-3’	58	50	Rev	AOX1 Promotor (594-617)
R310	5’-GTAATGCGGAGCTTGTTGC-3’	56	53	Rev	AOX1 Promotor (310-328)
R20	5’-CAACCTTTCGTCTTTGGATG-3’	53	45	Rev	AOX1 Promotor (9-28)

BIBLIOGRAPHY

Appendix 2 References

Abrahao-Machado L.F., Scapulatempo-Neto C. (2016) “HER2 testing in gastric cancer: An update.” World J Gastroenterol 22(19): 4619-4625

Adams, G. P., Schier, R. *et al.* (1998). "Prolonged in vivo tumour retention of a human diabody targeting the extracellular domain of human HER2/neu." British Journal of Cancer 77(9): 1405-1412.

Agdeppa, E.D., Spiker, M.E. (2009) “A review of Imaging Agent Development” AAPS J. 11(2): 286-299.

Ahn, H.S., Kim, S.H., Kodera, Y., Yang, H.-K. (2013) “Gastric Cancer Staging with Radiologic Imaging Modalities and UICC Staging System.” Dig Surg 30:142-149.

Anderson DC. and Reilly DE. (2004) “Production technologies for monoclonal antibodies and their fragments.” Current Opinion in Biotechnology. 15(5): 456-462

Barton C, Vigor K, Scott R, *et al.* (2016) “Beta-glucan contamination of pharmaceutical products: How much should we accept?” Cancer Immunol Immunother. 65(11):1289-1301.

Baxevanis, C. N., Perez, S. A., Papamichail, M. (2009) “Combinatorial treatments including vaccines, chemotherapy and monoclonal antibodies for cancer therapy.” Cancer Immunol. Immunother. 58:317-324.

Besselink, T., Liu, M., Ottens, M., van Beckhoven, R., Janssen A.E.M., Boom, R.M. (2013) “Comparison of activated chromatography resins for protein immobilisation.” J. Sep. Sci. 36; 1185-1191.

Bryant JL. (2006) “HERCEPTIN Adjuvant Therapy” 20060275305

Blažek D. and Celer C. (2003) “The Production and Application of Single-Chain Antibody Fragments.” Folia Microbiol. 48(5): 687-698.

Boersna Y.L., Chao, G., Steiner, D., Wittrup, K.D., Plückthun, A. (2011) “Bispecific Designed Ankyrin Repeat Proteins (DARPins) Targeting Epidermal Growth Factor Receptor Inhibit A431 Cell Proliferation and Receptor Recycling.” The Journal of Biological Chemistry 286 (48); 41273-41285.

Boersma,YL. Plückthurn, A. (2011) “DARPins and other repeat protein scaffolds: advances in engineering and applications.” Current Opinion in Biotechnology 22:849–857.

Cabanne, C., Raedts, M., Zavadzky, E., Santarelli, X. (2007) “Evaluation of radial chromatography versus axial chromatography, practical approach.” Journal of Chromatography B 845: 191-199.

Capala J., Bouchelouche, K. (2012) “Molecular imaging of HER2-positive breast cancer – a step toward an individualized “Image and Treat” strategy.” Curr Opin Oncol. 22(6) 559-566.

Carta. G., Jungbauer, A. (2010). “Downstream Processing of Biotechnology Products.” Protein Chromatography: Process Development and Scale-Up. Wiley-VCH. ISBN: 978-3-527-31819-3.

Chisti, Y. and Moo-Young, M. (1990) “Large scale protein separations: Engineering aspects of chromatography.” Biotech. Adv. 8: 699-708.

Cregg, JM., Vedvick, T.S., Raschke, WC. (1993) “Recent advances in the expression of foreign genes in Pichia pastoris.” Nature Biotechnology 11: 905-910.

De Leon-Rodriguez, L.M., Kovacs, Z. (2008) “The Synthesis and Chelation Chemistry of DOTA-Peptide Conjugates.” Bioconjugate Chem. 19(2): 391-402.

Demirci, A., Leu, F., Bailey, F.J. (2012) “Comparison of Radial and Axial Flow Chromatography for Monoclonal Antibody Downstream Processing at Bench and Pilot Scales.” American Journal of Biochemistry and Biotechnology 8(4); 255-262.

DiMasi J.A., Grabowski HG. (2007) “The cost of biopharmaceutical R&D: is biotech different? Managerial and Decision Economics, 28: 469-479

Duvall M., Bradley N. and Fiorini RN. (2011) “A Novel Platform to Produce Human Monoclonal Antibodies” *mAbs* 3(2): 203-208.

Ebrahimpour M., Shahavi M.H., Jahanshahi M. and Najafpour G. (2009) “Nanotechnology in Process Biotechnology: Recovery and Purification of Nanoparticulate Bioproducts Using Expanded Bed Absorption.” Dynamic Biochemistry, Process Biotechnology and Molecular Biology 3 (Special Issue 2), 57-60

Elgundi Z., Reslan M., Cruz E., Sifniotis, V., Kayser V. (2017) “The state-of-play and future of antibody therapeutics” *Advanced Drug Delivery Reviews* 122: 2-19

Epa V.C., Dolezal O, Doughty L, Xiao X, Jost C, et al. (2013) “Structural Model for the Interaction of a Designed Ankyrin Repeat Protein with the Human Epidermal Growth Factor Receptor 2.” PLoS ONE 8(3): e59163.

Fazlollahi, L., Remotti, E.E, Luga, A., Yang, H.-M., et al. (2018) “HER2 Heterogeniety in Gastroesophageal Cancer Detected by Testing Biopsy and Resection Specimens” Arch Pathol Lab Med 142:516-522.

Frenzel A, Schirrmann T, Hust M. “Phage display-derived human antibodies in clinical development and therapy.” MAbs. 8(7):1177-1194.

Gaspar, N., Sharp, S. Y., Eccles, S. A.; Gowan, S., Popov, S., Jones, C., Pearson, A., Vassal, G., Workman, P. (2010). “Mechanistic Evaluation of the Novel HSP90 Inhibitor NVP-AUY922 in Adult and Pediatric Glioblastoma”. Molecular Cancer Therapeutics. 9 (5): 1219–1233.

Gasser B, Prielhofer R, Marx H et al. (2013) “*Pichia pastoris*: protein production host and model organism for biomedical research.” Future Microbiol. 8:191–208.

Gebhart, G., Flamen, P., De Vries, E. et al. (2016) “Imaging Diagnostic and Therapeutic Targets: Human Epidermal Growth Factor Receptor 2.” Journal of Nuclear Medicine 57: 81-88.

Goldstein, R., Sosabowski, J., Livanos, M. et al. (2015) “Development of the designed ankyrin repeat protein (DARPin) G3 FOR HER2 molecular imaging.” Eur. J. Nucl. Med. Mol. Imaging 42:288-301

Gupta, S.K. and Shukla, P. (2017) “Sophisticated Cloning, Fermentation, and Purification Technologies for an Enhanced Therapeutic Protein Production: A Review.” Front. Pharmacol. 8:419.

Hacker DL., De Jesus M., Wurm FM. (2009) “25 years of recombinant proteins from reactor-grown cells – where do we go from here?” *Biotechnology Advances* 27: 1023-1027.

Harth, S., Ten Haaf, A., Loew, C., Frisch, C., & Knappik, A. (2018). “Generation by phage display and characterization of drug-target complex-specific antibodies for pharmacokinetic analysis of biotherapeutics.” mAbs, 11(1), 178-190.

Hibbert, D.B. (2012) “Experimental design in chromatography: A tutorial review.” J. Chromatogr. B, 910:2-13.

Hofstrom C, Altai M, Honarvar H, Strand J, Malmberg J, *et al*. (2013) “HAHAHA, HEHEHE, HIHIHI, or HKHKHK: influence of position and composition of histidine containing tags on biodistribution of [(99m)Tc(CO)3](+)-labelled affibody molecules.” J Med Chem. 56:4966–74.

Hofstrom C, Orlova A, Altai M,Wangsell F, Graslund T, Tolmachev V. (2011) “Use of a HEHEHE purification tag instead of a hexahistidine tag improves biodistribution of affibody molecules site-specifically labelled with (99m)Tc, (111)In, and (125)I.” J Med Chem. 54:3817–26.

Holliger P. and Hudson PJ. (2005) “Engineered antibody fragments and the rise of single domains” Nature Biotechnology. 23: 1126-1136

Hopf, P. P. (1947) Radial chromatography in industry. Ind. Eng. Chem. 39: 938–940.

Renaud Jacquemart, Melissa Vandersluis, Mochao Zhao, Karan Sukhija, Navneet Sidhu, Jim Stout, A. (2016) “Single-use Strategy to Enable Manufacturing of Affordable Biologics.” Computational and Structural Biotechnology Journal 14; 309-318

Jia, H., Guo, Y., Song, X., Shao, C. et al. (2016) “Elimination of N-glycosylation by site mutation further prolongs the half-life of IFN-a/Fc fusion proteins expressed in *P. pastoris*.” Microb Cell Fact 15:209.

Joshi, K.K., Sahni, G. (2010) “Molecular cloning, expression, purification and characterization of truncated forms of human plasminogen in Pichia pastoris expression system.” Process Biochemistry 45: 1251-1260.

Kajander, T., Cortajarena, A., Regan, L. (2007). “Consensus Design as a Tool for Engineering Repeat Proteins.” Methods in Molecular Biology 340:151-170.

Kalman, B., Szep, E., Garzuly, F. et al. (2013) “Epidermal Growth Factor Receptor as a Therapeutic Target in Glioblastoma.” Neuromol Med 15: 420.

Köhler, G. & Milstein, C. (1975) “Continuous Cultures of Fused Cells Secreting Antibody of Predefined Specificity” *Nature* 256: 52-53

Konstantinidis, S., Welsh, J.P., Roush, D.J., Velayudhan, A. (2016) “Application of Simplex-Based Experimental Optimization to Challenging Bioprocess Development Problems: Case Studies in Downstream Processing.” Biotechnol. Prog. 32(2):404-419.

Konstantinidis, S., Titchener-Hooker, N., Velayudhan, A. (2017) “Simplex-based optimization of numerical and categorical inputs in early bioprocess development: Case studies in HT chromatography.” Biotechnol, J. 12: 1700174

Lee, J.S., Kim, S.H., Im, S.-A., Kim, M.A., Han, J.K. (2017) “Human Epidermal Growth Factor Receptor 2 Expression in Unresectable Gastric Cancers: Relationship with CT Characteristics.” Korean J Radiol 18(5):809-820.

Lin-Cereghino, G.P., Stark, C.M., Kim, D. et al. (2013) “The effect of a-mating factor secretion signal mutations on recombinant protein expression in *Pichia pastoris*.” Gene 519: 311-317.

Liu H. and May K. (2012) “Disulphide bond structures of IgG molecules; Structural variations, chemical modifications and possible impacts to stability and biological function.” mAbs. 4(1): 17-23

Lofblom, J,. Frejd, F. Y., Stahl, S. (2011) “Non-Immunoglobulin based protein scaffolds” Current Opinion in Biotechnology 22(6): 843-848

Love, K.R., Dalvie, N.C., Love, C. (2018) “The yeast stands alone: the future of protein biologic production.” Current Opinion in Biotechnology” 53; 50-58.

Macauley-Patrick, S., Fazenda, M., McNeil, B. and Harvey, LM. (2005) “Heterologous protein production using Pichia pastoris expression system.” Yeast 22: 249-270.

Meehl, M.A. and Stadheim, TA. (2014) “Biopharmaceutical discovery and production in yeast.” Current Opinion in Biotechnology 30:120-127.

Mizukami, A., Caron, AL., Picanco-Castro, V. and Swiech, K. (2018) “Platforms for Recombinant Therapeutic Glycoprotein Production.” Recombinant Glycoprotein Production: Methods and Protocols, Methods in Molecular Biology vol. 1674, DOI 10.1007/978-1-4939-7312-5

Nixon, A.E., Sexton, D.J., Ladner, R.C. (2014) “Drugs derived from phage display. From candidate identification to clinical practice.” MAbs. 6(1): 73-85.

Okui, T., Shimo, T., Hassan, N.M,. Fukazawa, T., Kurio, N., Takaoka, M., Naomoto, Y., Sasaki, A. (2011). “Antitumor effect of novel HSP90 inhibitor NVP-AUY922 against oral squamous cell carcinoma”. Anticancer Research. 31 (4): 1197–204

Pavlou, A. K., & Reichert, J. M. (2004). “Recombinant protein therapeutics – success rates, market trends and values to 2010.’’ Nature Biotechnology 22(12): 1513-1519.

Pimlott, S.L. (2014). “Radioisotopes for medical imaging.” International Journal of Modern Physics A 29(4): 1441003

Plückthun, A. (2015) “Designed Ankyrin Repeat Proteins (DARPins): Binding Proteins for Research, Diagnostics, and Therapy.’’ Annual Review of Pharmacology and Toxicology 55:489-511.

Pollock, J., Coffman, J., Ho, S.V., Farid, S. (2017) “Integrated continuous bioprocessing: Economic, operational and environmental feasibility for clinical and commercial antibody manufacture.” Biotechnology Progress 33(4)

Prelaj, A., Rebuzzi, S.E., Caffarena, G., Giròn Berrìos, J.R., Pecorari, S., Fusto, C. Caporlingua, A., Caporlingua, F., Di Palma, A., Magliocca, F. M., Salvati, M., Tomao, S., Bianco, V. (2018).

Therapeutic approach in glioblastoma multiforme with primitive neuroectodermal tumor components: Case report and review of the literature. Oncology Letters, 15, 6641-6647.

Rahmim, A., Zaidi, H. (2008) " PET versus SPECT: strengths, limitations and challenges." Nuclear Medicine Communications 29: 193-207

Rushore, A.S., Kumar D. and Kateja N. (2018) "Recent developments in chromatographic purification of biopharmaceuticals." Biotechnol. Lett. 40:895-905

Saraswat, M., Musante, L., Ravida, A., Shortt, B.B., Holthofer, H. (2013) "Preparative Purification of Recombinant Proteins: Current Status and Future Trends." Bioned Res Int 312709.

Schettini, F., Buono, G. Cardalesi, C., *et al.* (2016) "Hormone Receptor / Human Epidermal Growth Factor Receptor 2-positive breast cancer: Where we are now and where we are going." Cancer Treatment Reviews 46: 20-26

Speranza, G., Anderson, L., Chen, A.P. et al. (2018) "First-in –human study of the epichaperome inhibitor PU-H71: clinical results and metabolic profile." Invest New Drugs 36(2): 230-239.

Shekhawat, L.K., Godara, A., Kumar, V., Rathore, A.S. (2018) "Design of experiments applications in bioprocessing: Chromatography process development using split design of experiments." Biotechnology Progress 35(1)

Sinha, J., Plantz, B.A., Zhang, W., Gouthro, M., *et al.* (2003). "Improved production of recombinant ovine interferon-H by Mut+ strain of Pichia pastoris using an optimized methanol feed profile." Biotechnol. Prog. 19:794–802.

Skrlec, K., Strukelj, Borut., Berlec, Ales. (2015) "Non-Immunoglobulin scaffolds: a focus on their targets." Trends in Biotechnology 33(7): 408-418.

Somasundaram, B., Pleitt, K., Shave, E., Baker, K., Lua, L. (2018) "Progression of continuous downstream processing of monoclonal antibodies: Current trends and challenges." Biotechnology and Bioengineering. 115:2893-2907.
Stasiuk, G.J., Long, N.J. (2013) "The ubiquitous DOTA and its derivatives: the impact of 1,4,7,10-tetraazacyclododecane-1,4,7,10-tetraaceticacid on biomedical imaging." Chem. Commun. 49: 2732-2746

Tamaskovic, R., Simon, M., Stefan, N., *et al.* (2012) "Designed Ankyrin Repeat Proteins (DARPins): From Research to Therapy." Methods in Enzymology 503: 101-134.

Tjandra JJ., Ramadi L., McKenzie IFC. (1990) "Development of human anti-murine antibody (HAMA) response in patients" *Immunology and Cell Biology*. 68(6): 367-376.

Tolmachev, V., Hofstrom, C., Malmberg, J. *et al*. (2010) "HEHEHE-Tagged Affibody Molecule May Be Purified by IMAC, Is Conveniently Labelled with [$^{99m}Tc(CO)_3$], and Shows Improved Biodistribution with Reduced Hepatic Radioactivity Accumulation." Bioconjugate Chem. 21: 2013-2022.

Tolner, B., Smith, L., Begent, R., Chester, KA. (2006) "Production of recombinant protein in *Pichia Pastoris* by fermentation." Nature Protocols 1(2): 1006-1021.

Tolner, B. Bhavsar, G., Foster, B., Vigor, K., Chester K.A. (2012) "Production of Recombinant Proteins from Picia pastoris: Interfacing Fermentation and Immobilized Metal Ion Affinity Chromatograpy." Laboratory Protocols in Fungal Biology. Chapter 37.

Umscheid, C.A., Margolis, D.J., Grossman, CE. (2011) "Key Concepts of Clinical Trials: A Narrative Review" Postgrad Med. 123(5): 194-204.

Von Gall, C., Maniawski, P., Verzijlbergen F., Carrio, I., Beyer, T., Kalemis, A. (2017) "Saving costs in cancer patient management through molecular imaging." Eur J Nucl Med Mol Imaging (2017) 44:2153–2157

Wakankar AA., Wang J., Canova-Davis E., Ma S., Schmalzing D., et al. (2010) "On Developing a Process for Conducting Extractable-Leachable Assessment of Components Used for Storage of Biopharmaceuticals." Journal of Pharmaceutical Sciences, 99(5): 2209-2218

Wang, W., Ignatius, A.A., Thakkar, SV. (2014) "Impact of Residual Impurities and Contaminants on Protein Stability." Journal of Pharmaceutical Sciences 103: 1315-1330.

Wang, H., Lu, M., Yao, M., Zhu, W. (2016) "Effects of treatment with an HSP90 inhibitor in tumors based on 15 phase II clinical trials." Molecular and Clinical Oncology 5:326-334

Wang, W., Zhao, J., Wen, X., Lin, C. et al. (2017) "MicroPET/CT Imaging of AXL Downregulation by HSP90 Inhibition in Triple-Negative Breast Cancer." Contrast Media & Molecular Imaging 1686525

Weninger A, Hatzl AM, Schmid C et al. (2016) "Combinatorial optimization of CRISPR/Cas9 expression enables precision genome engineering in the methylotrophic yeast *Pichia pastoris*." J Biotechnol. 235:139–49.

Westphal, M., Maire, C. L., Lamszus, K. (2017). "EGFR as a Target for Glioblastoma Treatment: An Unfulfilled Promise." CNS drugs *31*(9); 723-735.

Xu, H., Zong, H., Ma, C., *et al.* (2017) "Epidermal growth factor receptor in glioblastoma." *Oncol Lett.* 14(1): 512-516.

Xu X., Hirpara J., Epting K., Jin M., Ghose S., Rieble S. and Li ZJ. (2014) "Clarification and Capture of High-Concentration Refold Pools for *E.coli*-Based Therapeutics Using Expanded Bed Adsorption Chromatography." *Biotechnol. Prog.* 30(1): 113-123.

Yang S., Kuang Y., Liu Y., Hui X., *et al.* (2013) Enhanced production of Recombinant Secretory Proteins in Pichia pastoris by Optimizing Kex2 P1' site' PLoS ONE 8(9):e75347

Zahnd, C., Wyler, E., Schwenk, JM., *et al.* (2007) "A Designed Ankyrin Repeat Protein Evolved to Picomolar Affinity to Her2." Journal of Molecular Biology 369: 1015-1028.

Zhang, Y., Liu, R., Wu, X. (2007) "The proteolytic systems and heterologous proteins degradation in the methylotrophic yeast Pichia pastoris." Annals of Microbiology 57(4): 553-560

PUBLICATIONS

Eur J Nucl Med Mol Imaging (2015) 42:288–301
DOI 10.1007/s00259-014-2940-2

ORIGINAL ARTICLE

Development of the designed ankyrin repeat protein (DARPin) G3 for HER2 molecular imaging

Robert Goldstein · Jane Sosabowski · Maria Livanos · Julius Leyton · Kim Vigor · Gaurav Bhavsar · Gabriela Nagy-Davidescu · Mohammed Rashid · Enrique Miranda · Jenny Yeung · Berend Tolner · Andreas Plückthun · Stephen Mather · Tim Meyer · Kerry Chester

Received: 4 July 2014 / Accepted: 9 October 2014 / Published online: 13 November 2014

Abstract
Purpose Human epidermal growth factor receptor-2 (HER2) overexpression is a predictor of response to anti-HER2 therapy in breast and gastric cancer. Currently, HER2 status is assessed by tumour biopsy, but this may not be representative of the larger tumour mass or other metastatic sites, risking misclassification and selection of suboptimal therapy. The designed ankyrin repeat protein (DARPin) G3 binds HER2 with high affinity at an epitope that does not overlap with trastuzumab and is biologically inert. We hypothesized that radiolabelled DARPin G3 would be capable of selectively imaging HER2-positive tumours, and aimed to identify a suitable format for clinical application.
Methods G3 DARPins tagged with hexahistidine (His_6) or with histidine glutamate $(HE)_3$ and untagged G3 DARPins were manufactured using a GMP-compatible *Pichia pastoris* protocol and radiolabelled with ^{125}I, or with ^{111}In via DOTA linked to a C-terminal cysteine. BALB/c mice were injected with radiolabelled G3 and tissue biodistribution was evaluated by gamma counting. The lead construct ($(HE)_3$-G3) was assessed in mice bearing HER2-positive human breast tumour (BT474) xenografts.
Results For both isotopes, $(HE)_3$-G3 had significantly lower liver uptake than His_6-G3 and untagged G3 counterparts in non-tumour-bearing mice, and there was no significantly different liver uptake between His_6-G3 and untagged G3. $(HE)_3$-G3 was taken forward for evaluation in mice bearing HER2-positive tumour xenografts. The results demonstrated that radioactivity from ^{111}In-$(HE)_3$-G3 was better maintained in tumours and cleared faster from serum than radioactivity from ^{125}I-$(HE)_3$-G3, achieving superior tumour-to-blood ratios (343.7±161.3 vs. 22.0±11.3 at 24 h, respectively). On microSPECT/CT, ^{111}In-labelled and ^{125}I-labelled $(HE)_3$-G3 could image HER2-positive tumours at 4 h after administration, but there was less normal tissue uptake of radioactivity with ^{111}In-$(HE)_3$-G3. Preadministration of trastuzumab did not affect the uptake of $(HE)_3$-G3 by HER2-positive tumours.
Conclusion Radiolabelled DARPin $(HE)_3$-G3 is a versatile radioligand with potential to allow the acquisition of whole-body HER2 scans on the day of administration.

Keywords DARPin · HER2 · Molecular imaging · Breast cancer · SPECT

Electronic supplementary material The online version of this article (doi:10.1007/s00259-014-2940-2) contains supplementary material, which is available to authorized users.

R. Goldstein · M. Livanos · G. Bhavsar · M. Rashid · E. Miranda · J. Yeung · B. Tolner · T. Meyer · K. Chester (✉)
UCL Cancer Institute, Paul O'Gorman Building, 72 Huntley St, WC1E 6DD London, UK
e-mail: k.chester@ucl.ac.uk

R. Goldstein
e-mail: robert.goldstein@ucl.ac.uk

J. Yeung
UCL Institute of Child Health, 30 Guilford Street, London WC1N 1EH, UK

J. Sosabowski · J. Leyton · S. Mather
Centre for Molecular Oncology, Barts Cancer Institute, Queen Mary University of London, Charterhouse Square, London EC1M 6BQ, UK

G. Nagy-Davidescu · A. Plückthun
Biochemisches Institut, Universität Zürich, Winterthurerstr. 190, 8057 Zürich, Switzerland

K. Vigor
Biotherapeutics Development Unit, Cancer Research UK, Clare Hall Laboratories, Blanche Lane, South Mimms EN6 3LD, UK

Introduction

Overexpression of human epidermal growth factor receptor-2 (HER2) enhances signal transduction through the PI3K/Akt and the Ras/Raf/MEK/MAPK pathways, enabling cancer cell proliferation and survival [1]. HER2 is overexpressed in 20 – 25 % of patients with breast cancer and gastrooesophageal cancer, and in these cancers HER2 is an established therapeutic target [2, 3]. There are a range of HER2-targeted therapies, including the monoclonal antibody trastuzumab, licensed for the treatment of breast and gastric cancers, and the trastuzumab–drug conjugate, T-DM1, licensed for the treatment of breast cancer [3, 4]. Novel therapies targeting the HER2 receptor, downstream effectors and compensatory signalling pathways are in clinical development [1].

Currently, patients are selected for anti-HER2 therapy based on histological analysis, using immunohistochemistry or fluorescence in situ hybridization (FISH) of biopsied or surgically resected tissues [5]. These analyses are limited by the use of single-site and single time-point sampling, and furthermore they fail to provide information about heterogeneity of expression or changes in expression that occur over time [6]. Dependence on histological analyses risks misclassifying patients' HER2 status and selecting a suboptimal therapy. Discordance in HER2 status between the primary breast tumour and synchronous as well as metachronous metastases has consistently been reported [7]. HER2 status has also been reported to change, from negative to positive and vice versa, and also between metastatic disease relapses [8, 9]. Although the impact of HER2 misclassification on clinical outcomes is unclear, 20 – 30 % of patients with HER2-positive advanced breast cancer do not respond to first-line treatment combinations, despite advances in anti-HER2 therapies [10]. In the adjuvant setting, some patients with breast cancer histologically classified as HER2-negative benefit from adjuvant anti-HER2 therapy, casting doubt on their classification [11].

HER2 molecular imaging could potentially overcome the limitations of histological analysis by providing new information on HER2 expression at all metastatic sites. Radiolabelled trastuzumab has been used for this purpose, but although the pharmacokinetics of trastuzumab are well suited to therapy, its long half-life compromises tumour-to-blood ratios needed for imaging. Consequently, HER2 scans must be performed at least 2 days after radiolabelled trastuzumab administration, and even then tumours in highly vascular regions may be difficult to visualize [12]. In clinical studies, SPECT imaging with ^{111}In-trastuzumab and PET imaging with both ^{64}Cu-trastuzumab and ^{89}Zr-trastuzumab have shown lower rates of tumour detection in patients with advanced HER2-positive breast cancer than conventional imaging, including CT [12–14]. Therefore, a novel approach is needed to overcome these limitations, potentially utilizing low molecular weight high-affinity proteins [15].

Designed ankyrin repeat proteins (DARPins) are recombinant binding proteins composed of ankyrin repeats, which stack together to make a contiguous binding surface [16, 17]. Each ankyrin repeat consists of 33 amino acids, which form a β-turn followed by two anti-parallel α-helices and a loop binding to the β-turn of the next ankyrin repeat [18, 19]. Synthetic DARPin libraries have been designed [18], from which specific binders can be selected and further evolved by methods such as ribosome display [20].

The DARPin G3 is a low molecular weight protein (14 – 15 kDa) with picomolar affinity (91 pmol/L) for HER2 [21–23]. It has a short half-life in mice (<3 min), lacks biological activity and binds to HER2 in the presence of trastuzumab and pertuzumab in vitro [21, 23]. The DARPin G3 tagged with hexahistidine (His_6) and labelled with ^{99m}Tc-tricarbonyl ($[^{99m}Tc(CO)_3]^+$) can be used to visualize HER2-positive tumours [21]. Our goal was to use the DARPin G3 for routine clinical HER2 SPECT and PET imaging, and we set out to generate and evaluate different radiolabelled G3 formats to select a lead for clinical development.

The His_6 tag can be employed for purification of recombinant proteins by immobilized metal affinity chromatography (IMAC). We evaluated the effect of the His_6 tag on DARPin G3 biodistribution and compared it with the DARPin G3 tagged with histidine glutamate $(HE)_3$, which has a negative excess charge at physiological pH. The $(HE)_3$ tag has been reported to reduce background liver uptake in some cases, while still allowing tag-mediated IMAC [24, 25]. We developed a GMP-compatible *Pichia pastoris* production platform that allows cleavage of histidine-based tags after IMAC purification, enabling comparisons among variants of G3.

We hypothesized that the DARPin G3 would be capable of selectively imaging HER2-positive tumours and aimed to identify a suitable format for clinical application. Thus, we systematically investigated the effect of tag and label on the quality of imaging. First, we assessed the sensitivity and specificity of DARPin G3 radiolabelled with $[^{99m}Tc(CO)_3]^+$ via a His_6 tag in HER2-positive and HER2-negative tumour-bearing mice. Subsequently, we assessed the biodistribution of His_6-G3, $(HE)_3$-G3 and untagged G3 DARPins radiolabelled with ^{111}In and ^{125}I in non-tumour-bearing mice. Thus, both residualizing and non-residualizing radioisotopes were tested, as they have different cellular fates which can affect tumour-to-normal tissue ratios. Finally, the construct with the lowest normal tissue uptake was taken forward for evaluation as an imaging agent.

Materials and methods

Details of DARPin G3 constructs (Supplementary Fig. 1), production, purification, conjugation with 1,4,7,10-tetraazacyclododecane-1,4,7-Tris-acetic acid-10-

maleimidoethylacetamide (mal-DOTA) and radiolabelling are provided in the Supplementary Materials and methods.

DARPin G3 radiolabelling

DOTA-conjugated DARPins (5 – 60 μg) in 0.2 M ammonium acetate, pH 6.5, were mixed with a solution of $^{111}InCl_3$ (Covidien, The Netherlands; 10 – 30 MBq) and incubated for 2 h at 37 °C (reaction volumes 40 – 60 μl). The reactions were stopped by adding 0.1 M disodium edetate (EDTA) and the radiolabelled DARPins were purified by elution into PBS using a NAP-5 column (GE Healthcare, Little Chalfont, UK) pre-equilibrated with PBS. Radiochemical purity was determined using instant thin-layer chromatography (iTLC), using iTLC silica gel (SG) strips (Varian, Palo Alto, CA). To test for ^{111}In-EDTA, iTLC strips were eluted with 0.1 M ammonium acetate containing 25 mM EDTA (final pH 5.5) in which system ^{111}In-EDTA eluted to the solvent front, while ^{111}In-G3 DARPin and insoluble material remained at the origin. Formation of radioactive insoluble material was evaluated using iTLC-SG eluted with 35 % ammonia (v/v)/ethanol/water (1:2:5), in which system ^{111}In-DOTA-G3 DARPin and ^{111}In-EDTA both had Rf values >0.5, while any insoluble material present in the reaction mixture remained at the origin. If insoluble material was detected, reaction mixtures were filtered through a 0.2-μm sterile syringe filter with a Supor membrane (Pall Life Science, Portsmouth, UK). The radiochemical purity of ^{111}In-G3 DARPins was 70 – 80 % before purification and >95 % after purification (see below for specific activities, SA).

Iodine radiolabelling was performed in precoated Pierce iodination tubes (Thermo Scientific, Runcorn, UK) with unconjugated G3 DARPins (5 – 60 μg) in PBS for 10 min at room temperature, using either 10 MBq ^{125}I (PerkinElmer, Llantrisant, UK) or 15 – 20 MBq ^{123}I (GE Healthcare). The iodination reactions were stopped by adding sodium metabisulphite to a final concentration of 1 μM. Radioiodinated DARPins were purified by buffer exchange into PBS with a NAP-5 column. Radiochemical purity was assessed with iTLC-SG strips (Varian) using 0.1 M ammonium acetate containing 25 mM disodium EDTA (final pH 5.5) as $^{123/125}$I-G3 DARPin remained at the origin and free $^{123/125}$I eluted at the solvent front. Radiochemical purity increased from 60 – 70 % before purification to >95 % after purification (see below for SA). An equivalent molar amount of 'cold' potassium iodide (3.4×10^{-10} mol) was coadministered with ^{123}I-G3 DARPin to minimize normal tissue uptake of 'free' ^{123}I (formed by deiodination in vivo).

iTLC analysis was supplemented with size-exclusion high-performance liquid chromatography (HPLC). A Beckman System Gold 128 solvent module and a 168 UV detector module (monitoring at 280 and 220 nm; Beckman Coulter, High Wycombe, UK), combined with a Raytest GABi radiochemical detector (Raytest, Straubenhardt, Germany) were used. The radiolabelled DARPin G3 was eluted from a YMC-Pack Diol-60 (YMC Europe, Dinslaken, Germany) column, dimensions 300 mm length × 8.0 mm inner diameter, spherical shape, 5 μm particle size and 6 nm pore size, using a mobile phase of 0.2 M phosphate buffer (pH 6.8) at a flow rate of 0.5 ml/min.

In vitro assessment

The unconjugated and DOTA-conjugated G3 counterparts had comparable subnanomolar binding affinities for the HER2 extracellular domain (ECD) assessed by surface plasmon resonance, indicating that DOTA conjugation to the C-terminus does not compromise binding to HER2 (data not shown). Saturation binding assays of radiolabelled DARPin G3 were performed with BT474 HER2-expressing human breast cancer cells (ATCC, Manassas, VA) as previously described [26]. On BT474 cell-binding assays, ^{111}In-$(HE)_3$-G3 and ^{125}I-$(HE)_3$-G3 had saturable binding and similar binding affinities to each other.

To assess stability of the label, aliquots of radiolabelled DARPin G3 were incubated in PBS or in human serum/PBS (1:1). Serum stability was assessed at 37 °C for 24 h, while PBS stability was assessed at 4, 20 and 37 °C for 24 h after radiolabelling by iTLC, as previously outlined. After incubation, the stability of radiolabelled G3 was assessed by SDS-PAGE using non-reducing conditions, followed by autoradiography using a Cyclone storage phosphor system (PerkinElmer).

Biodistribution studies

All animal studies were ethically reviewed and performed in accordance with the UK Animals (Scientific Procedures) Act 1986, UK Home Office regulations and local regulations.

For non-tumour studies, female BALB/c mice (Charles River, Erkrath, Germany) aged 6 – 11 weeks (mean weight 19 g) received an intravenous dose of 0.3 MBq of ^{111}In-G3 DARPin (2.2 μg, SA 2.0 MBq/nmol, to 4.3 μg, SA 1 MBq/nmol) or ^{125}I-G3 DARPin (2.8 μg, SA 1.6 MBq/nmol, to 4.3 μg, SA 1 MBq/nmol) in 200 μl of PBS/0.1 % BSA. Mice were killed at 4 h (four mice) or 24 h (four mice) after administration. Tissues were removed and radioactivity measured in a gamma counter (1282 CompuGamma CS, LKB Wallac). Uptakes are expressed as means±SD of the percentage of injected radioactive dose per gram of tissue (% ID/g).

For tumour studies, a single 60-day release 0.72-mg 17β-oestradiol pellet (Innovative Research of America, Sarasota, FL) was inserted into the scruff of female SCID-beige mice (Charles River) aged 6 – 8 weeks (mean weight 17 g). The following day, the mice were inoculated with BT474 cells by subcutaneous injection (7.5×10^6 cells; ATCC) in PBS mixed

with equal volumes of Matrigel (BD Biosciences, Oxford, UK). When tumours reached 25 – 100 mm^2 (5 – 7 weeks after inoculation) the mice received 0.3 MBq of ^{111}In-G3 DARPin (2 μg, SA 2.2 MBq/nmol) or 0.3 MBq of ^{125}I-G3 DARPin (3 μg, SA 1.5 MBq/nmol) and biodistribution was calculated as outlined. Excised BT474 tumours from untreated SCID-beige mice were HER2-positive (immunohistochemistry 3+, defined as consistent with circumferential membrane staining that is complete, intense and within >10 % of tumour cells) as assessed using the HercepTest (Dako, Ely, UK) according to the manufacturer's instructions [5].

In the trastuzumab blocking study, three female SCID-beige mice with BT474 tumours received intravenous trastuzumab (14.2 mg/kg) 24 h prior to intravenous injection of ^{111}In-G3 DARPin. Three control mice received ^{111}In-G3 DARPin alone. The mice were killed at 4 h after administration of 0.3 MBq ^{111}In-G3 DARPin (1.9 μg per mouse, SA 2.3 MBq/nmol).

MicroSPECT/CT imaging

Female SCID-beige mice bearing BT474 tumours were injected intravenously with either 10.5 MBq of ^{123}I-G3 (2.1 MBq/μg, SA 30.1 MBq/nmol) or 8.4 MBq of ^{111}In-G3 (4 MBq/μg, SA 58 MBq/nmol). Preliminary work had demonstrated that HER2-positive tumour signals on SPECT scans were compromised at lower SAs of radiolabelled G3 DARPin (data not shown). Thus, the SA for imaging was increased compared to the biodistribution studies to enhance the quality of images, but mice assessed for biodistribution and imaging studies received a similar molar dose of G3 DARPin. The radiolabelling reactions for imaging studies were performed with both a lower amount of G3 DARPin and higher radiation activity within the parameters outlined in the radiolabelling section.

Imaging was performed under 2 % isoflurane anaesthesia 4 h after administration using a microSPECT/CT animal scanner (Bioscan, Poway, CA). Helical SPECT images were acquired in 20 projections over 30 – 40 min using a four-headed camera with 4×9 (1.4 mm) pinhole collimators. The CT images were acquired in 180 projections with an exposure time of 1,000 ms using a peak kilovoltage of 45 kVp over 6 min. Radionuclide images were reconstructed using HiSPECT (Scivis, Göttingen, Germany) iterative reconstruction software and fused with CT images using proprietary InVivoScope (Bioscan) software.

DARPin G3 specificity for HER2 in vivo

Mice were inoculated with tumours as previously described. G3 DARPins were radiolabelled with $[^{99m}Tc(CO)_3]^+$ via a C-terminal His_6 tag ($[^{99m}Tc(CO)_3]^+$-G3 DARPin-His_6) according to the published protocol [27]. Briefly, $[^{99m}Tc(CO)_3]^+$ was prepared using an IsoLink kit (Mallinckrodt, Petten, The Netherlands) according to the manufacturer's instructions. Following neutralization and the addition of 150 μg of G3 DARPin, the mixture was reacted at room temperature for 30 min. Radiolabelling efficiency was determined by size exclusion HPLC using the same methods as previously outlined. The product was purified from 50 % to 100 % radiochemical purity using a NAP-10 column (GE Healthcare). MicroSPECT/CT imaging was performed 1 h after administration of about 30 MBq $[^{99m}Tc(CO)_3]^+$-G3 DARPin-His_6 (10 μg, SA 44 MBq/nmol) to three mice with HER2-positive (BT474) tumours and three mice with HER2-negative (MDA-MB-468) tumours, as previously described. Mice were killed at 24 h.

DARPin G3 specificity for HER2 in vitro

The DOTA-conjugated G3 DARPins were labelled using naturally abundant indium chloride ($^{nat}InCl_3$; Sigma-Aldrich, St. Louis, MO) in 0.05 M HCl solution, and unconjugated G3 DARPins were labelled using $Na^{nat}I$ (Sigma-Aldrich) in 0.1 M sodium hydroxide, using the same conditions required for ^{111}In and ^{125}I radiolabelling reactions, respectively.

Competition assay

BT474 cells (ATCC) were seeded at a density of 1×10^6 per well into Cellstar six-well plates (Greiner bio-one, Frickenhausen, Germany) and grown to confluence over 24 h. The confluent cells were incubated in triplicate with 0.1 nM $[^{99m}Tc(CO)_3]^+$-G3 DARPin-His_6 with or without 1,000 nM ^{nat}In-DARPin or ^{nat}I-DARPin in Dulbecco's modified Eagle's medium (DMEM) with high glucose concentration (4.5 g/L) containing 1 % fetal calf serum (Biosera, Boussens, France) and 0.1 % sodium azide (Sigma-Aldrich) for 1 h 30 min at 20 °C. An unlabelled epidermal growth factor receptor (EGFR) binding DARPin (K. Chester, unpublished) was used as a control.

The assays were stopped by removing the medium and washing the cells with 2 ml ice-cold PBS. The cells were lysed with 1 ml of 1 M sodium hydroxide and the lysate was collected. The wells were washed twice with 1 ml of PBS. The washes were pooled with the cell lysate for analysis. The radioactivity was measured in a gamma counter. The mean percentage of radioactivity was calculated for each condition in relation to the controls treated with $[^{99m}Tc(CO)_3]^+$-G3 DARPin-His_6 alone.

Flow cytometry analysis

BT474 (ATCC), MDA-MB-468 (ATCC) and OE-19 (Sigma-Aldrich) cells were individually prepared for flow cytometry by removal of medium and incubation with 5 ml of 0.2 %

EDTA for 10 min. The cells were then transferred to tubes and centrifuged (4 °C, 4 min, 1,000 rpm). The EDTA solution was removed and 5 ml of fresh medium was added. Cells were counted and diluted to 1 million/ml, and 1 ml was used for each test condition. After washing with cold PBS, 200 μl of DARPin at 10 μg/ml was added followed by incubation for 1 h at 4 °C. Cells were washed with cold PBS and incubated with 200 μl of mouse anti-DARPin (K. Chester, unpublished) for 1 h at 4 °C. Subsequently the cells were washed with cold PBS and incubated with 200 μl of Alexa Fluor® 488 goat anti-mouse IgG (Life Technologies, Paisley, UK) for 30 min at 4 °C. After further washing with cold PBS, the cells were suspended in 500 μl of cold PBS. Samples were analysed on a CyAn ADP high-performance flow cytometer (Becton Dickinson, Oxford, UK); cells were gated according to size scattering, forward scattering and pulse width so only single cells were analysed. A total of 10,000 cell events were recorded per sample and data were analysed using FlowJo software (Tree Star, Ashland, OR).

Statistical analysis

An independent samples *t* test was performed with SPSS Statistics 21 software (IBM, Armonk, NY) to compare normal liver uptake between the different radiolabelled G3 DARPins (p values <0.05 were considered statistically significant).

Results

In vitro stability of label

Over 24 h, ^{111}In-$(HE)_3$-G3 DARPin was stable in PBS at 4, 20 and 37 °C and in serum at 37 °C, as >95 % of radiation activity remained bound to $(HE)_3$-G3 and each sample contained a single-sized radiolabelled protein that had the appropriate molecular weight (Supplementary Table 1 and Supplementary Fig. 2).

Specificity for HER2

HER2 tumour specificity was first established with $[^{99m}Tc(CO)_3]^+$-G3 DARPin-His_6, which had 3.5-fold higher uptake in HER2-positive (BT474) tumours than in HER2-negative (MDA-MB-468) tumours (3.5±1.1 vs. 1.0±0.2 % ID/g at 24 h after administration). Uptake in normal tissues was similar in the HER2-positive and HER2-negative tumour-bearing mice (Table 1). The differences in tumour uptake were also apparent on microSPECT/CT scanning (Fig. 1). However, $[^{99m}Tc(CO)_3]^+$-G3 DARPin-His_6 did not appear optimal for imaging, since the tumour-to-liver ratios were low (1.2:1 at 24 h) and the tumour-to-blood ratios were not optimal (26:1 at 24 h). Thus, there was a need to optimize G3 by assessing the effects of histidine-based tags on the biodistribution of G3 in normal tissue.

Table 1 Biodistribution of $[^{99m}Tc(CO)_3]^+$-G3 DARPin-His_6 in HER2-positive and HER2-negative tumour-bearing SCID-beige mice

Organ	HER2-positive (BT474) tumours at 24 h, mean % ID/g±SD (n=3)	HER2-negative (MDA-MB-468) tumours at 24 h, mean % ID/g± SD (n=3)
Tumour	3.5±1.1	1.0±0.2
Spleen	0.9±0.2	1.0±0.3
Kidney	108.0±7.7	108.6±10.6
Liver	3.0±0.2	2.7±0.7
Lung	0.5±0.1	0.5±0.2
Blood	0.1±0.0	0.1±0.00
Muscle	0.3±0.1	0.2±0.1

A competition assay showed that the His_6-G3 labelled with cold indium and cold iodine, $(HE)_3$-G3 and untagged G3 all competed with $[^{99m}Tc(CO)_3]^+$-G3 DARPin-His_6 for binding to HER2-positive human breast cancer cells (BT474). By contrast, non-labelled EGFR-targeting DARPin did not compete with $[^{99m}Tc(CO)_3]^+$-G3 DARPin-His_6 for binding to BT474 cells (Fig. 2).

Flow cytometry demonstrated that G3 DARPins labelled with cold indium and cold iodine bound to HER2-positive human breast cancer cells (BT474) and HER2-positive human gastrooesophageal junction (OE-19) adenocarcinoma cells, but did not bind to HER2-negative human breast adenocarcinoma cells (MDA-MB-468). The non-labelled G3 DARPin-His_6 and the assessed cold-labelled DARPins demonstrated HER2 specificity in vitro (Fig. 3). Thus, HER2 specificity of His_6-G3, $(HE)_3$-G3 and untagged G3 DARPins in vitro was confirmed.

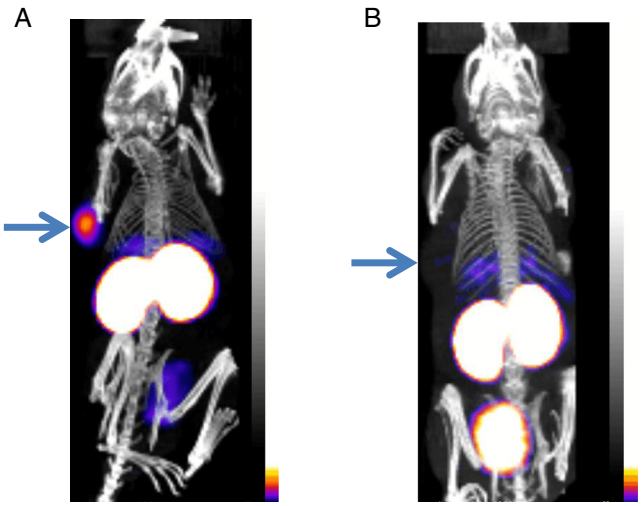

Fig. 1 microSPECT/CT scan of $[^{99m}Tc(CO)_3]^+$-G3 DARPin-His_6 at 1 h in SCID-beige mice bearing: **a** HER2-positive human breast tumour (BT474), and **b** HER2-negative human breast tumour (MDA-MB-468). Tumours (*arrows*) assessed at same sensitivity level

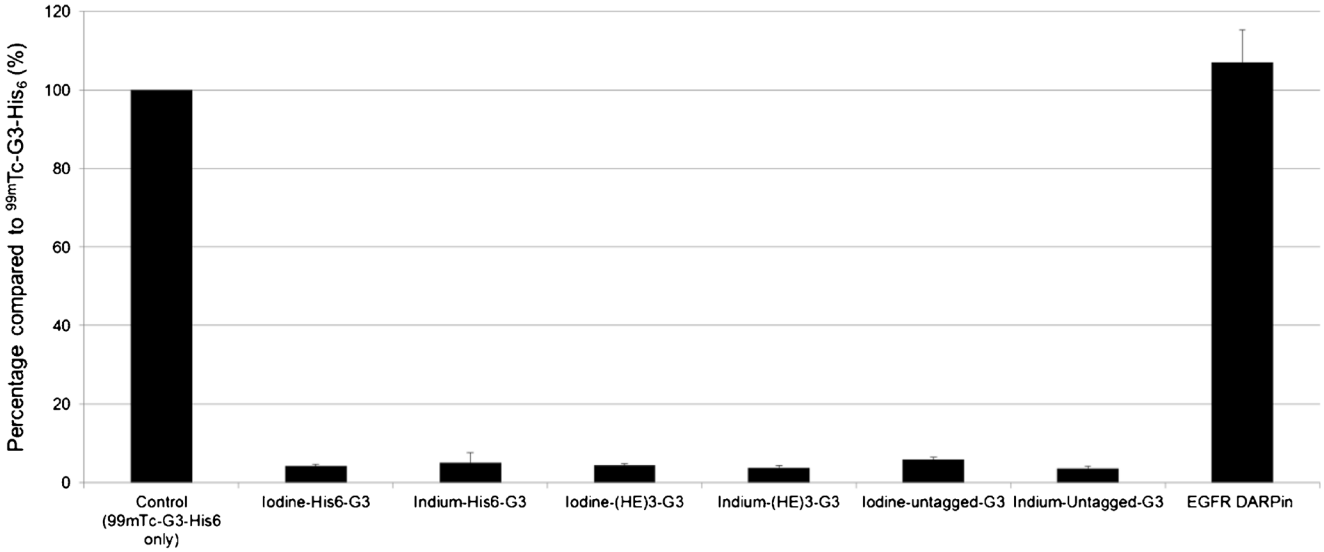

Fig. 2 Competition assay using BT474 cells, treated with 0.1 nM $[^{99m}Tc(CO)_3]^+$-G3 DARPin-His_6 with or without 1,000 nM cold DARPins. Each condition was assessed in triplicate and expressed as percentage of radioactivity in relation to the control treated with 0.1 nM $[^{99m}Tc(CO)_3]^+$-G3 DARPin-His_6 alone (means±SD)

Biodistribution in non-tumour-bearing mice

Normal tissue uptake of His_6-G3, $(HE)_3$-G3 and untagged G3 DARPins radiolabelled with ^{111}In and ^{125}I was first assessed in non-tumour-bearing mice. ^{111}In-$(HE)_3$-G3 DARPin had lower uptake in the spleen, stomach, liver and bone marrow at 4 h and 24 h than ^{111}In-His_6-G3 and ^{111}In-untagged-G3. In other normal tissues, ^{111}In-$(HE)_3$-G3 had either similar or lower uptake at 4 h and 24 h than its ^{111}In radiolabelled counterparts (Fig. 4 and Supplementary Table 2).

At 4 h, ^{111}In-$(HE)_3$-G3 had significantly lower liver uptake than ^{111}In-His_6-G3 ($p=0.001$) and ^{111}In-untagged-G3 ($p=0.001$). Also at 24 h after administration, ^{111}In-$(HE)_3$-G3 liver uptake was significantly lower than that of ^{111}In-untagged-G3 ($p=0.002$) and ^{111}In-His_6-G3 ($p=0.001$). Interestingly, there was no significant difference in liver uptake between the ^{111}In-untagged-G3 and ^{111}In-His_6-G3 at 4 and 24 h after administration (Fig. 4). This suggests a specific favourable influence of the $(HE)_3$-tag, rather than some level of liver targeting of the His_6 tag. Bone uptake was largely attributed to the marrow, as marrow uptake was similar to intact bone uptake. Kidney uptake was greater than 200 % ID/g for all ^{111}In-G3 DARPins at 4 h (Fig. 4 and Supplementary Table 2).

In the study of the radioiodinated DARPins (Fig. 5), where we also have to take enzymatic dehalogenation into account, ^{125}I-$(HE)_3$-G3 and ^{125}I-untagged-G3 showed the lowest uptake in all normal tissues at 4 h. At 24 h, liver uptake of ^{125}I-$(HE)_3$-G3 was significantly lower than those of ^{125}I-untagged-G3 ($p=0.004$) and His_6-G3 ($p=0.003$). There was no significant difference in normal liver uptake between ^{125}I-His_6-G3 and ^{125}I-untagged-G3 at 4 h and 24 h (Fig. 5 and Supplementary Table 3).

Normal tissue uptake of ^{125}I was <1.3 % ID/g for the ^{125}I-labelled G3 DARPins at 24 h, while for ^{111}In-G3 DARPins normal tissue uptake was better maintained between 4 and 24 h (Figs. 4 and 5).

Biodistribution in mice bearing HER2-positive tumours

The biodistribution of $(HE)_3$-G3 was assessed in HER2 tumour-bearing mice, and this construct was chosen on the basis of its lower normal tissue uptake (Figs. 4 and 5), which could facilitate imaging of HER2-positive tumours by achieving greater contrast between tumours and normal tissues. The normal tissue uptake of both ^{111}In-$(HE)_3$-G3 and ^{125}I-$(HE)_3$-G3 in tumour-bearing mice was similar to that in non-tumour-bearing mice (Supplementary Figs. 3 and 4). Similarly, normal tissue uptake of ^{111}In-$(HE)_3$-G3 in tumour-bearing mice was lower than that of ^{125}I-$(HE)_3$-G3 at 4 h, except in the kidneys. At 24 h, the differences in normal tissue uptake between ^{111}In-$(HE)_3$-G3 and ^{125}I-$(HE)_3$-G3 were smaller (Supplementary Table 4). Kidney uptake of ^{111}In-$(HE)_3$-G3 was higher than that in other tissues tested; it peaked at 4 h after administration at 232.0±24.1 % ID/g and decreased to 196.5±31.0 % ID/g at 24 h after administration (Fig. 6a, b and Supplementary Table 4).

The measured tumour uptake of ^{125}I-$(HE)_3$-G3 and ^{111}In-$(HE)_3$-G3 was similar at 4 h (11.3±3.2 and 8.8±1.3 % ID/g, respectively). However, the radioactivity from ^{111}In-$(HE)_3$-G3 in the tumour was better maintained, so that by 24 h ^{111}In-$(HE)_3$-G3 tumour radioactivity was over

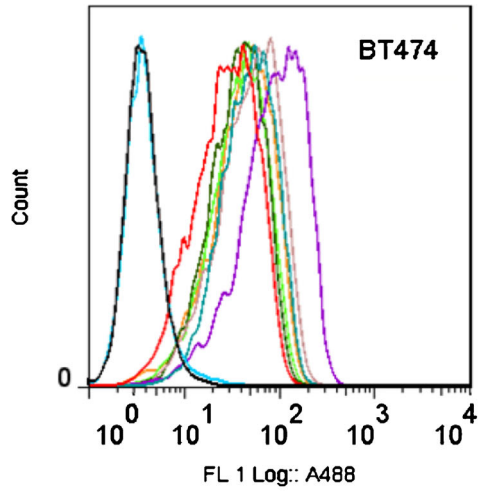

Sample Name	Percentage
Cells.fcs	1.5
Omission control.fcs	3.2
G3-his6.fcs	86.0
Indium untagged-G3.fcs	97.8
Iodine untagged-G3.fcs	97.8
Indium His6-G3.fcs	95.4
Iodine His6-G3.fcs	94.6
Indium (HE)3-G3.fcs	94.1
Iodine (HE)3-G3.fcs	93.1

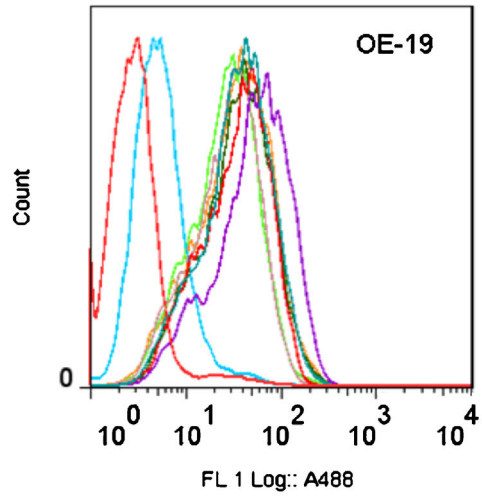

Sample Name	Percentage
Cells.fcs	4.0
Omission control.fcs	10.0
G3-His6.fcs	85.2
Indium untagged-G3.fcs	86.4
Iodine untagged-G3.fcs	90.5
Indium His6-G3.fcs	81.0
Iodine His6-G3.fcs	85.9
Indium (HE)3-G3.fcs	80.7
Iodine (HE)3-G3.fcs	83.5

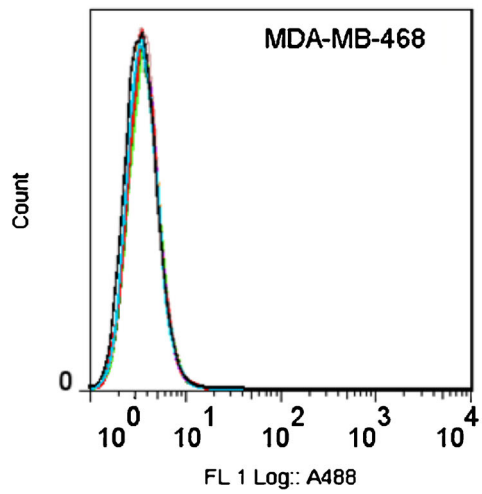

Sample Name	Percentage
Cells.fcs	1.2
Omission control.fcs	0.6
G3-His6.fcs	0.6
Indium untagged-G3.fcs	0.5
Iodine untagged-G3.fcs	0.7
Indium His6-G3.fcs	0.6
Iodine His6-G3.fcs	0.6
Indium (HE)3-G3.fcs	0.5
Iodine (HE)3-G3.fcs	0.6

Fig. 3 Flow cytometry of G3 DARPins labelled with cold indium and cold iodine assessed in human HER2-positive breast cancer cells (BT474) and gastrooesophageal junction (OE-19) adenocarcinoma cells, as well as in human HER2-negative breast adenocarcinoma cells (MDA-MB-468). $G3\text{-}His_6$ was unlabelled and omission controls were treated with cells and antibodies in the absence of G3 DARPin. Percentages are percentage of cells with G3 DARPin binding (*fcs* flow cytometry study)

threefold higher than that of $^{125}I\text{-}(HE)_3\text{-}G3$ (8.1±0.9 vs. 2.5±0.6 % ID/g; Fig. 6a, b and Supplementary Table 4).

In comparison with $^{125}I\text{-}(HE)_3\text{-}G3$, $^{111}In\text{-}(HE)_3\text{-}G3$ had higher tumour-to-normal ratios for all tissues except the

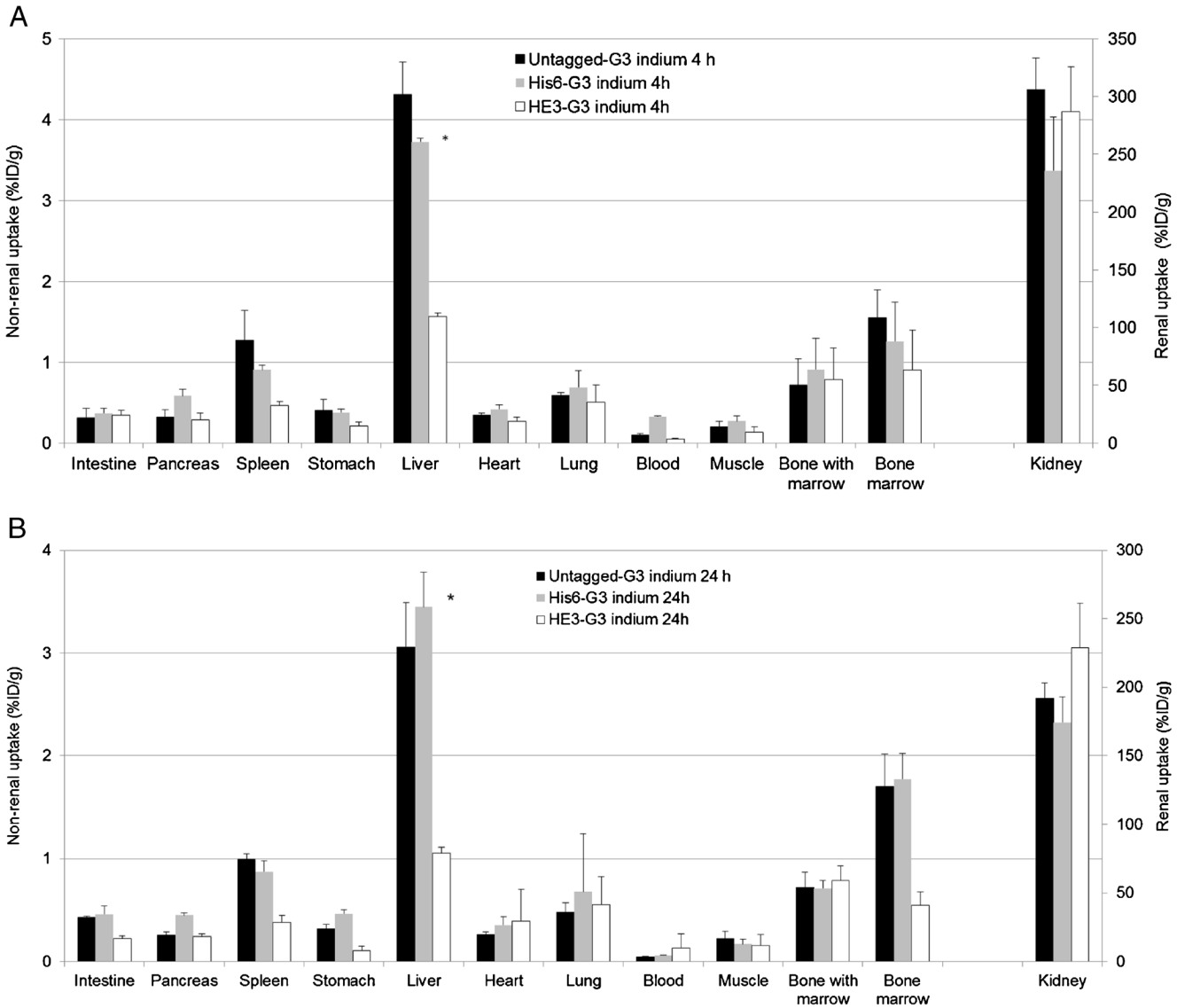

Fig. 4 Biodistribution of ^{111}In-G3 DARPins **a** 4 h and **b** 24 h after administration in female BALB/c mice (mean % ID/g±SD). *$p<0.05$, DARPins $(HE)_3$-G3 vs. His_6-G3 and untagged G3 (liver uptake)

kidneys at 4 h (Table 2). Tumour-to-blood ratios for ^{111}In-$(HE)_3$-G3 were 174.7±26.1 at 4 h and 343.7±161.3 at 24 h, compared with 4.4±3.4 at 4 h and 22.0±9.6 at 24 h for ^{125}I-$(HE)_3$-G3 (Table 2).

DARPin G3 tumour uptake in the presence of trastuzumab

Intravenous administration of an 18-fold molar excess of non-radiolabelled trastuzumab 24 h prior to administration of ^{111}In-$(HE)_3$-G3 did not alter HER2-positive tumour uptake at 4 h compared with that in control mice receiving only ^{111}In-$(HE)_3$-G3 (7.2±1.3 vs. 7.1±1.9 % ID/g, respectively; Fig. 6c). Although trastuzumab and G3 bind to domain IV of the HER2 ECD, G3 can bind in the presence of trastuzumab [23].

MicroSPECT/CT imaging

HER2 tumour uptake could be detected on the 4-h ^{123}I-$(HE)_3$-G3 microSPECT/CT scan but there was non-specific uptake in the stomach, kidneys, bladder and thyroid. In contrast, on the 4-h ^{111}In-$(HE)_3$-G3 microSPECT/CT scan, HER2 tumour uptake was detected and there was minimal non-specific uptake in non-renal organs (Fig. 7).

Discussion

^{111}In-$(HE)_3$-G3 DARPin was found to be better for HER2 imaging than all other formats tested in this study. There are limitations in comparing HER2 radioligands assessed in

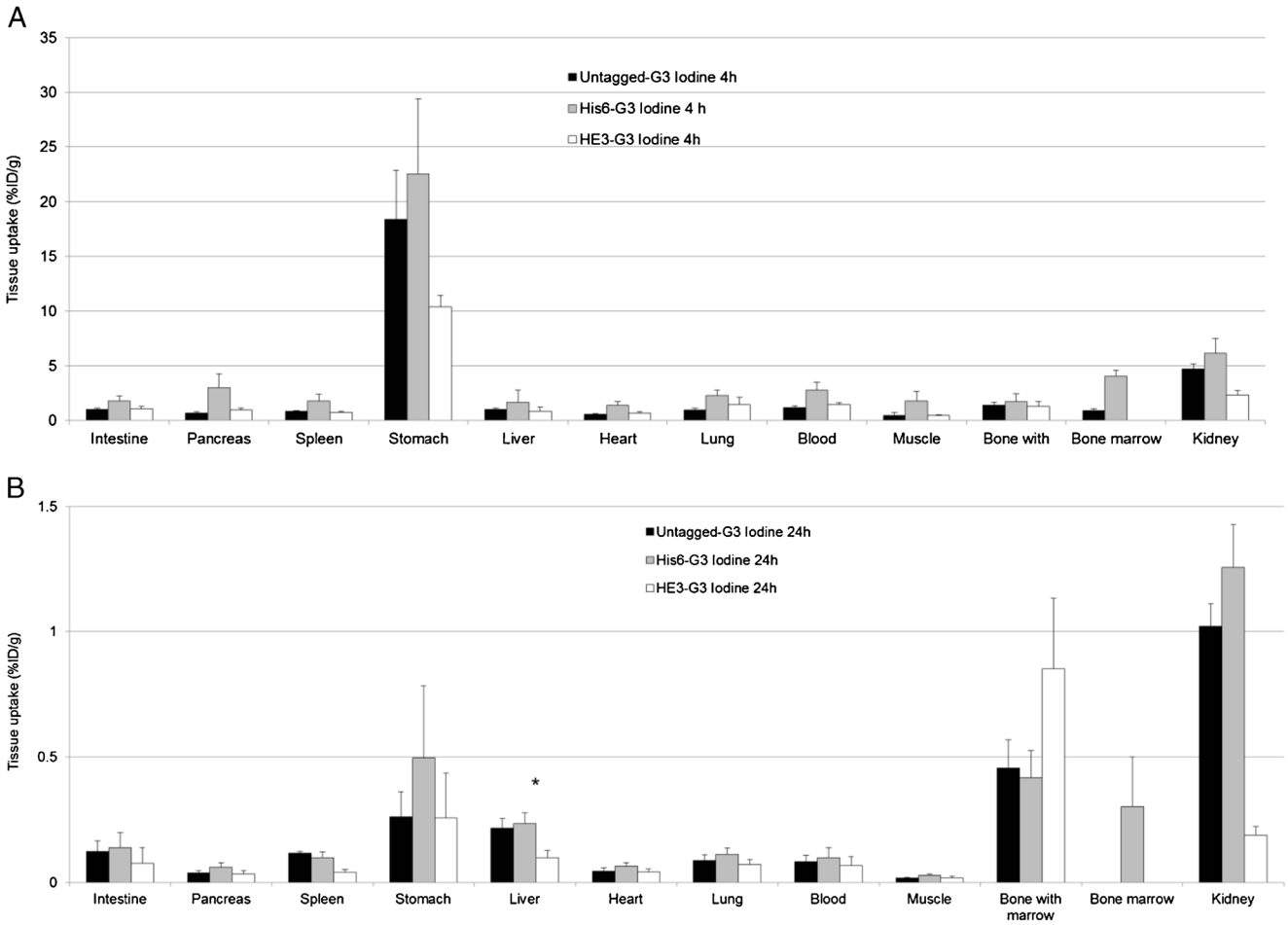

Fig. 5 Biodistribution of ^{125}I-G3 DARPins **a** 4 h and **b** 24 h after administration in female BALB/c mice (mean % ID/g±SD). *$p<0.05$, DARPins $(HE)_3$-G3 vs. His_6-G3 and untagged G3 (liver uptake)

different HER2-positive human tumour xenografts, including different levels of HER2 expression. However, within 24 h of administration to mice bearing HER2-positive tumours, ^{111}In-$(HE)_3$-G3 DARPin achieved higher tumour-to-blood ratios than other reported HER2 radioligands, including whole antibodies, Fab fragments of antibodies and small high-affinity proteins [28–31]. ^{111}In-$(HE)_3$-G3 also had greater potential for HER2 imaging than ^{125}I-$(HE)_3$-G3, reflected by superior microSPECT/CT scans.

The BT474 tumour-bearing mice were confirmed to have immunohistochemistry scores of 3+ with the HercepTest. The HER2-positive tumour uptake of ^{111}In-$(HE)_3$-G3 and ^{125}I-$(HE)_3$-G3 achieved at 4 h was 8.82±1.25 % ID/g and 11.29±3.24 % ID/g, respectively. By contrast, ^{111}In-DOTA-$Z_{HER2:342\text{-}pep2}$ achieved 39.9 percentage of injected activity per gram tissue (% IA/g) [32]. Although higher HER2-positive tumour uptake could have been anticipated, the tumour uptake was sufficient for microSPECT/CT imaging and impressive tumour-to-blood ratios were achieved.

The G3 DARPins were radioiodinated directly at their tyrosine residues. It is likely that only one of the two tyrosine residues within each G3 DARPin was radioiodinated, owing to the molar ratios of radioiodide and G3 DARPin used for radiolabelling. Although direct radioiodination is convenient and the most widely used methodology, it is recognized that the radioligand is likely to undergo in vivo dehalogenation. In future studies, we plan to compare methods using bifunctional coupling agents, to determine whether this approach can improve in vivo stability of radioiodinated G3 DARPins [33]. Nanobodies (12 – 15 kDa) are isolated from the heavy chain of Camelidae antibodies. The anti-HER2 5F7GGC Nanobody radioiodinated via the residualizing agent *N*-succinimidyl 4-guanidinomethyl 3-$^{125/131}$I-iodobenzoate (*I-SGMIB-Nanobody) has superior targeting of HER2-positive human breast carcinoma in vitro and in vivo than its directly radioiodinated counterpart, as *I-SGMIB-Nanobody has enhanced tumour retention of radioactivity [34].

Importantly, we observed that ^{111}In-$(HE)_3$-G3 was able to bind to HER2 in the presence of trastuzumab. This confirms the results of structural modelling which demonstrate that DARPin G3 and trastuzumab bind to non-overlapping epitopes of HER2 domain IV [35]. Thus, ^{111}In-$(HE)_3$-G3

DARPin has the potential to image both treatment-naive patients and patients receiving concomitant trastuzumab without requiring a delay to treatment.

^{111}In-(HE)$_3$-G3 imaging would provide completely new information with the potential to improve understanding of HER2 breast cancer evolution and heterogeneity. Current literature based on biopsy sampling is inconsistent with a wide-range of reported rates of HER2 expression discordance between primary and metastatic sites, from 0 to 34 % [7]. Whole-body assessment of HER2 expression at tumour sites over time and during therapy with HER2 imaging is both more feasible and acceptable to patients than serial and multiple biopsies. Furthermore, considerably less is known about gastric cancer HER2 biology, and ^{111}In-(HE)$_3$-G3 imaging could help address this knowledge gap [36].

HER2 is an important therapeutic target in cancer. DARPin HER2 imaging could be used to improve the selection of patients for anti-HER2 therapy, by identifying increased HER2 expression and the need to introduce anti-HER2 therapy, as well as HER2 loss, necessitating discontinuation of anti-HER2 therapy [1]. This could not only save patients from unnecessary treatments, but also improve healthcare economics by ensuring appropriate use of expensive anti-HER2 therapies.

The pharmacokinetics of ^{111}In-(HE)$_3$-G3, including short half-life in serum, high tumour-to-blood ratios and low non-renal tissue uptake, are well suited to HER2 imaging. The kidneys received the highest radiation dose. However, based on medical internal radiation dose (MIRD) estimates, the maximum absorbed kidney dose in patients with the proposed clinical dose of ^{111}In-(HE)$_3$-G3 (300 MBq) is 1,000-fold lower than the dose associated with a 5 % rate of radiation nephritis within 5 years of administration ($TD_{5/5}$; 9.75 mGy vs. 10 Gy) [37].

Imaging trials of most HER2 radioligands have had disappointing results due to limitations related to their pharmacokinetics for imaging which were already apparent in preclinical assessment [28–31]. It should be noted that the majority of clinical HER2 imaging studies have not assessed HER2 tumour status histologically for correlation with HER2 scans, thus limiting the evaluation of these imaging agents. Trastuzumab radiolabelled with ^{64}Cu, ^{89}Zr or ^{111}In has demonstrated the potential for HER2 imaging by identifying known and/or previously unknown tumour lesions in patients, but lacks sensitivity compared with conventional imaging owing to a long half-life and high blood pool activity [12–14]. Fab fragments of trastuzumab were developed for HER2 imaging because their lower molecular weight is associated with a shorter half-life in serum and faster clearance of background radiation from the blood compared with trastuzumab. However, ^{68}Ga-F(ab')$_2$-trastuzumab PET imaging failed to identify any tumours among four of the eight patients with metastatic HER2-positive breast cancer assessed, due to relatively high liver uptake and blood pool activity as well as potential competition with therapeutically administered trastuzumab [38].

Fig. 6 Biodistribution of (HE)$_3$-G3 in female SCID-beige mice bearing HER2-positive human breast tumours (BT474) (mean % ID/g±SD) pretreated with trastuzumab 24 h prior to DARPin administration (**a** ^{111}In-(HE)$_3$-G3 DARPin, **b** ^{125}I-(HE)$_3$-G3 DARPin. **c** ^{111}In-(HE)$_3$-G3 DARPin). Controls received only ^{111}In-(HE)$_3$-G3

A radiolabelled HER2 binding Affibody molecule, $Z_{HER2:342}$ (about 7 kDa), was used to assess three patients with HER2-positive metastatic breast cancer by PET and/or SPECT imaging. Although not all known tumour lesions were identified in two patients, there was limited tumour biopsy sampling to systematically evaluate the accuracy of HER2 Affibody molecule imaging. Unfortunately, there was high background liver uptake in this initial study [39]. Recently, a phase I trial demonstrated that the second generation Affibody ^{111}In-ABY-025 has improved distribution, dosimetry and accuracy in assessing patients with HER2-positive and HER2-negative metastatic breast cancer. There was a good correlation between HER2 status assessed by SPECT/CT ^{111}In-ABY-025 imaging and immunohistochemistry with the HercepTest, including confirmation that a patient who had had HER2-positive primary disease developed HER2-negative metastases [15].

In our evaluation of the DARPin G3, the (HE)$_3$ tag is a beneficial component as it appeared to lower normal liver uptake of the DARPin G3 without compromising uptake in other assessed normal tissues. This is advantageous for clinical application as HER2 molecular imaging requires high tumour-to-liver tissue ratios and the liver is a common site for breast cancer metastases, yet is also involved in drug metabolism and excretion. Histidine-based tags enable IMAC purification and can also be used for chelation of $[^{99m}Tc(CO)_3]^+$ [21, 27]. The His_6 tag is well established and has been used safely in patients [40], but (HE)$_3$-G3 DARPin was superior to His_6-G3. Affibody molecules with an (HE)$_3$ tag also have lower normal liver uptake than counterparts with alternative histidine-based tags [24, 25]. The G3 DARPins assessed in this study only differed by the presence or composition of their tags and thus the study was able to confirm that (HE)$_3$-G3 DARPin had the lowest normal liver uptake.

The mechanism of (HE)$_3$ tag-mediated reduction in liver uptake of DARPin G3 has not been established. For Affibody molecules it has been proposed that positive charge and hydrophobicity in the tag play a crucial role in liver uptake [25]. However, the untagged and His_6-tagged Affibody molecules have basic isoelectric points (pI), which are brought to a more acidic region by switching to an (HE)$_3$ tag, such that the overall pI of the different Affibody constructs tested differed greatly. By contrast the (HE)$_3$-tagged, His_6-tagged and untagged G3 DARPins have similar pI values of 4.79, 5.41 and 4.71, respectively [25]. Furthermore, the (HE)$_3$-tagged, His_6-tagged and untagged G3 DARPins have similar grand average

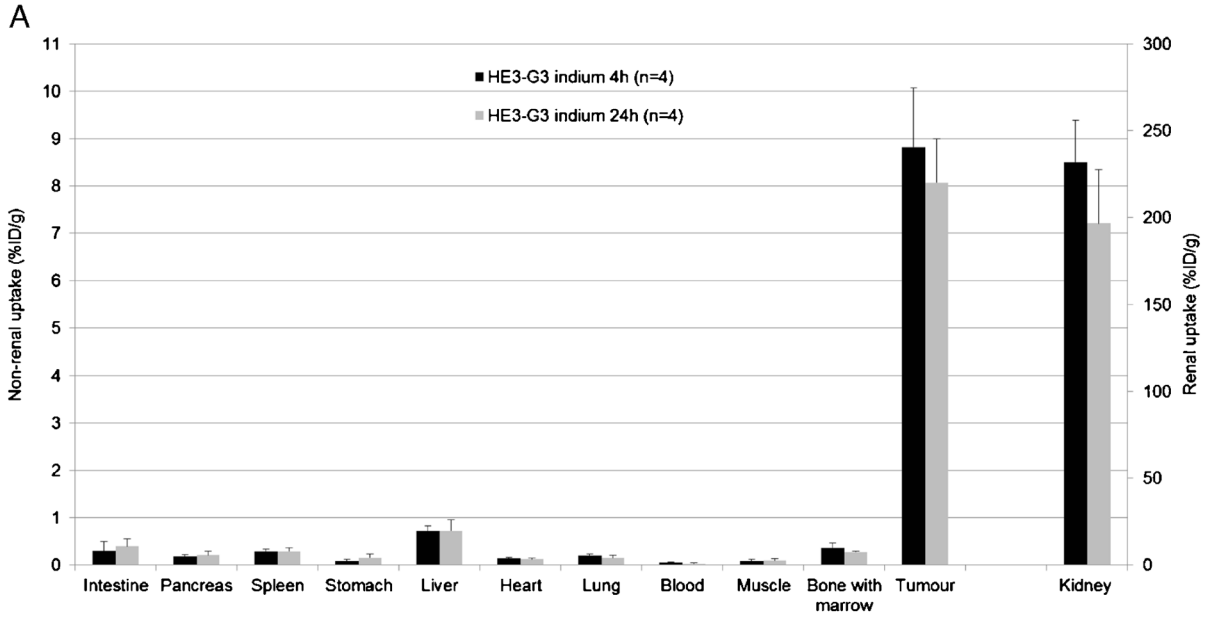
A
HE3-G3 indium 4h (n=4)
HE3-G3 indium 24h (n=4)
Non-renal uptake (%ID/g)
Renal uptake (%ID/g)
Intestine
Pancreas
Spleen
Stomach
Liver
Heart
Lung
Blood
Muscle
Bone with marrow
Tumour
Kidney

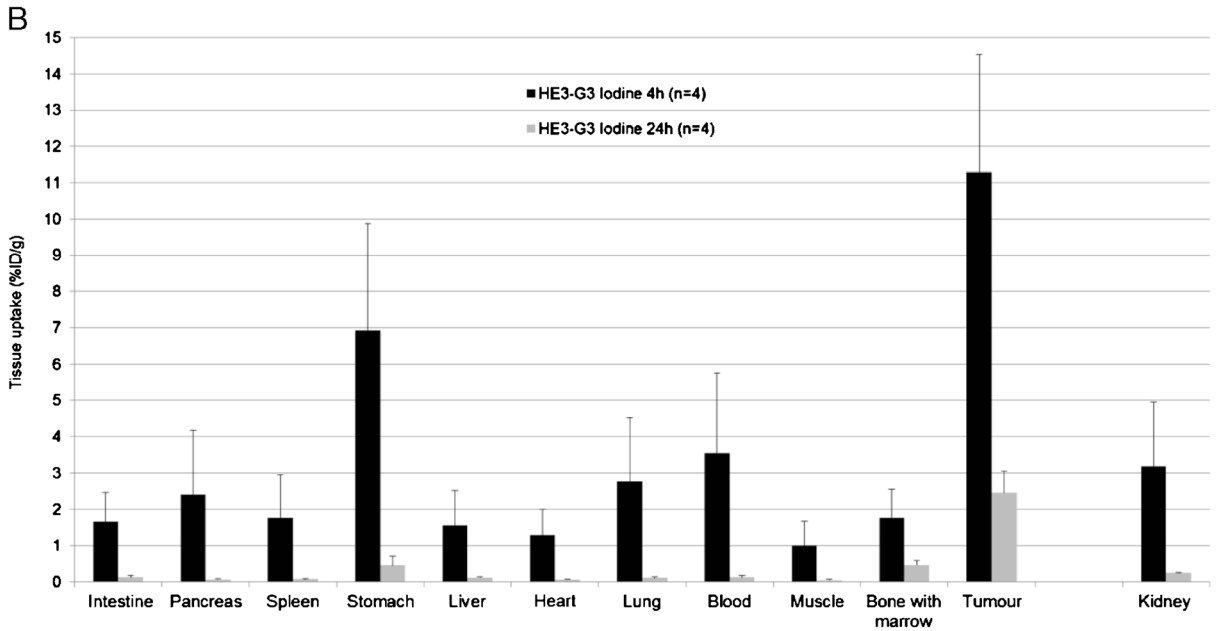
B
HE3-G3 Iodine 4h (n=4)
HE3-G3 Iodine 24h (n=4)
Tissue uptake (%ID/g)
Intestine
Pancreas
Spleen
Stomach
Liver
Heart
Lung
Blood
Muscle
Bone with marrow
Tumour
Kidney

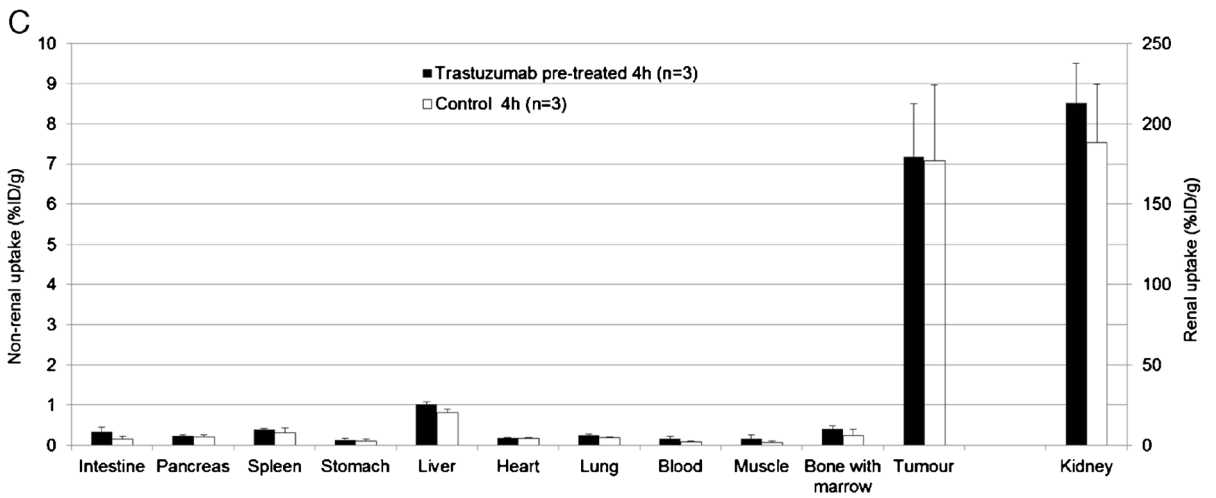
C
Trastuzumab pre-treated 4h (n=3)
Control 4h (n=3)
Non-renal uptake (%ID/g)
Renal uptake (%ID/g)
Intestine
Pancreas
Spleen
Stomach
Liver
Heart
Lung
Blood
Muscle
Bone with marrow
Tumour
Kidney

Table 2 Tumour-to-normal tissue ratios of ^{111}In-(HE)$_3$-G3 and ^{125}I-(HE)$_3$-G3 in female SCID-beige mice bearing HER2-positive human breast tumours (BT474)

Tissue	Tumour-to-tissue ratio			
	^{111}In-(HE)$_3$-G3		^{125}I-(HE)$_3$-G3	
	4 h (n=4)	24 h (n=4)	4 h (n=4)	24 h (n=4)
Tumour	1.0±0	1.0±0	1.0±0	1.0±0
Intestine	39.4±21.1	21.8±5.1	8.0±3.6	20.8±10.9
Pancreas	50.1±15.3	41.5±12.7	6.6±4.2	36.2±11.6
Spleen	32.3±9.6	28.6±5.0	8.5±5.1	34.2±11.2
Stomach	148.8±91.1	67.5±46.6	1.3±0.8	6.4±2.501
Kidney	0.04±0.008	0.04±0.005	4.3±2.2	9.8±2.5
Liver	12.4±1.8	12.0±3.6	9.3±5.7	21.0±8.1
Heart	69.3±25.2	66.5±8.1	10.4±5.1	37.8±11.5
Lung	46.4±12.6	60.8±24.9	5.4±3.6	23.2±9.1
Blood	174.7±26.1	343.7±161.3	4.4±3.4	22.0±11.3
Muscle	114.3±55.5	105.8±51.7	18.6±17.0	58.0±26.6
Bone with marrow	25.9±8.3	28.1±2.7	6.9±2.0	5.2±0.4

of hydropathy (GRAVY) scores of −0.12, −0.12 and +0.02, respectively, indicating that other factors are involved, while the corresponding Affibody molecules have slightly more divergent scores of −1.03, −0.97 and −0.85.

Although in preclinical studies histidine-tagged proteins have been shown to exert greater immunogenicity than their untagged counterparts, several histidine-tagged proteins have been well tolerated in human trials [40]. For example, Endostar a novel recombinant human endostatin which inhibits angiogenesis has a histidine tag, and was safe and well tolerated in large clinical trials [41]. Interestingly, a Blast search (NCBI) for a short input sequence with HEHEHE as the query, yielded a variety of hits in the database of almost identical sequences, e.g. HEHEH in the human zinc transporter (gene ID SLC39A9) and HEHEQE in kinase 3 (gene ID TAOK3). The HHHHHH sequence cannot be found using a Blast search in the *Homo sapiens* database. Instead clusters of histidine are found that are coordinated with metal ions, e.g. Ca^{2+}, Mg^{2+} and Zn^{2+}. The occurrence of the HEHEH sequence in human proteins could mean that the HE_3 tag is a potentially safer alternative to the His_6 tag.

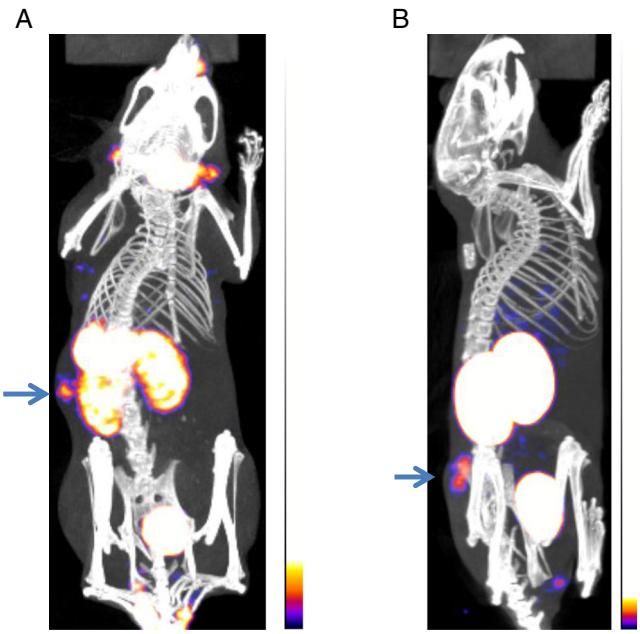

Fig. 7 MicroSPECT/CT scans of SCID-beige mice bearing HER2-positive (BT474) tumours (*arrows*) performed at 4 h (**a** ^{123}I-(HE)$_3$-G3 DARPin, **b** ^{111}In-(HE)$_3$-G3 DARPin)

Conclusion

A clinically valuable radioligand for HER2 molecular imaging in breast cancer and gastric cancer would require minimal normal liver and stomach uptake, as well as the ability to bind to HER2 in the presence of concomitant anti-HER2 therapy. We have demonstrated that ^{111}In-(HE)$_3$-G3 DARPin has specificity for HER2, binds in the presence of trastuzumab, and achieves high tumour-to-blood ratios and reasonable tumour to non-renal tissue ratios, including tumour-to-liver and tumour-to-stomach ratios. Based on the presented preclinical data, ^{111}In-(HE)$_3$-G3 could realize the clinical potential of HER2 imaging and may be suitable for assessment in a first-in-human study.

Acknowledgments This research was funded by the Seventh Framework Programme (FP7) for HER Imaging and Molecular Interaction Mapping in Breast Cancer (Imagint EC grant 259881) and the Breast Cancer Campaign. The research was supported by the National Institute for Health Research University College London Hospitals Biomedical Research Centre.

Conflicts of interest A.P. is a cofounder and shareholder of Molecular Partners, who are commercializing the DARPin technology.

References

1. Arteaga CL, Sliwkowski MX, Osborne CK, Perez EA, Puglisi F, Gianni L. Treatment of HER2-positive breast cancer: current status and future perspectives. Nat Rev Clin Oncol. 2012;9:16–32. doi:10.1038/nrclinonc.2011.177.
2. Ross JS. Breast cancer biomarkers and HER2 testing after 10 years of anti-HER2 therapy. Drug News Perspect. 2009;22:93–106. doi:10.1358/dnp.2009.22.2.1334452.

3. Bang YJ, Van Cutsem E, Feyereislova A, Chung HC, Shen L, Sawaki A, et al. Trastuzumab in combination with chemotherapy versus chemotherapy alone for treatment of HER2-positive advanced gastric or gastro-oesophageal junction cancer (ToGA): a phase 3, open-label, randomised controlled trial. Lancet. 2010;376:687–97. doi:10.1016/S0140-6736(10)61121-X.
4. Verma S, Miles D, Gianni L, Krop IE, Welslau M, Baselga J, et al. Trastuzumab emtansine for HER2-positive advanced breast cancer. N Engl J Med. 2012;367:1783–91. doi:10.1056/NEJMoa1209124.
5. Wolff AC, Hammond ME, Hicks DG, Dowsett M, McShane LM, Allison KH, et al. Recommendations for human epidermal growth factor receptor 2 testing in breast cancer: American Society of Clinical Oncology/College of American Pathologists clinical practice guideline update. J Clin Oncol. 2013;31:3997–4013. doi:10.1200/JCO.2013.50.9984.
6. Goldstein R, Sosabowski J, Vigor K, Chester K, Meyer T. Developments in single photon emission computed tomography and PET-based HER2 molecular imaging for breast cancer. Expert Rev Anticancer Ther. 2013;13:359–73. doi:10.1586/era.13.11.
7. Turner NH, Di Leo A. HER2 discordance between primary and metastatic breast cancer: assessing the clinical impact. Cancer Treat Rev. 2013;39:947–57. doi:10.1016/j.ctrv.2013.05.003.
8. Lindstrom LS, Karlsson E, Wilking UM, Johansson U, Hartman J, Lidbrink EK, et al. Clinically used breast cancer markers such as estrogen receptor, progesterone receptor, and human epidermal growth factor receptor 2 are unstable throughout tumor progression. J Clin Oncol. 2012;30:2601–8. doi:10.1200/JCO.2011.37.2482.
9. Gancberg D, Di Leo A, Cardoso F, Rouas G, Pedrocchi M, Paesmans M, et al. Comparison of HER-2 status between primary breast cancer and corresponding distant metastatic sites. Ann Oncol. 2002;13:1036–43.
10. Baselga J, Cortes J, Kim SB, Im SA, Hegg R, Im YH, et al. Pertuzumab plus trastuzumab plus docetaxel for metastatic breast cancer. N Engl J Med. 2012;366:109–19. doi:10.1056/NEJMoa1113216.
11. Paik S, Kim C, Wolmark N. HER2 status and benefit from adjuvant trastuzumab in breast cancer. N Engl J Med. 2008;358:1409–11. doi:10.1056/NEJMc0801440.
12. Mortimer JE, Bading JR, Colcher DM, Conti PS, Frankel PH, Carroll MI, et al. Functional imaging of human epidermal growth factor receptor 2-positive metastatic breast cancer using 64Cu-DOTA-trastuzumab PET. J Nucl Med. 2013;55:23–9. doi:10.2967/jnumed.113.122630.
13. Dijkers EC, Oude Munnink TH, Kosterink JG, Brouwers AH, Jager PL, de Jong JR, et al. Biodistribution of 89Zr-trastuzumab and PET imaging of HER2-positive lesions in patients with metastatic breast cancer. Clin Pharmacol Ther. 2010;87:586–92. doi:10.1038/clpt.2010.12.
14. Perik PJ, Lub-De Hooge MN, Gietema JA, van der Graaf WT, de Korte MA, Jonkman S, et al. Indium-111-labeled trastuzumab scintigraphy in patients with human epidermal growth factor receptor 2-positive metastatic breast cancer. J Clin Oncol. 2006;24:2276–82. doi:10.1200/JCO.2005.03.8448.
15. Sorensen J, Sandberg D, Sandstrom M, Wennborg A, Feldwisch J, Tolmachev V, et al. First-in-human molecular imaging of HER2 expression in breast cancer metastases using the 111In-ABY-025 affibody molecule. J Nucl Med. 2014;55:730–5. doi:10.2967/jnumed.113.131243.
16. Binz HK, Amstutz P, Kohl A, Stumpp MT, Briand C, Forrer P, et al. High-affinity binders selected from designed ankyrin repeat protein libraries. Nat Biotechnol. 2004;22:575–82. doi:10.1038/nbt962.
17. Boersma YL, Pluckthun A. DARPins and other repeat protein scaffolds: advances in engineering and applications. Curr Opin Biotechnol. 2011;22:849–57. doi:10.1016/j.copbio.2011.06.004.
18. Binz HK, Stumpp MT, Forrer P, Amstutz P, Pluckthun A. Designing repeat proteins: well-expressed, soluble and stable proteins from combinatorial libraries of consensus ankyrin repeat proteins. J Mol Biol. 2003;332:489–503.
19. Schilling J, Schoppe J, Pluckthun A. From DARPins to LoopDARPins: novel LoopDARPin design allows the selection of low picomolar binders in a single round of ribosome display. J Mol Biol. 2014;426:691–721. doi:10.1016/j.jmb.2013.10.026.
20. Dreier B, Pluckthun A. Rapid selection of high-affinity binders using ribosome display. Methods Mol Biol. 2012;805:261–86. doi:10.1007/978-1-61779-379-0_15.
21. Zahnd C, Kawe M, Stumpp MT, de Pasquale C, Tamaskovic R, Nagy-Davidescu G, et al. Efficient tumor targeting with high-affinity designed ankyrin repeat proteins: effects of affinity and molecular size. Cancer Res. 2010;70:1595–605. doi:10.1158/0008-5472.CAN-09-2724.
22. Zahnd C, Wyler E, Schwenk JM, Steiner D, Lawrence MC, McKern NM, et al. A designed ankyrin repeat protein evolved to picomolar affinity to Her2. J Mol Biol. 2007;369:1015–28. doi:10.1016/j.jmb.2007.03.028.
23. Jost C, Schilling J, Tamaskovic R, Schwill M, Honegger A, Pluckthun A. Structural basis for eliciting a cytotoxic effect in HER2-overexpressing cancer cells via binding to the extracellular domain of HER2. Structure. 2013;21:1979–91. doi:10.1016/j.str.2013.08.020.
24. Hofstrom C, Orlova A, Altai M, Wangsell F, Graslund T, Tolmachev V. Use of a HEHEHE purification tag instead of a hexahistidine tag improves biodistribution of affibody molecules site-specifically labeled with (99m)Tc, (111)In, and (125)I. J Med Chem. 2011;54:3817–26. doi:10.1021/jm200065e.
25. Hofstrom C, Altai M, Honarvar H, Strand J, Malmberg J, Hosseinimehr SJ, et al. HAHAHA, HEHEHE, HIHIHI, or HKHKHK: influence of position and composition of histidine containing tags on biodistribution of [(99m)Tc(CO)3](+)-labeled affibody molecules. J Med Chem. 2013;56:4966–74. doi:10.1021/jm400218y.
26. Sosabowski JK, Matzow T, Foster JM, Finucane C, Ellison D, Watson SA, et al. Targeting of CCK-2 receptor-expressing tumors using a radiolabeled divalent gastrin peptide. J Nucl Med. 2009;50:2082–9. doi:10.2967/jnumed.109.064808.
27. Waibel R, Alberto R, Willuda J, Finnern R, Schibli R, Stichelberger A, et al. Stable one-step technetium-99m labeling of His-tagged recombinant proteins with a novel Tc(I)-carbonyl complex. Nat Biotechnol. 1999;17:897–901. doi:10.1038/12890.
28. Dijkers EC, Kosterink JG, Rademaker AP, Perk LR, van Dongen GA, Bart J, et al. Development and characterization of clinical-grade 89Zr-trastuzumab for HER2/neu immunoPET imaging. J Nucl Med. 2009;50:974–81. doi:10.2967/jnumed.108.060392.
29. Smith-Jones PM, Solit DB, Akhurst T, Afroze F, Rosen N, Larson SM. Imaging the pharmacodynamics of HER2 degradation in response to Hsp90 inhibitors. Nat Biotechnol. 2004;22:701–6. doi:10.1038/nbt968.
30. Reddy S, Shaller CC, Doss M, Shchaveleva I, Marks JD, Yu JQ, et al. Evaluation of the anti-HER2 C6.5 diabody as a PET radiotracer to monitor HER2 status and predict response to trastuzumab treatment. Clin Cancer Res. 2011;17:1509–20. doi:10.1158/1078-0432.CCR-10-1654.
31. Perols A, Honarvar H, Strand J, Selvaraju R, Orlova A, Karlstrom AE, et al. Influence of DOTA chelator position on biodistribution and targeting properties of (111)In-labeled synthetic anti-HER2 affibody molecules. Bioconjug Chem. 2012;23:1661–70. doi:10.1021/bc3002369.
32. Orlova A, Tolmachev V, Pehrson R, Lindborg M, Tran T, Sandstrom M, et al. Synthetic affibody molecules: a novel class of affinity ligands for molecular imaging of HER2-expressing malignant tumors. Cancer Res. 2007;67:2178–86. doi:10.1158/0008-5472.CAN-06-2887.
33. Sosabowsky J, Melendez-Alafort L, Mather S. Radiolabelling of peptides for diagnosis and therapy of non-oncological diseases. Q J Nucl Med. 2003;47:223–37.

34. Pruszynski M, Koumarianou E, Vaidyanathan G, Revets H, Devoogdt N, Lahoutte T, et al. Improved tumor targeting of anti-HER2 nanobody through N-succinimidyl 4-guanidinomethyl-3-iodobenzoate radiolabeling. J Nucl Med. 2014;55:650–6. doi:10.2967/jnumed.113.127100.
35. Epa VC, Dolezal O, Doughty L, Xiao X, Jost C, Pluckthun A, et al. Structural model for the interaction of a designed ankyrin repeat protein with the human epidermal growth factor receptor 2. PLoS One. 2013;8:e59163. doi:10.1371/journal.pone.0059163.
36. Boku N. HER2-positive gastric cancer. Gastric Cancer. 2014;17:1–12. doi:10.1007/s10120-013-0252-z.
37. Wessels BW, Konijnenberg MW, Dale RG, Breitz HB, Cremonesi M, Meredith RF, et al. MIRD pamphlet No. 20: the effect of model assumptions on kidney dosimetry and response – implications for radionuclide therapy. J Nucl Med. 2008;49:1884–99. doi:10.2967/jnumed.108.053173.
38. Beylergil V, Morris PG, Smith-Jones PM, Modi S, Solit D, Hudis CA, et al. Pilot study of 68Ga-DOTA-F(ab')2-trastuzumab in patients with breast cancer. Nucl Med Commun. 2013;34:1157–65. doi:10.1097/MNM.0b013e328365d99b.
39. Baum RP, Prasad V, Muller D, Schuchardt C, Orlova A, Wennborg A, et al. Molecular imaging of HER2-expressing malignant tumors in breast cancer patients using synthetic 111In- or 68Ga-labeled affibody molecules. J Nucl Med. 2010;51:892–7. doi:10.2967/jnumed.109.073239.
40. Tolner B, Bhavsar G, Foster B, Vigor K, Chester K. Production of recombinant proteins from Pichia pastoris: interfacing fermentation and immobilized metal ion affinity chromatography. In: Gupta VK, Tuohy MG, O'Donovan A, editors. Laboratory protocols in fungal biology. Current methods in fungal biology. New York: Springer; 2013; p. 407–420
41. Han BH, Xiu QY, Wang HM, Shen J, Gu AQ, Luo Y, et al. A multicenter, randomized, double-blind, placebo-controlled safety study to evaluate the clinical effects and quality of life of paclitaxel-carboplatin (PC) alone or combined with endostar for advanced non-small cell lung cancer (NSCLC). Zhonghua Zhong Liu Za Zhi. 2011;33:854–9.